New Polymers for Application in Thermally Activated Delayed Fluorescence Organic Light-Emitting Diodes

The University Of Sheffield.

A thesis submitted in partial fulfilment of the requirements for the degree of Doctor of Philosophy
By

Yazeed Mohammed H Asiri

Department of Chemistry

June 2022

Declaration

I hereby declare that this thesis is submitted for the degree of doctorate of philosophy (PhD) at the University of Sheffield, having been submitted for no other degrees. It records the research carried out at the University of Sheffield from February 2018 to June 2022. It is entirely my original work, unless where referenced.

Signed…….

Date …….

Acknowledgements

This project could not be done without the kind help and support of many individuals throughout my PhD journey, I would want to offer my heartfelt gratitude and appreciation to each and every one of them.

First of all, I would like to express my gratitude to Allah (God) for providing me with the strength, talent, knowledge, and chance to seek, endure and accomplish this research project. This achievement would not have been possible without his blessings.

Furthermore, my most sincere thanks and appreciation go to my supervisor, Dr. Ahmed Iraqi for his invaluable support, guidance and advice in formulating the methodology and research topic, and for his help in writing up this thesis. This project could not be completed without him. It is a great honour to have had him as a supervisor.

Moreover, I would want to acknowledge and thank all the staff in the chemistry department for their important role in providing and easing things. it is impossible to name them all, but a special thank extend to Simon Thorpe, Nick Smith, Keith Owen, Mahomed Okhai, and the others. I would also send my deepest thanks and appreciation to my formal and current laboratory colleagues for their cooperation and help throughout my period of study.

Additionally, I would like to thank my mother and dedicate this project to the memory of my father. I am thankful for both for believing in me and providing everything that I needed from my birthday. I also thank my brothers and sisters for all their support and prayers.

Above all, my heartfelt gratitude goes out to my beloved wife Shatha for her countless love and support, and for being patient with me during my studies. To my lovely sons Mohammed and Haitham, I would say I am very proud to have both of you in my life and I am extremely thankful to you for being nice and cheering me up all the time. Words cannot explain how I am grateful to have you all in my life. This work could not be completed without my wife and children. Finally, my deep sense of appreciation goes to Taif University for their financial support of my scholarship.

Abstract

Organic light-emitting diodes (OLEDs) can emit light producing a wide range of colors. Their potential to be used in a variety of other applications makes them an important research topic as they are already utilized in solid-state lighting and color flat panel displays. In contrast to most small molecular organic materials, which are deposited as films through high-vacuum thermal deposition procedures, relatively simple solution processes can be used to deposit electroluminescent conjugated and non-conjugated polymers. Solution-processed polymer light-emitting diodes (PLEDs) are a center of interest to both industry and academia because they can be processed cost-effectively, they are flexible, and can be mass-produced over huge areas while being thermally stable.

Because of spin statistic rules, OLEDs based on standard fluorescent materials have generally limited external quantum efficiencies (EQEs) of about 5%, which severely limits their applicability. However, the internal quantum efficiency (IQE) of OLED devices which include organometallic phosphors is about 100 per cent as both singlet and triplet excitons can be used simultaneously in the emission process. However, noble metals like Ir and Pt, which are rare and expensive, are ubiquitous components in heavy-metal complexed phosphorescent materials used in OLEDs. Because these minerals are rare, their application in the manufacture of devices is expensive, prompting the quest for lower-priced alternatives. Because the IQE can theoretically collect both singlet and triplet excitons, thermally activated delayed fluorescence (TADF) OLEDs could be a viable choice. The reverse intersystem crossing (RISC) requires pure organic molecules with particular physical characteristics, which are relatively inexpensive.

This study focuses on the synthesis of a series of polymers with carbazole and fluorene derivatives suitable as host materials for TADF molecules because of their high triplet energies and good hole-transporting (HT) properties. Through Suzuki or Sonogashira co-polycondensation reactions of various substituted monomers, we grafted 10-(4-(5-phenyl-1,3,4-oxadiazol-2-yl)phenyl)-10H phenoxazine (TRZ-PXZ) through alkyl side chains onto the main-chain of polymers. In Chapter 1, we show how to make an efficient high triplet host that contains silicon in its chemical structure which is then incorporated into TADF polymers with different ratios. The chemical purity of all compounds was investigated and studied using ^{1}H-NMR, ^{13}C-NMR, elemental analysis, and mass spectrometry techniques. Ultraviolet-visible spectroscopy (UV-vis), cyclic voltammetry (CV), and thermal gravimetric analysis were also employed to determine the optical, electrochemical, and thermal properties of the resultant TADF copolymers.

Table of Contents

List of Figures

List of Schemes

List of Tables

List of abbreviations

Ar	Argon gas
b	Broad (NMR)
bm	Broad multiplet (NMR)
br	Broad peak (NMR)
bs	Broad singlet (NMR)
CB	Conduction Band
CV	Cyclic voltammetry
Cz	Carbazole
d	Doublet (NMR)
D	Electron donor
D-A	Donor-Acceptor
DCM	Dichloromethane
dd	Doublet of doublet (NMR)
DF	delayed fluorescence
DMF	N,N-Dimethylformamide
DMSO	Dimethyl sulfoxide
DP	Degree of polymerization
Eg (elec)	Electrochemical band gap
Eg (opt)	Optical band gap
eV	Electron Volt
Fc	Ferrocene
FWHM	Full Width Half Maximum
GPC	Gel Permeation Chromatography
HOMO	Highest Occupied Molecular Orbital
ICT	Intramolecular charge transfer
IQE	internal quantum yield
ITO	Indium Tin Oxide
J	Coupling constant (NMR)
J-V	Current-Voltage
JSC	Short Circuit Voltage

LUMO	Lowest Unoccupied Molecular Orbital
m	Multiplet (NMR)
M.p	Melting Point
m/z	Mass to charge ratio (MS)
Mn	Number-average molecular weight
MOT	Molecular Orbital Theory
MS	Mass spectrometry
Mw	Weight-average molecular weight
NBS	N-Bromosuccinimide
NMR	Nuclear Magnetic Resonance
OLED	Organic light emitting diode
P(o-tol)3	Tris(ortho-tolyl)phosphine
P3P3HT	Poly(3-hexylthiophene)
PC70BM	Phenyl-C70-Butyric Acid Methyl Ester
PDI	Polydispersity Index
PF	Prompt fluorescence
PL	Photoluminescence
PLQYs	photoluminescence quantum yields
ppm	Part per million
RISC	Reverse intersystem crossing
RT	Room temperature
s	Singlet (NMR)
t	Triplet (NMR)
TADF	Thermally activated delayed fluorescence
Td	Onset of Decomposition
TGA	Thermogravimetric analysis
THF	Tetrahydrofuran
UV-vis	Ultra-Violet-visible spectroscopy
VB	Valence Band

Chapter1: Introduction

1. Introduction

1.1 Organic Light Emitting Diodes

1.1.1 History of Organic Light Emitting Diodes

Electroluminescence is a phenomenon, where an electric current passing through materials, causes them to emit light.[1] The first attempt of creating light from electricity was done in the early nineteenth century when Thomas Edison invented the glowing bulb.[1] The efficiency of the invented bulb was low, as the conversion of electrons to photons was less than 6%. Then, improved higher efficiency devices (fluorescent tubes) were created, which is known as the second generation of artificial lights.[1] Enhanced fluorescent tubes are still widely used today. However, because of some disadvantages of these devices, such as toxic mercury components, the third generation of artificial lights was developed.[1] Organic light emitting diodes (OLEDs) started attracting the interest of researchers after the amazing work and their invention by Tang and Van Slyke in 1987[2]. Since then, there have been rapid developments in their applications as lightning sources and full colour displays.[3] OLEDs factor heavily in modern life, widely used in large flat screens, solid lighting devices and small display devices, such as smartwatches and mobile phones. Their beneficial features of being low in cost and voltage, lightweight, and responding very rapidly make OLEDs particularly useful for application in flat panel displays.[3] Unlike solar cells, where the electricity is generated from light, OLEDs produce light from electricity. The light is produced when the electron-hole pairs recombine to make excitons. The recombination takes place between the cathode and the anode where there are different layers, specifically, hole transport layers, electron transport layers and emissive layers.[4] The recombination process occurs when charge transport layers extract holes from the anode and electrons from the cathode and inject them into the emissive layers, resulting in a 1:3 singlet to triplet excitons ratio.[4] While the energy of triplet excitons is non-radiative and dissipates as heat, the radiative energy of singlet excitons emits light. This introduces a challenge in terms of internal quantum efficiency (IQE). The IQE of fluorescent OLEDs is limited to 25% due to the fact that only 25% of the excitons generated are singlet. The IQE of phosphorescent OLEDs, on the other hand, may theoretically approach 100 per cent by harvesting both singlet and triplet excitons via intersystem crossing (ISC).[5]

The limitation of phosphorescent OLEDs is using expensive heavy transition metals, such as platinum and iridium. Because of their toxicity, rarity and cost, these are not suitable for use in OLED devices.[6] Researchers have successfully found alternatives to those toxic metals for use

in OLED devices. Thermally activated delayed fluorescence (TADF) is considered one of the greatest successes in OLEDs. Adachi et al. successfully used pure organic compounds to obtain an external quantum efficiency (EQE) larger than 20%.[7] TADF-OLEDs use reverse intersystem crossing (RISC); these TADF systems harvest both (S) and (T) excitons which theoretically enhance the IQE of the emissive molecules.[8,9]

1.1.2 Structures of OLED Devices

OLEDs are usually classified as π-conjugated materials into two categories. One is related to small molecules, and is known as (SMOLEDs), while the second type uses larger molecules, (polymers), hence they are known as POLEDs. The properties of OLED materials include high flexibility, self-luminescence, strong resolution, wide viewing angle low power consumption and excellent EL efficiency; these qualities make OLED-based devices among the most promising. However, external effects, for example, photo-absorption mechanical stress, and electric fields may alos lead to cold body radiation, which can then cause luminescence[10–12]. Light in electroluminescent processes occurs due to the electrons-holes recombination.

OLED devices are typically solid-state devices. The simplest OLED devices consist of one organic layer sandwiched between two conductive electrodes. Light is emitted when holes are recombined with electrons within this layer. Thus, the organic layer must have a good transporting property for both electrons and holes. Mostly, these devices are comprised of two organic layers. The layer that connects to the cathode has good electron-transporting properties, and the other layer, which is connected to the anode, has good hole-transporting properties. The light is produced when the electrons and holes are recombined at the interface. The emissive organic layer is located between the transporting layers (Figure 1. 1). The various wavelengths of the emitted light are determined by the difference in the highest occupied molecular orbitals (HOMO) and the lowest occupied molecular orbitals (LUMO) of the emissive organic layer materials. In more complex OLED devices, more layers are used to inject holes and electrons efficiently from both the cathode and anode. In order to minimize Schottky barriers, these layers possess work functions that match the electrodes, which enhances the carrier injection.

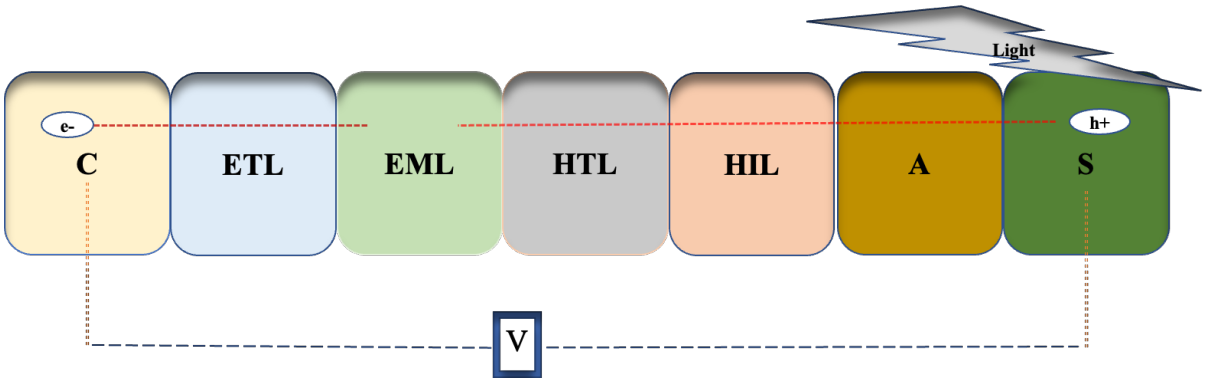

Figure 1. 1 General structure of OLED devices.

C: cathode, EML: emitting layer, HTL: hole transport layer, ETL: electron transport layer, HIL: hole injection layer, A: anode, S: substrate.

1.1.3 Working Concept of OLEDs Devices

The anode is a high-performance electrode (large work function) and is mostly made of indium tin oxide (ITO). This type of anode is known for its higher work function usually greater than 4.8eV. The anode is mostly a transparent electrode, which owns a high work function. The ITO anode layer shows very good transparency and has a small sheet resistance. Although it has these amazing features, indium is an expensive and rare material. Thus, there are ongoing efforts to create alternative anodes from carbon nanotubes, polymers and graphene.[13–15]

Secondly, the hole-injection layer (HIL) is deposited on the anode, where it takes the holes from the anode layer and injects them into the device.[16] The quality of the HIL is important for efficiency, operating voltage, device stability and its lifetime.[17] To minimise the barrier to hole injection in this layer and to enhance the hole transporting capability, different types of inorganic and organic semiconductors materials have been used for the HIL of OLEDs.[17] Different materials are used for HIL, such as transition metal oxides (TMOs) and metal halide materials. Because TMOs have a good energy band structure and close conduction band to ITO anode Fermi level, they are used to increase the OLEDs performance.[18,19] Copper iodide metal (CUI) is considered the best metal halide for this type of layer due to its unique features. It has a very high transparency, especially in the range of the visible spectrum; it also possesses great conductivity, matched work function as well as low temperature for thermal evaporation.[20,21]

The third layer of an OLED structure is the hole-transporting layer. In addition to the requirement of transparency for this layer, its HOMO must match the anode work function. Moreover, the hole-transporting layer (HTL) must be a good conductor of holes and should

have the ability to block the electrons, which increases the chance for the electrons and holes to collide and recombine in the emissive layer. Recently, 4,40-bis[N-(1-naphthyl)-N-phenylamino] biphenyl (NPB) has been proposed as a potential material for the hole injection layer.[22]

In OLEDs, the emissive layer is generally located between HTL and ETL. The organic emissive layer is at the centre of the OLED, where the light is formed. This layer contains a colour-realizing emitter that is doped into the host. The light is made in this layer after being converted from electrical energy.[21] The recombination between the electrons and holes to form excitons takes place in this layer. The energy difference between the HOMO levels and LUMO levels of this layer determines the light wavelength (λ) that is produced by the OLED device.

The electron-transporting layer mainly works to support the movements of the electrons through it, into the emissive layer. The Schottky barrier should be taken into account in this layer, and should be minimised; as a result, electrons can be injected into the organic emissive layer.[23] In addition, this layer should act as a good hole blocking layer; thus, the holes may stay in the emissive layer, thereby increasing the possibility of electron-hole recombination and emission of light.[24,25]

The electrons are inserted through the negatively charged cathode into the organic emissive layer. Typically, the cathode comprises a low work function metal (< 4 eV). Magnesium and calcium are examples of such metals that have low work function. Even though these metals have ideal values of work function, they are not stable in ambient settings, making them unsuitable for use in OLED displays. However, Aluminium is a good alternative to these metals. The work function for aluminium is approximately 4.3 eV. Therefore, aluminium is mostly used as a cathode in OLEDs.[22] Figure 1.2 illustrates the basic polymeric OLEDs operation processes, starting from all molecules being in the first ground state, and ending with the formation of excitons.

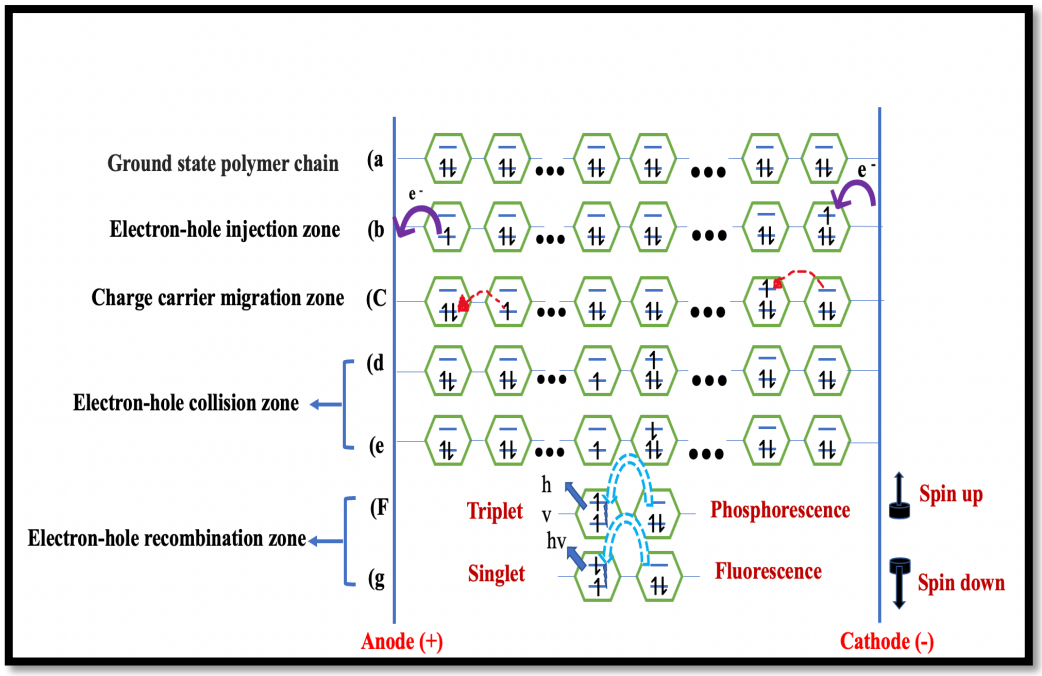

Figure 1. 2 Basic operation of OLED in polymeric chains.[23]

1.1.4 Application of OLED Devices

Since better-efficiency devices (fluorescent tubes, which are known as the second generation of artificial lights) were generated, studies into supplying the commercial market with higher-efficiency devices are ongoing. Recently, a large number of studies have developed solid-state lighting technologies. For instance, quantum dot light-emitting diodes (QDLED) and most importantly organic light-emitting diodes.[26] The importance of OLED devices comes from their strong commercial demands. Furthermore, they exhibit interesting characteristics, such as quick response, simpler preparation, and inexpensive and safe applications. OLED devices are the most common technology available in the market due to their nature of self-emission, which makes them easier to manufacture with high quality, efficiency and low weight. They are versatile and have been used and performed in a wide range of applications.[27]

Mobile phones and modern televisions have highly efficient, quality screens, which are examples of the commercial application of OLEDs. Compared to earlier LED products, OLED devices show excellent resolution images; also, OLEDs are self-illuminating, show a wider viewing angle, and provide thinner and lighter displays.[24,28] Recently, many improvements have been made to enhance the operational lifetime for OLED screens. The first OLED devices were publicly released in early 2013; their commercial use has continued to increase since then. There is now a numerous range of OLEDs on the market, from smartwatches to OLED

wallpaper. Moreover, companies work with researchers to investigate and enhance OLED devices and the materials used to make them. There are various companies interested in OLEDs, such as LG Chem, Merck, DuPont and Nissan Chemical Industries. Examples of OLED applications are shown in Figure 1.3.

Figure 1. 3 Examples of OLED applications.

1.2 The Development of OLEDs

1.2.1 Categories of Organic Materials Used in OLEDs

Since the early innovation of vapour-deposited OLED, several attempts have been made to make improved materials and to understand fully the physical concepts behind them. There are two types of OLEDs. The first type is devices that consist of small organic molecules (SMOLEDs), while the second class is made from large organic polymers (POLEDs).[29] The light generated by SMOLEDs is either fluorescence or phosphorescence. Various molecules are commonly used to make the organic layers in this class of OLEDs. The materials used for the hole transporting layers include (1,4-bis(1-naphthylphenylamino)biphenyl) (NPB) and (N,N-diphenyl-N,N-bis(3-methylphenyl)-1,1-biphenyl-4,4-diamine) (TPD), while the electron transporting layers contain (1,3,5-tris(N-phenylbenzimidizol-2-yl)benzene) (TPBI), (2-(4-biphenyl)-5-(4-t-butylphenyl)-1,3,4-oxadiazole) (PBD) and (tris(8-hydroxyquinoline)aluminium) (Alq_3).[30] However, both fluorescence and phosphorescence of

SMOLEDs are determined by the class of the emissive layer. On the other hand, the design of POLEDs layers consists of polymers. The main difference between these two types is HTL and EML. The emissive layer of this class is still under research. Examples of emissive layers include derivatives of poly(p-phenylene), poly(p-phenylenevinylene) and poly(fluorene).[31,32] The hole-transporting layer of POLEDs mostly contains PEDOT-PSS (polyethylene dioxythiophene polystyrene sulphonate).[33]

1.3 Generations of OLED Devices

1.3.1 Fluorescence-based Devices

The efficiency to convert electrons to photons is the most acceptable description for OLED efficiency; it can be distinguished by either the power efficacy or the quantum efficiency (QE). As the electrons and holes are recombined after being inserted from the cathode and the anode, both singlet and triplet excitation is going to form with a 1:3 ratio.[34] The decay of singlet excitons happens rapidly, producing quick electroluminescence (fluorescence). Fluorescent-based OLED devices are known as the first generation of OLEDs. Only 25% of singlet excitation can decay and emit fluorescence.

The excitons can be either radiative or non-radiative (NR). When radiative emission is at its maximum, the internal conversion will release the exited excitons back to the lower state. On the other hand, non-radiative excitons decay and produce heat with no light emission. In fluorescence-based materials, the photon is emitted as light when the excitons decay from the singlet excited state (S_1) relative to the ground state (S_0).[35] As a result, singlet states are the only state capable of emitting light.

However, the efficiency of this type of device is not ideal because of the quantum mechanics selection rules, which prohibit the transition from triplet states to singlet states. Therefore, the maximum internal quantum yield for fluorescent devices is limited to less than 26%.[36] Aluminium-tris-(8-hydroxyquinoline) and fluorene derivative polymers are typical examples of OLED fluorescent emitters.[37] (Figure 1.4).

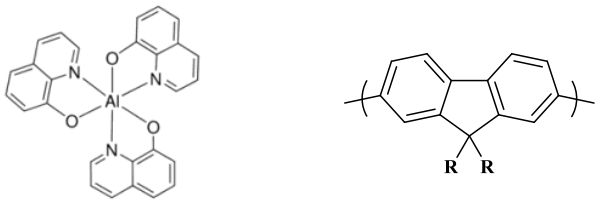

a b

Figure 1. 4 Examples of OLEDs fluorescent emitter (a) Aluminium-tris-(8-hydroxyquinoline)[29] and (b) general structure of fluorene polymer.

1.3.2 Phosphorescent Emitting OLEDs (PHOLEDs)

Phosphorescent-based devices are the second generation of OLEDs. They were introduced to increase the internal quantum efficiency. However, using a pure organic compound is not applicable in this generation. Thus, heavy metals such as platinum, and iridium, are incorporated with organic molecules in order to enhance the spin-orbit coupling between the exciton's orbital angular momentum and spin angular momentum, as a sequence, the triplet state turns to an emissive state.[38] Rather than fluorescent-based devices, phosphorescent molecules have a large value in terms of energy difference ($\Delta E_{(S-T)}$). Furthermore, intersystem crossing (ISC) is a very strong process, so it leads to the transfer of 75% of promoted excitons to the triplet-excited state. Using heavy metals (figure 1.5), such as osmium, platinum and iridium, make the transition between triplet-excited state (T_1) and singlet-ground state (S_0) possible.[39] Thus, all generated excitons are harvested by the phosphorescent emitter. Despite the advantageous properties of this type of emitter, limitations are still present. The operational life of the blue-coloured component of phosphorescent-based devices is insufficient. Furthermore, the spin-orbit coupling and ISC of PHOLEDs depends on expensive rare heavy metals.[40,41] PHOLED was the only choice for harvesting both singlet and triplet excitons until the discovery of the third generation of OLEDs, which was introduced as thermally activated delayed fluorescence (TADF).

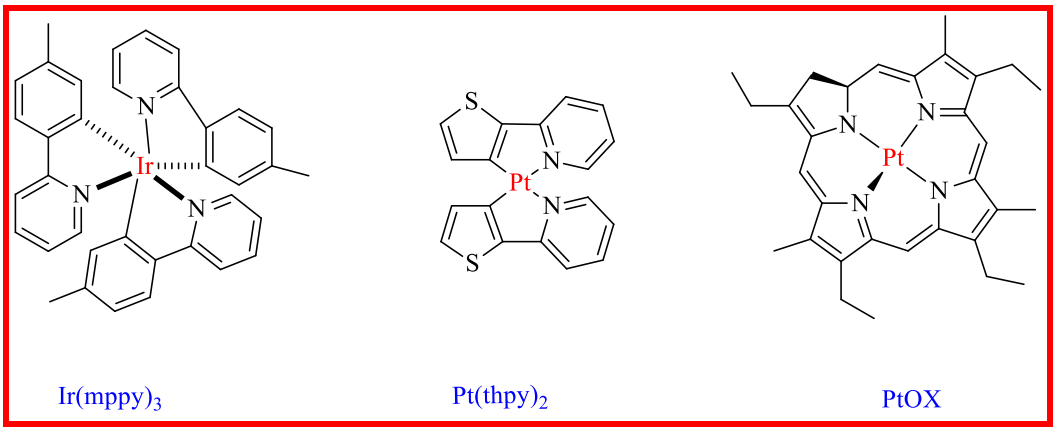

Figure 1. 5 Examples of OLED phosphorescent molecules.[42]

1.3.3 Third Generation of OLEDs

TADF is the newest form of OLED devices. TADF based materials create light by capturing both singlet and triplet excitons without rare heavy metals present in the emissive molecules. Their use for the molecular design and structure of OLEDs has increased rapidly in the last few years. In 2012, the Adachi group successfully used organic material to produce light with an efficiency comparable to that of phosphorescence-based devices.[7] The energy difference between the singlet and triplet state ($\Delta E_{(S-T)}$) of TADF molecules is low, which allows RISC to take the excitons back from the triplet excited state (T_1) to the singlet excited state (S_1). The lifetime of the excited state in TADF is usually in the order of microseconds, where it is less in normal fluorescence, often in the nanoseconds.[43–45] Introducing TADF emitters with such advantageous properties helps to avoid the triplet-triplet annihilation, which is common in PHOLEDs emitters.[46] Moreover, TADF molecules and emitters are less expensive since they are free from noble metals. High triplet energy and thermal stability are other features of TADF. On the other hand, there are some limitations and challenges present with TADFs such as degradation, and a broad emission spectrum. Figure 1.6 below shows a comparison between the three generations of OLEDs.

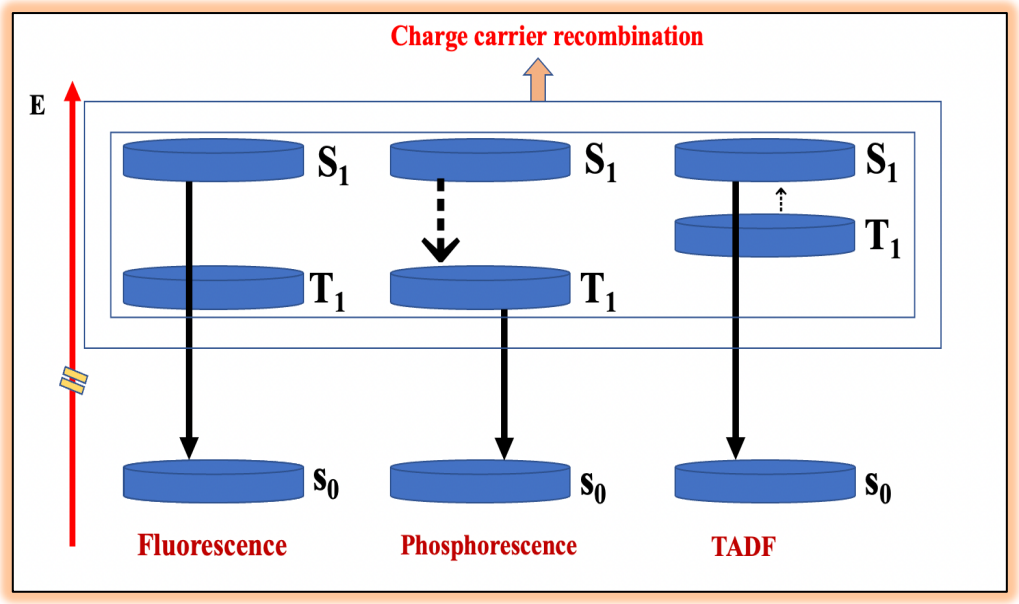

Figure 1. 6 Comparison between fluorescence, phosphoresce and TADF.[47]

1.4 Thermally Activated Delayed Fluorescence

1.4.1 Introduction

TADF materials are the latest generation of materials for use in efficient OLEDs that possess many advantages compared with the first two generations, such as avoiding the use of heavy metals and their high internal quantum efficiency. Thus, TADF-based materials are considered the most competitive materials for use in OLEDs. Furthermore, TADF-small molecule materials are proven to have a very good quantum yield and are capable of covering the full colour spectrum from blue to red. However, there remain some challenges in maximizing quantum efficiency and enhancing device output. These two criteria can be improved by focusing on the preparation methods and designs of the polymers used. Developing well-designed polymers results in low-cost materials suitable for processing.

TADF has been shown to be one the best solutions for high-efficiency fluorescence emitters; synthesising and developing such materials as either emitters or hosts is an important topic of research nowadays. Also, TADF molecules have been used as a cheaper electroluminescent replacement of organic phosphorescent materials, as they exhibit high-quality displays but are less expensive than phosphorescent molecules.[48]. In 1961, Parker and Hatchard discovered eosin dye, which exhibits TADF behaviour. [49] Nineteen years later, the first TADF complex (Cu(I)-complex) was prepared by Blasse et al;[50] more TADF materials have been synthesized

since then. The research and studies of TADF incorporated into OLEDs have increased significantly since 2009. The interest in using TADF in OLED devices peaked in 2012 after the discovery of Adachi et al[7]. Creating OLED devices with 30% of external quantum efficiency has become possible with newly high effective TADF molecules. In addition, the TADF emitter increased the EQE of OLED blue devices by almost 20%, while the EQE increment in green devices can be as high as 30%.

1.4.2 Mechanism of TADF Luminescence

The general structure of OLEDs is composed of a cathode, a metal anode and a different number of organic layers. The structure of OLED devices is usually classified into four types that are based on the number of layers. That is, multilayer structure, double-layer structure, single-layer structure and three-layer structure, which is the most used in OLEDs.[51,52] The structure of these organic layers includes HTL, ETL and EML, which is important in terms of increasing the device performance.

Applying an external voltage results in electrons being inserted from the cathode and holes being injected from the anode. They combine to form excitons in the organic emitting layer.[53] Because of their different spin states, those formed excitons have both singlet and triplet excitons (S_1) (T_1), and the ratio of singlet excitons to triplet excitons is 1:3 based on the quantum theory.[54] Those excitations then emit from the radiative excited first state of singlet or triplet excitons to the ground state. Photons generated in this process are emitted from the EML, which is responsible for the efficiencies of OLEDs.

The mechanism of OLED devices involves two methods as shown in Figure 1.7. One is common fluorescence and phosphorescence, and the other mechanism is TADF, which takes place through two unimolecular mechanisms. The first mechanism is promoted fluorescence (PF), and the second step is commonly known as delayed fluorescence (DF).[55,56] In promoting fluorescence, after the molecule is excited, fast emission occurs immediately. The process of emission is typically taking place within nanoseconds when the excitons decay from (S_1) to (S_0). On the other hand, the delayed fluorescence mechanism involves the (T_1), which is converted to (S_1) before the exciton's decay. The DF process includes a RISC; therefore, the fluorescence emission will take a longer time before taking place (microseconds).

In OLEDs, after injection of charges in TADF materials, both (S_1) and (T_1) are generated in a 1 to 3 ratio. Although the PE mechanism and DF mechanism have similarities in terms of their

spectral distribution as typical fluorescence, they exhibit different fluorescence lifetimes. In addition, the TADF emission process must have some key factors to operate in OLEDs effectively. First, electrons and holes are moving to create both singlet and triplet excitons with the ratio of 1:3.[57] Moreover, internal conversion (IC) and vibrational relaxation (VR) cause the higher energy excitons states (S_2, S_3...T_2, T_3,...) to move to the lowest energy states (S_1, T_1). Then under thermal activation conditions, the triplet excitons at the lowest triplet excited state are reversibly converted to a singlet-excited state *via* the RISC process. Finally, all excitons at the singlet-excited state, including the generated singlet excitons and transferred triplet excitons, will decay to the ground singlet state (S_0) with different luminescence lifetimes based upon the PF mechanism and DF mechanism.[58] The more T_1 conversion that occurs, the higher the efficiency of DF. Since the ratio of triplet conversion depends on the RISC process. Reducing the difference in the energy level between T_1 and S_1 is one way to boost the RISC procedure. That means that the first triplet excited state and the first singlet excited state have small energy splitting (E_{ST}).[48,58] However, the energy levels of the first singlet state and first triplet state in TADF molecules are as close to each other as less than 0.3 eV. The RISC of T_1 to S_1 is achieved by using ambient heat; consequently, all the triplet excitons (75%) are converted to singlet excitons, which produce DF of longer lifetimes (microseconds). In addition, the remaining excitons (25%) are also produced *via* PF. As a result, TADF materials could reach 100% internal quantum efficiency. The spectrum of both processes (DF and PF) is identical because they are both formed from S_1 emissions. The emission of TADF molecules is typically based on the spatial separation of the LUMO and the HOMO of excited state materials of charge transfer.[59] TADF materials have a small (ΔE_{ST}) due to their molecular design which usually involves bulky structure. It is possible to accomplish the RISC through thermal conditions. Consequently, all triplet excitons are converted to S_1, which then achieve 100% of internal quantum efficiency.

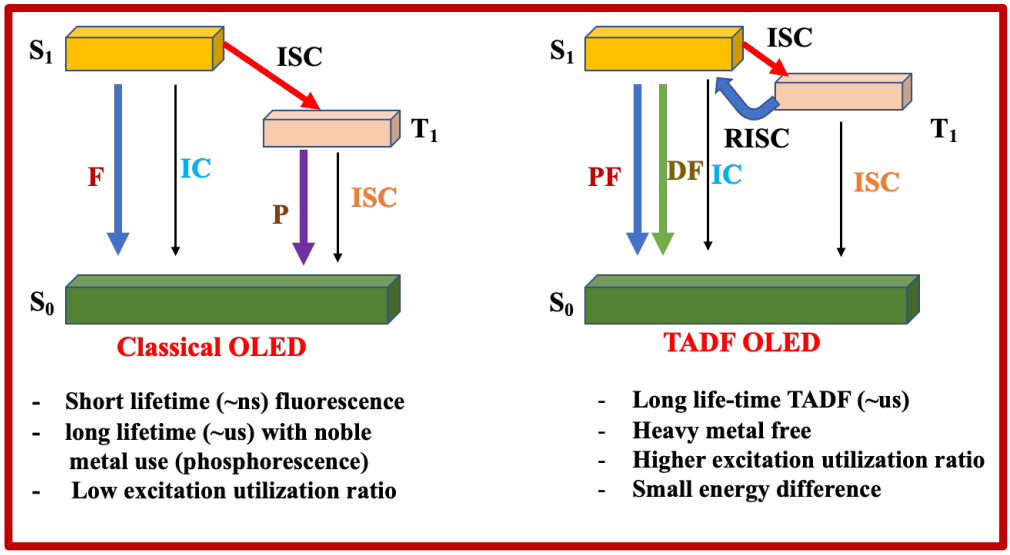

Figure 1. 7 Mechanism of Luminescence showing (F, IC, P, ISC, PF, DF, RIC, TADF). [60]

1.4.3 Molecular Construction Design of TADF Molecules

1.4.3.1 TADF Emitters Structure Rules

The design of TADF emitters is very important for efficient emission and for long-lifetime devices. The light-emitting features are linked to photoluminescence quantum yield (PLQY), and a small energy difference between S1 and T1 Δ_{EST}, which have been the main objectives of TADF emitters. These factors along with material stability and full width at half-maximum (FWHM) are important to be taken into consideration when designing TADF emitters. Since the parameters are interrelated, the TADF emitters were developed to enhance the parameters at the same time with a small sacrifice of other factors.[61]

In fact, many researchers have shown that the donor-acceptor structure is the ideal method of making TADF emitters, and current emitters are built using a donor-acceptor molecular architecture with significant separation between the HOMO and LUMO. [61,62] The LUMO is generally located on the electron acceptor moiety of the molecule, while the HOMO is on the electron donor part. In the case of TADF emitters based on small molecules, large steric hindrance groups are usually introduced between the acceptor (A) and the donor (D) of the TADF molecule.[63–65] Thus, the required separation of LUMO and HOMO is achieved, resulting in a better charge transfer state.[66] The molecular design strategy of TADF polymers follows the same manner of the D-A design.[67,68] The RISC process could be improved by controlling the interaction between the degree of electron cloud overlap and both HOMO and LUMO

orbitals to decrease the ΔE_{ST}.[69] The polymers of TADF materials must have a rigid structure to minimize the recombination of the molecules' energy. Thus, overcoming the non-radiative transition and raising the possibility of radiation decay.[70]

Two major limitations of the simple D-A-based molecular design come from i) the broad light emission spectrum, which is mainly due to the emission from the charge transfer emissive state. ii) the short lifetime arising from the instability of the chemical structure. Furthermore, the poor device lifetime is associated with the instability of the molecular structure. The broad spectrum is reflected in the low purity of the colour of TADF-OLED devices. Taking these points into consideration, attempts have been made to follow the donor-acceptor design while trying to overcome these obstacles.[71] Features of TADF devices, such as lifetime, external quantum efficiency, efficiency roll-off and colour purity, are generally based on the above-mentioned factors. In the case of colour purity, the responsible factor is the full width at half maximum (FWHM). PLQY is the dominant parameter for EQE. While the efficiency roll-off is determined by the delayed fluorescence's lifetime, the devices' lifetime is associated with material stability. Figure 1.8 illustrates the TADF materials structure method, the device output and required parameters.

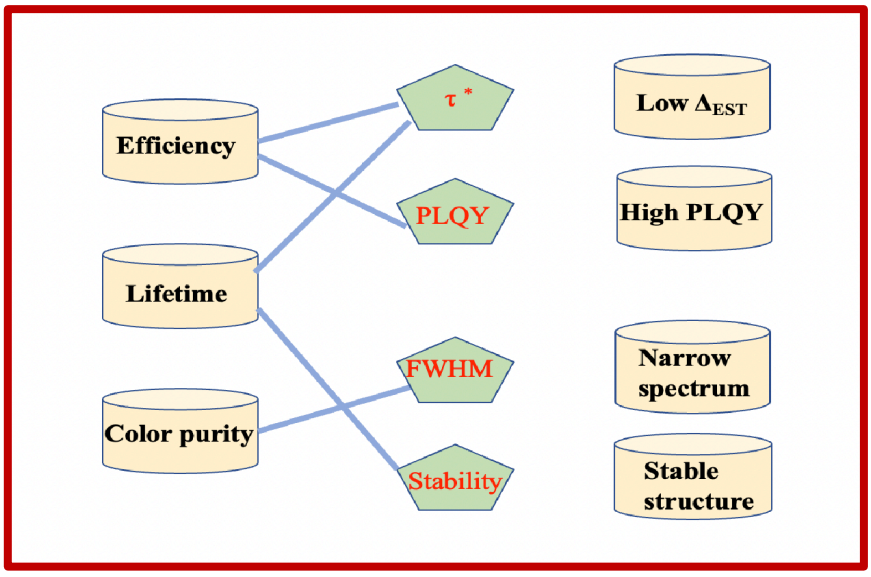

Figure 1. 8 The TADF materials structure method, the device output and required parameters.[62]

1.4.3.2 Short life DF Molecular Design

TADF Emitters in the light emission process have both fluorescence (F) and delayed fluorescence (DF), where the timescales are different from each other. While the fast electron decay of fluorescence has no true effect on the loss process of non-radiative decay, the slow rate decay of DF that characterises the process includes reducing non-radiative mechanisms, such as triplet-triplet annihilation and triplet polaron annihilation. This is because electrons in the triplet-excited state are sustained for a longer duration (microsecond) before moving back to the singlet-excited state. Based on this, it is extremely important to construct emitters that can limit τ with respect to DF. The common strategy of molecular design for delayed fluorescence should include lowering the energy difference between S_1 and T_1, so k_{RISC} increases, leading to achieving the required τ of delayed fluorescence.[72] Moreover, it is worth mentioning that some factors are considered quite important in managing the ΔE_{ST} of TADF molecules. These parameters involve the donor and acceptor distortion from linkers and increase the material's donor and acceptor strength. Carefully managing these two approaches proved to enhance the yield and performance significantly when applied for small ΔE_{ST} and short τ.[62,72,73]

1.4.3.3 Electron Donors and Electron Acceptors in TADF Molecular Design

The electroluminescence donor and acceptor mechanism in organic materials is essentially linked to an intramolecular charge transfer ICT in the excited state.[74] The involved ΔE_{ST} in TADF emitters should be minimized and the best way to do that is to use very strong electron acceptor and electron donor units. The charge transfer (CT) character of the excited state in these emitters will be elevated, which will increase the stability of singlet-excited energy. Different strong acceptors have been used, such as CN heteroaromatics, while phenothiazine, phenazine and acridan are the most usable as strong donors.[62] Furthermore, improving the CT character will support lowering ΔE_{ST} and limit τ. The design in which the distorted backbone aligns between the donor and acceptor units also determines the materials' characteristics. As the steric hindrance of both acceptor and donor elevates the dihedral angle in TADF polymers, efficiency could be enhanced by linking the donor and acceptor through an ortho-positioned phenyl linker.[62,75,76] Thus, it is extremely important to study the molecular design of TADF molecules carefully.

Many functional groups have been reported and used as the electron donor and the electron acceptor units. These units should be connected to each other in such a way as to achieve the

maximum TADF effect. Currently, the electron acceptor in the D-A system of TADF polymers should mainly contain groups that show three essential features: firstly, a strong ability to withdraw electrons; secondly, have an easily modified structure, and finally, possess a high electron-conjugated system. Various molecules seem to have these properties; the most usable ones are derivatives of nitrogen heterocycles, cyanobenzenes, benzophenones and diphenylsulfones.[77] For electron donor units, TADF polymers usually include nitrogen-containing aromatic groups in the structure. Those are considered to be good electron donor units, and they have been used widely in the structure of TADF polymers due to their strong donating power, which requires excellent stability, very high triplet energy, and good carrier transport capacity. Examples of these units involve derivatives of phenoxazine, acridine, aniline and carbazole.[78]

1.4.3.4 Molecular Construction for TADF Stability

Lifetime is one of the most important characteristics of OLED devices. In practical applications, OLED devices with short lifetimes cannot be used. The TADF emitters should therefore be designed to withstand degradation during OLED operation. Thus, incorporating durability is an important part of the TADF structure. More research work is needed to address this problem. In terms of chemical structure, stable moieties are all used to boost TADF operational stability.[79] During the operation of TADF-based devices, the emitters are exposed to excitons, positive polarons and negative polarons. Thus, they must show high stability under charged states. Molecular stability can be measured under either positive or negative polarons by evaluating the bond dissociation energy (BDE). In a class of acceptor moieties, the values of BDE of diphenyltrizine and benzonitrile types are mostly large, whereas in diphenylsulfone oxide and diphenylphosphine acceptors, the BDE values are negligible.[62] In the donor moieties units, carbazole-based donors are associated with high levels of BDE, while acridan and aromatic amine-type donors tend to have reduced BDE values under negative polarons.

Taking these points into consideration, researchers have successfully produced TADF operational materials, including D-A moieties using different derivatives, such as carbazole, triazine and benzonitrile. [59] **4CzIPN**, which has a lifetime of 1380 h at 1000 cd/m^2, is proven to be one of the most stable green TADF emitting materials.[80] The good chemical stability of **4CzIPN** comes from its structure, which involves four carbazole donor moieties and two CN acceptor moieties. Furthermore, high doping densities of **4CzIPN** strongly trap the electron, which results in optimising the lifetime of the device. Longer lifetime in highly doped

concentration of **4CzIPN**-based devices is also due to electron mobility through this type of emitters.[81]

Merging a triazine acceptor with a derivative of carbazole donor is another method of molecular design that is used to increase the stability, and therefore, the devices' lifetime. **DDCzTrz** is a molecule of this class, which is a good representative for TADF blue emitter. The chemical structure stability of **DDCzTrz** is due to triphenyltrizine's planar structure and carbazole moieties. Although not all triplet excitons can be harvested in **DDCzTrz**-based devices, the achieved lifetime is about 52 h at 500 cd/m^2. However, more research work needs to be done to increase the triplet excitons that can be harvested. Additionally, there are other carbazole-triazine compounds reported as having long TADF blue emission life, such as **TrzBCz**, **pBFCzTrz, mBFCzTrz** and **oBFCzTrz**.[82]

It is worth noting that there are yet not enough reported data regarding TADF lifetime. That is attributed to two general reasons; firstly, many derivatives of acridan donors are not suitable for stabilising TADF emitter designs. Secondly, many acceptors are not chemically stable; examples of these are arylboron, benzophenone and diphenylsulfone. Figure 1.9 shows some examples of stable TADF materials.

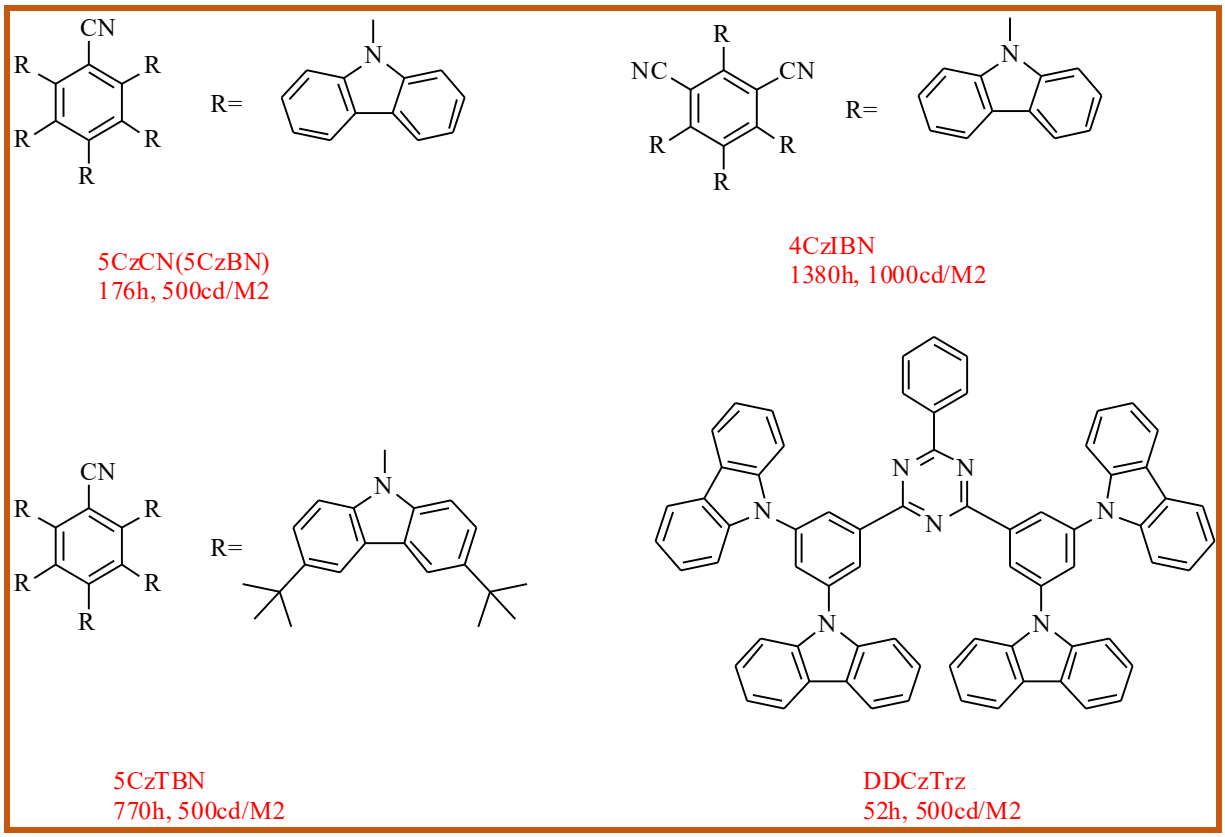

Figure 1. 9 Chemical structure, lifetime and initial luminesce of some stable TADF materials.[62]

1.5 TADF Hosts

1.5.1 Requirements and Mechanisms of TADF Host Molecules

As mentioned above, the emission of TADF materials typically involves the triplet-excited state. Unlike the singlet-excited state, the triplet-excited state has a longer lifetime, which could significantly lead to some drawbacks such as triplet-triplet annihilation, exciton migration and concentration quenching.[83] Thus, the resulting devices with these emitters usually exhibit poor performance, because of these triplet excited state issues. However, dispersing a suitable concentration of TADF emitters into an appropriate host can resolve the triplet excited state issues and so increase device efficiency. The commonly used host matrix for TADF-OLED often have their own unique features. The essential functions of the used hosts are the ability to generate excitons, transport carriers, and most importantly, to transfer the generated exciton energy to the TADF emitters. TADF hosts have the same mechanism of phosphorescence hosts, which mostly transport the injected electrons and holes from charge transporting layers to the emitters. Moreover, excitons are typically generated in the TADF host after the recombination

of holes and electrons. The host exciton energy is then transferred to the dopants *via* both Dexter energy transfer (DET) mechanism, and Förster energy transfer (FET) processes. As a result, the light emitted is generated by the dopant, with support from the host to overcome the exciton quenching and the intermolecular interaction.[84]

To dilute emitters into hosts, there are some requirements that hosts should have. 1) The host should have a balanced and high charge mobility to support the recombination of widely dispersed holes and electrons into emitting layer. 2) The ΔE_{ST} between the HOMO and LUMO must be small and in close arrangement with adjacent layers as to decrease the barrier of charge injection. 3) The triplet energy of the TADF host must be above 2.7 eV to avert the possibility of inverse energy transfer from the emitter to the host. 4) It is necessary to use a thermally and chemically stable host to increase the lifetime.[85] It is very important to look to the triplet energy level while making host materials, particularly when they are to be used for the blue emitters, which require hosts to have a triplet energy level of around 3eV. At present, different hosts have been reported and have been used for blue light emitters. Monopolar host materials that incorporate groups like phosphine oxide are known to have an appropriate triplet energy for blue emitters. DPEPO and PPT, which have high triplet energy, are examples of this type of host. However, the limited stability of monopolar hosts is still an issue.[86–89]

Many carbazole-based hosts have been reported, which were developed to improve the monopolar types. Some of these hosts, such as mCP, mCBP and CBP, are also used in the generation of phosphorescence.[85] Additionally, in order to have a balanced charge carrier mobility, bipolar carbazole-based hosts that incorporate acceptor units groups, such as phosphine oxide, triazine and cyano, into the structure have been developed.[90–93] These bipolar hosts cannot be used in pure blue emitters due to their low triplet energies (< 3 eV). Thus, they are mostly used in greenish-blue emitters.[94,95] Moreover, to avoid the issue of finding an appropriate host for each emitter, non-doped emitting materials may be used in layers that require sterically hindered molecules like dendrimers; however, they still have lower efficiencies than doped emitting layers.[96] Many TADF hosts have been developed that satisfy the required standards. Although the TADF-OLED devices' lifetime and external quantum efficiency have been improved over the years, the lifetime of blue OLED devices is not very long, and more research is needed to explore suitable chemical structures and design strategies. However, more emitters have been developed compared to the host materials; therefore, some procedures and guidelines could be useful to improve this field.

1.5.2 Categories of High Triplet Energy Hosts

The materials of higher triplet energy host can be divided into two classes, first a class of single host materials, and secondly mixed host materials. While the single hosts include bipolar transport host materials, electron transport type host (n-type), TADF hosts, hole transport type material (p-type), and pure-hydrocarbon materials, the mixed hosts materials involve electroplax hosts, exciplex-free type mixed hosts and incorporate exciplex hosts.[97] The n-type hosts dominate the nature of electron transport, and hole transport nature is controlled by p-type hosts. Bipolar host materials can move electrons and holes also relatively to the n-type and p-type. Thus, due to a wide recombination zone and a well-balanced charge density in the emitting layer, devices based on bipolar hosts are commonly better than those devices based on n-type and p-type hosts. Furthermore, TADF hosts can also be considered bipolar transporting because they contain electron and hole transport units.

Also, host materials can be categorized into three classes according to device function and its components; these are a single TADF host, an exciplex TADF host and an assistant host. The single host type consists of only one component that belongs to the intramolecular TADF class. Meanwhile, exciplex hosts, which are also known as intermolecular hosts, have both n-type and p-type components. An assistant host of TADF acts as an intermediary, transferring the triplet and singlet excitons energy to the emitter layers without losing energy.[98] TADF hosts are currently the most powerful hosts for long-lifetime and high-efficiency devices.

1.5.2.1 Bipolar Host for OLEDs

Currently, the most beneficial approach for developing bipolar host materials is to link the n-type group of acceptors with the p-type group of donors whether directly or via a π-connector. The donor units and acceptor units, which represent n-type and p-type, can respectively carry holes and electrons, which can enhance the injection and transporting properties. The emitting layer has hence balanced charge transport with a very wide electron/hole recombination zone.[99] Thus, bipolar hosts based on D-A and D–π–A molecular designs are optimised OLED devices. The common donor groups in this type of host include arylamine and carbazole, while the most used acceptor units include phosphine oxide, triazole, sulfone, triazine, cyano, diarylborane, imidazole, carboline and pyridine compounds. The best-known π-linker groups in this class include thiophene, spirofluorene, furfuran and aromatic rings. Bipolar hosts can be further classified based on their n-type units, which usually determine the performance and the efficiency of OLED devices.[80]

1.5.2.1.1 Bipolar Hosts According to n-Type Groups

The first class in this criterion include phosphine oxide (PO). The PO moiety is known to have high triplet energy and good solubility as needed to transport electrons in the emitting layer. It improves the electron injection feature by heightening the LUMO. The following features are important for constructing a PO-based host: i) the moiety of n-type (PO) links directly to p-type, ii) the PO acceptor is attached to the donor unit by a connector, iii) PO works as another acceptor to combine with other n-type groups, iv) PO should be inserted through p-types and should perform as non-conjugated π-linker.

Using a PO moiety as an n-type unit with different acceptor groups together with a non-conjugated connector maximises the triplet energy of the bipolar electron transport host. PO-based hosts are particularly considered to be the best among n-type hosts due to their tetrahedral geometry, which improves the triplet energy and increases the probability of electron transfer. Therefore, bipolar derivative hosts of PO proved to be effective in terms of harvesting triplet excitons of TADF emitters, resulting in OLEDs with high external quantum efficiency.[100] Although, bipolar hosts of PO have many advantages compared to others, some limitations are still present. These disadvantages involve serious chemical degradation, which is due to the week C-P single bond.[101] Therefore, low operation lifetime of OLEDs.

Many bipolar hosts are based on cyano groups. CN is known to be a good electron-withdrawing unit; when it is included in organic structures, it stimulates electron deficiency and improves the electron transportation property. Despite a small triplet energy degradation due to excessive conjugation, cyano-based hosts show very good chemical stability with large values of bond dissociation energy. In terms of molecular design, the most often used design is one that relies on modifying electron-rich carbazole structures by incorporating one cyano or two cyano units to minimise the electron density of the carbazole ring. Another strategy is to use a π-linker to connect the carbazole's electrons with other aromatic rings. Another approach that has been reported is to introduce a cyano unit into the different aromatic moieties to make bipolar transporting hosts.[102] Whether incorporated into the donor, linked through a π-linker or other aromatic units, CN-based bipolar transporting hosts demonstrated enhanced charge transport property and increased the devices' external quantum efficiency by improving the electron injection transport. Interestingly, due to CN unit and large bond dissociation energy values, the device lifetime of this class is better than lifetime of devices based on other types of hosts. The substitution numbers and positions of the cyano group significantly affect the device's lifetime

and other characteristics. Taking this into consideration, the substation around CN should be controlled carefully in order to have low driving voltage, large triplet energy, high external quantum efficiency and a device with a long lifetime.

Pyridine-electron bipolar hosts are another type of host, recognised for the moiety's electron transporting character, which is known to have a deep level of LUMO and strong electron affinity. This type of host is widely used in electron transport. The pyridine is introduced into the molecular design, together with p-type moieties to create a good bipolar host material. Carbazole is a common p-type moiety, which weakly combines with pyridine derivatives, resulting in a well- balanced carrier and high efficiency. Therefore, carbazole has served successfully as a donor moiety for n-type pyridine derivatives.[103] However, efficiency of OLED devices based on pyridine bipolar host is less than those based on PO and cyano. This type of host is not suitable for deep blue devices, due to degradation of the triplet energy by excessive conjugation of pyridine moiety.[104] The CN and PO moieties have a little impact on host E_T, unlike the pyridine moieties. Therefore, it is recommended that the design of pyridine-derived bipolar hosts be designed in such a way to reduce the number of conjugations that may arise. This may be achieved by modifying the main skeleton or linkage of the molecular structures.

Carboline bipolar hosts are also widely used to increase electron transporting properties. The design of this class relies on modifying the carbazole unit with a nitrogen atom. While this design enhances the electron transport character, it also maintains the carbazole triplet energy. Therefore, due to the high stability of carbazole moieties, carboline is useful for improving the stability of blue devices. Due to their high triplet energy (> 3.1eV), carboline and its derivatives have been used effectively to make blue hosts.[105] Like pyridine bipolar hosts, carboline and its derivatives are usually mixed with a carbazole moiety. In general, those carboline-based bipolar hosts have shown strong potential as hosts for deep blue devices.

Carbazole-based bipolar hosts are promising candidates for TADF-OLEDs and many derivatives of this class have been reported. Carbazole units have a good ability to build blocks due to their high E_T. CPB is an ideal example of carbazole-based bipolar host, where the carbazole unit is incorporated into benzene rings. A series of host materials using structures CPB has been developed and their performance compared. Many of the hosts synthesised involve heterocycles with various connections. Carbazole-based host materials often exhibit good chemical and thermal stability.[106] Carbazole-based bipolar hosts mostly consist of

carbazole units with other units such as CN acceptors, carbazole polyaromatic hosts and carbazole containing a silane core, etc. All those hosts share common features, including high triplet energy, good thermal stability and strong electron/hole transport properties.[88]

Apart from the bipolar hosts mentionned above, other electron transport moieties have been incorporated into hole-transport carbazole units. Derivatives of triazine, such as diphenyl-triazine, are commonly used as electron transport moieties, which are introduced in the molecular design of bipolar host molecules.[107] When mixed with a hole-transport carbazole, the diphenyl triazine moiety exhibits good charge transport properties due to its strong electron deficiency. However, it is difficult to reach a high triplet energy because of the planar structure which is generated when the electron transport moiety is linked to aromatic units. Furthermore, it is worth mentioning other common bipolar hosts include those based on benzimidazole, sulfone, boron and chromenopyrazole. All those hosts have been known to possess high triplet energy and they have been used in different light ranges for TADF-OLEDs.[108] Figure 1.10 illustrates some examples of bipolar host materials.

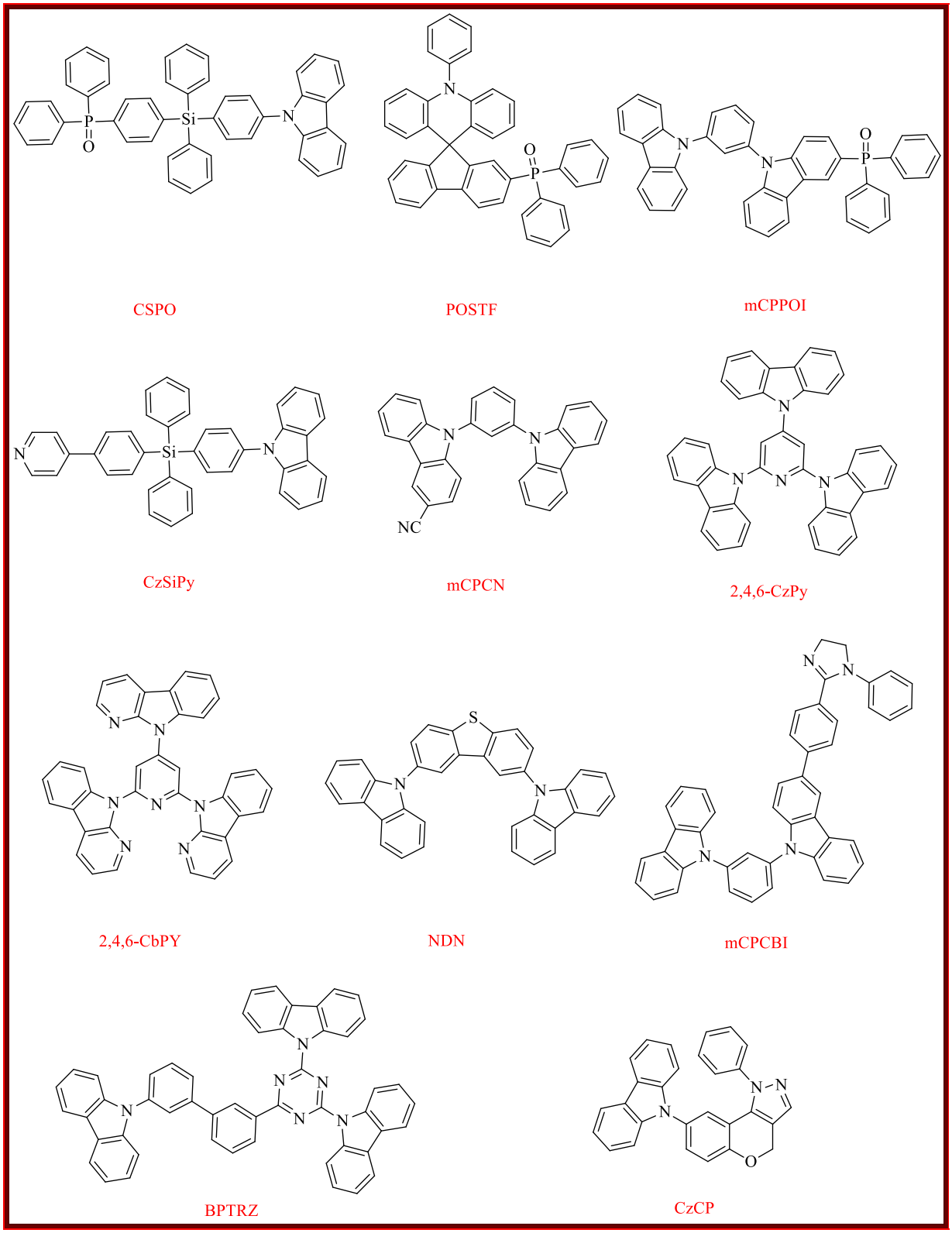

Figure 1. 10 The molecular structure of some common bipolar hosts.

1.5.2.2 Single TADF Host

TADF hosts are generally introduced to solve the efficiency issues of bipolar transport hosts. The triplet excitons for those bipolar-based hosts, such as PO and CN derivatives, are non-radiative like conventional fluorescence. TADF single hosts are capable of converting all non-radiative (NR) T_1 into radiative S_1, which is followed by Förster transfer of the energy to the fluorescent dopant. The device efficiency is therefore improved by harvesting all of the excitons of the fluorescent dopant. The ideal single host of TADF should fulfil the general requirements of the known host, as well as other requirements including small energy differences between the triplet-excited state and singlet-excited state, and should possess high k_{RISC} to facilitate the quick conversion process of T_1 to S_1 and minimise the probability of triple-triplet annihilation.[109] The twisted design of a D-A system leads to a small energy separation between HOMO and LUMO with high k_{RISC}.[7] The selection of acceptor and donor is extremely important as the acceptor with strong withdrawing nature and donor with a strong electron-donating nature result in strong intramolecular charge transfer, thus reducing both singlet and triplet energies. The acceptor moieties are mostly selected from phosphine oxide, pyrimidine, triazine, diphenyl sulfone, etc.; meanwhile, donor moieties are typically chosen from acridine, carbazole, carbazole derivatives, etc.

1.5.2.3 TADF Assistant Host

TADF emitters mostly experience concentrated triplet-triplet annihilation, which quenches the emission process because of the triplet excitons' long lifetime. Thus, TADF self-host may cause efficiency roll-off.[111] TADF assistant hosts have been devised to solve this issue; they are doped in with a higher triplet host. The system usually consists of three components: the emitter, the assistant host of TADF and another host with a wide energy gap. The emitter and TADF assistant host should have a lower E_T and E_S than those of wide energy gap host; they must also have a high k_{RISC} to enable their effective use as TADF materials. Additionally, the emitter should have a higher k_{RISC} and lower E_T and E_S than the TADF assistant host. The emitters can be fluorescent materials or TADF materials. To emit light, those emitters should show relatively high radiative decay. Because the quenching process is caused by the concentration and lifetime of triplet exciton, it is necessary to manage the concentration by controlling device engineering. Using these hosts is useful for low-efficiency roll-off and high device efficiency due to their ability to harvest singlet and triple excitons. Furthermore, devices based on TADF assistant hosts are proven to be thermally, morphologically and chemically

stable, which supports the device lifetime. Figure 1.11 explains and compares the mechanisms of TADF-self hosts and TADF assistant hosts.

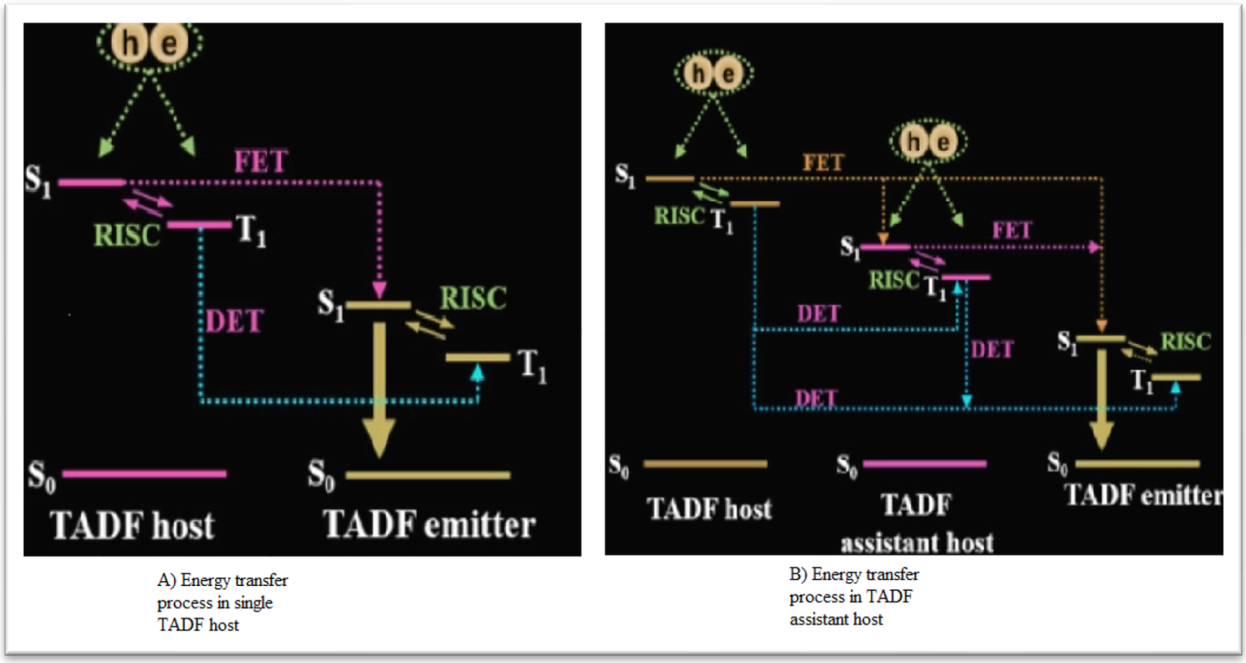

Figure 1. 11 The difference between a) single TADF energy transfer mechanism and b) TADF assistant host energy transfer mechanism.

1.6 Solution-Processable TADF Materials for OLEDs

1.6.1 Molecular Structure for Solution Processable TADF Materials

There are several requirements that TADF materials should fulfil to show good solution processability. Firstly, they need high solubility and good film forming ability; secondly, they need a very efficient TADF character, and thirdly, they need to be thermally stable as a solution-processable film.[112] They must also match the requirements of TADF materials, such as the rate of reverse intersystem crossing and other parameters, which were discussed previously. Because solution processable TADF small molecules mostly suffer from poor film-forming capability and weak solubility, the deposition of these materials as thin films is usually undertaken using the vacuum deposition strategy. Therefore, some modifications need to be introduced, such as inserting some known alkyl groups to facilitate film-forming properties. Strong thermal stability conditions are extremely important to avoid crystallisation during the operation of TADF-OLEDs. In addition, to enhance the film stability, it is very important to maximise the glass transition temperature (T_g). It can be increased by using rigid moieties such as carbazole and biphenyl, and by enlarging the molecular size.

In contrast to small molecules, dendrimers and polymers are good choices for solution processing due to their good solubility and amorphous properties.[113] The molecular design of ideal TADF polymers includes forming the main chain by polymerising TADF monomers or inserting the TADF units into a polymer side chain. The TADF polymer character is formed during the polymerisation process. In the case of TADF dendrimers, the molecular design often follows a core dendrons strategy, which is favourable to cancel the concentration quenching effect.[114] The dendrimer can be based on an acceptor molecule, such as benzophenone and triazine or TADF molecule. The acceptor molecule is mainly formed from electron-donating dendrons. An example is dendrons that use carbazole because of its perfect cross-linkage capabilities, strong thermal stability and its high hole-transport character.

1.6.2 TADF Small Molecules

For many years, advanced developments of TADF small molecules have been an excellent topic for research. Improving the solubility of many small molecules is important to enable their use as emitters in solution processable-based OLEDs. To create an excellent solution-processable small molecule for TADF, the TADF nature must be investigated. The full internal quantum yield cannot be achieved without considering the characteristics of TADF, which is important to harvest all triplet excitons. Common organic solvents are used to enable solution-based procedures. The morphological rigidity and most importantly to enhance the stability of solution-processed film in connection to charges and temperature in order to stabilise the device. Using TADF small molecules, which have balanced charge injection and transport, can facilitate the complex structure of TADF-OLEDs.[115] However, not many groups of TADF-small molecules satisfy these conditions. Compared with polymers, small molecules are not suitable for solution processing and are mostly used for thermal evaporation. Therefore, More research is needed to enhance the solution processability and film forming properties of small molecules for OLEDs.

1.6.3 TADF Polymers

Due to their good efficiency and high solution-processing fabrication capacity, TADF polymers and dendrimers have also been interesting topics of research. Emissive materials based on polymers are considered ideal for solution-processed OLEDs.[116] Unlike small molecules and dendritic molecules, synthesising TADF polymers is challenging. Some simple solution processing, such as ink-jet printing and spin coating, can be applied to reduce the cost

of production and increase efficiency. TADF polymers are proven to be more morphologically stable and highly solution processable. Thus, TADF polymers can support developments of low cost and highly efficient OLEDs by solution processing.[117,118] There are different molecular designs used to generate polymers with TADF properties, and many of those are based on a range of functional units. However, there are two main classes of TADF polymers. The first is named main chain TADF polymers, whose structure relies on alternate arrangement of acceptors and donors through their backbone, or on using conjugated linkages to graft the acceptors onto the donors. A side-chain type is another class of TADF polymer, in which the TADF building blocks are grafted into polymer backbone through non-conjugated linkages. The features and the performance of devices based on these classes of polymers are addressed in the following section.

1.6.3.1 Main-chain TADF Polymers

The design and synthesis of main-chain TADF polymers are typically based on donor and acceptor units. These polymers have shown a potential TADF character with a small ΔE_{STs}, and wide recombination zone, which can be optimised by controlling the number of acceptor and donor units. The donor unit in the chain is usually the TADF active part, which is connected to the polymer's backbone. Other parts of the TADF active units and the main chain have a significant impact upon each other. In the case of non-conjugated main-chain TADF polymers, Nikolaenko et.al. (2014) reported a new strategy named 'intermonomer TADF' to make TADF active unit indirectly by polymerizing accepter and donor monomers. .[119] They synthesised the main chain light-emitting polymers by combining triphenylamine (5%) as a donor unit, triphenyl triazine (50%) as the acceptor monomer and a high triplet non conjugated host (45%) as a spacer linked to the main chain as shown in figure 1.12. While triazine manages the location of the recombination zone and forms charge transfer units, the spacer ensures that the emitters are dispersed in the light-emitting polymer.[119] The fabrication of non-doped OLEDs was achieved by solution processing, in which TADF polymers worked as the emissive layer, and exhibited a small ΔE_{ST} value (0.22 eV) and an appropriate value of PLQY. In the case of conjugated main-chain TADF polymers, the acceptor units are linked alternately in the backbone of conjugated polymers. It is extremely difficult to synthesise this type of alternating D-A with TADF properties because this design strategy can cause large overlapping between acceptors and donor units, therefore losing TADF properties in these conjugated polymers. However, a few TADF were still developed according to this method such as pCzBP and pAcBP.[120c](Figure 1.13).

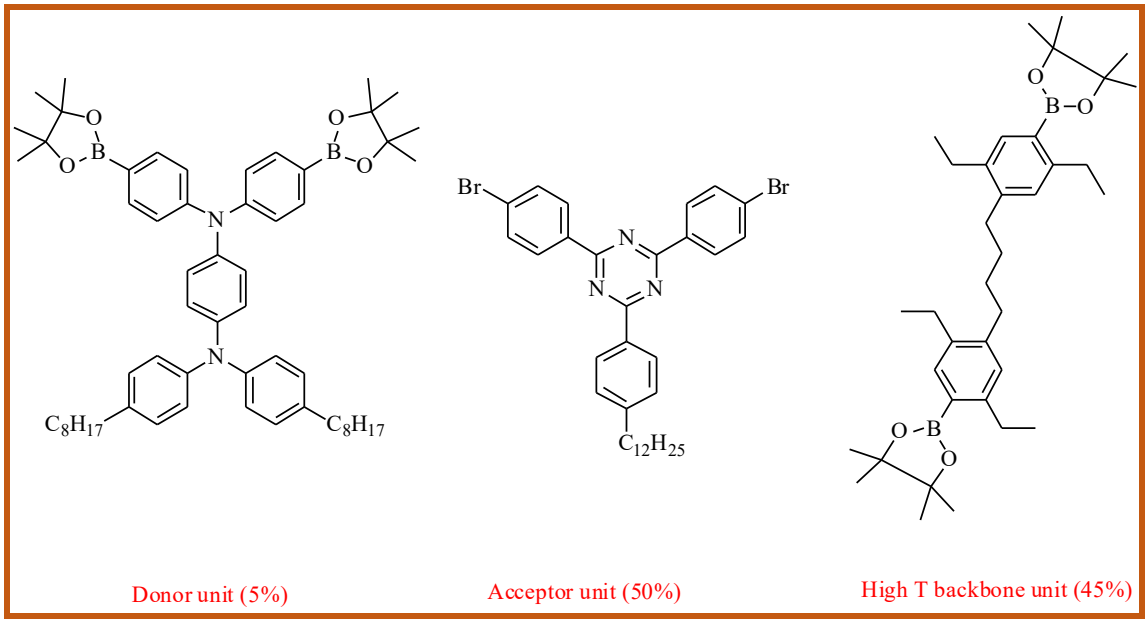

Figure 1. 12 Examples of TADF main chain ' intermonomer' structure'. [119]

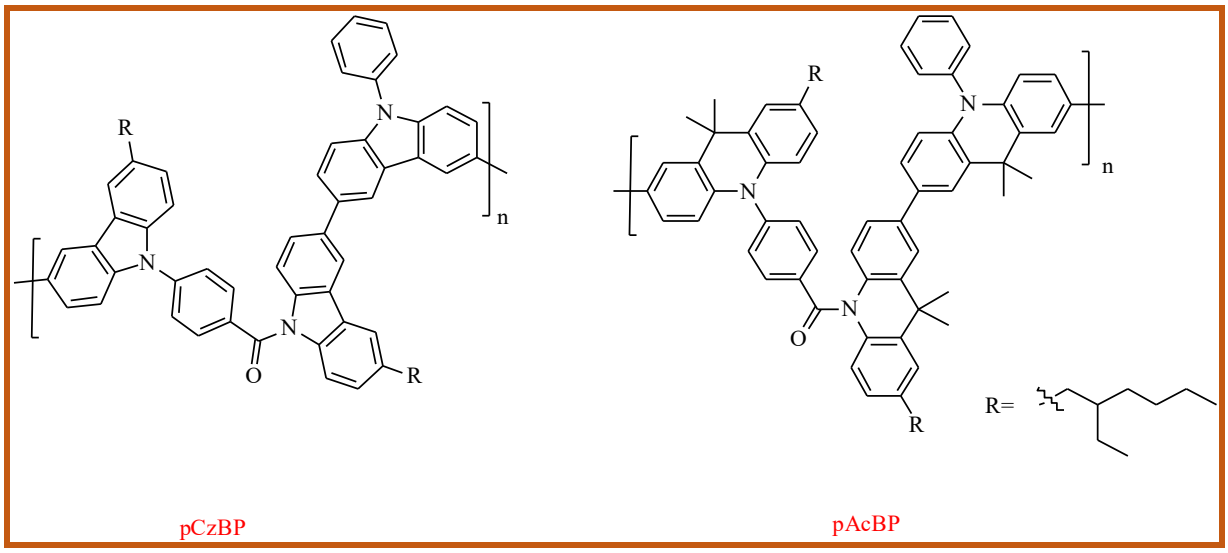

Figure 1. 13 structure of pCzBP and pAcBP [120]

1.6.3.2 Side-chain TADF Polymers

The side chain engineering strategy is the most useful strategy that has been utilised for TADF polymers.[121] These polymers mainly consist of side chain functionalised with TADF molecules grafted to the polymer backbone. The TADF properties, charge injection character and charge transport features, are all derived from the components of these polymers, whether that happens to be the backbone or side chain series. The major difference between this type of polymer and the main-chain type is that the chains that link the side chain and backbone are non-conjugated

in side-chain polymers. Therefore, the electronic properties of the backbone are not affected by the side chain. Unlike the main chain TADF type, it is not difficult to synthesise large conjugated structures of this type, and they offer large advantages in terms of processing the devices. In TADF polymers based on side chain structures, incorporation of the TADF-linked group into the polymer backbone is achieved through chemical bonding. Due to stable polymer backbone, these side chain polymers have been used successfully in high-efficiency blue OLEDs.[60] Emitters of TADF polymers could be achieved by grafting the TADF monomer onto the side chain of the polymer's backbone. Using TADF strategy is proven to increase the probability of excitation utilisation efficiency of the polymeric materials.[122-124]

Zhou et al. (2019) introduced a new engineering method to develop highly efficient solution processed TADF polymers. The idea of this strategy is to design and synthesise a series of TADF copolymers, where the character of TADF active unit is incorporated onto a side chain (Scheme 1.1). Additionally, the backbone of this polymer involves a conjugated unit (carbazole) and a non-conjugated unit (tetraphenylsilicon); therefore, the structure can achieve equilibrium.[125]

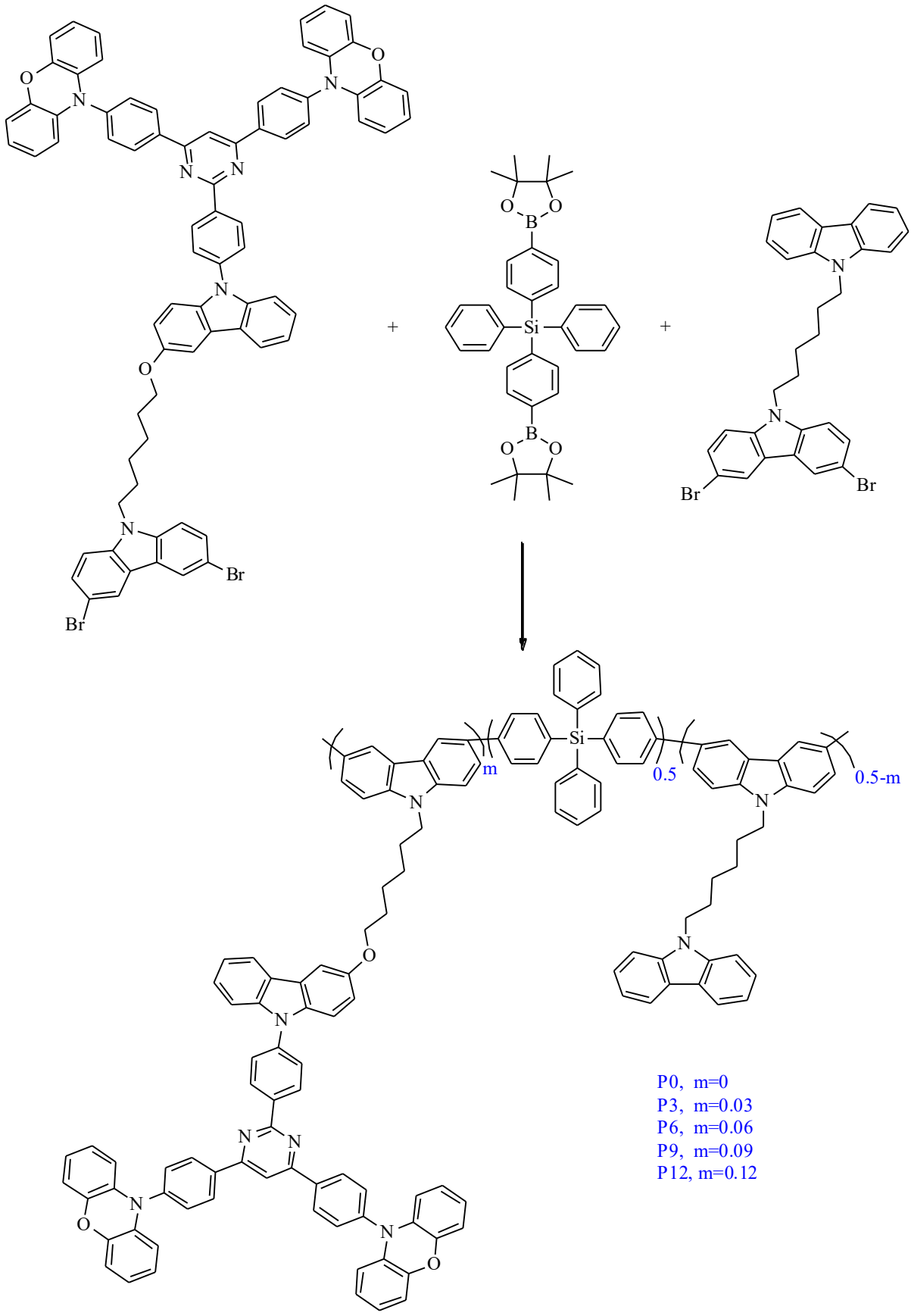

Scheme 1. 1 Synthesis route of TADF copolymer using various ratios of different monomers.[125]

1.6.4 Solution-processable TADF Dendrimers

Dendrimers can be considered to be a similar class to hyperbranched polymers with an excellent branched structure and precise molecular design.[126] Their structures usually contain a main core and a shell, which has repeated branched units and a central core. Macromolecules of dendritic TADF possess both the accurate molecular design similar to small molecules and the high molecular weight common to polymers. Therefore, the processing and photoelectric behaviours of materials can be improved by managing the molecular structure.[127] Although they have a large steric hindrance structure, they are amorphous and soluble. Furthermore, due to isolated chromophores at the core, they generally stop the concentration quenching process. The PLQY of condensed-state dendrimers is often high, which is attributed to their stable dendritic structures. Therefore, these TADF dendrimers are suitable for use in solution-processed OLED devices.

Several TADF dendrimer emitters have been reported so far. Their designs include integration of a TADF chromophore core with external branches, which determines the emission properties such as TADF character and colour. External branches include spatially separated HOMO distribution on the electron donor unit, as well as a spatially separated LUMO distribution on the electron acceptor unit. These branches work to increase the structure's solubility, transport the charge and improve the nature of the core TADF. There are two major classes of TADF dendrimers based on dendron- core connection; these are TADF dendrimers with conjugated linkages, and those with non-conjugated linkages as described in Figure 1.14.

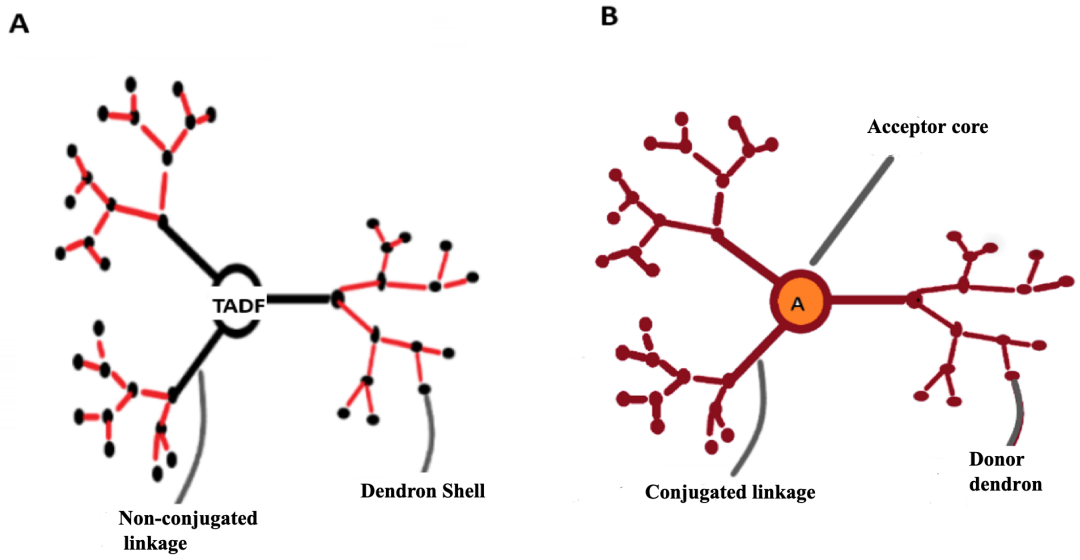

Figure 1. 14 A) Non-conjugated linkage of TADF dendrimers; B) Conjugated linkage of TADF dendrimers

1.6 Procedures for Synthesising TADF Polymers

1.6.1 Suzuki Cross-Coupling

In recent decades, many polymers have been synthesized using the Suzuki-Miyaura cross-coupling method. In this class of couplings, the sp2 hybridised orbitals of C atoms are used for generating C-C bonds.[128] Suzuki cross-coupling can be achieved with a high range of functional groups. The reaction is mostly carried out by using a base and a palladium catalyst. The C-C bond forming process takes place between aryl or vinyl boronic ester with aryl or vinyl halides; it can also occur between other boronic acid derivatives and aryl halides (Scheme 1.2). Moreover, the reaction usually requires mild conditions and various commercially available reagents. Most compounds used in this type of polymerisation, such as organoboron, are thermally stable, nontoxic and unreactive to oxygen and water. These features make the reaction suitable for large-scale use in manufacturing. The Suzuki coupling between aryl boronic esters and aryl halides is an extremely useful approach to prepare polyarylenes.[129] This strategy of coupling provides many advantages such as simplicity, low sensitivity to moisture and workable with monomers that possess functional groups. This coupling technique is adjustable; it enables the creation of alternative copolymers and can also tolerate many functional groups.

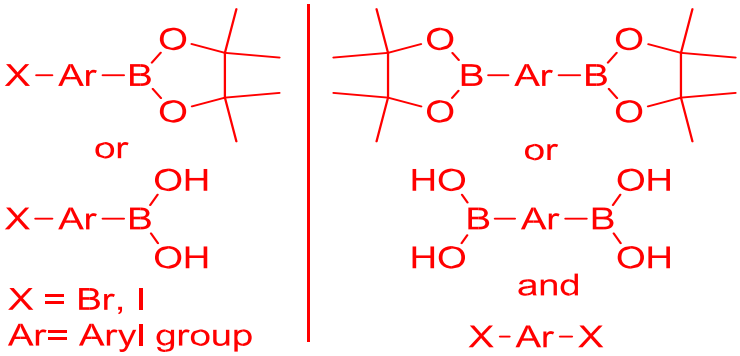

Scheme 1. 2 Monomers for Suzuki cross Coupling

The catalytic cycle for this type of reaction is illustrated in Scheme 1.3. The reaction cycle contains four steps. It begins with an oxidative reaction between the aryl halide and the palladium (0) centre to form a palladium (II) complex. The next step is the reaction with a base, which is generated from a hydroxide group producing an aryl Pd (II) complex; consequently, the ligand exchange takes place between the hydroxyl group and the halide. Therefore, the

electrophilic behaviour of the palladium complex is increased. Then the boron(ate) complex is generated from the coordination between the hydroxyl anion of the base with the boron atom in bis-bronic monomers. As a result, the boronated complex with the Ar-B bond becomes nucleophilically stronger. The transmetallation occurs next, where the Ar-B bond is cleaved and two palladium (II) complex ligands receive the organic group. In the final step, dimers of this complex are produced through a reductive elimination step.[130] The cycle can be repeated because the dimer still contains active end groups; therefore, a polymer forms by coupling with other dimers or monomers.

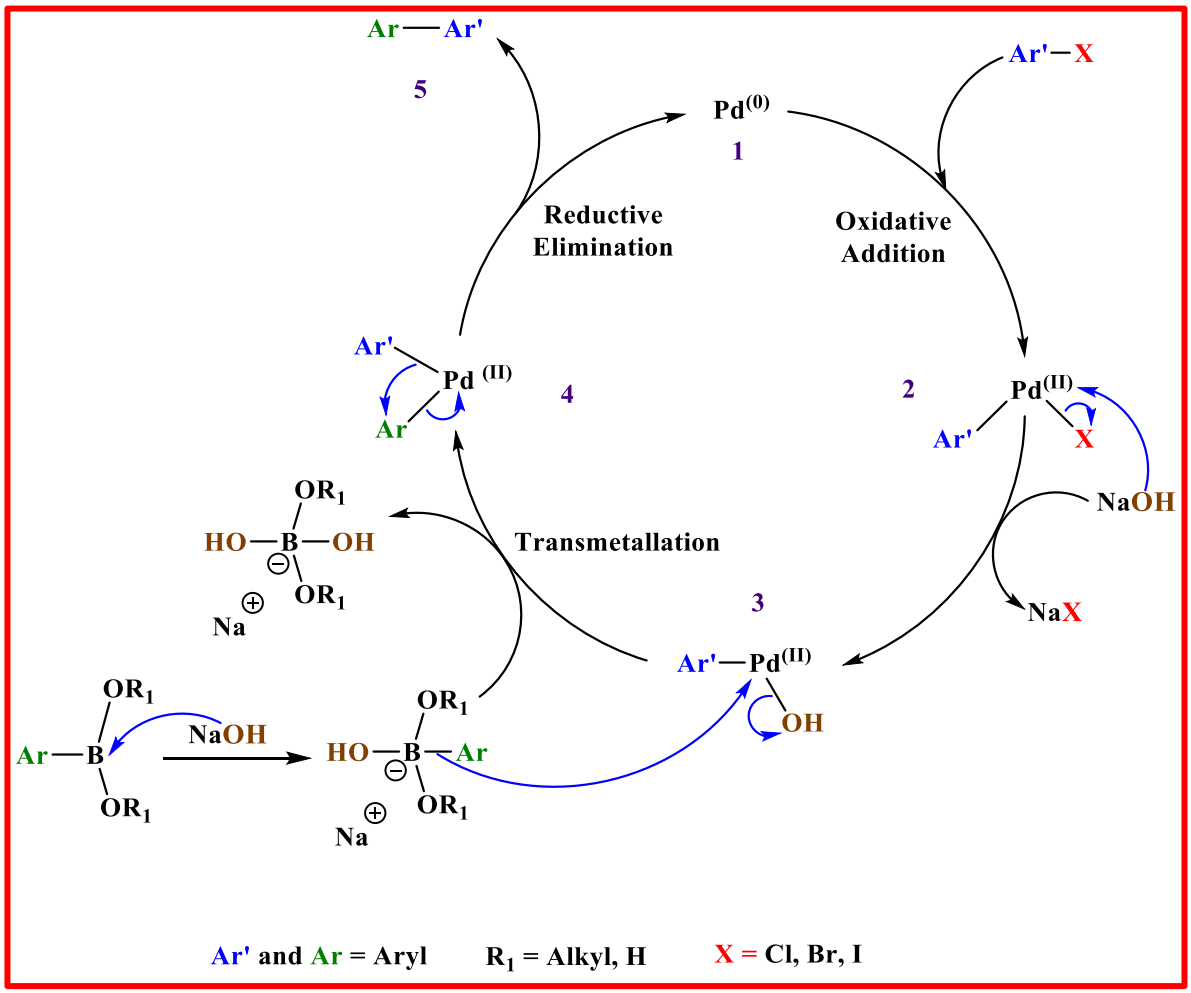

Scheme 1. 3 Suzuki Cross coupling Cycle

1.6.2 Sonogashira Coupling Reaction

The Sonogashira coupling reaction is a good C-C coupling reaction, where alkynes are one of the starting materials along with aryl halides. It is widely used because of its simplicity, versatility and value. The general reaction conditions in this class of coupling are shown in

Scheme 1.4.[131] The coupling between a terminal alkyne and a halide takes place *via* sp^2-sp palladium catalyst in the presence of a copper co-catalyst.

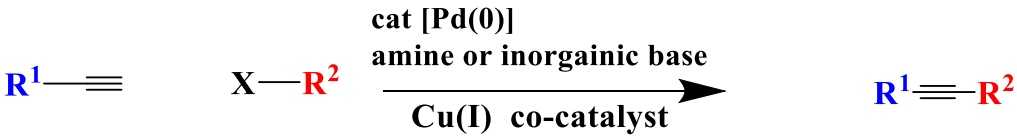

R^1= aryl, hetaryl, alkyl, SiR_3
R^2= aryl, hetaryl, Vinyl
X= Br, Cl, OTf

Scheme 1. 4 Sonogashira coupling conditions

However, the mechanism involving both palladium and copper catalysts in Sonogashira reaction is not fully understood. The common suggested catalytic cycle of the Sonogashira coupling reaction is shown in Scheme 1.5.[131–133] The proposed cycle involves the elementary steps that occur in transition metal-based coupling reactions containing reductive elimination, trans-metalation and oxidative addition. Furthermore, the catalytic process takes place through two different cycles, the palladium (cycle A), followed by copper (cycle B). In cycle A, the catalysis starts when [Pd(0)L_2] active species are formed from Pd(II). The reduction process is elevated by amines through sigma complexation, dehydropalladation and reductive elimination. The next step in this mechanism is the oxidative addition, which includes decreasing ligated Pd(0) by the addition of vinyl halide or aryl, resulting in increasing the oxidation number to +2. This is believed to be the reaction rate-limiting step.[134] Transmetallation is a step in which both catalytic cycles (Pd) and (Cu) are attached to each other. It is a necessary to create π-alkyne-copper complex to improve the terminal H acidity, which supports amines in deprotonating the alkyne then generates the anionic nucleophile that finally creates the Cu acetylide. Consequently, transmetallation occurs where alkyne is moved from the copper centre to the palladium centre. The transmetallation is then followed by cis-trans isomerisation, which finally goes through reductive elimination to give the desired product. The last step is the reductive elimination, which is the opposite of the oxidative addition process. Two bonds of metal ligands are terminated, and a new ligand-ligand bond is formed. The oxidation number of the palladium centre is reduced to 0 at the end of the reductive elimination, completing the catalytic cycle.

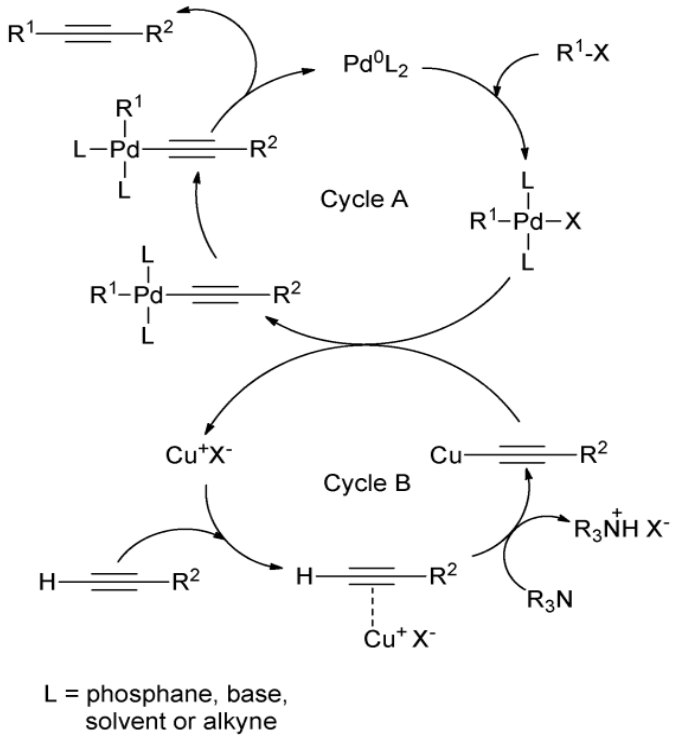

Scheme 1. 5 Catalytic Cycle of Sonogashira C-C coupling reaction

1.7 Features of Carbazole and Fluorene as OLED Materials

1.7.1 Carbazole

OLED materials based on carbazole derivatives have been used widely due to the unique features of carbazole structure, [135] such as processing and optoelectronic properties (Figure 1.15). Generally, there are two types of polycarbazoles. The classification is based on conductivity and linkage-position. The linkage through 3,6 positions facilitates a meta linked phenylene backbone. Thus, polymers of this type (linked through 3,6-positions) exhibit great advantages, including transparency and an electro-chemically stable oxidation process, but they display lower charge carrier mobilities. These type of carbazole polymers provide a remarkable advantage for OLED applications[136,137] and TADF devices. [138] In the case of poly (2,7-linked carbazole)s, the structure boosts both the degree of conjugation and the length of the conjugation segment. Therefore, these materials based on the 2,7-linkage positions of carbazole are considered to be serious candidates for applications requiring lower optical and lower electrochemical band gaps.[139]

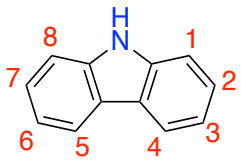

Figure 1. 15 chemical structure of carbazole

1.7.2 Fluorene

Fluorene and its derivatives have been proven to be good materials for use in OLEDs. As an example, poly(9,9'-dialkyl fluorene)s offers numerous advantages, such as stability under heat, straightforward synthesis and the ability to emit blue light in solid and solution states. Fluorene also shows high electron and hole mobilities properties in bulk materials. Polymers of fluorene belong to the rigid class of polymers that possess a rigid backbone structure as well as flexible sidechains. The rigidity of the backbone and flexibility of side chains is determined by functional groups at the carbon-9 position, resulting from the considerable acidity of CH at this position. However, following deprotonation in basic media, fluorene can be easily functionalised by a range of electrophiles.[140] General structure of polyfluorene as shown in figure 1.16.

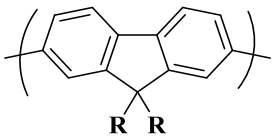

Figure 1. 16 General structure of polyfluorenes

1.8 Project Aim

Modern lifestyles have changed rapidly with the development of artificial lighting and the world is moving towards more eco-friendly products. Unlike fluorescent tubes, manufacturing OLED devices involves using fewer environmentally harmful substances, while producing highly efficient lighting panels. Many companies, such as LG, SONY, Philips, and Konica, have incorporated this technology into lighting panel products. OLED applications include computer monitors, TV screens, mobile phones and other devices.[140] As well as being environmentally friendly, OLEDs also offer advantages including flexibility, rollability and transparency. The high-quality outcome of OLEDs is eminent due to the predecessors, showing broader viewing angles, higher refresh rates and more contrast ratio. In terms of energy consumption, OLEDs use less energy than thin-liquid crystals, as they are only consumed by active pixels.

Considering all these features, OLEDs can re-innovate the fabrication of flat panels and smart device displays. To achieve high-quality displays, all possible methods of device manufacturing should be explored. Furthermore, it is important to research the possible mechanisms used to harvest the triplet excitons and convert them to singlet excitons to overcome the IQE barrier that has been determined by spin statistics. Three different generations of OLEDs have been introduced since their invention in 1987.[141] The first generation of OLEDs used fluorescent materials, while the second generation was based on phosphorescent materials. OLEDs based on TADF are the current generation. This third type of device use TADF properties which enable the use of triplet states generated in OLED devices *via* thermal energy through conversion to singlet states through the reverse intersystem crossing. This reverse intersystem crossing facilitates maximum values of internal quantum efficiency.

The aim of this project is to develop solution-processable materials for OLED applications. Efficient host polymers are targeted in this work in order to incorporate them in OLED emissive layers. Two major procedures are to be used to synthesise the required solution processible polymers, which are Sonogashira polymerisation and Suzuki polymerisation. This study focuses on the design and preparation of the main host polymers using the commonly known SiCz host molecule which is used extensively as a host material in OLED devices manufactured using *vacuum* deposition techniques. The prepared host polymers using SiCz units are to be explored for use to manufacture OLEDs through solution processing methods in order to reduce

the costs of the resulting OLEDs. The Suzuki polycondensation procedure is to be used to synthesise the copolymers. Furthermore, the TADF emitter, phenoxazine-2,4,6-triphenyl-1,3,5-triazine (PXZ-TRZ), is to be incorporated into the polymer side chains, resulting in a single polymer system with a TADF character. Thus, the polymer backbone works as a host and charge-transporting channel, while the side chains do not affect the electronic characteristics of the polymer backbone but facilitate different functionalities. Because of the features of polycarbazole and polyfluorene materials, such as their good hole-electron transporting properties and high triplet energy, they are to be used to make the polymer backbone in this study. However, polymers containing SiCz on the main chain must be free of conjugation along polymer chains, so the final polymers still have high-energy triplet states. To decrease conjugation of the polymers, the Sonogachira method is to be used to make copolymers containing 1,7-octadiyne. SiCz containing carbazole in its structure is to be used in the main chain of the polymers due to its good hole mobility, high triplet energy, and thermal and chemical stability. Introducing TADF units into the side chain of polymers is expected to enhance the lighting properties of the resulting materials.

1.9 References

(1) Horowitz, G.; Fichou, D.; Peng, X.; Xu, Z.; Garnier, F. A Field-Effect Transistor Based on Conjugated Alpha-Sexithienyl. *Solid State Communications* **1989**, *72* (4), 381–384.

(2) Koden, M. History of OLEDs. **2017**.

(3) Kunić, S.; Šego, Z. OLED Technology and Displays. In *Proceedings ELMAR-2012*; IEEE, 2012; pp 31–35.

(4) van der Holst, J. J. M.; van Oost, F. W. A.; Coehoorn, R.; Bobbert, P. A. Electron-Hole Recombination in Disordered Organic Semiconductors: Validity of the Langevin Formula. *Phys. Rev. B* **2009**, *80* (23), 235202. https://doi.org/10.1103/PhysRevB.80.235202.

(5) Moral, M.; Muccioli, L.; Son, W.-J.; Olivier, Y.; Sancho-Garcia, J.-C. Theoretical Rationalization of the Singlet–Triplet Gap in OLEDs Materials: Impact of Charge-Transfer Character. *Journal of Chemical Theory and Computation* **2015**, *11* (1), 168–177.

(6) Kappaun, S.; Slugovc, C.; List, E. J. W. Phosphorescent Organic Light-Emitting Devices: Working Principle and Iridium Based Emitter Materials. *International Journal of Molecular Sciences* **2008**, *9* (8), 1527–1547. https://doi.org/10.3390/ijms9081527.

(7) Uoyama, H.; Goushi, K.; Shizu, K.; Nomura, H.; Adachi, C. Highly Efficient Organic Light-Emitting Diodes from Delayed Fluorescence. *Nature* **2012**, *492* (7428), 234–238.

(8) Chen, X.-K.; Kim, D.; Brédas, J.-L. Thermally Activated Delayed Fluorescence (TADF) Path toward Efficient Electroluminescence in Purely Organic Materials: Molecular Level Insight. *Accounts of Chemical Research* **2018**, *51* (9), 2215–2224.

(9) Lyskov, I.; Marian, C. M. Climbing up the Ladder: Intermediate Triplet States Promote the Reverse Intersystem Crossing in the Efficient TADF Emitter ACRSA. *The Journal of Physical Chemistry C* **2017**, *121* (39), 21145–21153.

(10) Camara, C. G.; Escobar, J. V; Hird, J. R.; Putterman, S. J. Correlation between Nanosecond X-Ray Flashes and Stick–Slip Friction in Peeling Tape. *Nature* **2008**, *455* (7216), 1089–1092.

(11) Wei, X. Y.; Wang, X.; Kuang, S. Y.; Su, L.; Li, H. Y.; Wang, Y.; Pan, C.; Wang, Z. L.; Zhu, G. Dynamic Triboelectrification-induced Electroluminescence and Its Use in Visualized Sensing. *Advanced Materials* **2016**, *28* (31), 6656–6664.

(12) Ducrot, E.; Chen, Y.; Bulters, M.; Sijbesma, R. P.; Creton, C. Toughening Elastomers with Sacrificial Bonds and Watching Them Break. *Science* **2014**, *344* (6180), 186–189.

(13) Yersin, H. *Highly Efficient OLEDs: Materials Based on Thermally Activated Delayed Fluorescence*; John Wiley & Sons, 2019.

(14) Cinquino, M.; Prontera, C. T.; Pugliese, M.; Giannuzzi, R.; Taurino, D.; Gigli, G.; Maiorano, V. Light-Emitting Textiles: Device Architectures, Working Principles, and Applications. *Micromachines* **2021**, *12* (6), 652.

(15) Giovanella, U.; Pasini, M.; Botta, C. Organic Light-Emitting Diodes (OLEDs): Working Principles and Device Technology. In *Applied Photochemistry*; Springer, 2016; pp 145–196.

(16) Han, T.-H.; Song, W.; Lee, T.-W. Elucidating the Crucial Role of Hole Injection Layer in Degradation of Organic Light-Emitting Diodes. *ACS Applied Materials & Interfaces* **2015**, *7* (5), 3117–3125.

(17) Zhou, X.; Pfeiffer, M.; Blochwitz, J.; Werner, A.; Nollau, A.; Fritz, T.; Leo, K. Very-Low-Operating-Voltage Organic Light-Emitting Diodes Using AP-Doped Amorphous Hole Injection Layer. *Applied Physics Letters* **2001**, *78* (4), 410–412.

(18) Kröger, M.; Hamwi, S.; Meyer, J.; Riedl, T.; Kowalsky, W.; Kahn, A. Role of the Deep-Lying Electronic States of MoO_3 in the Enhancement of Hole-Injection in Organic Thin Films. *Applied Physics Letters* **2009**, *95* (12), 251.

(19) Zhou, X.; Pfeiffer, M.; Blochwitz, J.; Werner, A.; Nollau, A.; Fritz, T.; Leo, K. Very-Low-Operating-Voltage Organic Light-Emitting Diodes Using AP-Doped Amorphous Hole Injection Layer. *Applied Physics Letters* **2001**, *78* (4), 410–412.

(20) Vasilopoulou, M.; Papadimitropoulos, G.; Palilis, L. C.; Georgiadou, D. G.; Argitis, P.; Kennou, S.; Kostis, I.; Vourdas, N.; Stathopoulos, N. A.; Davazoglou, D. High Performance Organic Light Emitting Diodes Using Substoichiometric Tungsten Oxide as Efficient Hole Injection Layer. *Organic Electronics* **2012**, *13* (5), 796–806.

(21) Lee, J.-H.; Leem, D.-S.; Kim, J.-J. High Performance Top-Emitting Organic Light-Emitting Diodes with Copper Iodide-Doped Hole Injection Layer. *Organic Electronics* **2008**, *9* (5), 805–808.

(22) Kim, J.; Kim, M.; Won Kim, J.; Yi, Y.; Kang, H. Organic Light Emitting Diodes Using NaCl: N, N′-Bis (Naphthalene-1-Yl)-N, N′-Bis (Phenyl) Benzidine Composite as a Hole Injection Buffer Layer. *Journal of Applied Physics* **2010**, *108* (10), 103703.

(23) Strukelj, M.; Papadimitrakopoulos, F.; Miller, T. M.; Rothberg, L. J. Design and Application of Electron-Transporting Organic Materials. *Science* **1995**, *267* (5206), 1969–1972.

(24) Minaev, B.; Baryshnikov, G.; Agren, H. Principles of Phosphorescent Organic Light Emitting Devices. *Physical Chemistry Chemical Physics* **2014**, *16* (5), 1719–1758.

(25) Akcelrud, L. Electroluminescent Polymers. *Prog. Polym. Sci.* **2003**, *28* (6), 875–962

(26) Huang, Y.; Hsiang, E.-L.; Deng, M.-Y.; Wu, S.-T. Mini-LED, Micro-LED and OLED Displays: Present Status and Future Perspectives. *Light: Science & Applications* **2020**, *9* (1), 1–16.

(27) Zhang, D.; Huang, T.; Duan, L. Emerging Self-emissive Technologies for Flexible Displays. *Advanced Materials* **2020**, *32* (15), 1902391.

(28) Zhang, C.; Ji, C.; Park, Y.; Guo, L. J. Thin-Metal-Film-Based Transparent Conductors: Material Preparation, Optical Design, and Device Applications. *Adv. Opt. Mater.* **2021**, *9* (3), 2001298.

(29) Kreger, K.; Bäte, M.; Neuber, C.; Schmidt, H.; Strohriegl, P. Combinatorial Development of Blue OLEDs Based on Star Shaped Molecules. *Advanced Functional Materials* **2007**, *17* (17), 3456–3461.

(30) Karzazi, Y. Organic Light Emitting Diodes: Devices and Applications. *J. Mater. Environ. Sci* **2014**, *5* (1), 1–12.

(31) Perepichka, I. F.; Perepichka, D. F.; Meng, H.; Wudl, F. Light-emitting Polythiophenes. *Advanced Materials* **2005**, *17* (19), 2281–2305.

(32) Antoniadis, H. Overview of OLED Display Technology. *Cell* **2003**, *408*, 314–6460.

(33) Felton, M. J. Thinner, Lighter, Better, Brighter Organic Light-Emitting Diodes May Make Cathode Ray Tubes and Liquid Crystal Displays Obsolete. *TODAYS CHEMIST AT WORK* **2001**, *10* (11), 30–35.

(34) Zhao, Y.; Zhu, L.; Chen, J.; Ma, D. Improving Color Stability of Blue/Orange Complementary White OLEDs by Using Single-Host Double-Emissive Layer Structure: Comprehensive Experimental Investigation into the Device Working Mechanism. *Organic Electronics* **2012**, *13* (8), 1340–1348.

(35) Baldo, M. A.; O'brien, D. F.; Thompson, M. E.; Forrest, S. R. Excitonic Singlet-Triplet Ratio in a Semiconducting Organic Thin Film. *Physical Review B* **1999**, *60* (20), 14422.

(36) Adachi, C.; Baldo, M. A.; Thompson, M. E.; Forrest, S. R. Nearly 100% Internal Phosphorescence Efficiency in an Organic Light-Emitting Device. *Journal of Applied Physics* **2001**, *90* (10), 5048–5051.

(37) Kwong, C. Y.; Djurišić, A. B.; Choy, W. C. H.; Li, D.; Xie, M. H.; Chan, W. K.; Cheah, K. W.; Lai, P. T.; Chui, P. C. Efficiency and Stability of Different Tris (8-Hydroxyquinoline) Aluminium (Alq3) Derivatives in OLED Applications. *Materials Science and Engineering: B* **2005**, *116* (1), 75–81.

(38) Valeur, B.; Berberan-Santos, M. N. A Brief History of Fluorescence and Phosphorescence before the Emergence of Quantum Theory. *Journal of Chemical Education* **2011**, *88* (6), 731–738.

(39) Yersin, H.; Rausch, A. F.; Czerwieniec, R. Organometallic Emitters for OLEDs: Triplet Harvesting, Singlet Harvesting, Case Structures, and Trends. *Physics of Organic Semiconductors* **2012**, 371–424.

(40) Murawski, C.; Leo, K.; Gather, M. C. Efficiency Roll-off in Organic Light-emitting Diodes. *Advanced Materials* **2013**, *25* (47), 6801–6827.

(41) Zhang, Y.; Aslan, K.; Previte, M. J. R.; Geddes, C. D. Metal-Enhanced e-Type Fluorescence. *Applied Physics Letters* **2008**, *92* (1), 13905.

(42) Lamansky, S.; Kwong, R. C.; Nugent, M.; Djurovich, P. I.; Thompson, M. E. Molecularly Doped Polymer Light Emitting Diodes Utilizing Phosphorescent Pt (II) and Ir (III) Dopants. *Organic Electronics* **2001**, *2* (1), 53–62.

(43) Adachi, C. Third-Generation Organic Electroluminescence Materials. *Japanese Journal of Applied Physics* **2014**, *53* (6), 60101.

(44) Yersin, H.; Czerwieniec, R.; Hupfer, A. Singlet Harvesting with Brightly Emitting Cu (I) and Metal-Free Organic Compounds. In *Organic Photonics V*; International Society for Optics and Photonics, 2012; Vol. 8435, p 843508.

(45) Volz, D.; Cheng, Y.; Liu, R.; Wallesch, M.; Zink, D.; Göttlicher, J.; Steininger, R.; Flügge, H.; Fléchon, C.; Navarro, J. High-Efficiency OLEDs with Fully-Bridged PyrPHOS-Complexes Using Singlet Harvesting. *Adv. Mater* **2015**, *27*, 2538–2543.

(46) Tao, Y.; Yang, C.; Qin, J. Organic Host Materials for Phosphorescent Organic Light-Emitting Diodes. *Chemical Society Reviews* **2011**, *40* (5), 2943–2970.

(47) Volz, D. Review of Organic Light-Emitting Diodes with Thermally Activated Delayed Fluorescence Emitters for Energy-Efficient Sustainable Light Sources and Displays. *Journal of Photonics for Energy* **2016**, *6* (2), 020901. https://doi.org/10.1117/1.jpe.6.020901.

(48) Endo, A.; Ogasawara, M.; Takahashi, A.; Yokoyama, D.; Kato, Y.; Adachi, C. Thermally Activated Delayed Fluorescence from Sn4+–Porphyrin Complexes and Their Application to Organic Light Emitting Diodes—A Novel Mechanism for Electroluminescence. *Advanced Materials* **2009**, *21* (47), 4802–4806.

(49) Berberan-Santos, M. N.; Garcia, J. M. M. Unusually Strong Delayed Fluorescence of C70. *Journal of the American Chemical Society* **1996**, *118* (39), 9391–9394.

(50) Blasse, G.; McMILLIN, D. R. On the Luminescence of Bis (Triphenylphosphine) Phenanthroline Copper (I). *Chemical Physics Letters* **1980**, *70* (1), 1–3.

(51) Adachi, C.; Tokito, S.; Tsutsui, T.; Saito, S. Electroluminescence in Organic Films with Three-Layer Structure. *Japanese Journal of Applied Physics* **1988**, *27* (2A), L269.

(52) Guo-Zhang, D.; Hong-Jian, L.; Yan-Zhi, P.; Xiao-Yu, D.; Qiang, X. Energy Transfer Probability in Organic Electrophosphorescence Device with Dopant. *Chinese Physics* **2005**, *14* (12), 2590.

(53) Hung, L. S.; Chen, C. H. Recent Progress of Molecular Organic Electroluminescent Materials and Devices. *Materials Science and Engineering: R: Reports* **2002**, *39* (5–6), 143–222.

(54) Rothberg, L. J.; Lovinger, A. J. Status of and Prospects for Organic Electroluminescence. *Journal of Materials Research* **1996**, *11* (12), 3174–3187.

(55) Valeur, B.; Berberan-Santos, M. N. *Molecular Fluorescence: Principles and Applications*; John Wiley & Sons, 2012.

(56) Masters, B. R. Molecular Fluorescence: Principles and Applications. *Journal of Biomedical Optics* **2013**, *18* (3), 39901.

(57) Chen, A. C.-A.; Wallace, J. U.; Wei, S. K.-H.; Zeng, L.; Chen, S. H.; Blanton, T. N. Light-Emitting Organic Materials with Variable Charge Injection and Transport Properties. *Chemistry of Materials* **2006**, *18* (1), 204–213.

(58) Kondakov, D. Y. Role of Triplet-triplet Annihilation in Highly Efficient Fluorescent Devices. *Journal of The Society for Information Display* **2009**, *17* (2), 137–144.

(59) Peng, Q.; Li, W.; Zhang, S.; Chen, P.; Li, F.; Ma, Y. Evidence of the Reverse Intersystem Crossing in Intra-Molecular Charge-Transfer Fluorescence-Based Organic Light-Emitting Devices Through Magneto-Electroluminescence Measurements. *Advanced Optical Materials* **2013**, *1* (5), 362–366.

(60) Yin, X.; He, Y.; Wang, X.; Wu, Z.; Pang, E.; Xu, J.; Wang, J. Recent Advances in Thermally Activated Delayed Fluorescent Polymer—Molecular Designing Strategies. *Frontiers in Chemistry* **2020**, *8*.

(61) Hirata, S.; Sakai, Y.; Masui, K.; Tanaka, H.; Lee, S. Y.; Nomura, H.; Nakamura, N.; Yasumatsu, M.; Nakanotani, H.; Zhang, Q. Highly Efficient Blue Electroluminescence Based on Thermally Activated Delayed Fluorescence. *Nature Materials* **2015**, *14* (3), 330–336.

(62) Im, Y.; Kim, M.; Cho, Y. J.; Seo, J.-A.; Yook, K. S.; Lee, J. Y. Molecular Design Strategy of Organic Thermally Activated Delayed Fluorescence Emitters. *Chemistry of Materials* **2017**, *29* (5), 1946–1963.

(63) Méhes, G.; Nomura, H.; Zhang, Q.; Nakagawa, T.; Adachi, C. Enhanced Electroluminescence Efficiency in a Spiro-acridine Derivative through Thermally Activated Delayed Fluorescence. *Angewandte Chemie International Edition* **2012**, *51* (45), 11311–11315.

(64) Furue, R.; Nishimoto, T.; Park, I. S.; Lee, J.; Yasuda, T. Aggregation-Induced Delayed Fluorescence Based on Donor/Acceptor-Tethered Janus Carborane Triads: Unique Photophysical Properties of Nondoped OLEDs. *Angewandte Chemie International Edition* **2016**, *55* (25), 7171–7175.

(65) Zhang, Q.; Li, J.; Shizu, K.; Huang, S.; Hirata, S.; Miyazaki, H.; Adachi, C. Design of Efficient Thermally Activated Delayed Fluorescence Materials for Pure Blue Organic Light Emitting Diodes. *Journal of the American Chemical Society* **2012**, *134* (36), 14706–14709.

(66) Xie, Y.; Li, Z. Thermally Activated Delayed Fluorescent Polymers. *Journal of Polymer Science Part A: Polymer Chemistry* **2017**, *55* (4), 575–584.

(67) Suzuki, K.; Kubo, S.; Shizu, K.; Fukushima, T.; Wakamiya, A.; Murata, Y.; Adachi, C.; Kaji, H. Triarylboron-Based Fluorescent Organic Light-Emitting Diodes with External Quantum Efficiencies Exceeding 20%. *Angewandte Chemie International Edition* **2015**, *54* (50), 15231–15235.

(68) Zhang, Q.; Li, B.; Huang, S.; Nomura, H.; Tanaka, H.; Adachi, C. Efficient Blue Organic Light-Emitting Diodes Employing Thermally Activated Delayed Fluorescence. *Nature Photonics* **2014**, *8* (4), 326–332.

(69) Youn Lee, S.; Yasuda, T.; Nomura, H.; Adachi, C. High-Efficiency Organic Light-Emitting Diodes Utilizing Thermally Activated Delayed Fluorescence from Triazine-Based Donor–Acceptor Hybrid Molecules. *Applied Physics Letters* **2012**, *101* (9), 93306.

(70) Guo, J.; Li, X.; Nie, H.; Luo, W.; Gan, S.; Hu, S.; Hu, R.; Qin, A.; Zhao, Z.; Su, S. Achieving High-Performance Nondoped OLEDs with Extremely Small Efficiency Roll-Off by Combining Aggregation-Induced Emission and Thermally Activated Delayed Fluorescence. *Advanced Functional Materials* **2017**, *27* (13), 1606458.

(71) Teng, J.-M.; Wang, Y.-F.; Chen, C.-F. Recent Progress of Narrowband TADF Emitters and Their Applications in OLEDs. *Journal of Materials Chemistry C* **2020**, *8* (33), 11340–11353.

(72) Congrave, D. G.; Drummond, B. H.; Conaghan, P. J.; Francis, H.; Jones, S. T. E.; Grey, C. P.; Greenham, N. C.; Credgington, D.; Bronstein, H. A Simple Molecular Design Strategy for Delayed Fluorescence toward 1000 Nm. *Journal of the American Chemical Society* **2019**, *141* (46), 18390–18394.

(73) Liang, X.; Tu, Z.; Zheng, Y. Thermally Activated Delayed Fluorescence Materials: Towards Realization of High Efficiency through Strategic Small Molecular Design. *Chemistry–A European Journal* **2019**, *25* (22), 5623–5642.

(74) Reineke, S.; Thomschke, M.; Lüssem, B.; Leo, K. White Organic Light-Emitting Diodes: Status and Perspective. *Reviews of Modern Physics* **2013**, *85* (3), 1245.

(75) Tao, Y.; Chen, R.; Li, H.; Zheng, C.; Huang, W. Thermally Activated Delayed Fluorescence Materials Based on Donor–Acceptor Molecular Systems. *Highly Efficient OLEDs: Materials Based on Thermally Activated Delayed Fluorescence* **2018**, 377–423.

(76) Lee, K. H.; Jeon, S. O.; Chung, Y. S.; Numata, M.; Lee, H.; Lee, E. K.; Kwon, E. S.; Sim, M.; Choi, H.; Lee, J. Y. An Excited State Managing Molecular Design Platform of Blue Thermally Activated Delayed Fluorescence Emitters by π-Linker Engineering. *Journal of Materials Chemistry C* **2020**, *8* (5), 1736–1745.

(77) Volz, D. Review of Organic Light-Emitting Diodes with Thermally Activated Delayed Fluorescence Emitters for Energy-Efficient Sustainable Light Sources and Displays. *Journal of Photonics for Energy* **2016**, *6* (2), 020901. https://doi.org/10.1117/1.jpe.6.020901.

(78) Lv, X.; Sun, S.; Zhang, Q.; Ye, S.; Liu, W.; Wang, Y.; Guo, R.; Wang, L. A Strategy to Construct Multifunctional TADF Materials for Deep Blue and High Efficiency Yellow Fluorescent Devices. *Journal of Materials Chemistry C* **2020**, *8* (14), 4818–4826.

(79) Nguyen, T. B.; Nakanotani, H.; Hatakeyama, T.; Adachi, C. The Role of Reverse Intersystem Crossing Using a TADF-Type Acceptor Molecule on the Device Stability of Exciplex-Based Organic Light-Emitting Diodes. *Advanced Materials* **2020**, *32* (9), 1906614.

(80) Tsang, D. P.-K.; Matsushima, T.; Adachi, C. Operational Stability Enhancement in Organic Light-Emitting Diodes with Ultrathin Liq Interlayers. *Scientific Reports* **2016**, *6* (1), 1–10.

(81) Song, W.; Lee, W.; Kim, K. K.; Lee, J. Y. Correlation of Doping Concentration, Charge Transport of Host, and Lifetime of Thermally Activated Delayed Fluorescent Devices. *Organic Electronics* **2016**, *37*, 252–256.

(82) Kim, H. M.; Choi, J. M.; Lee, J. Y. Blue Thermally Activated Delayed Fluorescent Emitters Having a Bicarbazole Donor Moiety. *RSC Advances* **2016**, *6* (68), 64133–64139.

(83) Yang, Z.; Mao, Z.; Xie, Z.; Zhang, Y.; Liu, S.; Zhao, J.; Xu, J.; Chi, Z.; Aldred, M. P. Recent Advances in Organic Thermally Activated Delayed Fluorescence Materials. *Chemical Society Reviews* **2017**, *46* (3), 915–1016.

(84) Wang, Y.; Yun, J. H.; Wang, L.; Lee, J. Y. High Triplet Energy Hosts for Blue Organic Light-Emitting Diodes. *Advanced Functional Materials* **2021**, *31* (12), 2008332.

(85) Wong, M. Y.; Zysman-Colman, E. Purely Organic Thermally Activated Delayed Fluorescence Materials for Organic Light-emitting Diodes. *Advanced Materials* **2017**, *29* (22), 1605444.

(86) Kim, M.; Jeon, S. K.; Hwang, S.; Lee, J. Y. Stable Blue Thermally Activated Delayed Fluorescent Organic Light-emitting Diodes with Three Times Longer Lifetime than Phosphorescent Organic Light-emitting Diodes. *Advanced materials* **2015**, *27* (15), 2515–2520.

(87) Yook, K. S.; Lee, J. Y. Bipolar Host Materials for Organic Light-Emitting Diodes. *The Chemical Record* **2016**, *16* (1), 159–172.

(88) Chatterjee, T.; Wong, K. Perspective on Host Materials for Thermally Activated Delayed Fluorescence Organic Light Emitting Diodes. *Advanced Optical Materials* **2019**, *7* (1), 1800565.

(89) Han, C.; Zhao, Y.; Xu, H.; Chen, J.; Deng, Z.; Ma, D.; Li, Q.; Yan, P. A Simple Phosphine–Oxide Host with a Multi-insulating Structure: High Triplet Energy Level for Efficient Blue Electrophosphorescence. *Chemistry–A European Journal* **2011**, *17* (21), 5800–5803.

(90) Ding, D.; Zhang, Z.; Wei, Y.; Yan, P.; Xu, H. Spatially Optimized Quaternary Phosphine Oxide Host Materials for High-Efficiency Blue Phosphorescence and Thermally Activated Delayed Fluorescence Organic Light-Emitting Diodes. *Journal of Materials Chemistry C* **2015**, *3* (43), 11385–11396.

(91) Shin, S. K.; Han, S. H.; Lee, J. Y. High Triplet Energy Exciplex Host Derived from a CN Modified Carbazole Based N-Type Host for Improved Efficiency and Lifetime in Blue Phosphorescent Organic Light-Emitting Diodes. *Journal of Materials Chemistry C* **2018**, *6* (38), 10308–10314.

(92) Kukhta, N. A.; Matulaitis, T.; Volyniuk, D.; Ivaniuk, K.; Turyk, P.; Stakhira, P.; Grazulevicius, J. V; Monkman, A. P. Deep-Blue High-Efficiency TTA OLED Using

Para-and Meta-Conjugated Cyanotriphenylbenzene and Carbazole Derivatives as Emitter and Host. *The Journal of Physical Chemistry Letters* **2017**, *8* (24), 6199–6205.

(93) An, Z.; Chen, R.; Yin, J.; Xie, G.; Shi, H.; Tsuboi, T.; Huang, W. Conjugated Asymmetric Donor-Substituted 1, 3, 5-Triazines: New Host Materials for Blue Phosphorescent Organic Light-Emitting Diodes. *Chemistry–A European Journal* **2011**, *17* (39), 10871–10878.

(94) Ren, X.; Li, J.; Holmes, R. J.; Djurovich, P. I.; Forrest, S. R.; Thompson, M. E. Ultrahigh Energy Gap Hosts in Deep Blue Organic Electrophosphorescent Devices. *Chemistry of Materials* **2004**, *16* (23), 4743–4747.

(95) Nishimoto, T.; Yasuda, T.; Lee, S. Y.; Kondo, R.; Adachi, C. A Six-Carbazole-Decorated Cyclophosphazene as a Host with High Triplet Energy to Realize Efficient Delayed-Fluorescence OLEDs. *Materials Horizons* **2014**, *1* (2), 264–269.

(96) Wei, Q.; Ge, Z.; Voit, B. Thermally Activated Delayed Fluorescent Polymers: Structures, Properties, and Applications in OLED Devices. *Macromolecular Rapid Communications* **2019**, *40* (1), 1800570.

(97) Mahoro, G. U.; Fernandez-Cestau, J.; Renaud, J.; Coto, P. B.; Costa, R. D.; Gaillard, S. Recent Advances in Solid-State Lighting Devices Using Transition Metal Complexes Exhibiting Thermally Activated Delayed Fluorescent Emission Mechanism. *Advanced Optical Materials* **2020**, *8* (16), 2000260.

(98) Jung, M.; Lee, K. H.; Lee, J. Y.; Kim, T. A Bipolar Host Based High Triplet Energy Electroplex for an over 10000 h Lifetime in Pure Blue Phosphorescent Organic Light-Emitting Diodes. *Materials Horizons* **2020**, *7* (2), 559–565.

(99) Li, W.; Li, J.; Liu, D.; Wang, F.; Zhang, S. Bipolar Host Materials for High-Efficiency Blue Phosphorescent and Delayed-Fluorescence OLEDs. *Journal of Materials Chemistry C* **2015**, *3* (48), 12529–12538.

(100) Kim, M.; Lee, J. Y. Engineering of Interconnect Position of Bicarbazole for High External Quantum Efficiency in Green and Blue Phosphorescent Organic Light-Emitting Diodes. *ACS Applied materials & Interfaces* **2014**, *6* (17), 14874–14880.

(101) Lin, N.; Qiao, J.; Duan, L.; Wang, L.; Qiu, Y. Molecular Understanding of the Chemical Stability of Organic Materials for OLEDs: A Comparative Study on Sulfonyl,

Phosphine-Oxide, and Carbonyl-Containing Host Materials. *The Journal of Physical Chemistry C* **2014**, *118* (14), 7569–7578.

(102) Sharma, A.; Balasaravanan, R.; Thomas, K. R. J.; Ram, M.; Dubey, D. K.; Yadav, R. A. K.; Jou, J.-H. Tuning Photophysical and Electroluminescent Properties of Phenanthroimidazole Decorated Carbazoles with Donor and Acceptor Units: Beneficial Role of Cyano Substitution. *Dyes and Pigments* **2021**, *184*, 108830.

(103) Wang, Q.; Tian, Q.-S.; Zhang, Y.-L.; Tang, X.; Liao, L.-S. High-Efficiency Organic Light-Emitting Diodes with Exciplex Hosts. *Journal of Materials Chemistry C* **2019**, *7* (37), 11329–11360.

(104) Park, S.-R.; Kim, S.-M.; Kang, J.-H.; Lee, J.-H.; Suh, M. C. Bipolar Host Materials with Carbazole and Dipyridylamine Groups Showing High Triplet Energy for Blue Phosphorescent Organic Light Emitting Diodes. *Dyes and Pigments* **2017**, *141*, 217–224.

(105) Tan, J.; Wang, B.; Huang, Z.; Lv, X.; Yi, W.; Zhuang, S.; Wang, L. Design, Synthesis, Characterization and Application of a Novel Electron-Deficient Moiety 1, 5-Diazacarbazole in High Triplet Energy Host Materials. *Journal of Materials Chemistry C* **2016**, *4* (23), 5222–5230.

(106) Li, J.; Dong, S.-C.; Opitz, A.; Liao, L.-S.; Koch, N. Design Principles of Carbazole/Dibenzothiophene Derivatives as Host Material in Modern Efficient Organic Light-Emitting Diodes. *Journal of Materials Chemistry C* **2017**, *5* (28), 6989–6996.

(107) Zhao, X.-H.; Zhang, Z.-S.; Qian, Y.; Yi, M.-D.; Xie, L.-H.; Hu, C.-P.; Xie, G.-H.; Xu, H.; Han, C.-M.; Zhao, Y. A Bulky Pyridinylfluorene-Fuctionalizing Approach to Synthesize Diarylfluorene-Based Bipolar Host Materials for Efficient Red, Green, Blue and White Electrophosphorescent Devices. *Journal of Materials Chemistry C* **2013**, *1* (21), 3482–3490.

(108) Zhang, D.; Duan, L.; Li, Y.; Li, H.; Bin, Z.; Zhang, D.; Qiao, J.; Dong, G.; Wang, L.; Qiu, Y. Towards High Efficiency and Low Roll-off Orange Electrophosphorescent Devices by Fine Tuning Singlet and Triplet Energies of Bipolar Hosts Based on Indolocarbazole/1, 3, 5-triazine Hybrids. *Advanced Functional Materials* **2014**, *24* (23), 3551–3561.

(109) Lin, C.-C.; Huang, M.-J.; Chiu, M.-J.; Huang, M.-P.; Chang, C.-C.; Liao, C.-Y.; Chiang, K.-M.; Shiau, Y.-J.; Chou, T.-Y.; Chu, L.-K. Molecular Design of Highly Efficient Thermally Activated Delayed Fluorescence Hosts for Blue Phosphorescent and Fluorescent Organic Light-Emitting Diodes. *Chemistry of Materials* **2017**, *29* (4), 1527–1537.

(110) Xia, Y.; Liu, Z.; Li, J.; Fan, C.; Li, G.; Zhao, B.; Wu, Y.; Wang, H.; Guo, K. TADF Material with Non-Conjugated Rigid Donor for High-Performance Full-Color Phosphorescent OLEDs: Effects of Triplet Harvest and Charge Transport on Efficiency. *Organic Electronics* **2020**, *85*, 105826.

(111) Nakanotani, H.; Higuchi, T.; Furukawa, T.; Masui, K.; Morimoto, K.; Numata, M.; Tanaka, H.; Sagara, Y.; Yasuda, T.; Adachi, C. High-Efficiency Organic Light-Emitting Diodes with Fluorescent Emitters. *Nature Communications* **2014**, *5* (1), 1–7.

(112) Huang, T.; Jiang, W.; Duan, L. Recent Progress in Solution Processable TADF Materials for Organic Light-Emitting Diodes. *Journal of Materials Chemistry C* **2018**, *6* (21), 5577–5596.

(113) Shi, W.; Sun, M.; Hu, X.; Ren, B.; Cheng, J.; Li, C.; Duan, X.; Fu, X.; Zhang, J.; Chen, H. Structurally and Functionally Optimized Silk-fibroin–Gelatin Scaffold Using 3D Printing to Repair Cartilage Injury in Vitro and in Vivo. *Advanced Materials* **2017**, *29* (29), 1701089.

(114) Grayson, S. M.; Frechet, J. M. J. Convergent Dendrons and Dendrimers: From Synthesis to Applications. *Chemical Reviews* **2001**, *101* (12), 3819–3868.

(115) Zou, Y.; Gong, S.; Xie, G.; Yang, C. Design Strategy for Solution-Processable Thermally Activated Delayed Fluorescence Emitters and Their Applications in Organic Light-Emitting Diodes. *Advanced Optical Materials* **2018**, *6* (23), 1800568.

(116) Gong, S.; Yang, C.; Qin, J. Efficient Phosphorescent Polymer Light-Emitting Diodes by Suppressing Triplet Energy Back Transfer. *Chemical Society Reviews* **2012**, *41* (14), 4797–4807.

(117) Burroughes, J. H.; Bradley, D. D. C.; Brown, A. R.; Marks, R. N.; Mackay, K.; Friend, R. H.; Burns, P. L.; Holmes, A. B. Light-Emitting Diodes Based on Conjugated Polymers. *Nature* **1990**, *347* (6293), 539–541.

(118) Gustafsson, G. Y. Cao, GM Treacy, F. Klavetter, N. Colaneri, and AJ Heeger. *Nature* **1992**, *357*, 477.

(119) Nikolaenko, A. E.; Cass, M.; Bourcet, F.; Mohamad, D.; Roberts, M. Thermally Activated Delayed Fluorescence in Polymers: A New Route toward Highly Efficient Solution Processable OLEDs. *Advanced Materials* **2015**, *27* (44), 7236–7240.

(120) Lee, S. Y.; Yasuda, T.; Komiyama, H.; Lee, J.; Adachi, C. Thermally Activated Delayed Fluorescence Polymers for Efficient Solution-processed Organic Light-emitting Diodes. *Advanced Materials* **2016**, *28* (21), 4019–4024.

(121) Zhang, Y.; Zuniga, C.; Kim, S.-J.; Cai, D.; Barlow, S.; Salman, S.; Coropceanu, V.; Brédas, J.-L.; Kippelen, B.; Marder, S. Polymers with Carbazole-Oxadiazole Side Chains as Ambipolar Hosts for Phosphorescent Light-Emitting Diodes. *Chemistry of Materials* **2011**, *23* (17), 4002–4015.

(122) Luo, J.; Xie, G.; Gong, S.; Chen, T.; Yang, C. Creating a Thermally Activated Delayed Fluorescence Channel in a Single Polymer System to Enhance Exciton Utilization Efficiency for Bluish-Green Electroluminescence. *Chemical Communications* **2016**, *52* (11), 2292–2295.

(123) Zou, Y.; Gong, S.; Xie, G.; Yang, C. Design Strategy for Solution-Processable Thermally Activated Delayed Fluorescence Emitters and Their Applications in Organic Light-Emitting Diodes. *Advanced Optical Materials* **2018**, *6* (23), 1800568.

(124) Lin, X.; Zhu, Y.; Zhang, B.; Zhao, X.; Yao, B.; Cheng, Y.; Li, Z.; Qu, Y.; Xie, Z. Highly Efficient TADF Polymer Electroluminescence with Reduced Efficiency Roll-off via Interfacial Exciplex Host Strategy. *ACS Applied materials & Interfaces* **2018**, *10* (1), 47–52.

(125) Zhou, X.; Huang, M.; Zeng, X.; Chen, T.; Xie, G.; Yin, X.; Yang, C. Combining the Qualities of Carbazole and Tetraphenyl Silane in a Desirable Main Chain for Thermally Activated Delayed Fluorescence Polymers. *Polym. Chem.* **2019**, *10* (30), 4201–4208.

(126) Astruc, D.; Boisselier, E.; Ornelas, C. Dendrimers Designed for Functions: From Physical, Photophysical, and Supramolecular Properties to Applications in Sensing, Catalysis, Molecular Electronics, Photonics, and Nanomedicine. *Chemical Reviews* **2010**, *110* (4), 1857–1959.

(127) Burn, P. L.; Lo, S.; Samuel, I. D. W. The Development of Light-emitting Dendrimers for Displays. *Advanced Materials* **2007**, *19* (13), 1675–1688.

(128) Miyaura, N.; Suzuki, A. Palladium-Catalyzed Cross-Coupling Reactions of Organoboron Compounds. *Chemical Reviews* **1995**, *95* (7), 2457–2483.

(129) Schlüter, A. D. The Tenth Anniversary of Suzuki Polycondensation (SPC). *Journal of Polymer Science Part A: Polymer Chemistry* **2001**, *39* (10), 1533–1556.

(130) Suzuki, A. Organoboron Compounds in New Synthetic Reactions. *Pure and Applied Chemistry* **1985**, *57* (12), 1749–1758.

(131) Sonogashira, K.; Tohda, Y.; Hagihara, N. A Convenient Synthesis of Acetylenes: Catalytic Substitutions of Acetylenic Hydrogen with Bromoalkenes, Iodoarenes and Bromopyridines. *Tetrahedron Letters* **1975**, *16* (50), 4467–4470.

(132) Lenfant, S.; Viero, Y.; Krzeminski, C.; Vuillaume, D.; Demeter, D.; Dobra, I.; Oçafrain, M.; Blanchard, P.; Roncali, J.; Van Dyck, C. New Photomechanical Molecular Switch Based on a Linear π-Conjugated System. *The Journal of Physical Chemistry C* **2017**, *121* (22), 12416–12425.

(133) Tour, J. M. Molecular Electronics. Synthesis and Testing of Components. *Accounts of Chemical Research* **2000**, *33* (11), 791–804.

(134) Melchor, M. G. *A Theoretical Study of Pd-Catalyzed CC Cross-Coupling Reactions*; Springer Science & Business Media, 2013.

(135) Li, J.; Grimsdale, A. C. Carbazole-Based Polymers for Organic Photovoltaic Devices. *Chemical Society Reviews* **2010**, *39* (7), 2399–2410.

(136) Xu, F.; Kim, J.-H.; Kim, H. U.; Jang, J.-H.; Yook, K. S.; Lee, J. Y.; Hwang, D.-H. Synthesis of High-Triplet-Energy Host Polymer for Blue and White Electrophosphorescent Light-Emitting Diodes. *Macromolecules* **2014**, *47* (21), 7397–7406.

(137) Huang, J.; Niu, Y.; Yang, W.; Mo, Y.; Yuan, M.; Cao, Y. Novel Electroluminescent Polymers Derived from Carbazole and Benzothiadiazole. *Macromolecules* **2002**, *35* (16), 6080–6082.

(138) Shao, S.; Ding, J.; Wang, L.; Jing, X.; Wang, F. Highly Efficient Blue Electrophosphorescent Polymers with Fluorinated Poly (Arylene Ether Phosphine

Oxide) as Backbone. *Journal of the American Chemical Society* **2012**, *134* (37), 15189–15192.

(139) Geissler, U.; Hallensleben, M. L.; Rienecker, A.; Rohde, N. Polyarylenes on the Basis of Alkylpyrrole and Alkylcarbazole Derivatives and Their Oligomeric Model Systems. *Polymers for Advanced Technologies* **1997**, *8* (2), 87–92.

(140) Scherf, U.; List, E. J. W. Semiconducting Polyfluorenes—towards Reliable Structure-Property Relationships. *Advanced Materials* **2002**, *14* (7), 477–487.

(141) Tang, C. W.; VanSlyke, S. A. Organic Electroluminescent Diodes. *Applied Physics Letters* **1987**, *51* (12), 913–915.

CHAPTER 2: Design and Synthesis of non-Conjugated Backbone Polymers with TADF Emitters for Application of OLEDs

Abstract

Due to their unique features, TADF polymers have been a focus of interest for use in electroluminescent devices. A series of highly efficient copolymers, including various ratios of TADF units, were synthesised and developed following the side-chain engineering strategy. The green TADF emitter (PXZ-TRZ) was successfully attached to the side chain of polymers *via* Suzuki polycondensation. The copolymer's backbone involved derivative units of carbazole and non-conjugated tetrahedral silicon. Among the prepared polymers, P1 and P5 were made with TADF-free moieties for comparison purposes. The results of the synthesised polymers and their monomers are presented, together with their photophysical analysis, TGA and cyclic voltammetry analyses. Comparable optical band gap values (between 3.20 eV and 3.45 eV) were displayed for all polymers; this can be attributed to the non-conjugated nature of the materials. All polymers demonstrate good thermal stability with decomposition temperatures higher than 300 °C. In addition, a good solubility of these polymers was displayed in most common organic solvents, which makes them promising emitting-layer candidates for solution-processed polymers in light-emitting diode applications.

2.1. Introduction

OLEDs using emitters with TADF properties have attracted significant attention since the first report of high EQE materials (20%) by Adachi et al.[1,2] The internal quantum efficiency of TADF materials in devices can theoretically be 100%; this is possible *via* RISC, which enables those materials to harvest both singlet excitons from the lowest excited state and triplet excitons after being converted.[3,4] TADF molecules have a great feature of a small energy gap between the singlet and triplet state (ΔE_{ST})[5], which enables the promotion of excitons from the triplet excited state into the singlet excited state. This minimized energy level between the two states can be generated by managing the spatial separation between the LUMO and the HOMO orbitals of the molecules by including both electron-withdrawing and electron-donating moieties in their structures.[6,7]

Host materials are typically used in OLED emitting layers to enhance the efficiency of the device's performance.[8] Moreover, the candidate host materials for TADF-OLEDs should own several requirements for their use in OLED devices.[9] For example, they must have high triplet energy and the guest dopant should have lower triplet energy than the host materials to assure no energy transfer back to the host. Host molecules should also have appropriate HOMO and LUMO energy levels to enable transportation and charge injection. Other desirable host properties include a high glass transition temperature (T_g), balanced charge transportation to boost the recombination zone, and they must show high solubility in organic solution for solution processability purposes.[10–12]

Bipolar host materials are unlike unipolar types; they involve accepting and donating units to facilitate charge injection and increase the transporting character.[13,14] It is extremely important to increase the steric hindrance or to break the conjugation system in host materials so they could have high triplet energy. This is facilitated by introducing linkers, such as cyclohexane and silane, between accepting and donating entities in the host core structures.[15,16] This method is the most effective way for orbital separation. In this study, host molecules containing silane functional groups in their molecular structure, labelled as SiCz, were successfully designed and incorporated into polymers. (Figure 2.1)

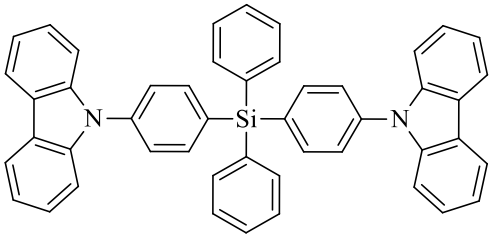

Figure 2.1 The structure of the targeted host molecule (SiCz)

There are three main considerations that should be taken into an account for TADF polymers; in addition to the choice of an efficient host, it is also extremely important to select an effective guest emitter for TADF polymers.[17] TADF polymer-engineering strategies could also determine the materials' outcome efficiency.[18,19] Following the main-chain strategy system, Lee et al. successfully designed TADF polymers that contain a combination of acridine derivatives or carbazole as donors and diphenyl ketone as acceptors.[20] The external quantum efficiency in this study was between 9% and 10% using orange and green emitters. Although a tremendous number of TADF polymers have been synthesised using this method, the interaction between the polymers' backbones, acceptors, and donors, which determines the TADF properties is yet unpredictable.

On the other hand, TADF polymers have been made effectively via the side-chain engineering technique in the past few years.[21,22] It is a manageable and convenient method because the polymers can possess the characteristics of the TADF moiety that is attached to the side chain. Furthermore, desirable charge transfer (CT) properties and the high triplet energy level of the polymer's backbone contribute to enhancing the electroluminescence, thus better device performance.[23–25]

A series of copolymers containing a conjugated carbazole moiety that optimises the charge transporting properties, and non-conjugated tetraphenyl silicon that maintains a high triplet energy level, was successfully designed by Yang et al.[26] By grafting 10,10′-((2-(4-(9*H*-carbazol-9-yl)phenyl)pyrimidine-4,6-diyl)bis(4,1-phenylene))bis(10*H*-phenoxazine), identified as (PXZ-Pm-MeOCz), onto the side chain, polymers with various molar ratios of TADF moiety were made as shown in Scheme 2.1. There was a full intra-chain and inter-chain energy transfer to the attached TADF unit from the polymer's backbone that was shown in photoluminescence spectra. By comparing these synthesised copolymers, the maximum emission peak in the neat thin-film moves gradually towards red-shifted as the molar ratio of

the TADF unit increase due to more aggregation present in the TADF unit, as a result, a high possibility of π–π interaction. This is also shown in this project, where different molar ratios of TADF unit (PXZ-TRZ) are present in the designed polymers.

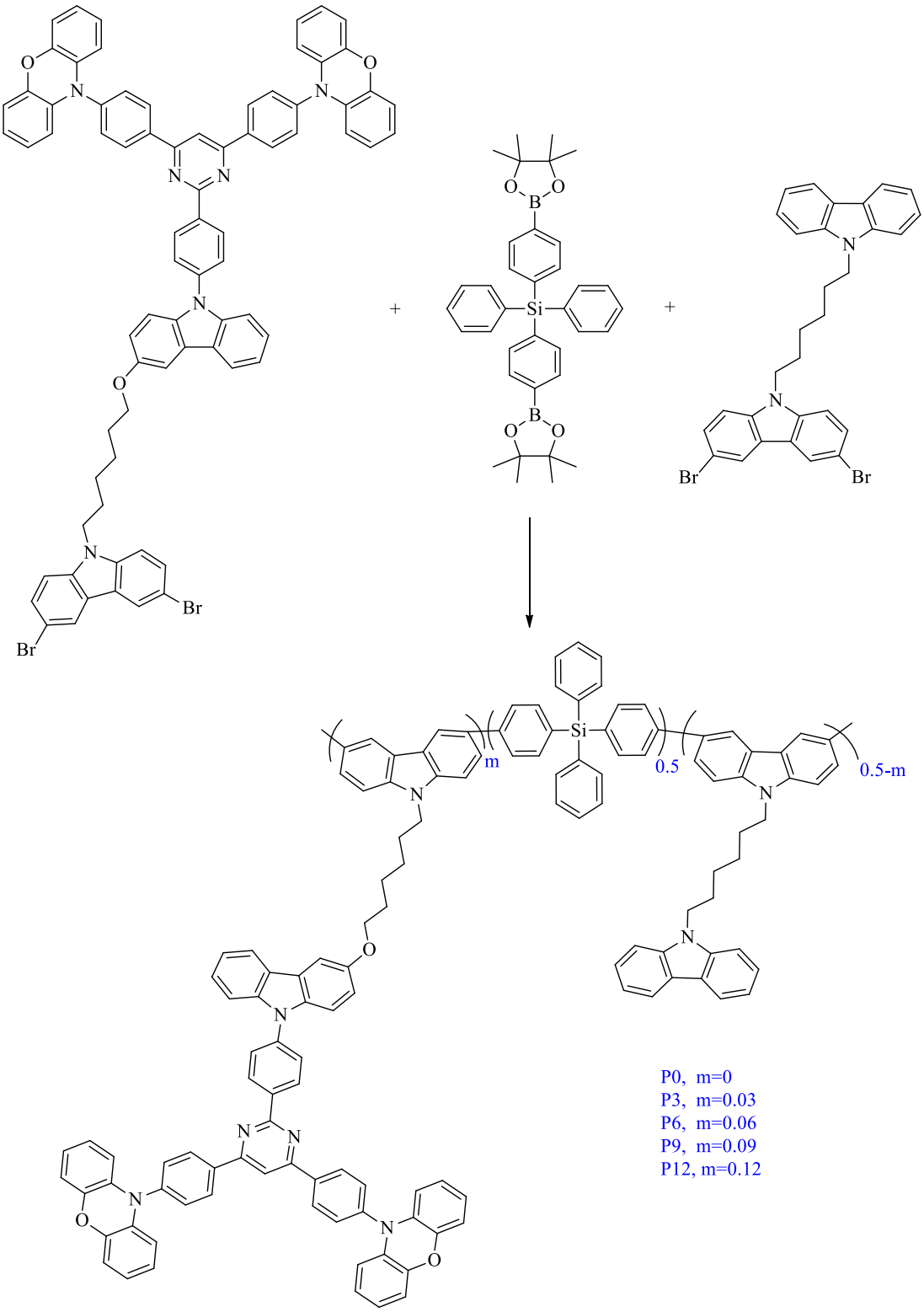

Scheme 2.1 Synthesis route of the TADF copolymers.

TADF polymers are more efficient than small molecules for the solution processing method due to their chemical stability, morphology and film-forming properties.[27–29] Even though solution-processed polymer materials are more suitable as emissive materials, the performance of devices can be restricted, as the polymers may affect the electroluminescence process by determining external quantum efficiency (EQE). However, the mechanisms of TADF, which use pure organic emissive molecules, offer a powerful strategy to optimise the EQE of polymeric materials. In addition, this study uses a side-chain engineering method to graft a TADF unit into polymers to build a single polymer system with a TADF channel. The attached emitter is linked through the side chain to the polymer backbone with no electronic conjugation between the polymer system and the TADF sites. In such systems, the polymer backbone serves as a host material and promotes charge and energy transport while the side chains with the linked TADF molecules act as guest emitters.

2.2. Results and Discussion

The target series of TADF polymers were designed as shown in Schemes 2.2 and 2.3 through a Suzuki polycondensation of M1, M2 and M3 with different feed molar ratios of 1:1:0 (P1), 0.9:1:0.1 (P2), 0.8:1:0.2 (P3) and 0.6:1:0.4 (P4) as described in Scheme 2.2. In addition, P5, P6, P7 and P8 were synthesised using the same method with various feed molar ratios of M1, M3 and M4. Furthermore, two polymers namely (P1) and (P5) do not include the TADF moiety in their polymer chains for comparison purposes, meanwhile, TADF units were grafted in gradually increasing ratios into the polymer side chains. In this study, 10-(4-(4,6-diphenyl-1,3,5-triazine-2-yl)phenyl)-10H-phenoxazine (PXZ -TRZ) was used as the TADF emitter. It is widely known as an effective TADF dye for OLEDs. It is commonly used in OLEDs where vacuum evaporation is required to afford the device's active layers. Because of the advantages of solution processing techniques, such as spray coating and spin coating from solutions, over the vacuum evaporation method, the TADF unit is attached to side chains of polymer backbones to enable the solution processing strategy. M1 contains silicon, which breaks the conjugation system and is selected together with carbazole to endow the polymers with high triplet energy and hole-transporting properties.

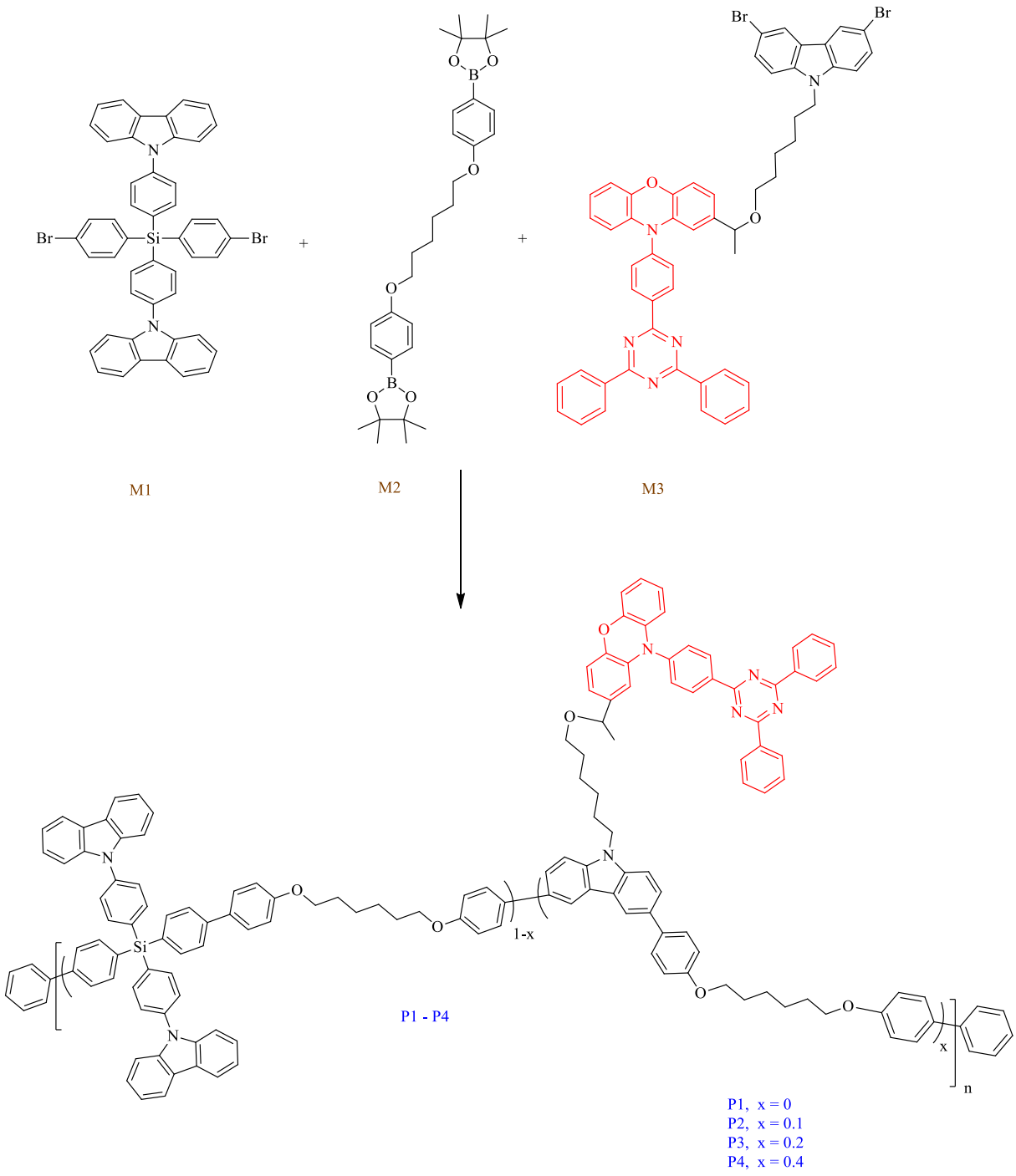

Scheme 2.2 Synthetic route for TADF polymers (P1-P4).

Reagents and conditions; $NaHCO_3$, $P(o\text{-}tol)_3$, $Pd(OAc)_2$, H_2O, THF, 85°C, 1 to 3 days.

The same monomer containing the (PXZ-TRZ) unit was also grafted onto the silane host backbone, as illustrated in Scheme 2.3. This was done to exploit the efficient electroluminescence exhibited and high charge carrier mobility. In addition, the solubility of all prepared polymers in this chapter ranged from good (for P5-P8) to excellent (for P1-P4) in

most known organic solvents, such as THF, chloroform, DCM and toluene, enabling them to be readily used as solution processing materials. As described in Scheme 2.3, the TADF copolymers (P5-P8) were prepared following the Suzuki polycondensation method of monomers: (M1), (M4) and (M3) with feed molar ratios of 50:50:0, 45:50:5, 40:50:10 and 30:50:20 to produce P5, P6, P7and P8 respectively.

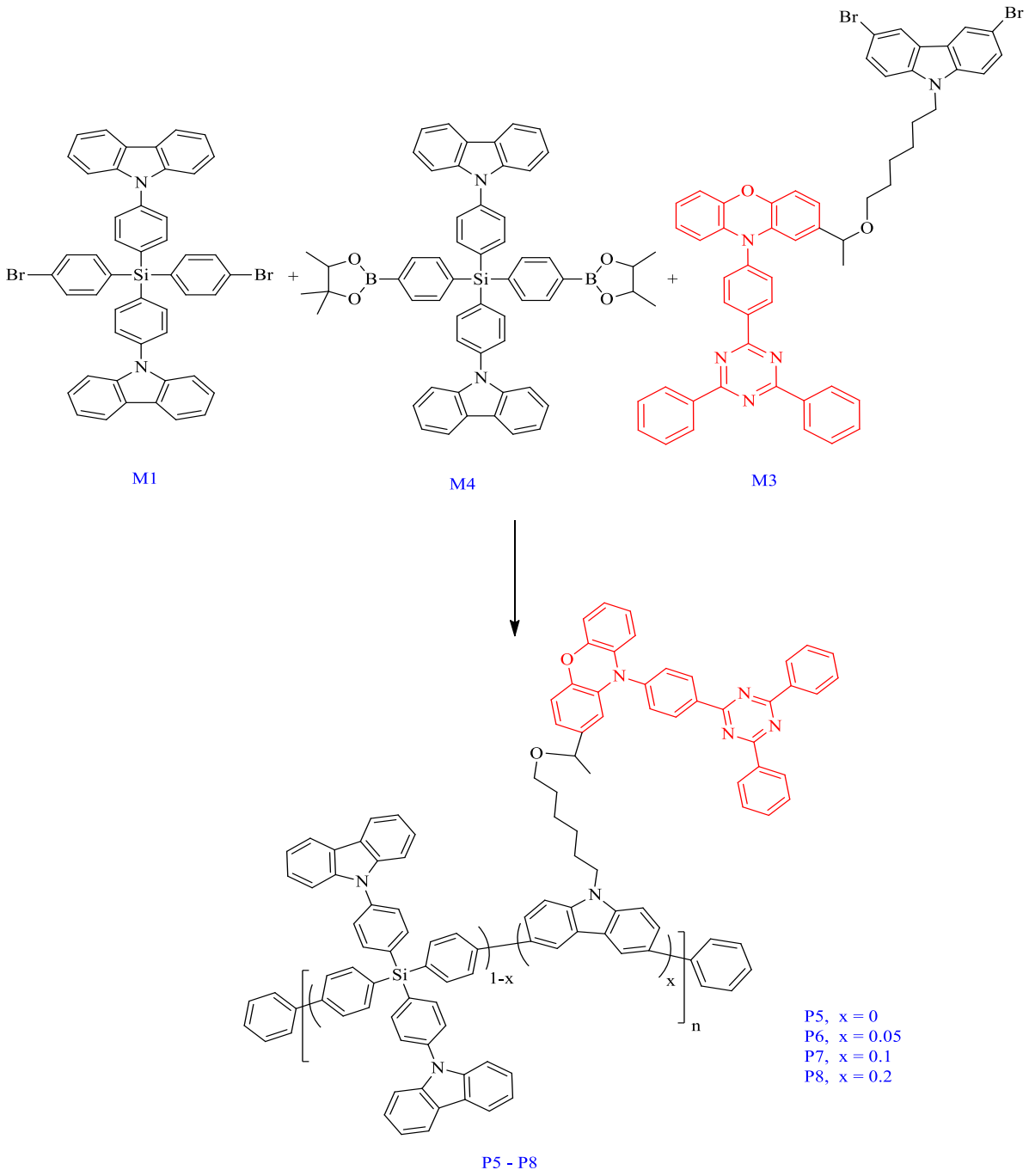

Scheme 2.3 Synthetic route for TADF polymers (P5-P8).

Reagents and conditions; $NaHCO_3$, $P(o\text{-}tol)_3$, $Pd(OAc)_2$, H_2O, THF, Ar, 90°C, 3d.

2.2.1 Monomers Synthesis

The first monomer 4-(9H-carbazol-9-yl)phenyl)bis(4-bromophenyl)silane (Br-SiCz-Br) is derived from the known host (SiCz), which was discussed earlier in this chapter. Scheme 2.4 describes the synthetic route of (Br-SiCz-Br) (M1). The purities of the prepared compounds were confirmed by ^{1}H- NMR, ^{13}C-NMR, elemental analysis and mass spectrometry.

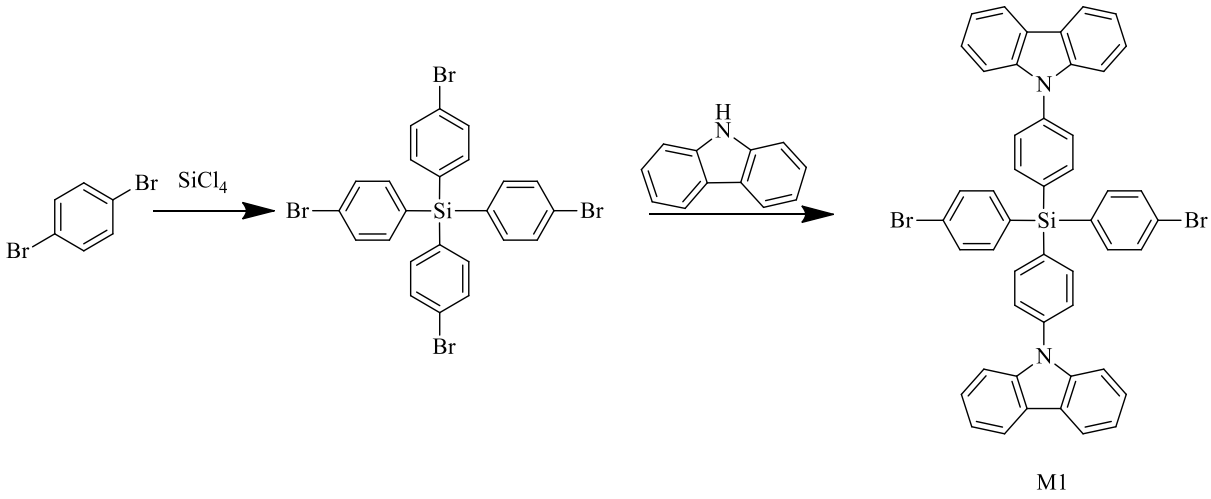

Scheme 2.4 Preparation route of (Br-SiCz-Br)

The appearance of M1 is a white solid. Dichloromethane (DCM) is used to extract the crude product, followed by purification through silica column chromatography, using 9:1 petroleum ether (PE) and dichloromethane (DCM). Then the polarity of the solvents is increased by modifying the used eluent to 2.7:1 (PE) and (DCM) to finally form the required compound as a white solid product. The monomer exhibits distinct doublet resonance at 8.17 ppm, which is attributed to the protons attached to the carbons at positions 4 and 5 in carbazole. It also displays new aromatic peaks at 7.44 ppm and 7.37 ppm, these are corresponding to the protons that are attached to the carbons at positions 2,7 and 3,6 in the carbazole ring. Meanwhile, the signal from N-H disappeared as shown in Figure 2.2. The mass spectrum of M1 displays the main integer signals at 822, 824 and 826 due to the presence of two isotopes of bromine (^{79}Br and ^{81}Br). The resulting ^{1}H- NMR, ^{13}C-NMR, elemental analysis and mass spectroscopy show an excellent match with the literature.[30]

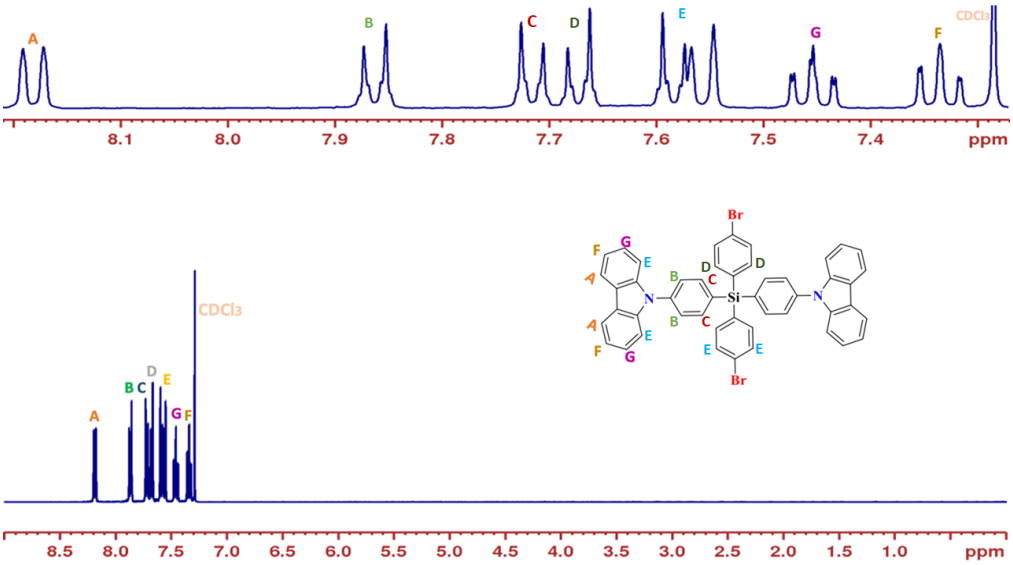

Figure 2.2 ^{1}H-NMR spectrum of M1 in $CDCl_3$.

The synthesis of the first monomer (M1) consists of two steps; the first one is making tetrakis(4-bromophenyl) silane from bromobenzene and silicon tetrachloride, followed by coupling with 9-H carbazole using the Ullman-coupling method to prepare the TADF host. The first step and its proposed mechanism are shown in Schemes 2.5 and 2.6 respectively.

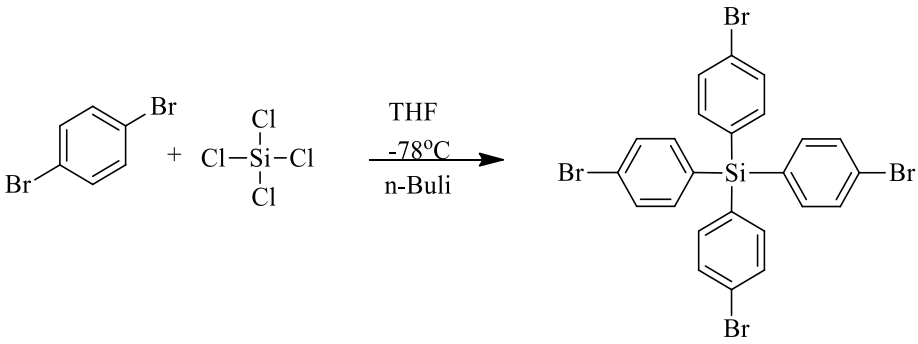

Scheme 2.5 The synthetic route of tetrakis(4-bromophenyl) silane

The preparation of the first product (tetrakis (4-bromophenyl) silane) takes place under dry conditions and at a very low temperature according to the procedure illustrated by Skorotetcky et al.; the mechanism is described in Scheme 2.6.[31] The white crystal substance formed after extracting the crude product with diethyl ether, followed by purification using column chromatography with hexane as eluent, then methanol for crystallisation. Thin-layer

chromatography (TLC) confirmed the purity of the product by showing one spot. Additionally, nuclear magnetic resonance (NMR) use to confirm the final chemical structure of the compound. A new doublet peak in ^{1}H NMR was displayed at 7.55 ppm, which corresponded to the aromatic protons close to the silicon. Also, The ^{13}C NMR spectrum exhibits four peaks for four different carbons in the aromatic region. Mass spectroscopy and elemental analysis results also show complete agreement with the literature. The responsible mechanism for this reaction is the lithiation of the 1,4-dibromo benzene starting material with butyllithium. In this step, halogen (Br)-lithium exchange takes place in which the corresponding organolithium is formed (phenyl lithium). Therefore, a new nucleophilic centre is formed, which then attacks the $SiCl_4$ to finally produce the product.

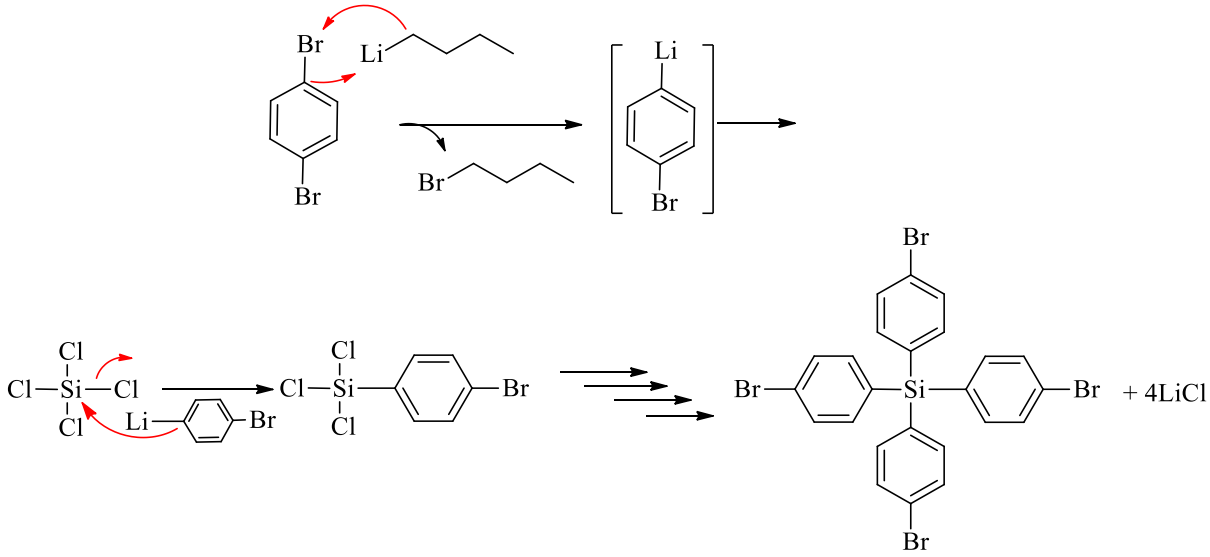

Scheme 2.6 The proposed mechanism for the preparation of tetrakis (4-bromophenyl) silane

The synthesis of the monomer is the second step in which the final monomer (M1) was successfully obtained with a 26% yield. A modified method of the procedure described by Liu, He et al, was followed, where the Ullman coupling strategy is used to form a C-N bond as shown in Scheme 2.7.[32] The Product is a white solid, and its structure was confirmed *via* both ^{1}H NMR and ^{13}C NMR. The ^{1}H NMR spectrum showed that one proton at 11.57 ppm had disappeared. This was understood to be a proton assigned to the carbazole ring, and the peak for this proton could be seen in the spectrum for the carbazole. The final structure had mass peaks at 822, 824 and 826 due to the presence of two isotopes of bromine (^{79}Br and ^{81}Br), which was in good agreement with the literature. Furthermore, elemental analysis of M1 gave

a result as follows: C,69.93: H, 3.90: Br, 19.40: N, 3.38 which match its proposed formula. All these results were an indication that the formation of the first monomer had been successful.

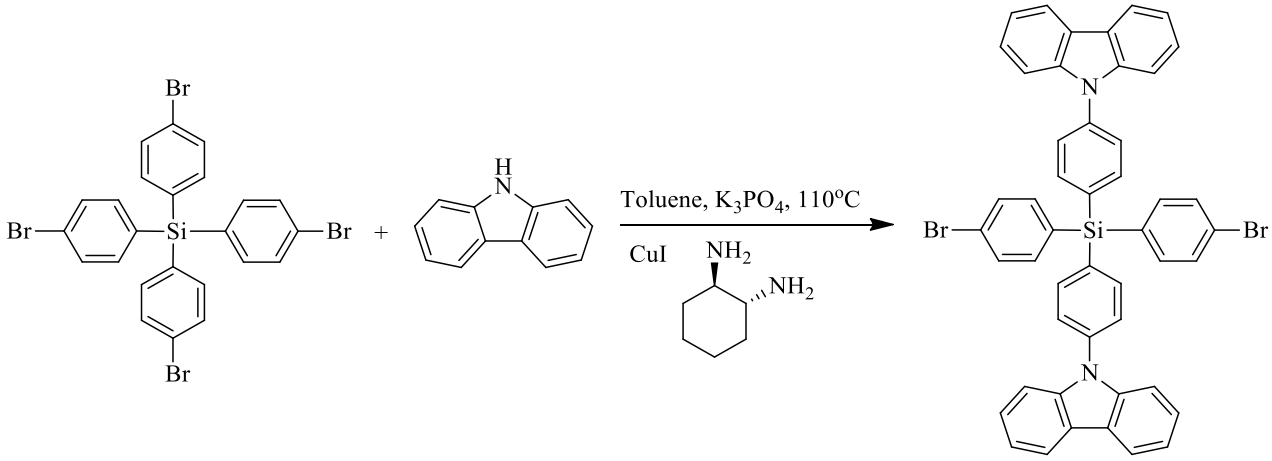

Scheme 2.7 The synthetic route of (M1)

This reaction followed the Ullman coupling procedure, in which the catalyst for this reaction was copper iodide, while the ligand was trans-1,2-diaminocyclohexane. However, the yield for this product was not very high, due to the regioselectivity. While different proposed mechanisms have been reported for Ullmann coupling reactions, using copper catalysis with ligands has been applied successfully to form C-N bonds as explained in Scheme 2.8. The first step of this procedure is oxidative addition, where the oxidation number of the copper increases and the coper aryl complex forms. This is followed by deprotonation of the bonded hydrogen (N-H), in which carbazole is coupled with the intermediate molecule. The last step is reductive elimination, where copper (I) is regenerated and C-N bonds form.

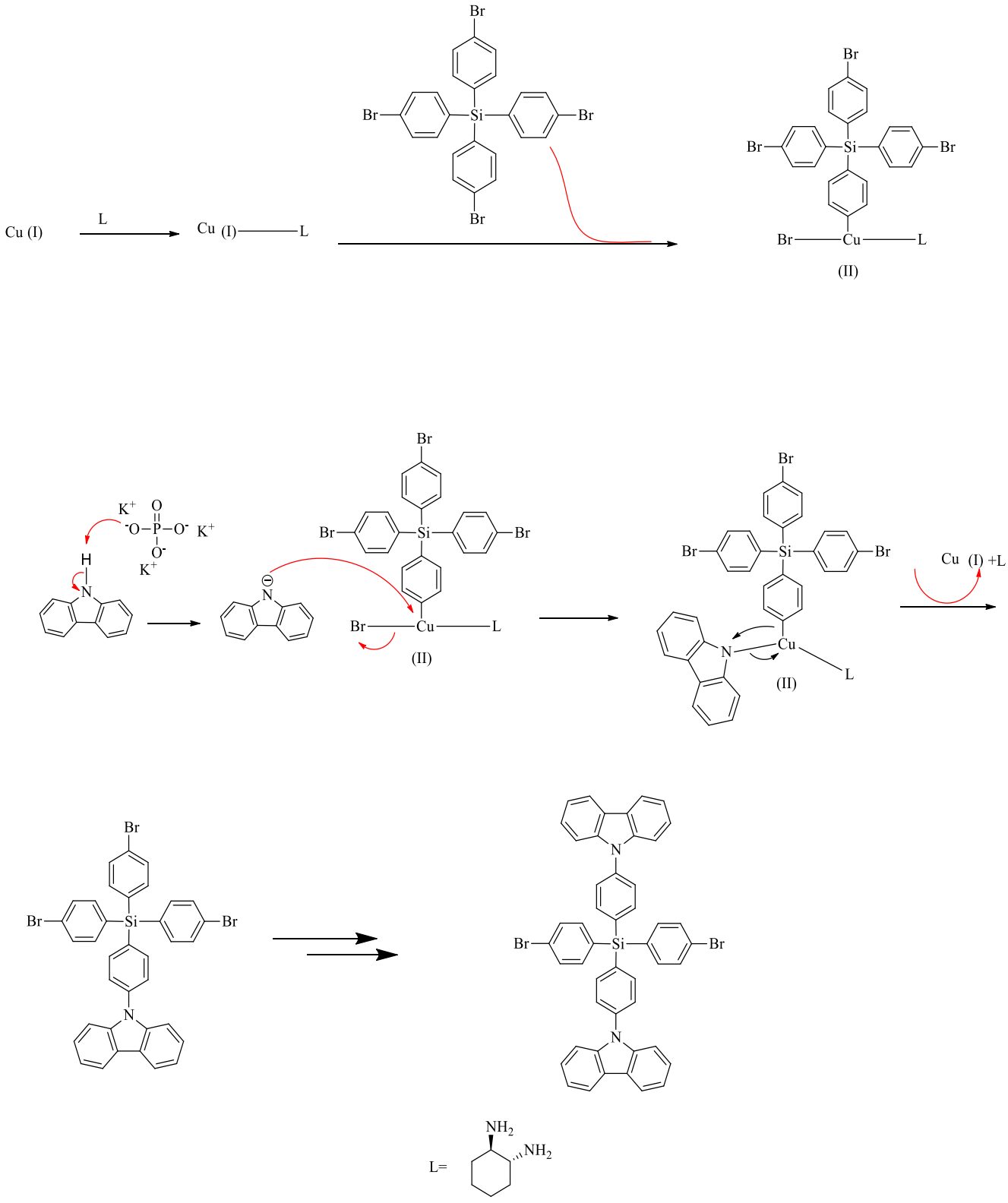

Scheme 2.8 Suggested mechanism for M1 synthesis

The target polymers in the first series in this chapter are also formed from M2 and M3. M2 is produced via a few steps using the procedure used by Hermann, Mathias, et al., and described in Scheme 2.9.[33]

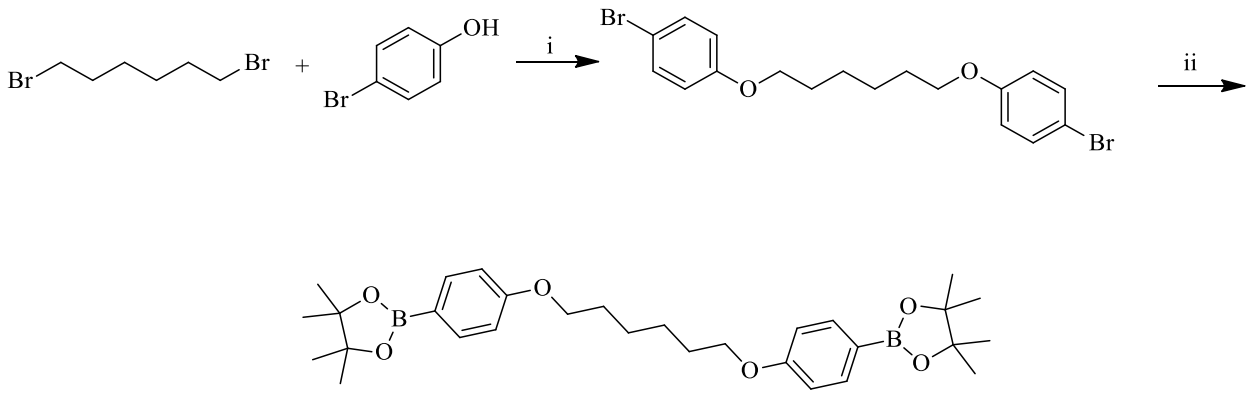

M2

Scheme 2.9 Synthetic route of (M2)

Reagents and conditions: i) K_2CO_3; DMF, 60°C, 2d; ii) n-Buli; i-PrOBpin, THF, -78°C 24h.

Column chromatography (SiO_2, petroleum ether/DCM 1:1 to 10:1) was used to purified the required compound (M2), a colourless solid finally was obtained with a 92 per cent yield. Proton and carbon NMR, mass spectrometry, and elemental analysis have confirmed the structure and purity of this compound. The ^1H NMR revealed a triplet peak at 4.01 ppm attributable to OCH_2 protons. (as shown in Figure 2.3).

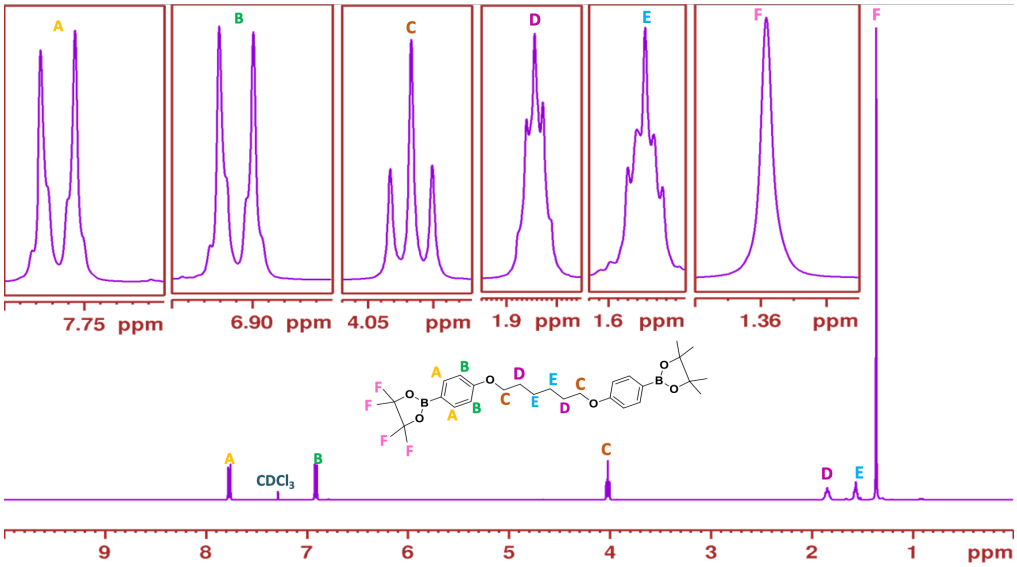

Figure 2.3 ^{1}H-NMR spectrum of (M2) in $CDCl_3$

1,6-Bis(4-bromophenoxy)hexane was prepared successfully according to the modified procedures described in the literature.[34] The ^{1}H NMR spectra of this substance displayed 4 protons in the aromatic region, whereas the hydroxyl group proton (at 5.33 ppm) vanished. Furthermore, the ^{13}C NMR spectrum of this product exhibited four peaks for four different carbons in the aromatic region and three peaks for three carbons of the n-hexyl chain in the aliphatic region. The proposed reaction mechanism of this product mainly involves two steps as illustrated in Scheme 2.10. It is based on the nucleophilic substitution (S_N2) mechanism. This type of mechanism commonly involves two steps: i) deprotonation of the hydroxyl group (OH) via a good base, such as potassium carbonate (k_2CO_3) to form a phenolate anion, ii) the generated ion then attacks the electrophilic 1,6-dibromohexane to produce the product 1,6-bis(4-bromophenoxy)hexane.

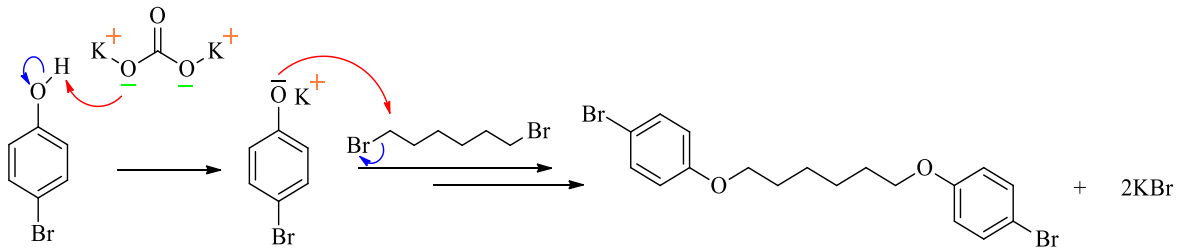

Scheme 2.10 Plausible mechanism for formation of compound (1)

After that, the second product, which is identified as M2, was successfully made using the procedure described by Hermann, Mathias, et al.[33] The final monomer (M2) was formed as a ghost-white solid with a 92% yield. It was purified via column chromatography and the final solid appears after recrystallisation in ethanol. The final structure was confirmed by all available analysis measurements. Mass spectrometry showed a major peak at m/z = 523 as expected. Furthermore, proton NMR displayed a large single peak at 1.34 ppm, which was assigned to 24 protons attached to the newly introduced pinacolato boron (Bpin) groups which were absent in the previous compound. The proposed mechanism for this reaction is illustrated in Scheme 2.11. In this mechanism, the intermediate product is formed after the lithiation of the starting material, which then attacks the i-PrOBpin to make the desired compound (M2).

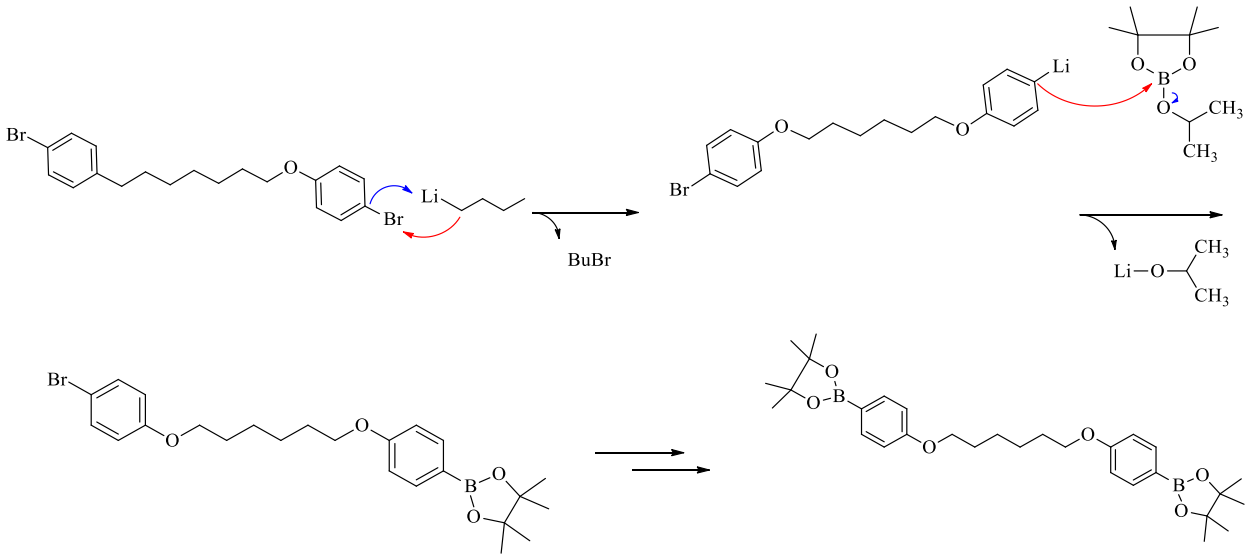

Scheme 2.11 Proposed mechanism for synthesising (M2)

In order to possess TADF character in the final polymers, the target polymers in this thesis, including those in this chapter, are required to possess TADF units in their design. Thus, M3, which includes a TADF moiety in its structure, was prepared in several steps, as will be explained in this chapter. Phenoxazine-2,4,6-triphenyl-1,3,5-triazine (PXZ-TRZ), which is known to be a good TADF emitter, was made and introduced as a pendant into M3. The synthetic path to this monomer began with acylation of 10-phenoxazine to generate functionalised PXZ-TRZ, which was finally coupled with the functionalised 9-H carbazole, as shown in Scheme 2.12.

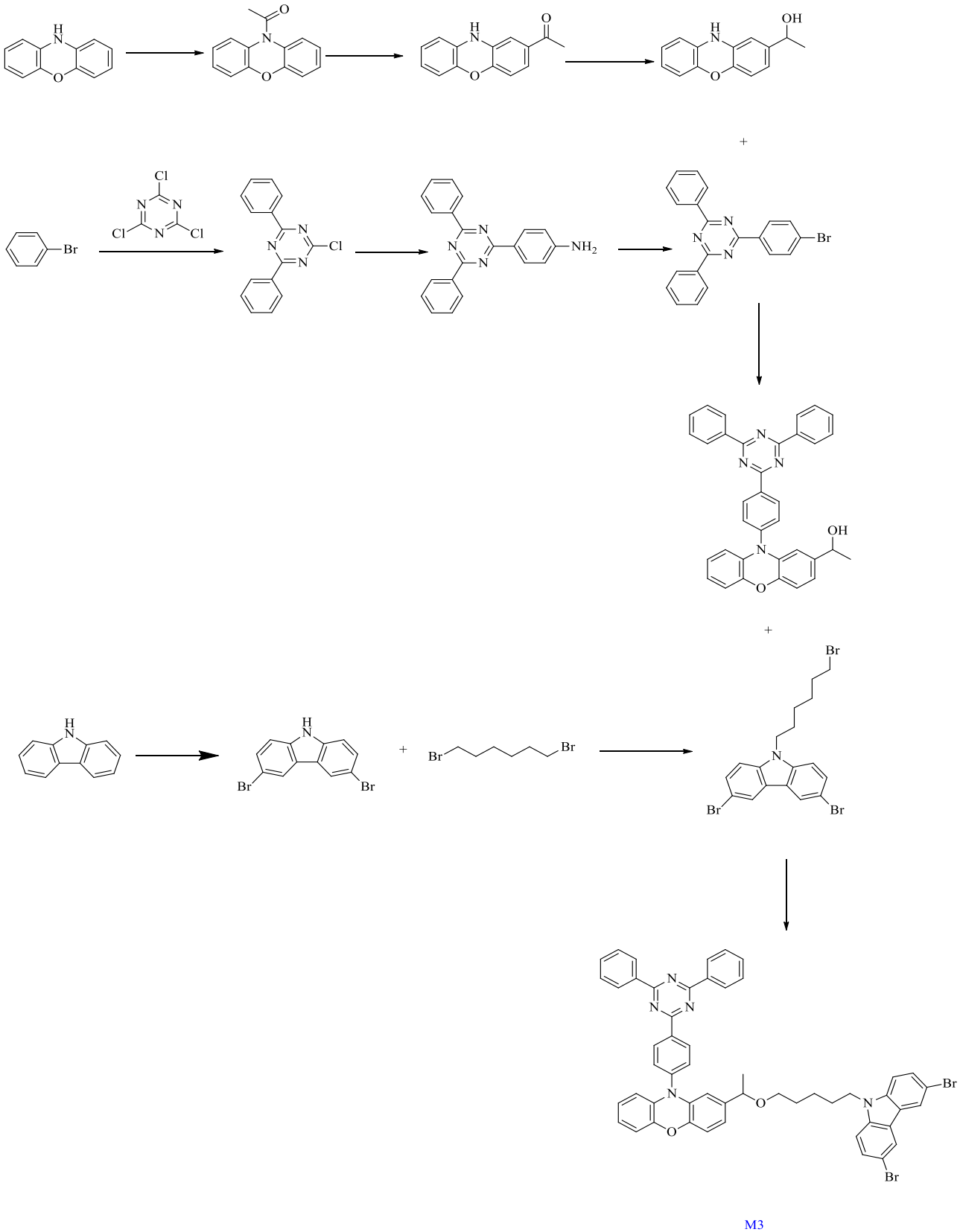

Scheme 2.12 Synthetic path to (M3)

The 1-(10H-phenoxazin-2-yl)-ethanol, which is labelled as compound (3) in Scheme 2.13, worked as a donor in the process of making the final monomer. The purity and structure of all compounds involved were verified via TLC, ^{1}H- NMR, ^{13}C-NMR, elemental analysis and mass spectrometry.

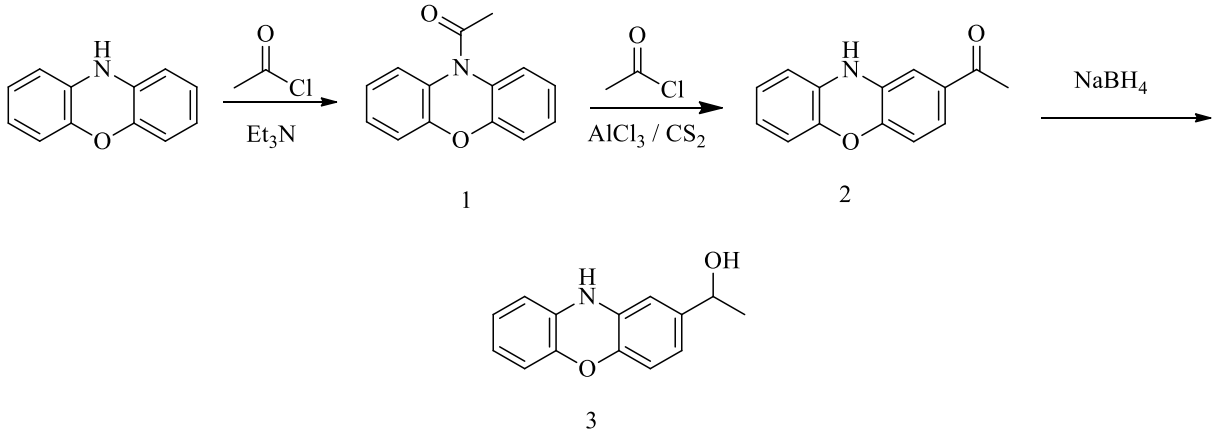

Scheme 2.13 Synthesis of 1-(10H-phenoxazin-2-yl)-ethanol

Compound (1) of monomer 3 was prepared as a light-white solid. The synthesis was carried out under dry conditions. After monitoring the reaction via TLC, de-ionised water and dichloromethane were used to extract the crude product. The purification of the compound was performed using column chromatography with silica as the stationary phase and a mixture of hexane and ethyl acetate (4:1) as the mobile phase. All results of the analytical measurements confirmed the structure and purity of the product. While the proton signal of N-H disappeared in ^{1}H NMR, a new singlet peak showed at 2.37 ppm, which corresponded to the new acetyl group. All other analytical results, such as mass spectrometry and elemental analysis, displayed good agreement with the literature. The mechanism of this reaction involves three steps. First, the lone pair of nitrogen on the amine group of phenoxazine acts as nucleophiles that attack the carbon of acetyl chloride. The second step is the elimination step in which a double bond is formed between the carbon and oxygen and the chlorine ion is given off. Lastly, the hydrogen is eliminated by triethylamine to finally form the product. Scheme 2.14 below shows the possible mechanism involved in preparing the product (1).

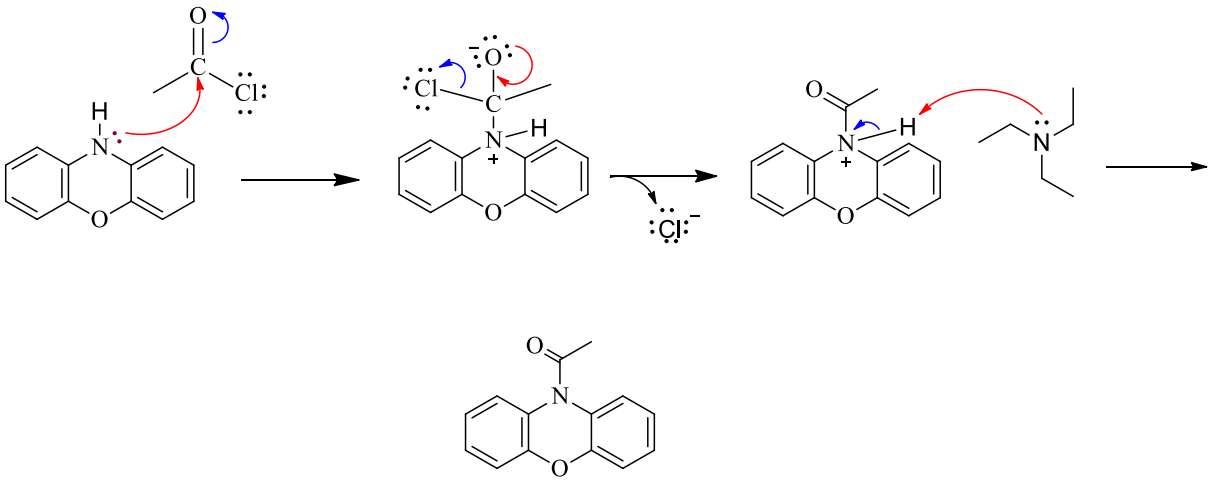

Scheme 2.14 Possible mechanism to prepare compound (1) of M3.

The second substance, 2-actetylphenoxazine labelled as (2) in Scheme 2.13, was made successfully following Vanderhaeghe's procedure; the suggested mechanism for this reaction is explained in Scheme 2.15.[35] The obtained product has a light green colour, and the crude product is purified firstly by extraction many times using DCM and water. The final desired substance was produced with 85% yield after precipitating the crude in ice methanol. In proton NMR spectra, singlet peaks are presented at 2.46 ppm and a broad singlet at 8.44 ppm, which represent the protons attached to the carbon bonded to the carbonyl group, and to the proton attached to the nitrogen atom in the phenoxazine respectively. The mass spectrum showed a large single peak at m/z 225 which was in total agreement with the proposed structure. The reaction mechanism underwent the Friedel-Crafts acylation and the final product was formed after hydrolysis. The first step of Friedel-Crafts acylation is using aluminium trichloride ($AlCl_3$) as a Lewis acid catalyst to react with acetyl chloride (CH_3COCl), forming a more electrophilic carbon (acylium ion). After that, the electrophilic carbon (C+) is attacked by the nucleophile that had formed previously at the para position of the aromatic carbon-carbon bond (C=C). Thus, the system of aromaticity breaks at this stage, forming an intermediate cation (cyclohexadienyl). In the end, the carbon=carbon aromaticity system is reformed together with reproducing the active catalyst via removing (H^+) from the sp^3 carbon adjacent to the acyl group and making HCl. The Fridel-craft acylation is followed by acid-catalyzed amide hydrolysis to finally produce the required product. The suggested mechanism for this reaction is described in Scheme 2.15.

A- Fridel-craft acylation

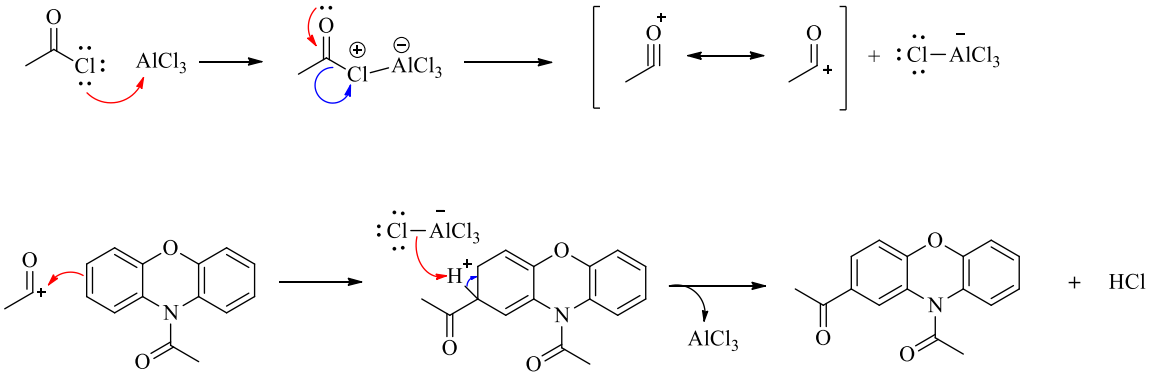

B- Hydrolysis of Amide

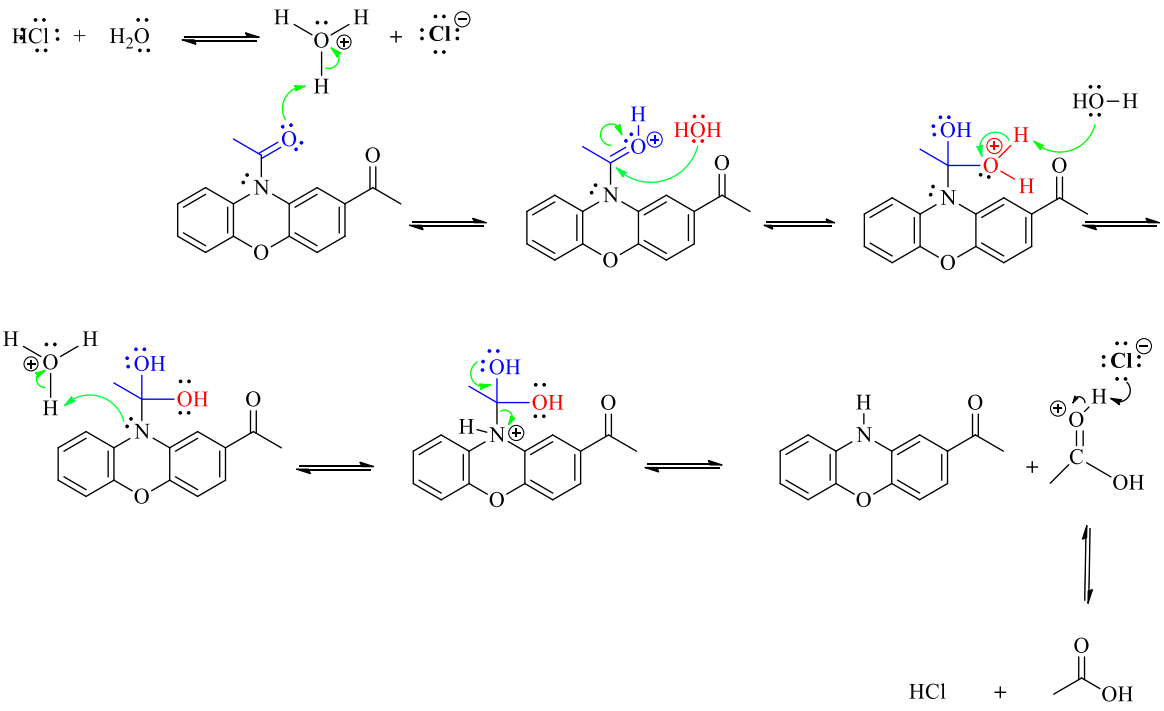

Scheme 2.15 Suggested mechanism to make product (2).

The last step is finally forming 1-(10H-phenoxazin-2-yl)-ethanol product (3). It was made successfully according to a modified method of Vanderhaeghe illustrated in Scheme 2.16.[35] The final pure product was obtained after recrystallising the resultant crude in a mixture of petroleum ether and toluene to give an off-white molecule with a 73% yield. The product showed only one spot in TLC, which indicates the removal of all side products. Other analyses such as ^{1}H NMR and mass spectrometry, were then used to identify the structure and purity of the product. The proton of the hydroxyl group displayed a broad singlet peak at 4.18 ppm in

^{1}H NMR. It is worth noting that the broad peak here is due to fast NMR proton exchange between the OH proton and the solvent proton.

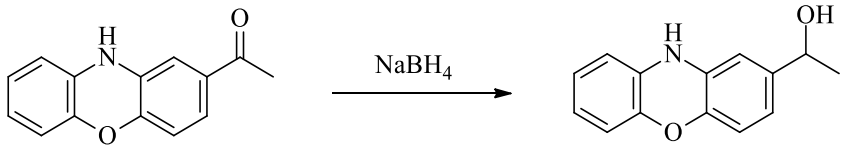

Scheme 2.16 The preparation of compound (3)

The mechanism of this reaction includes two different steps (addition and protonation) as shown in Scheme 2.17. The addition of the hydrogen occurs in the first step, as it detaches from the borohydride (BH_4^-) and moves to the carbonyl carbon in compound (2). Therefore, a carbon-hydrogen bond forms and a new lone pair on the oxygen is generated, which makes a negatively charged intermediate product. In the following step, the proton from the water is added to the intermediate to produce the desired alcohol.

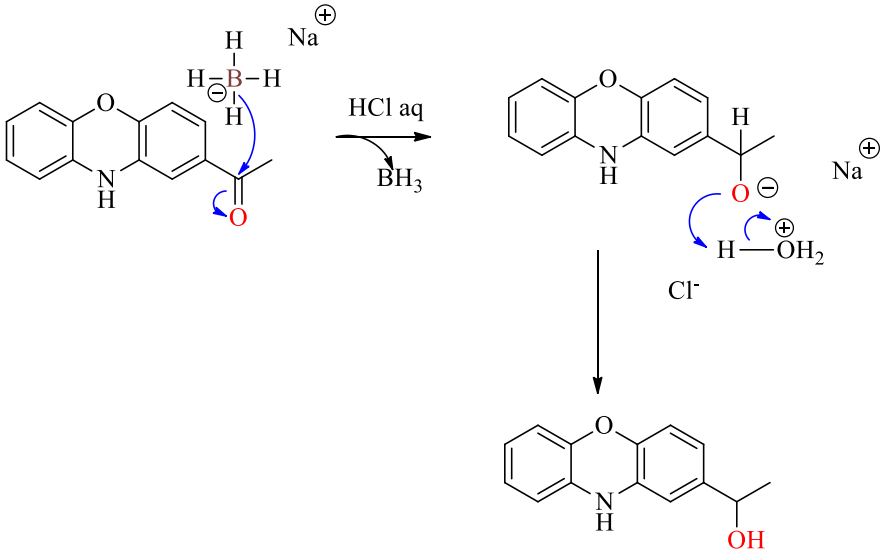

Scheme 2.17 The proposed reduction mechanism of 2-actetylphenoxazine

The preparation steps for the production of the 2-bromo-4,6-diphenyl-1,3,5-triazine labelled as compound (6), which coupled with 1-(10H-phenoxazin-2-yl)-ethanol (3), is illustrated in Scheme 2.18.

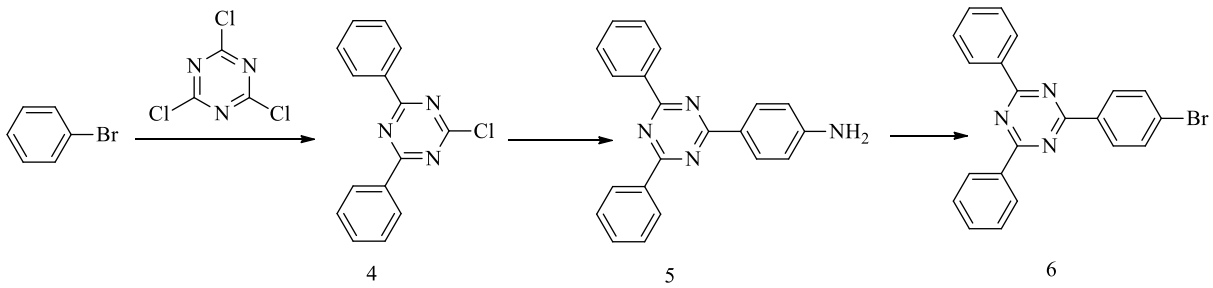

Scheme 2.18 The synthetic route to produce compound (6)

Compound (4) was obtained starting from 1-bromo benzene by following the procedure described by Liu et al.[36] The 2-chloro-4,6-diphenyl-1,3,5-triazine was obtained as a white solid with a yield of 70%. The final product gave only a single spot on the TLC indicating the purity of the product. Furthermore, elemental analysis and mass spectrometry verified the purity of the desired compound. The elemental analysis of this product (4) matches its proposed structure and gives the following result: C,67.51; N 15.73; H, 3.98. The main integer mass appeared at m/z 266.2, which gave further agreement with the expected structure. ^{1}H NMR and ^{13}C NMR were also applied to confirm the final structure of this compound. The ^{13}C NMR exhibited intense peaks at 173.6 ppm and 172.4 ppm, which is assigned to the carbons bonded between two nitrogen atoms and phenyl(ipso carbon to phenyl ring), and between two nitrogen atoms and chloride (ipso carbon to Cl) respectively. A plausible reaction mechanism is that of the Grignard mechanism, which consists of two steps, as shown in Scheme 2.19. Magnesium turning is used in the first step to react with bromo benzene to produce the Grignard reagent (phenyl magnesium bromide) forming very polar center. The intermediate reagent then attacks the 2,4,6-trichloro-1,3,5-triazine to yield the required product (4).

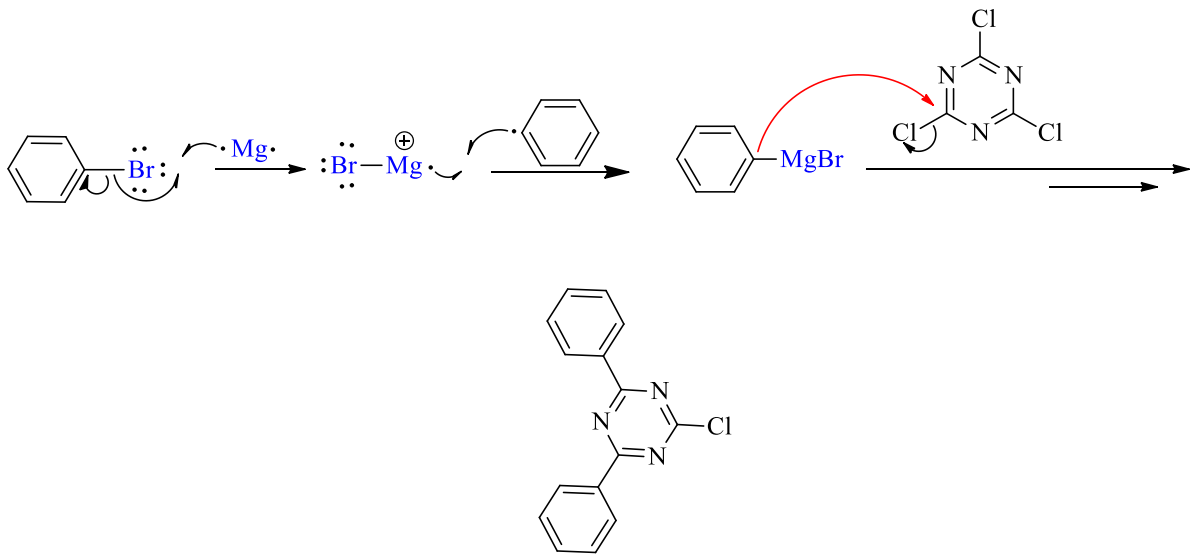

Scheme 2.19 Proposed mechanism to form product (4)

The next step toward M3 was making compound (5) from 2-chloro-4,6-diphenyl-1,3,5-triazine. It was synthesised according to a modified version of the procedure used by Tanaka et al.[37] 2-Amino-4,6-diphenyl-1,3,5-triazine (5) was obtained as a yellowish-brown solid, with a yield of 73%. The reaction was carried out between 2-chloro-4,6-diphenyl-1,3,5-triazine and 4-aminophenylboronic acid pinacol ester in dry conditions in the presence of a palladium catalyst, as shown in Scheme 2.20.

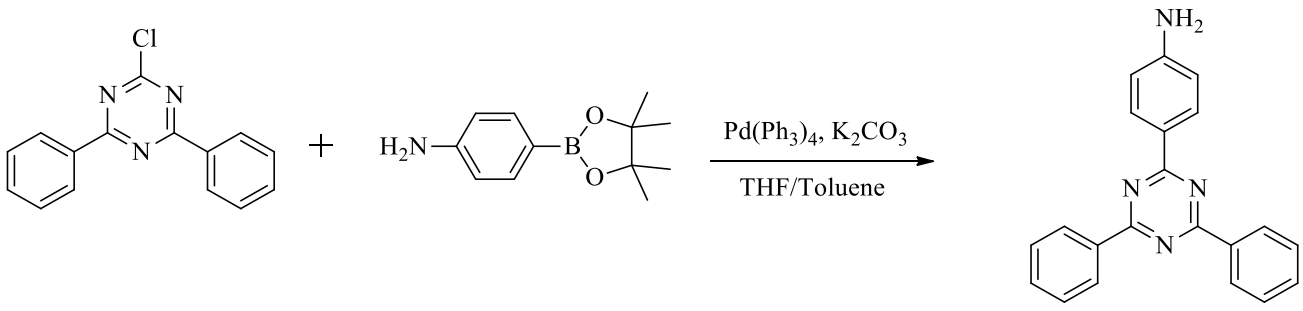

4 5

Scheme 2.20 Preparation of 2-amino-4,6-diphenyl-1,3,5-triazine.

The reaction was monitored using TLC. When the new spot became very dark under UV light, the reaction was stopped using deionised water, which was followed by crude extraction with dichloromethane three times. The crude product was purified via precipitating in methanol after it went through basic alumina to get rid of the acidic protons. The mass spectrometry and

elemental analysis also verified the purity of the compound (5). The ^{1}H NMR showed a distinctive broad singlet peak at 4.16 ppm, which was not present in compound (4) assigned to protons of NH_2. The reaction mechanism for this follows the Suzuki cross-coupling reaction that was described in Chapter 1.

In the next step, 2-(4-bromophenyl)-4,6-diphenyl-1,3,5-triazine (compound (6)), was prepared from the previous product (5). This molecule was made following the procedure carried out by Tanaka et.al.[37] The preparation route and the reagents used are shown in Scheme 2.21.

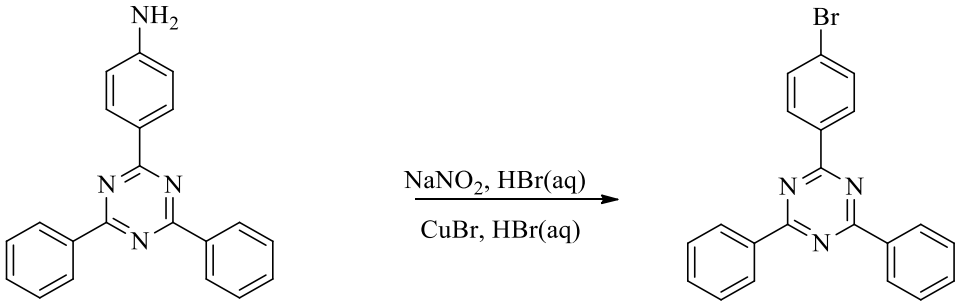

5 6

Scheme 2.21 Synthesis of 2-(4-bromophenyl)-4,6-diphenyl-1,3,5-triazine (6).

A white solid material was obtained with a yield of 52% after purifying the crude product using column chromatography (eluent: DCM/ PE 2:5). The TLC displayed only one spot, which assured the presence of only one product. Thus, both NMRs, elemental analysis and mass spectrometry were performed to confirm the structure and the purity of the resulting substance. All these analyses showed a good match with the literature. The first indication came from the ^{1}H NMR, where the peak of NH_2 protons (4.16 ppm) of the starting material (5) disappeared, and the aromatic peaks showed a downfield shift compared with those in the compound (5). The mass spectrometry and elemental analysis results verified the proposed structure of the desired product.The elemental analysis of compound (6) matches its proposed structure and gives the following result: C,74.42; N 15.71; H, 4.93.The suggested mechanism for this reaction is according to Sandmeyer and is shown in Scheme 2.22. It generally consists of four steps. The bromine ion and nitrosonium are generated during the reaction between hydrobromic acid and sodium nitrite, in which two protonations occur. In the second stage, the electrophilic nitrosonium converts the amine to salt (diazonium). After that, the oxidation number of Cu increases to 2, as the single electron migrates from it towards the diazonium salt,

to create a diazo radical, and from the bromide to Cu(I)Br ion to form Cu(II)Br. The desired compound is formed in the last stage, where the diazo radical releases nitrogen gas, resulting in the formation of a radical that reacts with Cu(II)Br to remake the copper (Cu(I)) and form the final product.

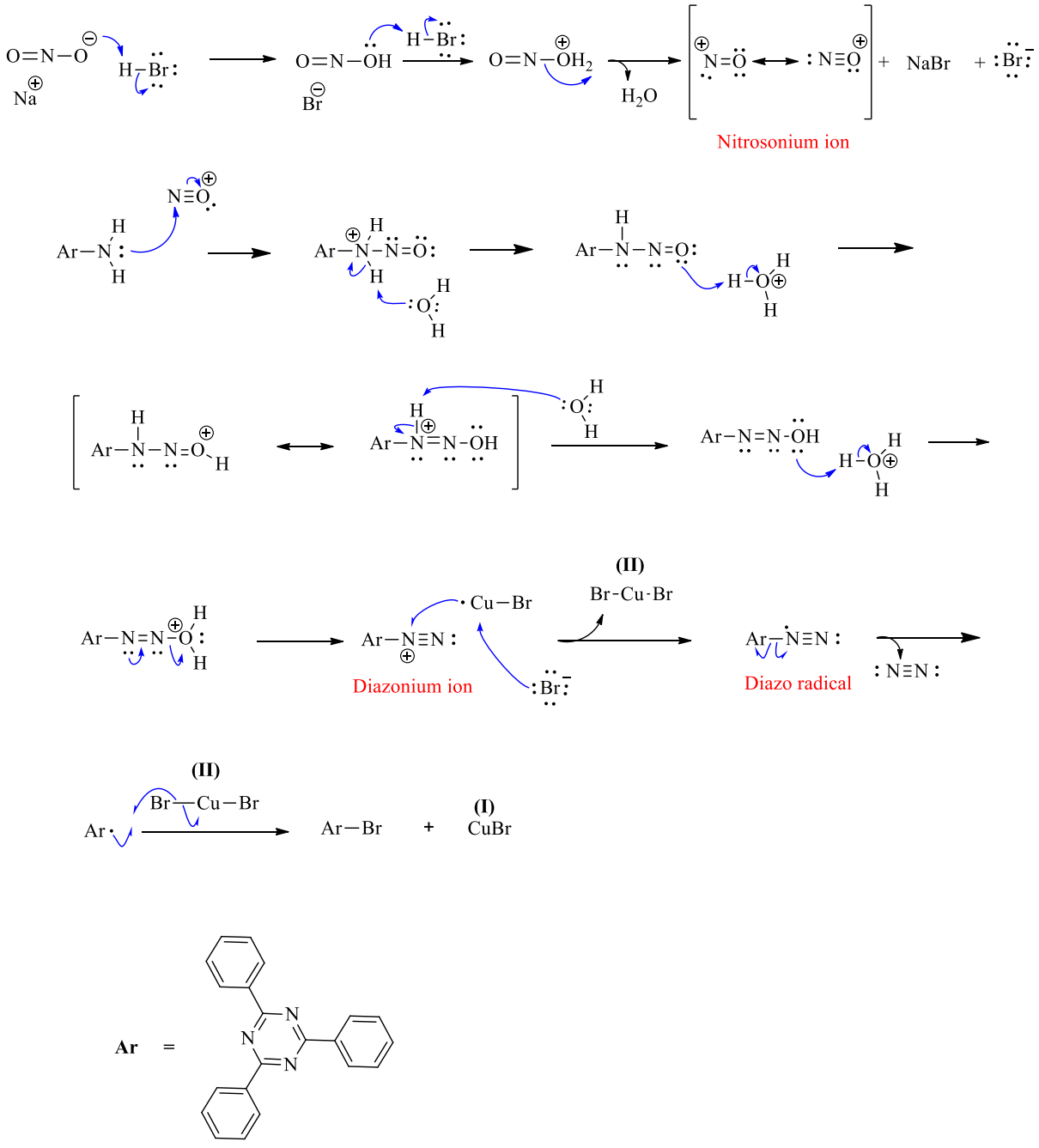

Scheme 2.22 Proposed Sandmeyer mechanism to synthesise product (6)

The next step featured a coupling reaction between product 6 and 1-(10H-phenoxazin-2-yl)-ethanol, to form a functionalised TADF moiety (7) as presented in Scheme 2.23. The formed compound was made following a modified version of that used by Tanaka et.al.[37]

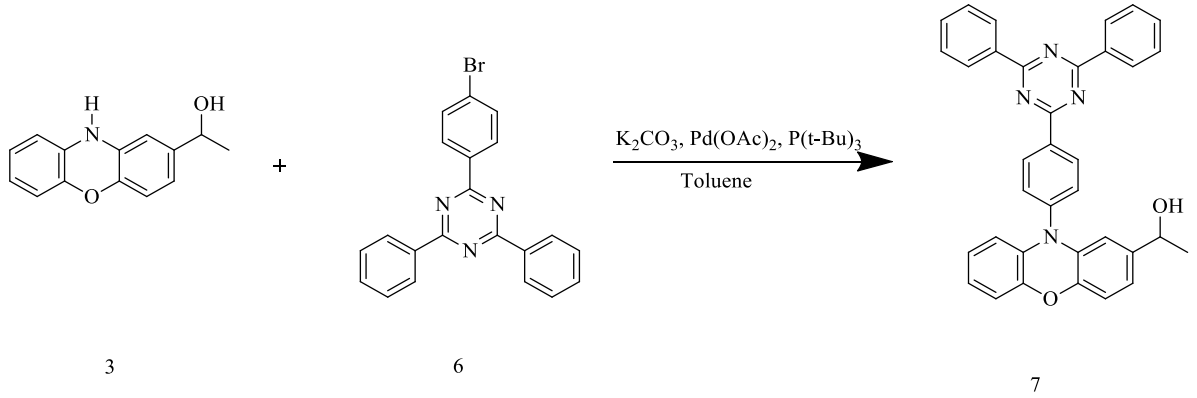

3 6 7

Scheme 2.23 Preparation of functionalised TADF moiety

The product is a result of the coupling reaction between carbon and nitrogen in the presence of potassium carbonate (K_2CO_3) as a base, palladium acetate ($Pd(OAc)_2$) as a catalyst and tri-tert-butyl-phosphine ($P(t\text{-}Bu)_3$) as an efficient ligand. The appearance of the final product was a light yellowish solid and was afforded after purifying the dark crude product by column chromatography using hexane, ethyl acetate, and methanol 4:1:1 as eluent. The ^{1}H NMR and ^{13}C NMR identified the structure of the resulting molecule. The peak for the proton N-H, which was displayed at 8.15 ppm in the starting material, had disappeared from the product ^{1}H NMR. In addition, the downfield shift can be seen between 6.75 ppm and 6.02 ppm which was understood to be protons associated with the ring system of phenoxazine, and these peaks could be observed in the spectrum for compound (3). Elemental analysis of this product (7) shows the following results: C,78.66: H, 5.05: N, 9.85. These results together with other analyses, provide strong confirmation that the desired product had been synthesised successfully. The reaction follows the Buchwald-Hartwig cross-coupling mechanism, as illustrated in Scheme 2.24. It is based on the palladium catalytic cycle, which involves multiple steps, starting with the alteration of the palladium oxidation state, followed by the oxidative addition of compound 6 to Pd. Compound (3) was then added to the oxidative complex. Finally, deprotonation took place, and the product was formed after reductive elimination.

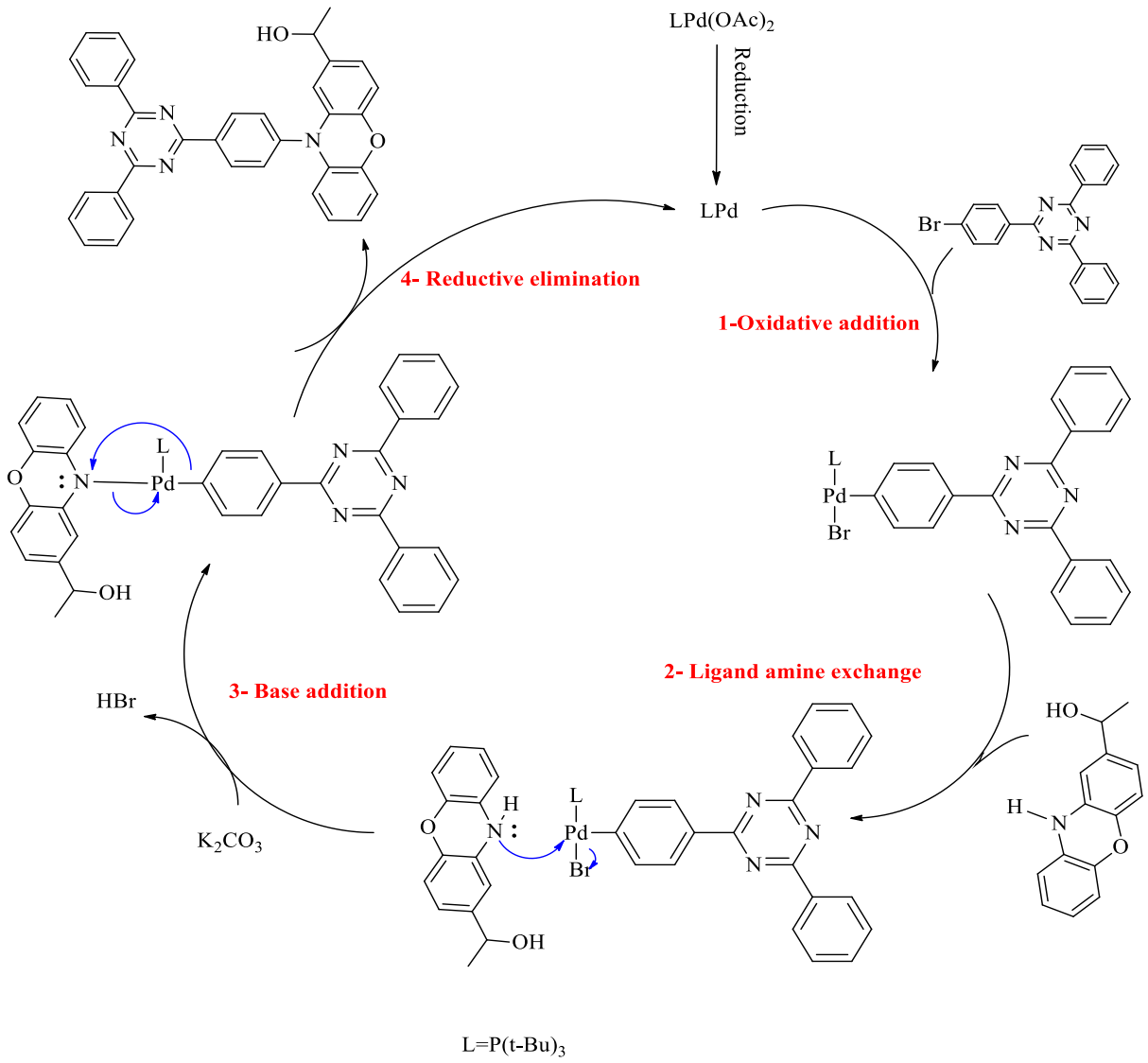

Scheme 2.24 Proposed mechanism route to compound 7.

The route to the third monomer continued by producing 3,6-dibromo-9-(6-bromohexyl)-9H-carbazole that started from commercially available 9-H-carbazole. The product was used to couple with compound 7, forming the M3. However, making the desired product involves two steps as described in Scheme 2.25. Firstly, N-bromosuccinimide (NBS) reacted with the carbazole to form 3,6-dibromo-9-H-carbazole, which was deprotonated to add the 1,6-dibromhexane.

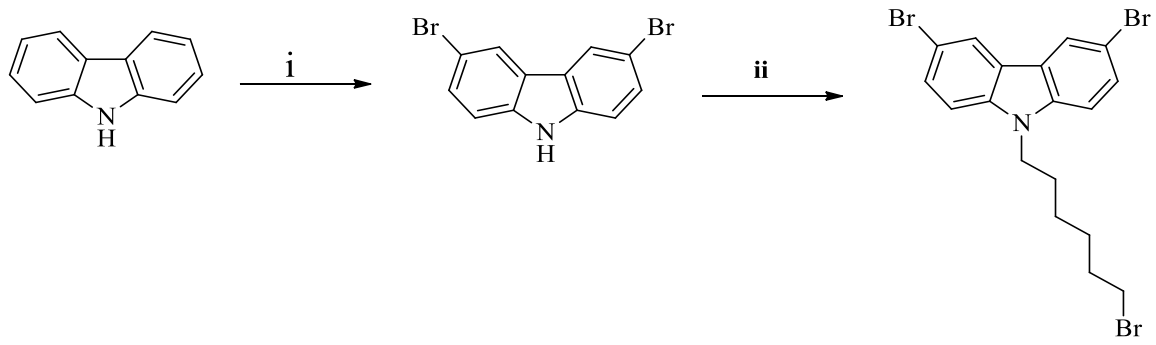

8 **9**

Scheme 2.25 Synthesis steps to 3,6-dibromo-9-(6-bromohexyl)-9H-carbazole

Reagents and conditions: i) NBS, Toluene, DMF, 0°C, 24h; ii) 1,6-dibromohexane, KOH, DMF, 60°C, 48h

Product 8 was successfully prepared with a very high yield (91%) in accordance with a modified procedure described by Feng et al.[38] The synthesis was carried out carefully under dry conditions using argon and non-oxidised solvents. It was also performed in a dark environment to avoid bromine radicals that might form due to light. The reaction was kept for a longer time to increase the product yield, which had been monitored via TLC. It stopped when only a very light spot of starting materials was presented in TLC. Although this reaction gave the required product at a very good yield, a small amount of side product appeared in the crude product, which turned out to be the 3-bromo-9H-carbazole. However, purification was performed using a flash column with PE and DCM as eluents, followed by recrystallisation in a mixture of 3:12 hexane: methanol to obtain white crystals. The structure and purity of the final product were identified by ^{1}H NMR, ^{13}C NMR, mass spectrometry and elemental analysis, which revealed the expected spectrum for the proposed structure. The aromatic protons in the carbazole ring showed at 7.46 ppm and 8.42 ppm in NMR spectra, and the proton of N-H in the carbazole ring also displayed a broad singlet peak at 11.57 ppm. Furthermore, the mass spectrometry spectra showed three peaks at m/z 322, 324 and 326, which can be attributed to the bromine isotopes ^{79}Br and ^{81}Br. N-Bromosuccinimide (NBS) was used in this reaction as a bromine source. It was used for bromination due to the low concentration of Br compared with Br_2. Therefore, reducing the possibility of bromination of double bonds. The mechanism of this reaction is an electrophilic aromatic substitution. The three and six position of the carbazole ring is extremely nucleophilic due to the carbazole's resonance effect, which results in an attack of the electrophilic Br of NBS. The succinimide anion then removes the proton on

the 9H-carbazole ring to generate the brominated ring. The process is repeated for another proton to produce the final product (8). A possible mechanism for this reaction is shown in Scheme 2.26.

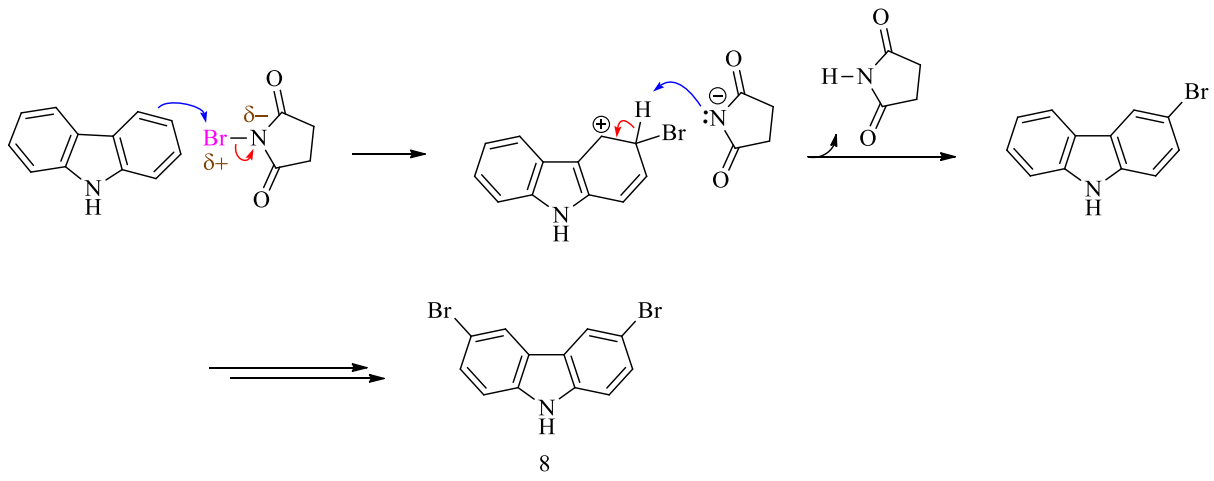

Scheme 2.26 Possible mechanism to prepare compound (8)

The next product 3,6-dibromo-9-(6-bromohexyl)-9H-carbazole (9) was made using a modified procedure that is described by Liu et al.[39] The bromo-alkylation was carried out at moderate temperature (60°C) in the presence of dry dimethylformamide (DMF) as a solvent and an excess of anhydrous potassium hydroxide (KOH) to force the deprotonation to take place. The compound was formed as a white solid, with a yield of 58% after recrystallisation from methyl alcohol. The desired product displayed only a single spot-on TLC. Then GC-MS was performed to confirm the purity of this substance, which in fact showed a peak at m/z 487.2 that matches the expected calculation for the proposed structure. In addition, ^{1}H NMR exhibited two essential indications, i); new peaks in aliphatic regions, which were assigned to the proton of the attached bromohexane; ii) disappearance of the proton peak of N-H at 11.57 ppm. All these analysis results confirmed the successful preparation of 3,6-dibromo-9-(6-bromohexyl)-9H-carbazole. The reaction follows the nucleophilic substitution mechanism (S_N2)This method involves two steps as demonstrated in Scheme 2.27. In the first step, a good base, such as a KOH, is introduced to deprotonate the amine group to generate the anion. This then attacks the 1,6-dibromohexane, as a nucleophile, to yield the required compound (9).

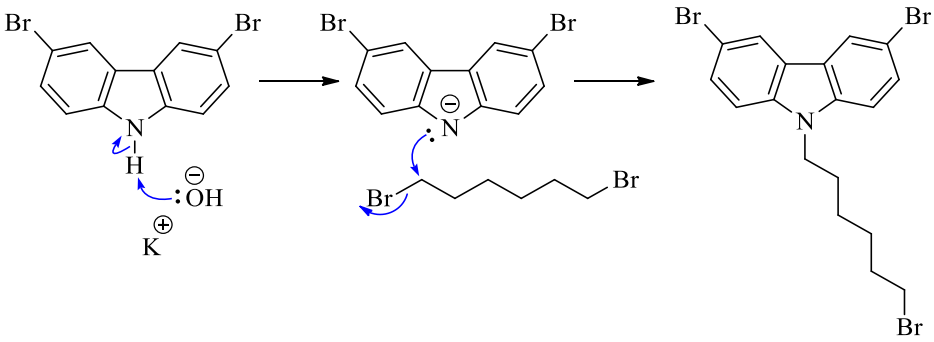

Scheme 2.27 The proposed SN^2 mechanism to synthesise compound (9)

The final step was making M3, which is a result of the reaction between compound 9 and product 7 that possess TADF features. The synthesis steps were similar to the one used to make 3,6-dibromo-9-(6-bromohexyl)-9H-carbazole. Scheme 2.28 describes the reaction and shows the conditions and reagents.

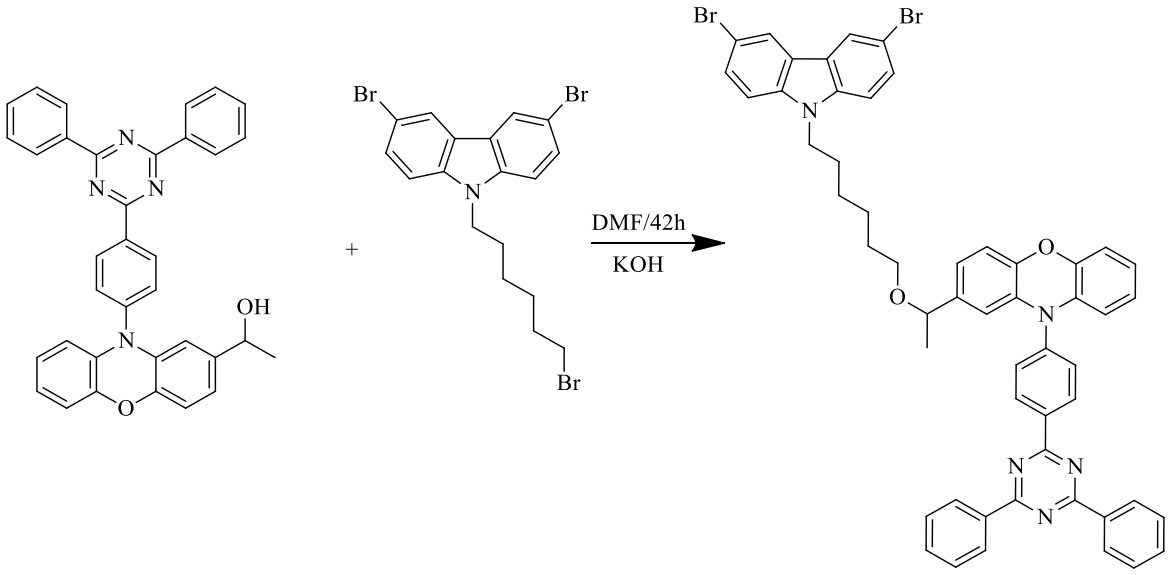

Scheme 2.28 The last synthesis step to M3

The reaction was stopped, and deionised water was used for workup, followed by extraction using ethyl acetate. The crude displayed three spots on TLC; thus, column chromatography with petroleum ether and ethyl acetate (10:1-10:4) as eluents was used to collect the product spot. The final pure monomer was then obtained as a yellow solid with a 40% yield. The purity of M3 was confirmed by ^{1}H NMR. It showed the six protons of the aromatic carbazole as a doublet at 8.02 ppm, a doublet of doublet at 7.40 ppm and a doublet at 7.12ppm. Based on the proton NMR studies for the product and starting materials, ^{1}H NMR of the product displayed

no signal at 4.22 ppm, which represents the proton of OH in the starting material. It also exhibited the expected number of protons in aliphatic regions as shown in figure 2.4. These NMR results, together with elemental analysis and mass spectrometry, which all offer considerable agreement with the proposed monomer structure, are substantial evidence that the M3 was prepared successfully. The reaction undergoes a nucleophilic substitution, which was explained in the synthesis of compound 9.

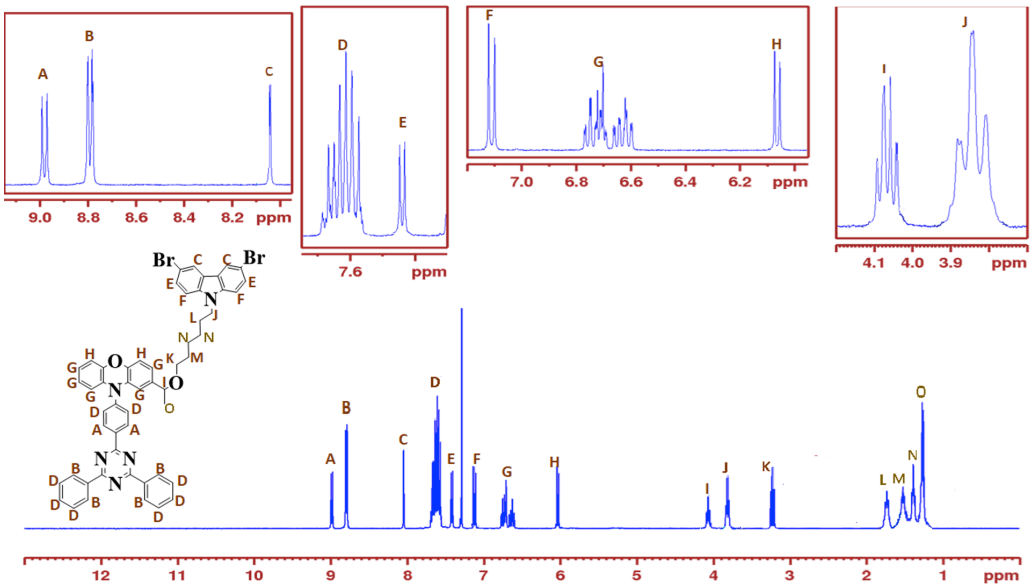

Figure 2. 4 ^{1}HNMR spectra of M3 in $CDCl_3$.

The next monomer (M4) was synthesised and derived from Br-SiCz-Br (M1) as depicted in Scheme 2.29.

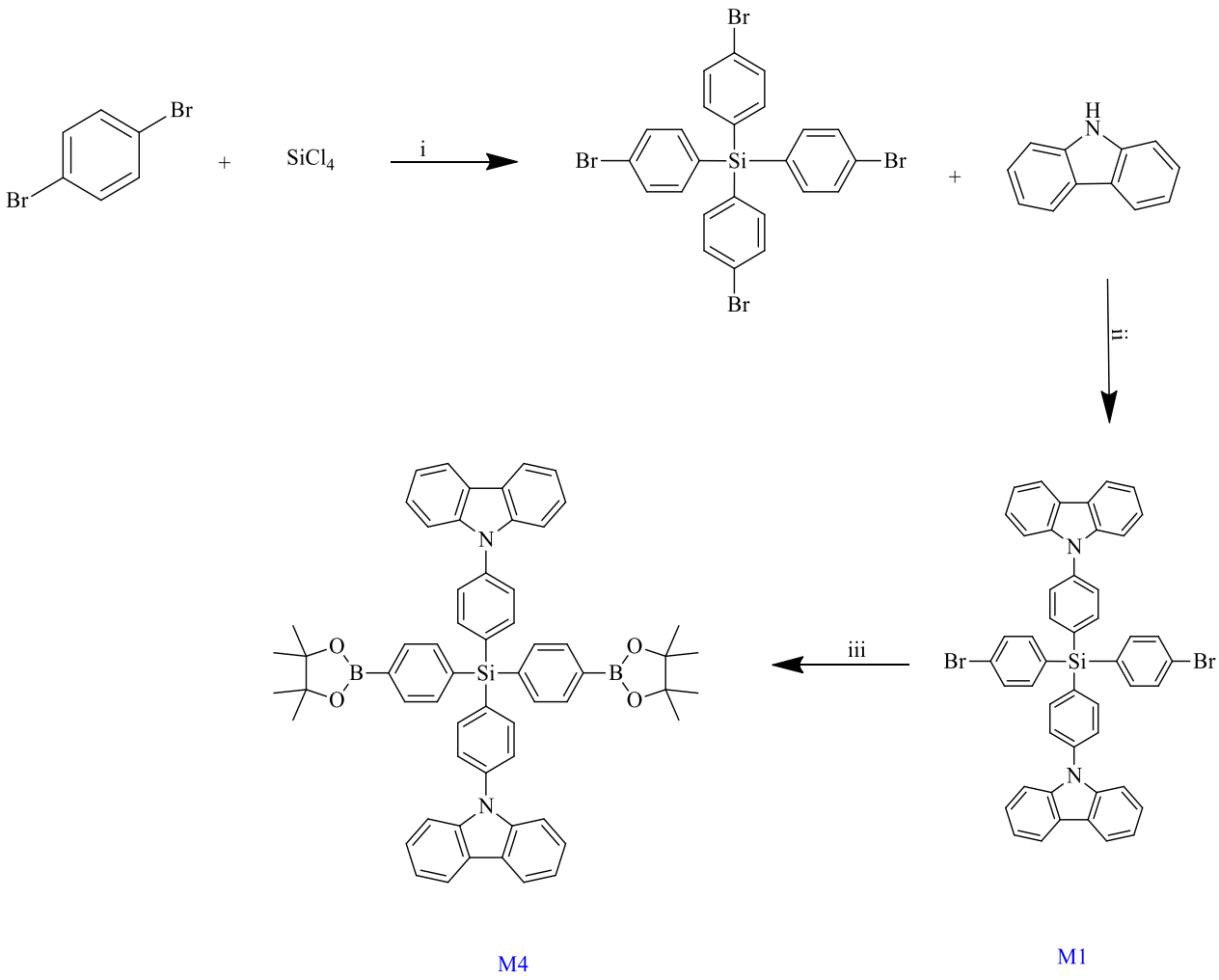

Scheme 2.29 The synthetic route of M4.

Reagents and Conditions: i) n-Buli, THF, -78°C, 24h; ii) K_3PO_4, CuI, trans-diaminocyclohexane, toluene, 110°C, 1d; iii) bis(pinacolato)diboron, KOAc, $Pd(dppf)Cl_2$, DMF, 100°C, 2d.

The reaction route to this monomer and the compounds involved are similar to those for the first monomer, which were described earlier in this chapter. However, bis(4-(9H-carbazol-9-yl)phenyl)bis(4-bromophenyl)silane (M1) reacted with bis(pinacolato)diboron according to a modified procedure used by Mathias et al to form the desired product.[40] The crude product formed a light brown oily substance, which was purified by precipitation in methyl alcohol and then passed through basic alumina to eliminate the acidic protons. The final pure product had a white solid appearance with a 55% yield. The purity was confirmed via ^{1}H NMR, ^{13}C NMR, elemental analysis and mass spectrometry. Mass spectrometry confirmed the purity of the product and gave three peaks at m/z 919, 920 and 921, which can be expected because of the

boron isotopes, B^{10} and B^{11}. ^{1}H NMR displayed a singlet peak at 1.34 ppm (Figure 2.5), which is assigned to the protons of the methyl groups attached to the boronic ester. The ^{13}C NMR spectrum of M4 shows sixteen peaks for 16 chemically different environments of carbons in which two of them displayed in the aliphatic region. These results indicate that the boronic ester product had formed from the brominated molecule (M1).

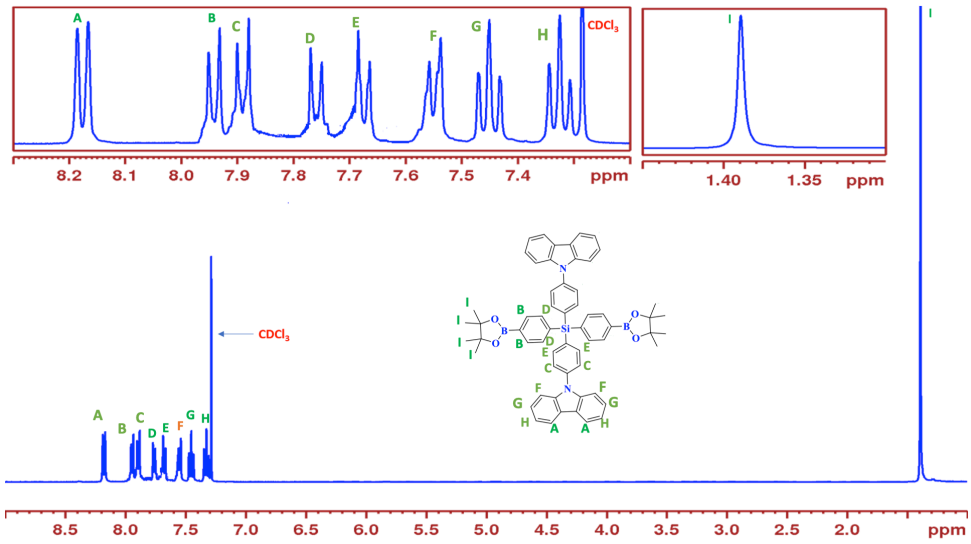

Figure 2. 5 ^{1}H-NMR spectrum of (M4) in $CDCl_3$.

The mechanism of this reaction follows the Suzuki-Miyaura coupling mechanism, which was described in Chapter 1.

2.2.2 Synthesis of TADF Copolymers

As shown in Schemes 2.30 and 2.31, TADF polymers P1-P4 and P5-P8 were successfully made using Suzuki polycondensation (SPC) of M1, M2 and M3 for P1-P4, and M1, M4 and M3 for P5, P6, P7 and P8. These polymers were made with different molar feed ratios, P1 (1:1:0), P2 (0.9:1:0.1), P3 (0.8:1:0.2) and P4 (0.6:1:0.4). Similarly, P5 (1:1:0), P6 (0.9:1:0.0.1), P7 (0.8:1:0.2) and P8 (0.6:1:0.4). It is worth pointing out that all polymers include TADF moiety in their chemical structures except polymer 1 and polymer 5, which for comparison purposes, were made without TADF monomer. The Suzuki polymerisation of prepared monomers all took place at 85°C using $NaHCO_3$ as a base and THF as solvent. The reaction relies on the catalysts palladium acetate ($Pd(OAc)_2$) and tris(*o*-tolyl)phosphine ($P(o\text{-}tol)_3$) with catalyst ratio of 1:2. The duration for full polymerisation is different from one polymer to another, according to the formed precipitates in the reaction flask. The first two polymers were stopped after 30

hours, as the produced precipitant's part were larger than the soluble part at the bottom of the reaction round flask. All other polymers were left for longer, with the time ranging between 48 hours and 80 hours. All polymerisations underwent the Suzuki cross-coupling mechanism, which was explored in Chapter 1.

All polymerisation reactions were stopped by adding bromobenzene and then phenyl boronic acid to end cap the reaction solutions. It is an important step to optimise the TADF polymers' solubility during the manufacturing of devices. The end-capping processing was carried out at high temperatures for 4 h. After that, polymers were transferred to a solution of chloroform, left under stirring followed by washing in a solution of NH_4OH to eliminate any remaining traces of Pd catalyst, which could negatively impact the efficiency of TADF devices.[41,42]

The polymers needed to be purified to remove all impurities and other side products including oligomers, small molecules and unreacted monomers. Thus, the polymers were purified and separated into fractions using the Soxhlet extraction technique with various solvents, including acetone, hexane and methyl alcohol to remove low molecular weight polymers and small molecules. In addition to the mentioned solvents, the polymers were purified further using toluene and chloroform; finally, they were precipitated in methanol.

.

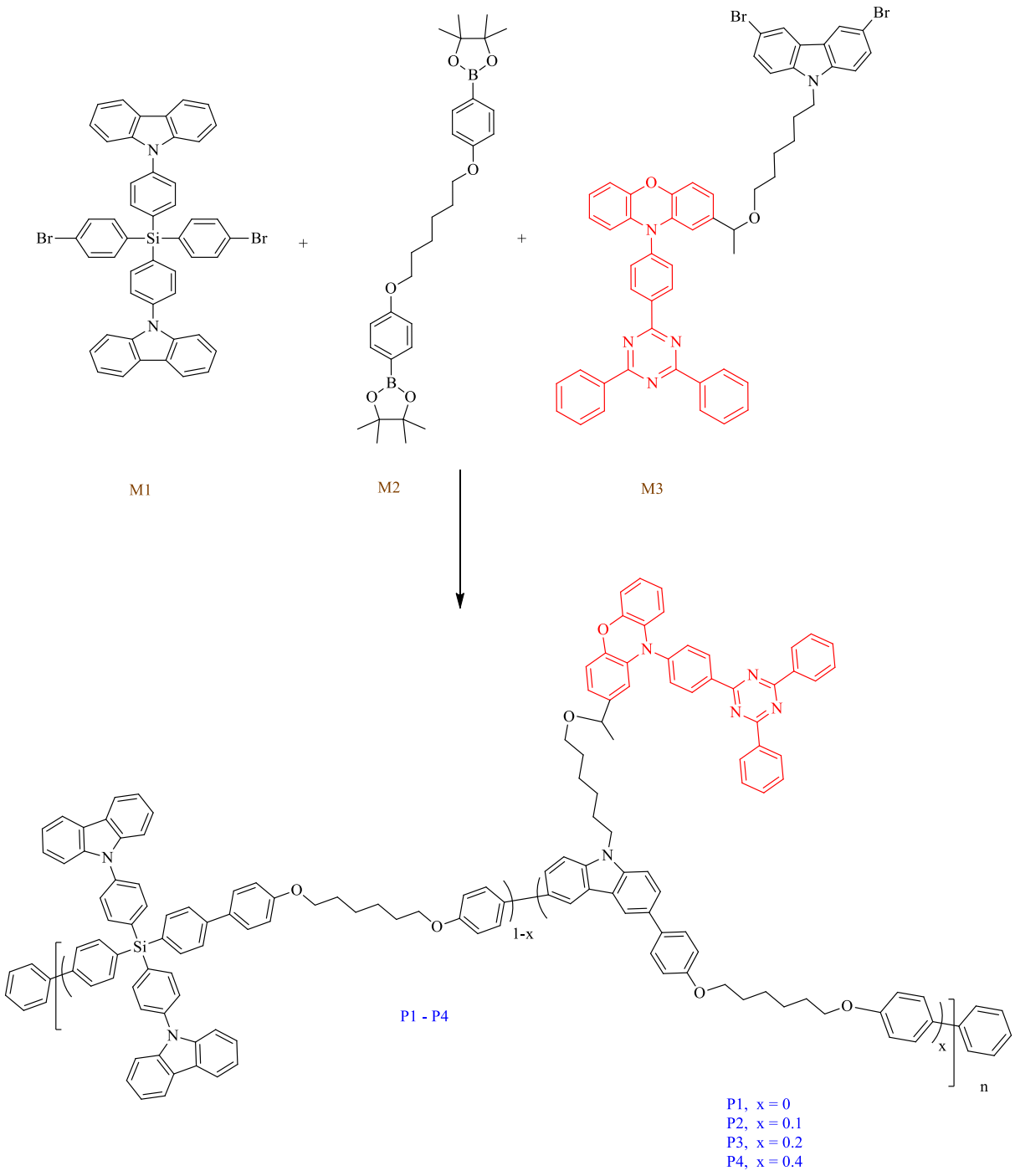

Scheme 2.30 Synthetic route of P1, P2, P3 and P4

Reagents & conditions $NaHCO_3$, $P(o\text{-}tol)_3$, $Pd(OAc)_2$, H_2O, THF, Ar, 90°C, 3d.

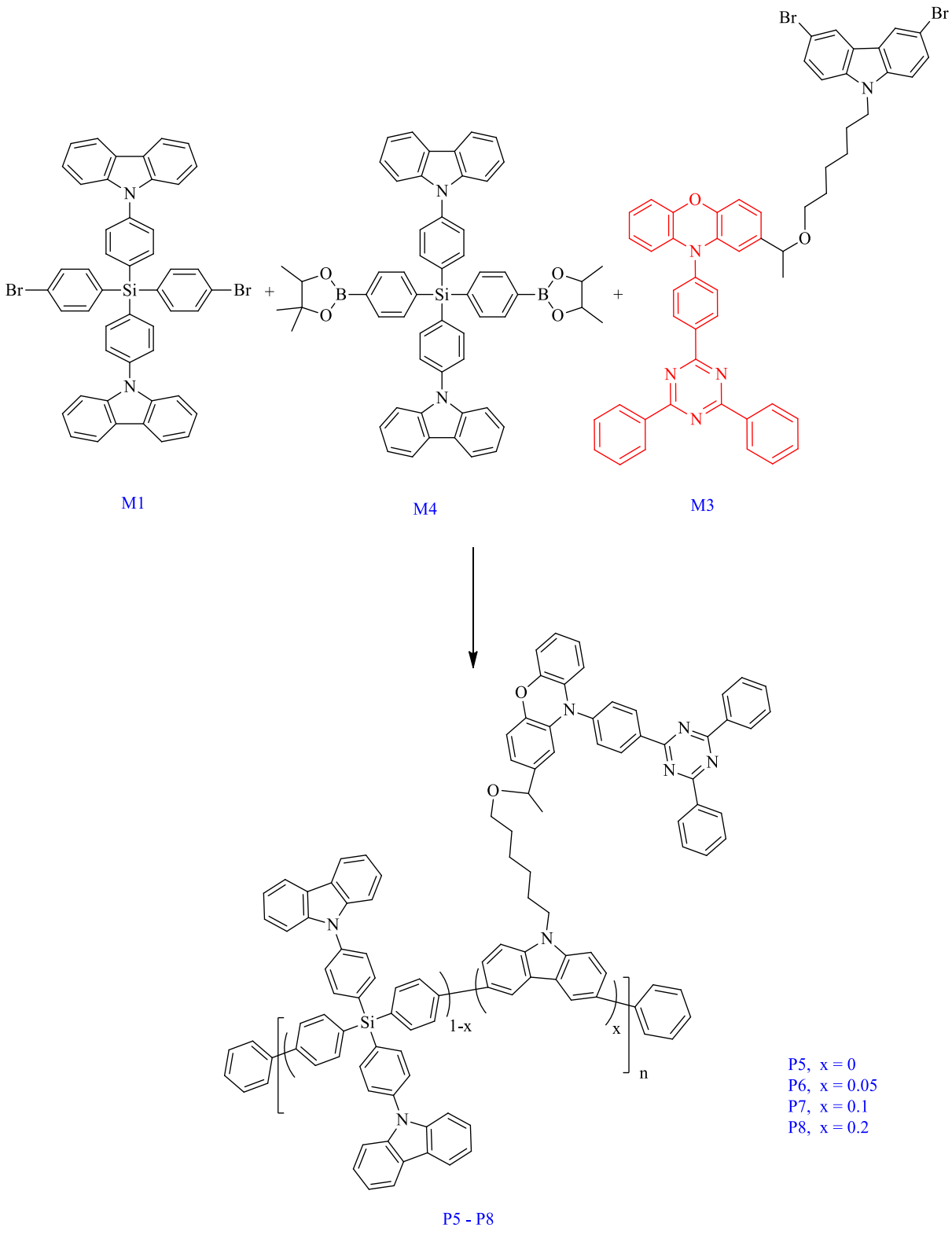

Scheme 2.31 Synthetic route for TADF polymers (P5-P8).

Reagents and conditions; $NaHCO_3$, $P(o\text{-}tol)_3$, $Pd(OAc)_2$, H_2O, THF, Ar, 85°C, 3d.

^{1}H NMR was performed to characterise the chemical structure of the synthesised polymers; the results displayed a good correlation with the polymers' structures. In addition, ^{1}H NMR was also used to calculate the actual ratio of TADF unit in these polymers. Table 1.1 below showed the accurate ratio of TADF in these polymers. The resultant spectrum of ^{1}H NMR showed peaks at 9.02, 8.80, 6.57 and 6.02 ppm, which corresponds to the protons of the TADF moiety in M3. It is noticeable that these peaks increased as the molar feed ratio increased from P2 to P4 and from P6 to P8. All polymers revealed characteristic peaks at 8.17, 7.44, 7.37 ppm which are related to hydrogen atoms in the carbazole ring in M1 and M4.

Table 2. 1 TADF percentage ratio From ^{1}H NMR spectra

Polymers	feed ratio	actual ratio
P1	0%	0%
P2	5%	5.5%
P3	10%	10.8%
P4	20%	22.3%
P5	0%	0%
P6	5%	4.3%
P7	10%	9%
P8	20%	18.6%

Moreover, the weight average molecular weight (Mw) and the number of average molecular weight (Mn) were calculated *via* gel-permeation-chromatography (GPC) using tetrahydrofuran as an eluent and polystyrene as molecular weight references standard. All synthesised polymers in this chapter show high solubility in many common organic solvents, such as

tetrachloromethane, toluene and tetrahydrofuran. All polymers were made with yields greater than 50%. The collected GPC data of designed polymers show that the first series of polymers (P1-P4) have larger Mn and Mw values than polymers P5, P6, P7 and P8. This can be explained as being due to the presence of the highly soluble chain attached to the phenyl group in M2. The presence of a high-solubility group enhances the polymer's solubility and results in additional polymerisation and large molecular weight polymers.

In contrast to the first four polymers (P1-P4), P5, P6, P7 and P8, which were formed from M1, M3 and M4, displayed lower Mn and Mw. This could be due to steric hindrance that present in these polymers. The number average Mn of these polymers (P5-P8) is between 4200 Da for P8 and 6800 Da for P6. Introducing monomer 4, which has more aromatic ring units than monomer 2, into the backbone of these polymers increases the steric hindrance, and decreases the solubility hence the lower Mw. In addition, the GPC results revealed that the first set of polymers (P1-P4) has a smaller polydispersity index (PDI) than the second group of polymers (P1-P4) in this chapter. This is could be understood due to the less steric hindrance structure of M2, which as a result allows chains to be as close in Mw as possible. On the other hand, increasing the steric hindrance of monomer (M4) results in an increase in the repulsion between polymers' chains in P5, P6, P7 and P8 leaving them with larger PDI. However, table 2.2 exhibits all GPC results for the polymers described in this chapter.

Table 2.2 GPC analysis results of P1-P8.

PDI = polydispersity index

Polymer	M_n(Da)	M_w(Da)	PDI	Yield	Fraction
P1	17100	22100	1.292	60%	Toluene
P2	20000	24900	1.245	62%	Toluene
P3	19000	22100	1.163	67%	Chloroform

P4	18000	21500	1.194	73%	Chloroform
P5	5400	15600	2.888	55%	Toluene
P6	6800	14800	2.176	61%	Chloroform
P7	6300	13400	2.127	62%	Chloroform
P8	4200	8600	2.04	60%	Chloroform

2.2.3 Optical Analysis and Properties

The optical features and properties of the synthesised polymers were all examined using UV-Vis spectroscopy in a diluted solution of chloroform (Figures 2.6a and 2.7a) and in the solid state as a thin film (Figures 2.6b and 2.7b). The optical band gaps were calculated according to the onset of absorption of polymers in a thin film. The values of maximum absorption in solution and film and onset values are summarised in Table 2.3.

Table 2.3 UV-Vis data of polymers (P1-P8)

Polymer	λ_{max} in Solution (nm)	λ_{max} in Film (nm)	λ_{max} Onset of thin film (nm)	$E_{g\ opt}$ (eV)
P1	307	316	379	3.27 ± 0.006
P2	306	319	388	3.19 ± 0.005
P3	305	318	387	3.20 ± 0.011
P4	303	314	380	3.26 ± 0.008
P5	308	318	400	3.10 ± 0.003
P6	306	319	389	3.18 ± 0.012

P7	307	317	392	3.16 ± 0.002
P8	305	316	381	3.25 ± 0.009

The maximum absorptions of all the polymers in this chapter are comparable to each other, and the values are between 303 nm and 308 nm in solution, and between 314 nm and 319 nm in the solid state (thin film). The short wavelength absorption of these polymers is clearly due to a non-conjugated system, which leads to a wider energy gap between π-π* transition, hence the shorter absorbance wavelength. The presence of silicon in the polymer backbone causes the conjugation to be disrupted. In addition, these polymers are unlike conjugated polymers, in which electron delocalisation takes place alongside the polymer's backbone resulting in optimised electronic conjugation and thus having a longer wavelength absorbance. Furthermore, the weak absorption at around 360 nm is due to the n- π* transition in the nitrogen atom.

When these designed TADF polymers were cast into a film, the absorption maxima (λ_{max}) were red-shifted. For example, the absorption maxima in $CHCl_3$ solution for P3 and P6 were at 305 nm and 306 nm while they were at 318 nm and 319 nm when cast into a thin film. Polymers exhibited red-shifted in the thin film due to the increase in the concentration of the sample. This leads to more molecular aggregation and stronger intermolecular interaction, which promotes a planner structure, hence, a better electron delocalization. The molecular aggregation in the solid state causes the π-π stacking which results in a red-shifted too. However, both solid state and solution showed comparable confirmation of the polymer's backbone, yet displayed larger planarity in the film.

Furthermore, all polymers' energy band gaps were calculated based on the absorption onset in the film solid state. By comparing the optical band gap of the first series of polymers (P1-P4) with the second series of polymers (P5-P8), it is obvious that P5-P8 have lower energy optical bandgap values than P1-P4. It is hypothesised that increasing the number of aromatic groups in a polymer's backbone enhances conjugation and electron delocalisation, hence decreasing the optical band gap values, as in P5-P8.

A TADF unit (PXZ-TRZ) was introduced as a pendant in M3. UV-Vis spectroscopy was used to determine the absorption of this molecule and compare it with the analysis of the designed

polymers as illustrated in Figures 2.6 and 2.7. However, the presence of PXZ-TRZ in P2, P3, P4, P5, P6, P7 and P8 was not clearly shown and barely seen in P4 and P8 (at 420 nm) UV spectra. This can be due to the low molar absorption coefficients of TADF substituents attached to these polymers

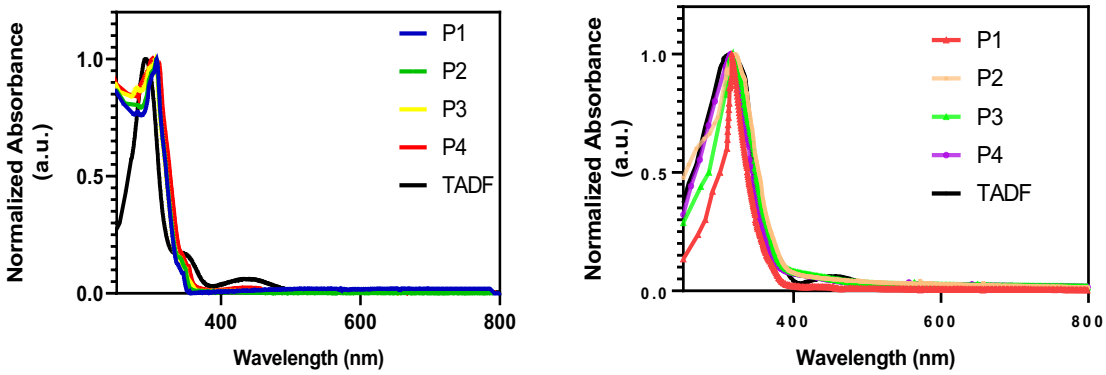

Figure 2. 6 Normalized UV-Vis absorption of P1, P2, P3, P4, and TADF unit in (a) chloroform solution; (b) solid-state film. (TADF unit = PXZ-TRZ)

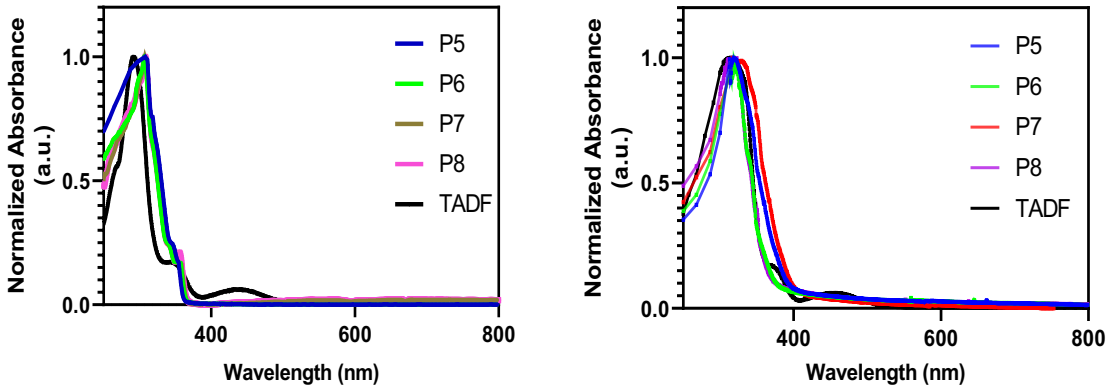

Figure 2. 7 Normalized UV-Vis absorption of P5, P6, P7, P8, and TADF unit in (a) chloroform solution; (b) solid-state film. (TADF unit = PXZ-TRZ)

As shown in Figures 2.8.a and 2.9.a, the photoluminescence spectrum peaks in toluene solution displayed that, the longer wavelength region (~545 nm) was proportionally enhanced as the M3 ratio in the polymer was increased, which may indicate tolerable inter-chain energy transfer from the polymer's backbone to the side chain TADF moieties as a result of M3 contribution. Dual emission peaks can be observed at ~ 385 nm and at ~ 545 nm in P2-P4, whereas P1 exhibited only one peak; the two emissions are coming from the polymer's backbone and the

TADF sidechain unit, respectively. Similarly, for P6-P8, the backbone peak appears at ~ 400 nm, the strongest TADF peak is from P8, which has the highest percentage of grafted TADF units. On the other hand, the PL spectra of P2-P4 and P6-P8 in the solid state presented completely different characteristics. All of the mentioned polymers showed intense peaks at a longer wavelength (around 535 nm), which is strong evidence for a complete energy transfer from the polymer's backbone to the attached TADF units; that is in good agreement with the literature.[43] Additionally, the emission peak of the main chain backbone was minimised, reaching the lowest peak in P4 and P8. Moreover, the net film PL spectra showed that as TADF units increase, the peak becomes red-shifted due to more aggregation impact as loading of M3 increases, thus P4 was more red-shifted than P2 and P3, similarly P8 >P7>P6. The trend of red-shifted emissions indicates that the TADF unit contributes more to the emission profile than the copolymers do. However, it is worth noting that the contribution of the TADF unit in the solution emission spectra promotes as the polymer concentration increases. This could be due to enhancing the aggregation effect as the chains of more neighbouring polymers became close to each other in the concentrated solution.

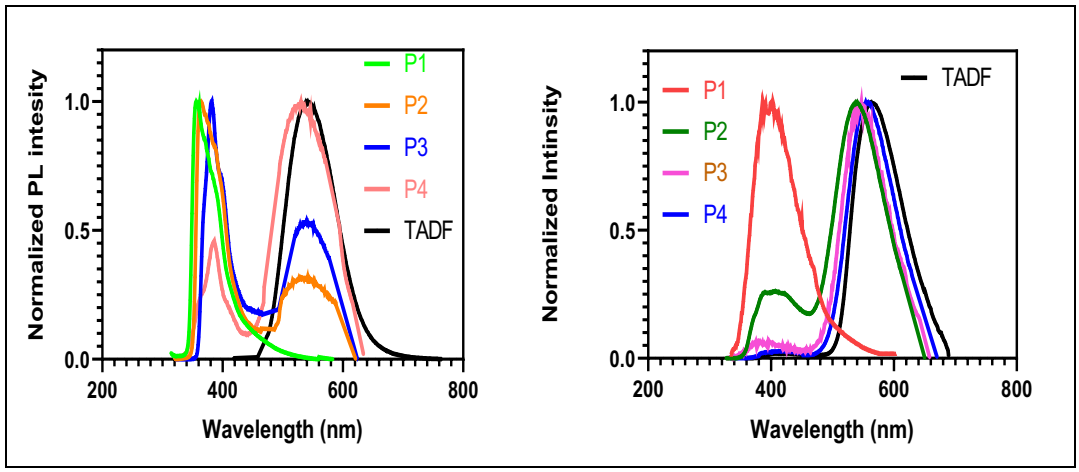

Figure 2.8 The normalised Pl spectra of P1-P4 in (a) toluene solution and (b) in neat film.

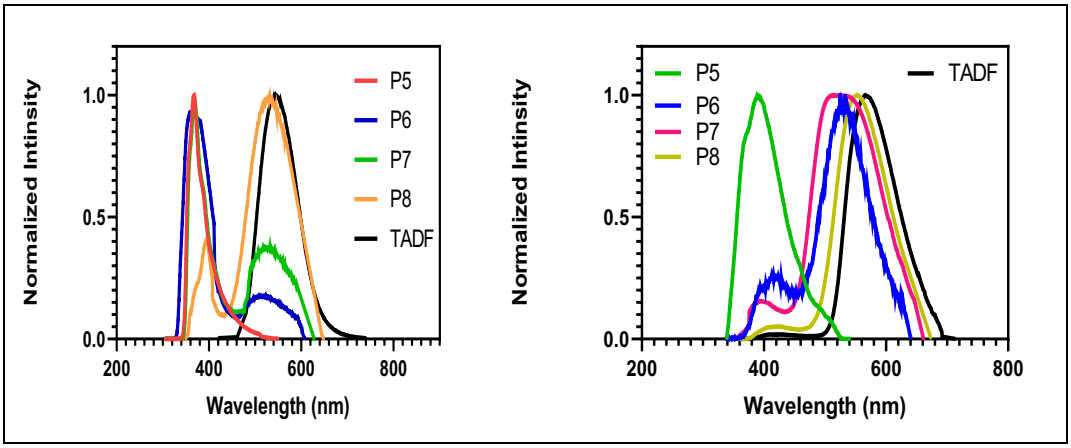

Figure 2.9 The normalised Pl spectra of P5-P8 in (a) toluene solution and (b) in neat film.

2.2.4. Electrochemical Analysis

Cyclic voltammetry (CV) was used to characterise and analyse the electrochemical characteristics of polymers (P1-P8), as shown in Figures 2.10 and 2.11. The reduction onset identified the polymers' lowest unoccupied molecular orbital (LUMO) energy levels, whereas the oxidation onset determined the polymers' highest occupied molecular orbital (HOMO) energy levels.

The CV measurements were performed in acetonitrile with tetrabutylammonium perchlorate as the electrolyte (0.1 M) and silver nitrate (Ag/Ag^{+}) as a reference electrode, on drop-cast polymer films using a platinum disc electrode as the working electrode at a scan rate of 100 mV s^{-1}. The electrochemical band gaps could be determined using the difference between the HOMO and LUMO energy values.

Table 2. 4 Electrochemical data of P1-P8.

Polymer	HOMO (eV)[a]	LUMO (eV)[b]	Eg (elec) (eV)[c]
P1	-5.43	-3.37	2.06 ± 0.0021
P2	-5.06	-3.40	1.66 ± 0.0015

P3	-5.02	-3.41	1.61 ± 0.0036
P4	-4.96	-3.42	1.54 ± 0.0027
P5	-5.35	-3.38	1.97 ± 0.0041
P6	-5.04	-3.39	1.65 ± 0.0012
P7	-5.00	-3.40	1.60 ± 0.0030
P8	-4.95	-3.40	1.55 ±.0009

a. HOMO energy levels estimated from the onset of the oxidation peak. b. LUMO energy levels calculated from the onset of the reduction peak. c. Electrochemical band gap.

The calculated HOMO and LUMO energy levels for all polymers are presented in Table 2.4. Polymers that contain the TADF unit generally showed a shallower HOMO level than those free of TADF units. Amongst all the polymers, P1 showed the deepest HOMO level, with a value of -5.43 eV, followed by P5 with a value of -5.35 eV. This is due to the effect of the larger nonconjugated system in the backbone of P1. Thus, the result is a wider band gap for this polymer. P4 and P8 displayed the shallowest HOMO level with values of -4.96 and -4.95, respectively. This is ascribed to the high percentage (~20%) of phenoxazine donors in these polymers. It is clear that the higher the TADF unit content in a polymer's structure, the shallower the HOMO level and the lower the electrical band gap. Conversely, the LUMO levels for all the polymers are comparable as seen in the above table and shown below in the figures. The LUMO levels for polymers P2-P4 and P6-P8 are a little deeper than for P1 and P5 owing to the presence of triazine acceptor units in their backbone structure.

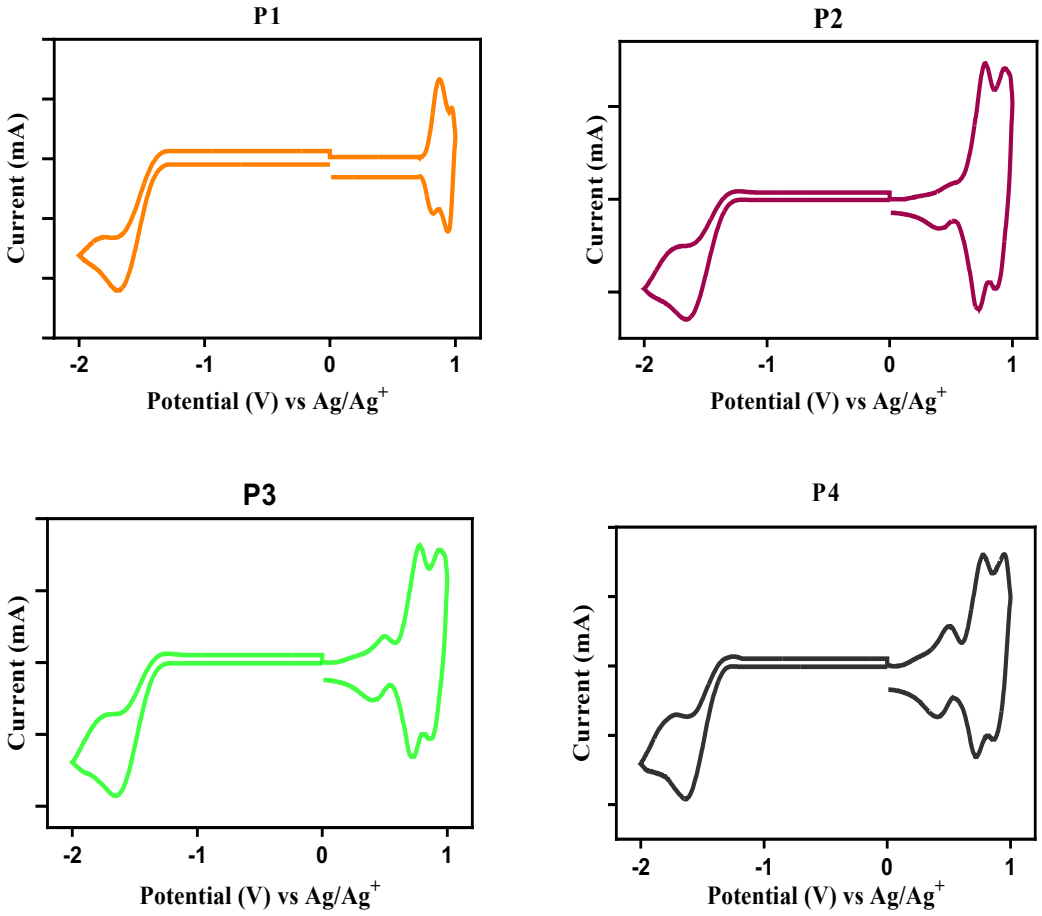

Figure 2. 10 Cyclic voltammograms for P1-P4

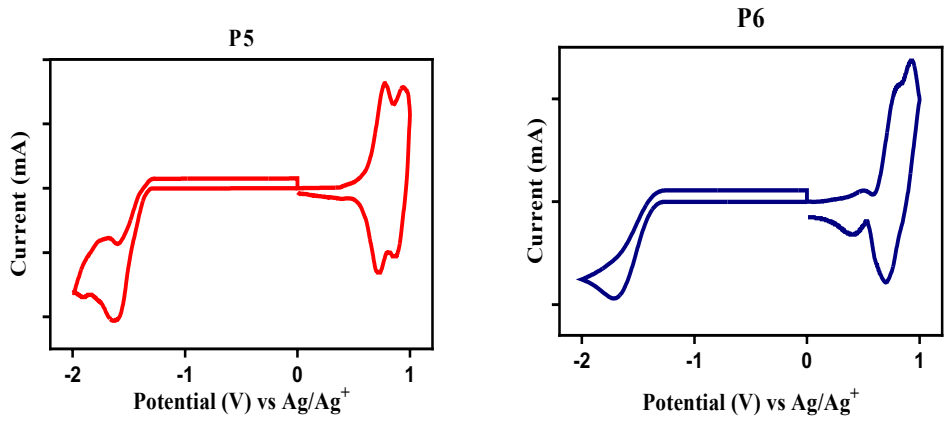

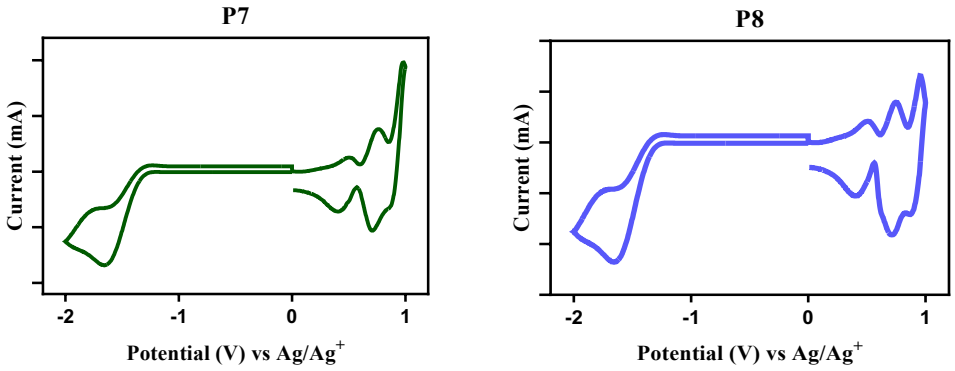

Figure 2. 11 Cyclic voltammograms for P5-P8.

As shown in Figures 2.10 and 2.11, P1 and P5 exhibited two chemical reversible oxidation peaks, which can be ascribed to the polymers' backbone, which includes a carbazole donor moiety, whereas P2-P4 and P6-P8 revealed three reversible oxidation peaks. The first oxidation peak in this polymer is located at around 0.60 V and belongs to the phenoxazine donor of the TADF unit, whereas the latter two peaks result from the polymer's backbone. The reduction peaks were similar for all polymers except for a slight shift when TADF is presented. The HOMO and LUMO values for all polymers were measured by the half-wave potential of the first oxidation and reduction peaks, respectively.

2.2.5 Thermal Analysis

TGA was used to determine the thermal stability of all the polymers. Figure 2.12 depicts the thermal degradation curves of the prepared polymers. Table 2.5 shows the temperatures at which decomposition begins. The experiments were carried out in an inert nitrogen atmosphere at a heating rate of 10 °C min^{-1}.

Table 2. 5 Thermal properties of polymers, P1-P8.

Polymers	Td (℃) [a]
P1	340
P2	342
P3	347

P4	354
P5	352
P6	354
P7	361
P8	363

[a] Degradation onset of polymers determined by thermogravimetric analysis with a heating rate of 10 ℃ min^{-1} in an inert nitrogen atmosphere.

All polymers, as shown in Figure 2.12, have good thermal stability, with thermal decomposition temperatures higher than 335 °C. Under 400 °C, most of these polymers lose less than 5% of their weight owing to decomposition. These findings suggest that these copolymers have excellent heat stability and can be successfully employed in solution-processed electronics devices. P1 and P5 displayed single degradation curves with the highest onset decomposition temperatures (Td) at 340 °C and 354 °C, respectively. This could be attributed to the alkyl chain cleavage from the polymers. The initial degradation of P2-P4 occurred between 342 °C and 352 °C, and between 354 °C and 363 °C for P6, P7 and P8. Unlike P1, polymers containing the TADF moiety in their structures (P2-P4) showed two degradation phases. These may be related to the cleavage of the alkyl chain and the decomposition of the residual polymer backbone.

Comparing the first series of polymers (P1-P4) with the second series (P5-P8) showed that the letters have a higher degradation temperature owing to their rigid chemical structure. The decomposition temperature decreases slightly by decreasing the TADF unit content, i.e., P1<P2<P3<P4 and P5<P6<P7<P8. This could be related to the resistance which rises as the molar ratio of M3 increases. All the synthesised polymers exhibit degradation until about 38% of the polymer remains; they then slowly degrade until reaching a steady rate of decomposition at around 800 °C. The reason for this may be related to the fact that polymers contain alkyl chains that are less volatile during combustion. As a result, a thick charring layer is formed on the virgin polymer, which prevents heat flux from reaching the virgin polymer owing to its low thermal conductivity. The heat degradation of the polymers would be delayed because of this process.[44]

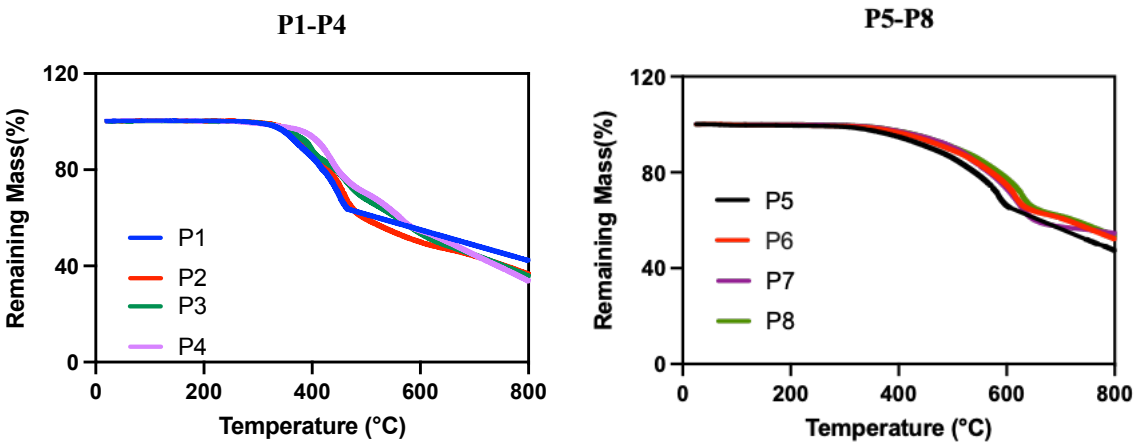

Figure 2. 12 Thermogravimetric analysis of polymers, P1-P8, carried out at a heating rate of 10 ^{o}C min^{-1} in an inert nitrogen atmosphere.

2.3. Conclusion

Organic emissive materials have seen tremendous expansion due to the commercial interest in their use in OLEDs as a new generation of displays and lighting sources. The new generation materials with TADF features can optimise the efficiency without the use of heavy metals to convert all triplet excitons into singlet excitons, resulting in almost 100% exciton utilisation. We introduced the TADF unit (PXZ-TRZ) into the polymer's structure following a side-chain engineering strategy. The TADF unit was grafted into the side chain of the polymer's backbone in P2-P4 and P6-P8. All TADF-based polymers described in this chapter were synthesised using the Suzuki cross-coupling procedure; their thermal, optical and electrochemical properties were demonstrated. In addition, silicon was integrated into the polymer's backbone to break the conjugation system, resulting in increasing the triplet energy as well as stability. Alkyl groups were also introduced into the polymers' structures to enhance their solubility in organic solvents. After successful synthesis of TADF-based polymers, GPC was used to determine the polymers molecular weight, which was found to be in the range of 17000-20000 Da (Mn) for P1-P4 and in the range of 4200-6800 Da (Mn) for P5-P8. The lower molecular weight values in the second series of TADF polymers (P5-P8) are assigned to the steric hindrance structure of the monomer used, which limits the chain growth during the polymerisation process.

The photoluminescence spectroscopy demonstrated that the introduction of the TADF pendant unit leads to energy transfer to the polymers' backbones. While P1 and P5, which were made without the TADF unit, showed only one peak at ~390 nm, other P2-P4 and P6-P8 in toluene exhibited dual emission peaks at ~390 nm and 547 nm respectively. The former peak corresponds to the polymer's backbone and the latter is ascribed to the emissions of the TADF unit. In addition, by increasing the molar ratio of the TADF monomer (M3), the intensity of the TADF peak (~547 nm) increased, which denotes more efficient energy transfer from the polymer's backbone to the TADF moiety. In neat film, the intensity of the peak at the tail of spectra (~550nm) is increased, while the polymer backbone peak is minimised, indicating that a complete energy transfer from the backbone to the TADF unit took place in the solid state.

The optical characteristics of all designed polymers were also investigated using UV-Vis spectroscopy in dilute chloroform solution and in neat film. In dilute $CHCl_3$, all polymers (P1-P8) demonstrated similar maximum absorption peaks in the ultraviolet-visable region (~300-309 nm). The relative low wavelength is due to breaking the conjugation system in the

polymer's backbones, which results in a reduction of the electronic delocalisation across the polymer's chains. Additionally, the energy band gap of all polymers was determined based upon absorption onset in neat film, which showed that P5-P8 had a lower energy band gap than their counterparts (P1-P4). This is assigned to the presence of a higher number of aromatic groups in P5-P8, which increase the conjugation.

Cyclic voltammetry (CV) and thermal gravimetric analysis were both performed to find out the electrochemical properties and thermal stability of these TADF-based polymers. The measurement of CV was carried out under inert conditions of argon in a dilute solution. All polymers displayed relative low HOMO levels. Moreover, all polymers exhibited good thermal stability versus increased temperature. Thermal stability and high solubility make these polymers good candidates for solution-processed OLED devices.

2.4. References

(1) Uoyama, H.; Goushi, K.; Shizu, K.; Nomura, H.; Adachi, C. Highly Efficient Organic Light-Emitting Diodes from Delayed Fluorescence. *Nature* **2012**, *492* (7428), 234–238.

(2) Adachi, C. Third-Generation Organic Electroluminescence Materials. *Japanese Journal of Applied Physics* **2014**, *53* (6), 060101.

(3) Tao, Y.; Yuan, K.; Chen, T.; Xu, P.; Li, H.; Chen, R.; Zheng, C.; Zhang, L.; Huang, W. Thermally Activated Delayed Fluorescence Materials towards the Breakthrough of Organoelectronics. *Advanced Materials* **2014**, *26* (47), 7931–7958.

(4) Ogiwara, T.; Wakikawa, Y.; Ikoma, T. Mechanism of Intersystem Crossing of Thermally Activated Delayed Fluorescence Molecules. *The Journal of Physical Chemistry A* **2015**, *119* (14), 3415–3418.

(5) Rajamalli, P.; Senthilkumar, N.; Gandeepan, P.; Ren-Wu, C.-C.; Lin, H.-W.; Cheng, C.-H. A Method for Reducing the Singlet–Triplet Energy Gaps of TADF Materials for Improving the Blue OLED Efficiency. *ACS Applied Materials & Interfaces* **2016**, *8* (40), 27026–27034.

(6) Godumala, M.; Choi, S.; Cho, M. J.; Choi, D. H. Thermally Activated Delayed Fluorescence Blue Dopants and Hosts: From the Design Strategy to Organic Light-Emitting Diode Applications. *Journal of Materials Chemistry C* **2016**, *4* (48), 11355–11381.

(7) Wang, L.; Ou, Q.; Peng, Q.; Shuai, Z. Theoretical Characterizations of TADF Materials: Roles of Δ G and the Singlet–Triplet Excited States Interconversion. *The Journal of Physical Chemistry A* **2021**, *125* (7), 1468–1475.

(8) Stavrou, K.; Franca, L. G.; Monkman, A. P. Photophysics of TADF Guest–Host Systems: Introducing the Idea of Hosting Potential. *ACS Applied Electronic Materials* **2020**, *2* (9), 2868–2881.

(9) Lin, C.-J.; Huang, H.-L.; Tseng, M.-R.; Cheng, C.-H. High Energy Gap OLED Host Materials for Green and Blue PhOLED Materials. *Journal of Display Technology* **2009**, *5* (6), 236–240.

(10) Yook, K. S.; Lee, J. Y. Small Molecule Host Materials for Solution Processed Phosphorescent Organic Light-emitting Diodes. *Advanced Materials* **2014**, *26* (25), 4218–4233.

(11) Ding, L.; Dong, S.; Jiang, Z.; Chen, H.; Liao, L. Orthogonal Molecular Structure for Better Host Material in Blue Phosphorescence and Larger OLED White Lighting Panel. *Advanced Functional Materials* **2015**, *25* (4), 645–650.

(12) Rodella, F.; Bagnich, S.; Duda, E.; Meier, T.; Kahle, J.; Athanasopoulos, S.; Köhler, A.; Strohriegl, P. High Triplet Energy Host Materials for Blue TADF OLEDs—A Tool Box Approach. *Frontiers in Chemistry* **2020**, *8*, 657.

(13) Li, W.; Li, J.; Liu, D.; Wang, F.; Zhang, S. Bipolar Host Materials for High-Efficiency Blue Phosphorescent and Delayed-Fluorescence OLEDs. *Journal of Materials Chemistry C* **2015**, *3* (48), 12529–12538.

(14) Jeon, S. O.; Yook, K. S.; Joo, C. W.; Lee, J. Y. High-Efficiency Deep-Blue-Phosphorescent Organic Light-Emitting Diodes Using a Phosphine Oxide and a Phosphine Sulfide High-Triplet-Energy Host Material with Bipolar Charge-Transport Properties. *Advanced Materials* **2010**, *22* (16), 1872–1876.

(15) Lin, T.; Chatterjee, T.; Tsai, W.; Lee, W.; Wu, M.; Jiao, M.; Pan, K.; Yi, C.; Chung, C.; Wong, K. Sky-blue Organic Light Emitting Diode with 37% External Quantum Efficiency Using Thermally Activated Delayed Fluorescence from Spiroacridine-triazine Hybrid. *Advanced Materials* **2016**, *28* (32), 6976–6983.

(16) Park, S.-R.; Kim, S.-M.; Kang, J.-H.; Lee, J.-H.; Suh, M. C. Bipolar Host Materials with Carbazole and Dipyridylamine Groups Showing High Triplet Energy for Blue Phosphorescent Organic Light Emitting Diodes. *Dyes and Pigments* **2017**, *141*, 217–224.

(17) Stavrou, K.; Franca, L. G.; Monkman, A. P. Photophysics of TADF Guest–Host Systems: Introducing the Idea of Hosting Potential. *ACS Applied Electronic Materials* **2020**, *2* (9), 2868–2881.

(18) Jhulki, S.; Cooper, M. W.; Barlow, S.; Marder, S. R. Phosphorescent and TADF Polymers and Dendrimers in Solution-Processed Self-Host Organic Light-Emitting Diodes: Structure Analysis and Design Perspectives. *Materials Chemistry Frontiers* **2019**, *3* (9), 1699–1721.

(19) Wei, Q.; Ge, Z.; Voit, B. Thermally Activated Delayed Fluorescent Polymers: Structures, Properties, and Applications in OLED Devices. *Macromolecular Rapid Communications* **2019**, *40* (1), 1800570.

(20) Lee, S. Y.; Yasuda, T.; Komiyama, H.; Lee, J.; Adachi, C. Thermally Activated Delayed Fluorescence Polymers for Efficient Solution-processed Organic Light-emitting Diodes. *Advanced Materials* **2016**, *28* (21), 4019–4024.

(21) Hu, Y.; Cai, W.; Ying, L.; Chen, D.; Yang, X.; Jiang, X.-F.; Su, S.; Huang, F.; Cao, Y. Novel Efficient Blue and Bluish-Green Light-Emitting Polymers with Delayed Fluorescence. *Journal of Materials Chemistry C* **2018**, *6* (11), 2690–2695.

(22) Li, C.; Nobuyasu, R. S.; Wang, Y.; Dias, F. B.; Ren, Z.; Bryce, M. R.; Yan, S. Solution-processable Thermally Activated Delayed Fluorescence White OLEDs Based on Dual-emission Polymers with Tunable Emission Colors and Aggregation-enhanced Emission Properties. *Advanced Optical Materials* **2017**, *5* (20), 1700435.

(23) Li, C.; Wang, Y.; Sun, D.; Li, H.; Sun, X.; Ma, D.; Ren, Z.; Yan, S. Thermally Activated Delayed Fluorescence Pendant Copolymers with Electron-and Hole-Transporting Spacers. *ACS Applied Materials & Interfaces* **2018**, *10* (6), 5731–5739.

(24) Shao, S.; Ding, J.; Wang, L.; Jing, X.; Wang, F. White Electroluminescence from All-Phosphorescent Single Polymers on a Fluorinated Poly (Arylene Ether Phosphine Oxide) Backbone Simultaneously Grafted with Blue and Yellow Phosphors. *Journal of the American Chemical Society* **2012**, *134* (50), 20290–20293.

(25) Shao, S.; Ding, J.; Ye, T.; Xie, Z.; Wang, L.; Jing, X.; Wang, F. A Novel, Bipolar Polymeric Host for Highly Efficient Blue Electrophosphorescence: A Non-Conjugated Poly (Aryl Ether) Containing Triphenylphosphine Oxide Units in the Electron-Transporting Main Chain and Carbazole Units in Hole-Transporting Side Chains. *Advanced Materials* **2011**, *23* (31), 3570–3574.

(26) Zhou, X.; Huang, M.; Zeng, X.; Chen, T.; Xie, G.; Yin, X.; Yang, C. Combining the Qualities of Carbazole and Tetraphenyl Silane in a Desirable Main Chain for Thermally Activated Delayed Fluorescence Polymers. *Polymer Chemistry* **2019**, *10* (30), 4201–4208.

(27) Kim, H. J.; Lee, C.; Godumala, M.; Choi, S.; Park, S. Y.; Cho, M. J.; Park, S.; Choi, D. H. Solution-Processed Thermally Activated Delayed Fluorescence Organic Light-Emitting Diodes Using a New Polymeric Emitter Containing Non-Conjugated Cyclohexane Units. *Polymer Chemistry* **2018**, *9* (11), 1318–1326.

(28) Yang, Y.; Wang, S.; Zhu, Y.; Wang, Y.; Zhan, H.; Cheng, Y. Thermally Activated Delayed Fluorescence Conjugated Polymers with Backbone-donor/Pendant-acceptor Architecture for Nondoped OLEDs with High External Quantum Efficiency and Low Roll-off. *Advanced Functional Materials* **2018**, *28* (10), 1706916.

(29) Zhu, Y.; Yang, Y.; Wang, Y.; Yao, B.; Lin, X.; Zhang, B.; Zhan, H.; Xie, Z.; Cheng, Y. Improving Luminescent Performances of Thermally Activated Delayed Fluorescence Conjugated Polymer by Inhibiting the Intra-and Interchain Quenching. *Advanced Optical Materials* **2018**, *6* (10), 1701320.

(30) Choi, S.; Godumala, M.; Lee, J. H.; Kim, G. H.; Moon, J. S.; Kim, J. Y.; Yoon, D.-W.; Yang, J. H.; Kim, J.; Cho, M. J. Optimised Structure of Silane-Core Containing Host Materials for Highly Efficient Blue TADF OLEDs. *Journal of Materials Chemistry C* **2017**, *5* (26), 6570–6577.

(31) Skorotetcky, M. S.; Borshchev, O. v; Cherkaev, G. v; Ponomarenko, S. A. Synthesis of Nanostructured Organosilicon Luminophores Based on Phenyloxazoles. *Russian Journal of Organic Chemistry* **2019**, *55* (1).

(32) Liu, H.; Cheng, G.; Hu, D.; Shen, F.; Lv, Y.; Sun, G.; Yang, B.; Lu, P.; Ma, Y. A Highly Efficient, Blue-Phosphorescent Device Based on a Wide-Bandgap Host/FIrpic: Rational Design of the Carbazole and Phosphine Oxide Moieties on Tetraphenylsilane. *Advanced Functional Materials* **2012**, *22* (13), 2830–2836.

(33) Hermann, M.; Wassy, D.; Kratzert, D.; Esser, B. Dibenzo [a, e] Pentalenophanes: Bending a Non-Alternant Hydrocarbon. *Chemistry–A European Journal* **2018**, *24* (29), 7374–7387.

(34) Komber, H.; Müllers, S.; Lombeck, F.; Held, A.; Walter, M.; Sommer, M. Soluble and Stable Alternating Main-Chain Merocyanine Copolymers through Quantitative Spiropyran–Merocyanine Conversion. *Polymer Chemistry* **2014**, *5* (2), 443–453.

(35) Vanderhaeghe, H. Phenoxazines. I. Ring-Substituted Derivatives. *The Journal of Organic Chemistry* **1960**, *25* (5), 747–753.

(36) Liu, X.-K.; Zheng, C.-J.; Xiao, J.; Ye, J.; Liu, C.-L.; Wang, S.-D.; Zhao, W.-M.; Zhang, X.-H. Novel Bipolar Host Materials Based on 1, 3, 5-Triazine Derivatives for Highly Efficient Phosphorescent OLEDs with Extremely Low Efficiency Roll-Off. *Physical Chemistry Chemical Physics* **2012**, *14* (41), 14255–14261.

(37) Tanaka, H.; Shizu, K.; Miyazaki, H.; Adachi, C. Efficient Green Thermally Activated Delayed Fluorescence (TADF) from a Phenoxazine–Triphenyltriazine (PXZ–TRZ) Derivative. *Chemical Communications* **2012**, *48* (93), 11392–11394.

(38) Feng, S.; Xu, H.; Zhang, C.; Chen, Y.; Zeng, J.; Jiang, D.; Jiang, J.-X. Bicarbazole-Based Redox-Active Covalent Organic Frameworks for Ultrahigh-Performance Energy Storage. *Chemical Communications* **2017**, *53* (82), 11334–11337.

(39) Suzuki, A. Organoboron Compounds in New Synthetic Reactions. *Pure and Applied Chemistry* **1985**, *57* (12), 1749–1758.

(40) Hermann, M.; Wassy, D.; Esser, B. Conjugated Nanohoops Incorporating Donor, Acceptor, Hetero-or Polycyclic Aromatics. *Angewandte Chemie International Edition* **2021**.

(41) Krebs, F. C.; Nyberg, R. B.; Jørgensen, M. Influence of Residual Catalyst on the Properties of Conjugated Polyphenylenevinylene Materials: Palladium Nanoparticles and Poor Electrical Performance. *Chemistry of Materials* **2004**, *16* (7), 1313–1318.

(42) Nielsen, K. T.; Bechgaard, K.; Krebs, F. C. Removal of Palladium Nanoparticles from Polymer Materials. *Macromolecules* **2005**, *38* (3), 658–659.

(43) Xie, G.; Luo, J.; Huang, M.; Chen, T.; Wu, K.; Gong, S.; Yang, C. Inheriting the Characteristics of TADF Small Molecule by Side-Chain Engineering Strategy to Enable Bluish-Green Polymers with High PLQYs up to 74% and External Quantum Efficiency over 16% in Light-Emitting Diodes. *Advanced Materials* **2017**, *29* (11), 1604223.

(44) Patel, P.; Hull, T. R.; Lyon, R. E.; Stoliarov, S. I.; Walters, R. N.; Crowley, S.; Safronava, N. Investigation of the thermal decomposition and flammability of PEEK and its carbon and glass-fibre composites. *Polymer Degradation and Stability* **2011**, 96 (1).

Chapter 3: Synthesis and development of New High Triplet Energy polymers with Pendant TADF Guests for OLEDs

Abstract

TADF polymers are mostly designed to be used in solution-processed OLED devices. While there are many attempts to synthesise suitable TADF polymers, not many efficient polymers have been reported. In this chapter, M3, which includes PXZ-TRZ as a TADF unit, was incorporated as a pendent into polymers using the Suzuki polymerisation reaction and Sonogashira coupling reaction methods. Polymers 9 and 10 were made via the Suzuki method, while P11 and P12 were synthesised according to the Sonogashira procedure. Moreover, P9 and P11 were made free of the TADF moiety for analysis comparison purposes. The purity and chemical structures of all the materials involved were confirmed using different analysis techniques, such as NMR, UV-Vis spectroscopy and elemental analysis. All of these copolymers exhibited thermal stability up to around 288°C. Unlike P9 and P11, P10 and P12 showed different emission peaks in both neat film and toluene solution. One peak was attributed to the polymer's backbone and the other one corresponded to the attached PXZ-TRZ unit. Polymers containing fluorene in their backbone (P9 and P10) showed lower energy band gap values, which is due to the extension of the conjugated system in their structure.

3.1 Introduction

Since the innovation of Tang and his co-researchers in the late eighties,[1] many attempts have been taking place to improve the OLEDs structure in terms of both affordability and efficiency for visual and lightening display applications. The first efficiency limitation appeared in common fluorescence emitters when non-radiative triplets are produced from three quatres of total excitons as a result of electrical excitation.[2] Despite that the single excitons can form from triplet-triplet annihilation, the total internal quantum efficiency is still theoretically limited to less than 65%.[3] Thus, phosphorescent emitters were introduced to optimise the maximum outcomes of internal quantum efficiency. These emitters, which incorporate heavy metals such as platinum and iridium in their molecular structures, successfully optimised the efficiency by harvesting both singlet and triplet excitons.[4] Fabrication of enhanced structures containing multiple layers using high vacuum deposition were possible and applied to make highly efficient OLEDs based phosphorescence emitters.[5–8] However, these emitters are very expensive and not eco-friendly due to the presence of heavy metals. This drawback of POLEDs encouraged researchers to find other, cheaper and eco-friendly alternatives. Among all types of devices deposition methods, the energy outcome of vacuum deposition is proven to have a higher energy outcome than other methods, such as printing or spin coating. Thus, studies and research are ongoing to develop solution processing made of full organic materials. [5,9,10]

It is essential to design organic materials with minimised singlet triplet energy difference to allow RISC to occur, thereby converting all excitons to singlet excitons, which is another term for energy exploiting. Endo et al. were successfully able to design the first type of pure organic TADF materials which was derived from triazine (TRZ). The photoluminescence quantum yield was first limited to around 40% with 33% efficiency of converting triplet excitons when 1,3-bis(N-carbazolyl) benzene (mCP) was used as a host.[11] The same group was then able to develop pure organic TADF emitter materials with an improved triplet conversion rate (~100%).[12] Considerable attempts have been made since then to synthesise full organic materials and controllable TADF molecules for multi-layered OLED devices. The aim behind that is to facilitate vapour deposition method and phase transition processes for the molecules that makes the OLEDs. [13–16]

The Sonogashira coupling reaction is a method in which the reaction mechanism relies on a palladium catalyst, which has a strong ability to form C-C bonds. The new carbon-carbon bond is formed as a result of a coupling between sp^2 hybridised carbon of vinyl halide or aryl and a

terminal sp carbon of an alkyne.[17] In 1975, the reaction method took Sonogashira's name, after he and his co-researchers discovered coupling using palladium derivatives as a catalyst with a supporting catalyst, such as copper, in the presence of an amine as a solvent to enable the reaction to be carried out at a moderate temperature.[18] On the other hand, other studies suggest that palladium-based coupling needs higher temperatures to be completed.[19,20] However, the contradictory finding of these studies successfully described a strong, new carbon-carbon bond formation pathway. Meanwhile, the success of an earlier study is due to copper trans-metalation of the terminal triple bond, which when united with palladium, builds high catalytic versatility and capacity.

In this chapter, Suzuki coupling is used to synthesise P9 and P10, where P9 is free of TADF moiety and around 5% of P10 is TADF. The main backbone of these polymers was designed from a mixture of a conjugated fluorene, carbazole and a non-conjugated tetraphenyl silicon unit. The non-conjugated host (Br-SiCz-Br) was selected due to its high triplet energy, which is a result of reducing a pi-conjugation system, and good thermal stability, which is because of the bulk rigid structure.[21] In addition, conjugated fluorene is used to enhance electron transportation and charge transfer properties. Furthermore, Sonogashira coupling is followed in this chapter to make P11 and P12, in which the former is prepared without a TADF unit for comparison. The polymer backbone in these polymers is spaced by alkyl along the polymer's chains. A non-conjugated silicon derivative was used here together with alkynes to minimise the electronic delocalisation along the chain, hence increasing the triplet energies.

3.2 Results and Discussions

To minimise the polymers' pi-conjugation system, a series of alternating copolymers containing silane and octa-1,7 diyne were designed. The polymers' backbone consists of fluorene and SiCz as repeating units; the fluorene unit was chosen for P9 and P10 due to its high fluorescence property. Fluorene is similar to carbazole in terms of its structure except for the nitrogen atom that is located in the middle of a carbazole ring. The physical properties and chemical structures of a non-conjugated host are highly important when it is incorporated into polymers to reduce conjugation. Thus, the hole property is promoted by the SiCz in these polymers. In addition, introducing alkyne chains into copolymers as in P11 and P12 is extremely beneficial to increasing the polymers' solubility. TADF, which had been synthesised as described in Chapter 2, was attached to the copolymers' sidechains. This type of TADF was used due to its quality, which is described in Chapters 1 and 2. The Suzuki polycondensation method was used to prepare P9 and P10 as shown in Scheme 3.1. P9 was made without a TADF unit, while 5% of P10 was PXZ-TRZ. P11 and P12 were designed according to the Sonogashira polymerisation procedure (Scheme 3.2). M3, which includes the TADF unit, was not involved in P11 in order to compare the physical properties with P12 that have a TADF unit in its structure.

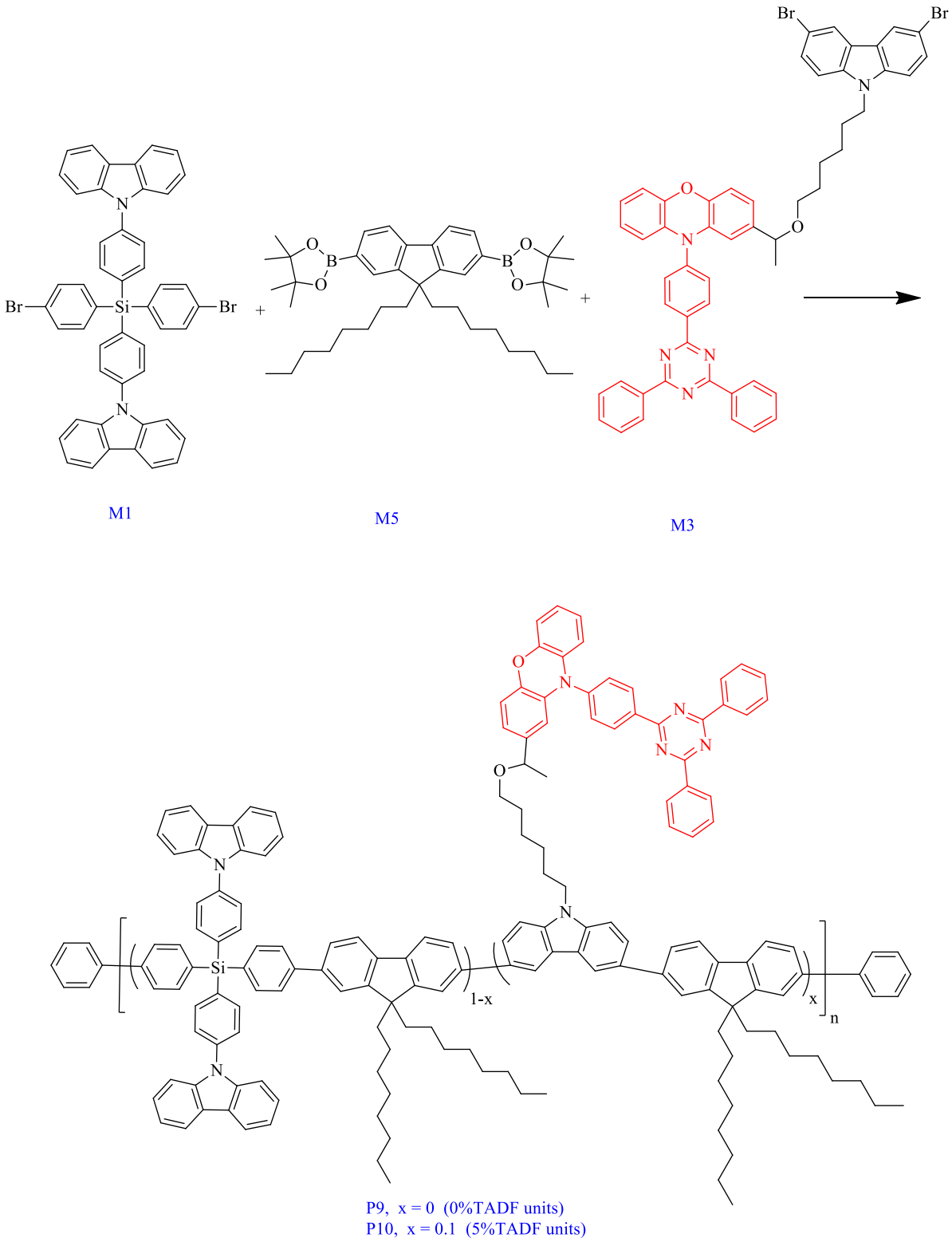

Scheme 3. 1 Preparation route to P9 and P10.

Reagents & conditions: $NaHCO_3$, $P(o\text{-}tol)_3$, $Pd(OAc)_2$, H_2O, THF, Ar, 90°C, 3d.

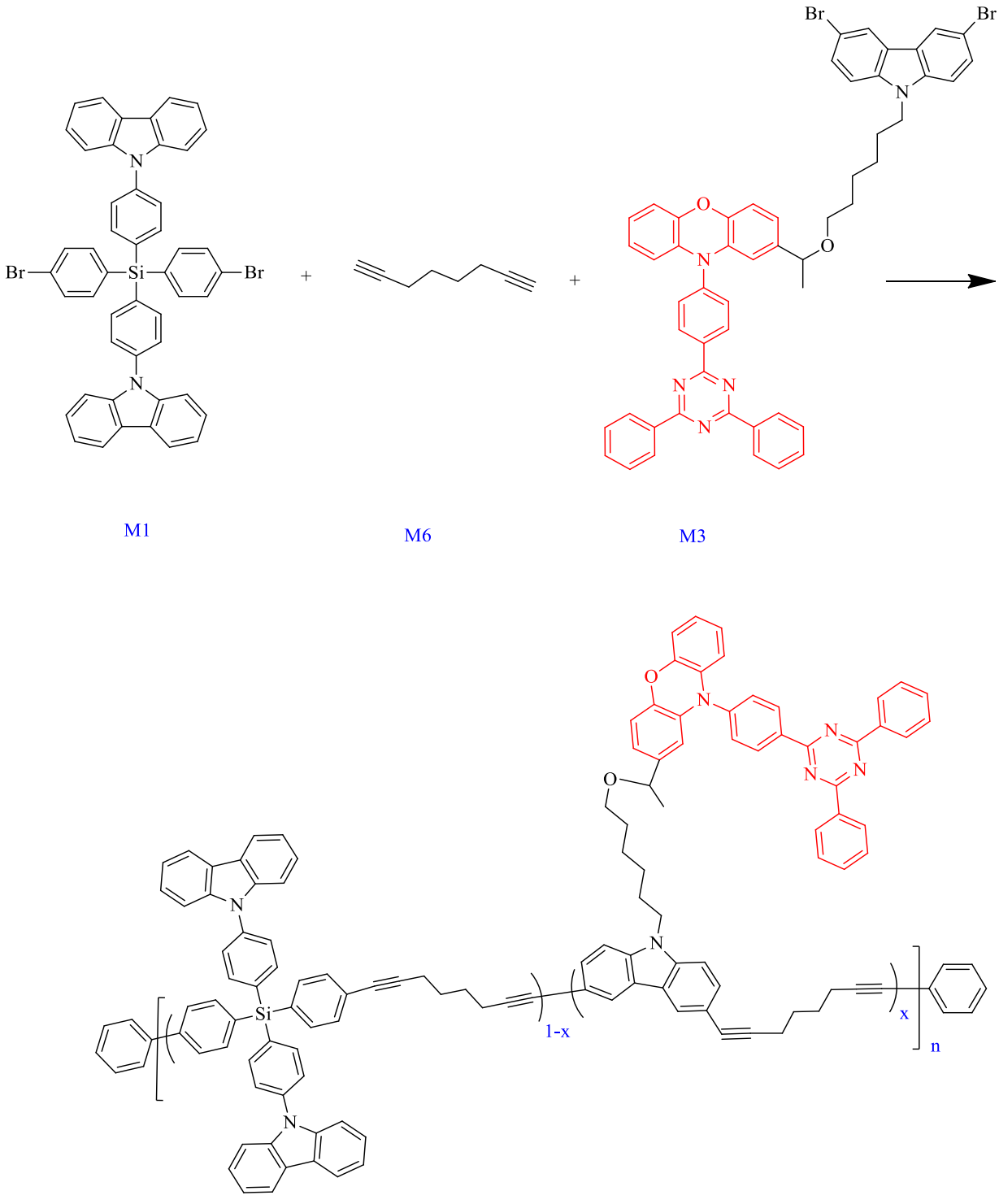

M1 M6 M3

P11, x = 0 (0%TADF units)
P12, x = 0.1 (5%TADF units)

Scheme 3.2 Synthetic path of P11 and P12.

Reagents & conditions: anhydrous THF, Cu(I), $Pd(PPh_3)_2Cl_2$, PPh_3, triethylamine, 80°C, 3d.

3.2.1 Monomer Preparation

The synthetic route for monomer 5 is shown in Scheme 3.3. M5 reacted with M1 to make P9 and reacted with M1 and M3 to prepare polymer 10. The preparation path of M1 (4-(9H-carbazol-9-yl) phenyl) bis(4-bromophenyl) silane (Br-SiCz-Br)) and compound M3 were described in the previous chapter.

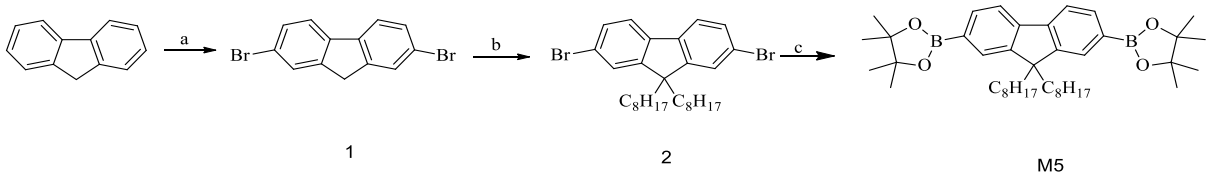

Scheme 3. 3 Preparation steps of M5

Br_2, dry chloroform, H_2SO_4, RT, 30h; b) KOH, KI, C_8H_{17}-Br, DMSO RT, 22h, c) bis(pinacolato)diboron, KOAc, $Pd(dppf)Cl_2$, DMF, 90°C, 52h.

Bromination of fluorene at 2- and 7-positions was carried out using bromine. The reaction took place at room temperature under dry conditions in presence of dry $CHCl_3$. To prevent the bromination of the protons of methylene, the reaction was carried out in a dark environment. The first product (dibromofluorene) was purified through column chromatography after TLC exhibited three spots of crude product. Petroleum ether and dichloromethane were used as the mobile phase eluent in purification, and the yield of the desired product was approximately 75%. The chemical structure and purity of this compound were determined and confirmed via TLC, NMRs, elemental analysis and mass spectrometry, which all show reasonable agreement with the literature. The ^1H NMR spectrum of this molecule showed a singlet peak at 3.90 ppm, which is attributed to protons at the 9-position of the fluorene. ^{13}C NMR of this product displayed 7 peaks for 7 different environments around the carbons and one of the peaks showed at 36.5 ppm, which is understood to be the carbon of methylene bridge in dibromofluorene. Scheme 3.4 illustrates the proposed mechanism of this reaction. As is shown, H_2SO_4 firstly reacts with the bromine to generate the complex (Br-Br^+-H) which increases the electrophilic nature of bromine. In the following step, the pi electrons in the aromatic C=C work as a nucleophile that attacks the electrophilic bromine (Br) to make an intermediate carbocation. In the final step, the proton of sp^3 adjacent to the bromo- group was removed to regenerate the carbon=carbon and the aromatic ring. $HSO4^-$ appeared to remove the mentioned proton to make dibromofluorene; then H_2SO_4 was regenerated as a catalyst.

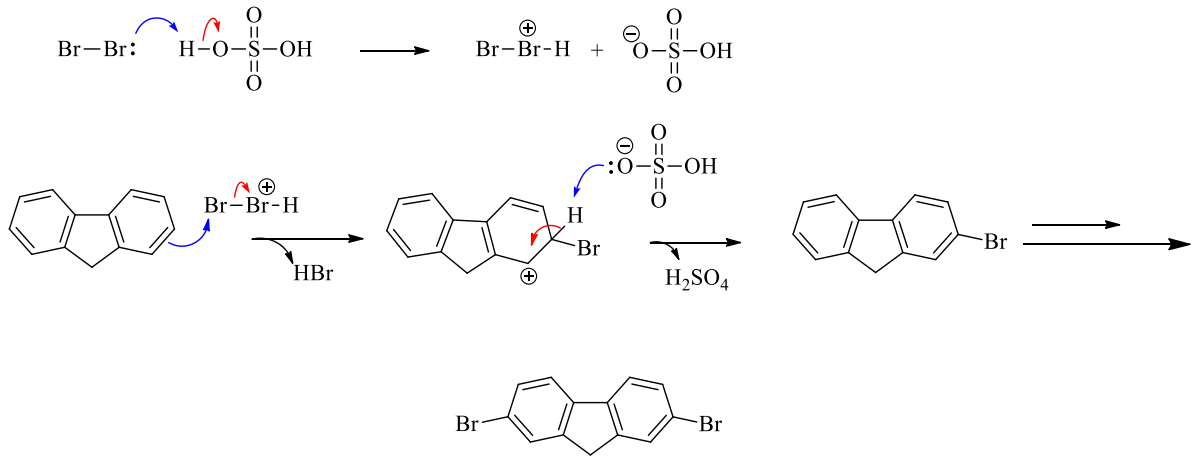

Scheme 3. 4 Proposed mechanism to yield 2,7-dibromofluorene.

The next step was the synthesis of compound 2, in which the reaction was carried out in liquid dry DMSO, where 2,7- dibromofluorene (1) reacted with 1-bromooctane at the 9-position in presence of KOH as a base and KI as a nucleophilic catalyst to yield the crude product. This crude was purified twice by recrystallisation from methyl alcohol and chloromethane to yield light yellowish crystals with a yield of 80%. The purity was confirmed through mass spectrometry, ^{1}H NMR and ^{13}C NMR. ^{1}H-NMR showed that the singlet peak of the 9-position proton vanished at 3.90 ppm. It also illustrated the expected number of protons in the aliphatic region. The mechanism of this reaction is a nucleophilic substitution, which is similar to that explained in Chapter 2. However, this mechanism involves two S_N2 reactions. i) iodide from KI replaces the (Br) from 2,7- dibromofluorene to form a better-leaving group (LG). Therefore, easier for nucleophilic attack on the neighbouring carbon. ii) the second nucleophilic substitution takes place in which (I) is left and product 2 is formed.

A modified procedure from Brunner was used to synthesise 2,7-bis(4,4,5,5-tetramethyl-1,3,2-dioxaborolan-2-yl)-9,9-di-n-octylfluorene (M5).[22] The reaction took place at high temperature under dry conditions in presence of the potassium acetate base and palladium catalyst. The final product obtained after purification was a white solid with 81% yield. It was purified by methanol precipitation, after which the acidic protons were removed by passing it through basic alumina. By using NMR, GC-MS and elemental analysis, the purity of the product, as well as its structure were confirmed. The ^{1}H NMR showed an intense single peak at 1.38 ppm, which was attributed to the protons of the methyl group in the attached boronic ester (as shown in Figure 3.1). In addition, there were peaks at m/z 642, 643 and 644 in the mass spectrum of monomer 5, which were due to the existence of the boron isotopes, ^{10}B and ^{11}B. The results of

the analysis and data are strong evidence that the brominated material (2) had been successfully converted to a boronic ester product (M5).

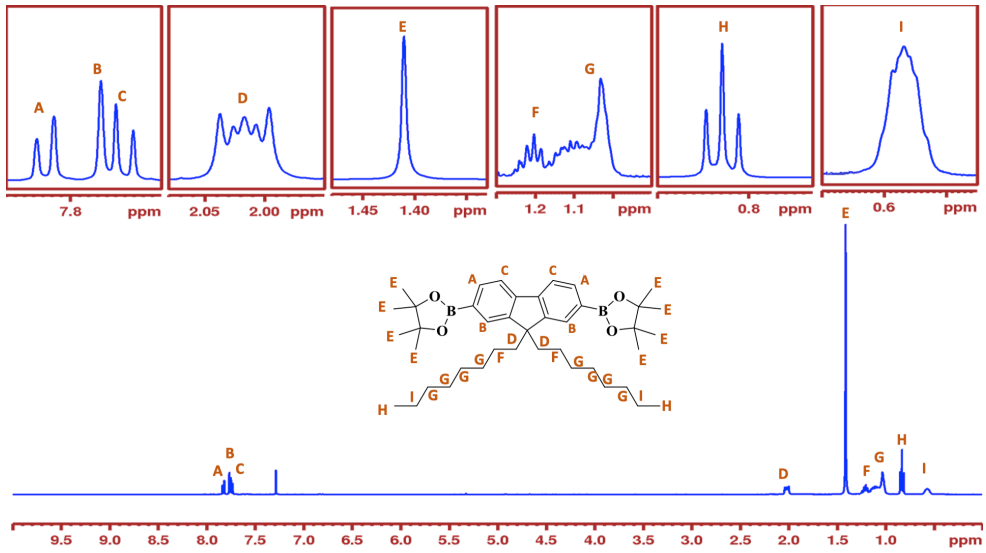

Figure 3. 1 ^{1}H-NMR spectrum of (M5) in $CDCl_3$.

Suzuki cross-coupling is the mechanism responsible for this reaction, which is similar to the mechanism described in the first two chapters.

In addition to M5, M1 and M3 were required to make all the polymers described in this chapter. The synthesis route and mechanism of these monomers were explained in detail in the previous chapter. It is worth noting that the PXZ-TRZ unit, which has TADF characteristics, was introduced into M3, which was gradually incorporated into the synthesised polymers. As mentioned before, the TADF unit was grafted onto the side chain of P10 and P12. Unlike M5, M6 (1,7-octadiyne) was purchased from a commercial supplier and used directly without any further modification. M6 is used for the Sonogashira polymerisation described in this chapter.

3.2.2 Polymers Preparation

Among all synthesised copolymers in this chapter, two polymers (P9 and P10) were designed using the Suzuki cross-coupling reaction, in which the reaction occurs between the di-brominated molecule and the boronic ester material as shown previously in Scheme 3.1. The polycondensation reaction was carried out *via* a similar procedure that was described in the second chapter. The polymerisation reaction was monitored to track the formed precipitate. The reaction to produce P9 was ended after two days, as a large amount of precipitate had

formed, while the P10 reaction was stopped after three days. The Suzuki cross-coupling mechanism is the one responsible for this reaction; the reaction mechanism including all steps was described in detail in Chapter 1.[23] End capping reagents were added to the polymers after stopping the polymerisation reaction. This step enhances the stability of the synthesised TADF polymers during fabrication of OLED devices. Finally, Soxhlet extraction was used to fractionate the polymers and different solvents used for this purpose such as chloroform, acetone, toluene, hexane and methanol.

Polymers P11 and P12 were also made. These two polymers were designed via Sonogashira polymerisation. P11 was formed from the reaction between the first monomer and M6, while P12 was made from M1, M6 and M3 with a molar feed ratio of 0.9:1:0.1, respectively. However, the accurate ratio was calculated from the ^{1}HNMR spectra and the results are presented in table 3.1. The reaction was carried out following a modified procedure that was used by Grätz et al.[24] This method of polymerisation usually relies on two catalysts; one is copper(I) iodide and the other is a palladium derivative. The reaction took place at 100°C in the presence of triethylamine as the base, and toluene as the solvent. It was stopped when the percentage of polymer precipitate was higher than the percentage of solvent in the sealed vessel. The crude product was then extracted using ethyl acetate, which was followed by washing and drying. The desired polymers were purified by precipitating in alcohol multiple times. P11 and P12 were formed as white solids. The chemical structure and purity of the polymers were identified through ^{1}H NMR and GPC. The ^{1}H NMR spectra for P11showed the peak of attached M1 between 7.20 ppm and 8.20 ppm, while the spectra of P12 displayed an extra peak for the TADF monomer with distinguishable small signals of PXZ-TRZ. The reaction mechanism of P11 and P12 were illustrated and explained in the introduction section.

Table 3. 1 ^{1}H NMR results of TADF percentage ratio in P9, P10, P11 and P12

Polymers	feed ratio	actual ratio
P9	0%	0%

P10	5%	4.1%
P11	0%	0%
P12	5%	3.3%

GPC was performed to estimate the weight average molecular weight (Mw) and the number-average molecular weight (Mn) using polystyrene as an internal standard and tetrahydrofuran (THF) as the eluent (Table 3.2). All prepared polymers demonstrated good solubility in most organic solvents at room temperature. The yield of all polymers was less than 65%. Among all polymers described in this chapter, P9 displayed the highest Mn and Mw, followed by P10, while Sonogashira polymers (P11 and P12) showed relatively lower Mn and Mw values. P9 has a larger Mw (38100 Da) compared to others; that can be explained by the conjugation effect of 2,7-linked fluorenes. Fluorene-based polymers (P9-P10) had a higher Mw due to the large alkyl soluble group, which increases the solubility of the polymers to enable further polymerization. On the other hand, the low Mn and Mw for P11 and P12 are attributed to the alkyne evaporation and aggregation of the alkyne as a result of the polymers' higher planar conformation.[25] It is worth noting that incorporating alkyne units in polymers' structure increases the aggregation and hence the planarity. This leads to polymers to display poor solubility with different solvents in Soxhlet, resulting in only low molecular weight of polymers that are extracted, whereas a large fraction of polymers is left in the Soxhlet apparatus. This is also the same reason why these polymers (P11 and P12) have lower yields.

Table 3. 2 GPC results of P9, P10, P11 and P12

Polymer	M_n (Da)	M_w (Da)	PDI	Yield	Fraction
P9	23600	38100	1.61	64%	Chloroform
P10	14200	18200	1.277	60%	Chloroform
P11	5700	7500	1.30	32%	Toluene
P12	3000	3400	1.12	35%	Toluene

3.2.3 UV-Vis Analysis and Photoluminescence Properties

The optical characteristics of polymers P9, P10, P11 and P12 in dilute chloroform solutions (Figures 3.2 and 3.3 (a)) and solid state as drop-cast thin films on quartz substrate (Figure 3.2 and 3.3 (b)) were investigated using UV-Vis spectroscopy. The onset of optical absorption of the polymers in the solid state was used to calculate the optical band gaps of all polymers. Table 3.3 summarises the measured optical characteristics of all polymers.

Table 3.3 UV-Vis values of P9, P10, P11 and P12

Polymers	λ_{max} Solution (nm)	λ_{max} Film (nm)	λ Onset in thin film (nm)	$E_{g\ opt}$ (eV)
P9	319	327	394	3.15 ± 0.011
P10	321	328.5	401	3.09 ± 0.023
P11	289	302	360	3.44 ± 0.006
P12	290	303	363	3.41 ± 0.017

Polymers 9, 10, 11 and 12 displayed different maximum absorptions in chloroform solution. TADF polymers containing fluorene in their molecular structure (P9 and P10) showed higher values (319 nm and 321 nm) respectively, compared with P11 and P12, which exhibited lower absorption values (289 nm and 290 nm) respectively. The blue shift of P11 and P12 is ascribed to the lower molecular weight of these polymers. The presence of fluorene in P9 and P10 structure enhances the π-π* transition, which increases the electron delocalisation, resulting in more red-shifted absorption. Moreover, the UV-Vis spectra of these polymers revealed a stronger bathochromic absorption in the thin film compared to their absorptions in chloroform solution. This might be understood as the polymers adopting a more planar shape in the solid state.

The polymers' optical band gaps were approximately calculated, according to the onset of optical absorption in the film; these were 3.15 eV, 3.09 eV, 3.44 eV and 3.41 eV for P9, P10, P11 and P12, respectively. The use of 2,7 fluorenes in P9 and P10 enabled a partial increase in the conjugation system, which enhanced the π-π stacking in the thin film. Thus, P9 and P10 showed narrower band gaps than P11 and P12.

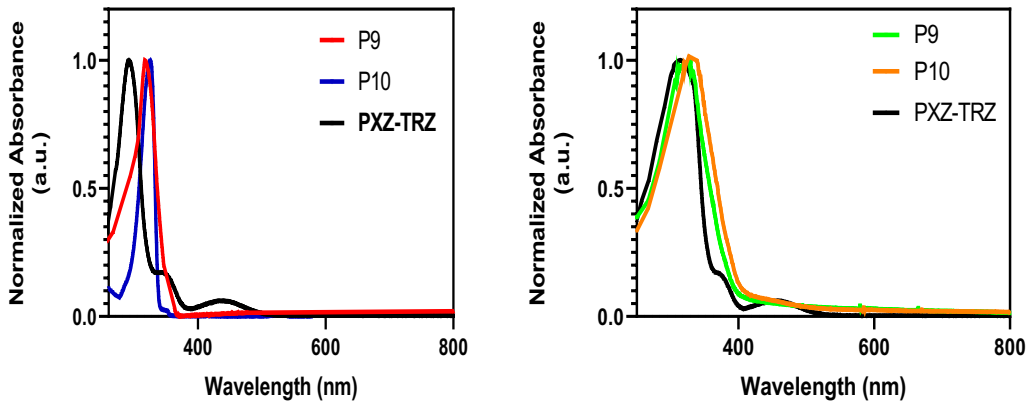

Figure 3. 2 Normalized UV-Vis absorption spectra of P9, P10, and TADF unit in a) chloroform solution and in b) thin film

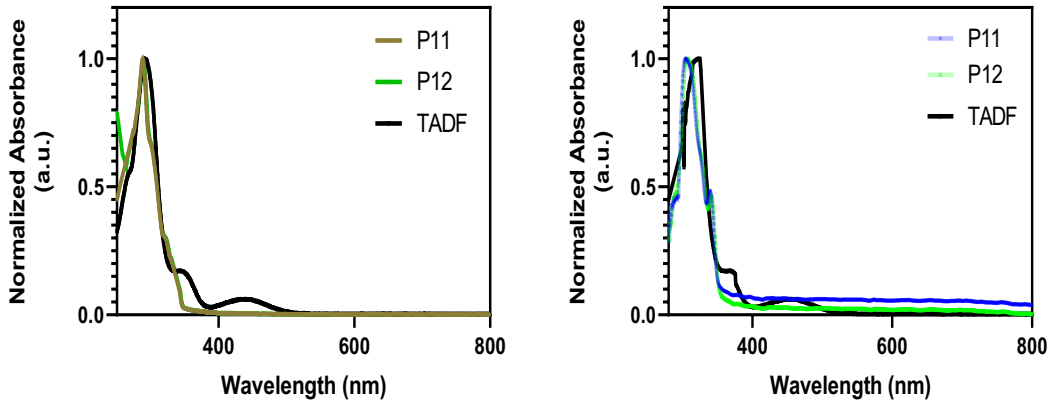

Figure 3. 3 Normalized UV-vis absorbance of P11, P12 and TADF unit in a) chloroform solution and in b) thin film

The photoluminescent spectra of the designed polymers and the PXZ-TRZ unit in toluene and in the solid state are shown in Figures 3.4 and Figure 3.5. While P9 and P11 display only one major emission peak, two peaks are detected from the emission spectra of P10 and P12. In solution, P10 exhibits two emission peaks. The strongest one is at around 390 nm and the less intense peak is at about 535 nm; these are attributed to the emissions of the polymer's backbone and the TADF unit. Similarly, Figure 3.5 (a) shows two emission peaks from P12. Therefore, there is a partial energy transfer to the TADF unit from the polymer chain in the solution state. Meanwhile, the solid-state photoluminescence spectra proved that a complete interchain energy transfer took place from the polymer backbone to the PXZ-TRZ unit. It shows the main peak of P10 and P12 to be around 535 nm, while the backbone emission is almost negligible.

It is apparent from the data that the TADF units play a significant role in the emission profile of the copolymers.

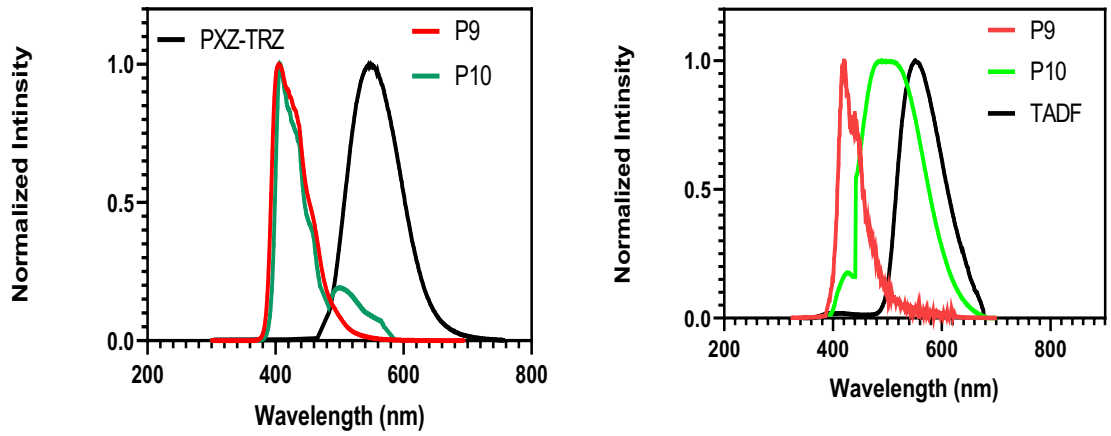

Figure 3. 4 Normalized intensity of P9, P10 and TADF unit in a) toluene solution and in b) thin film

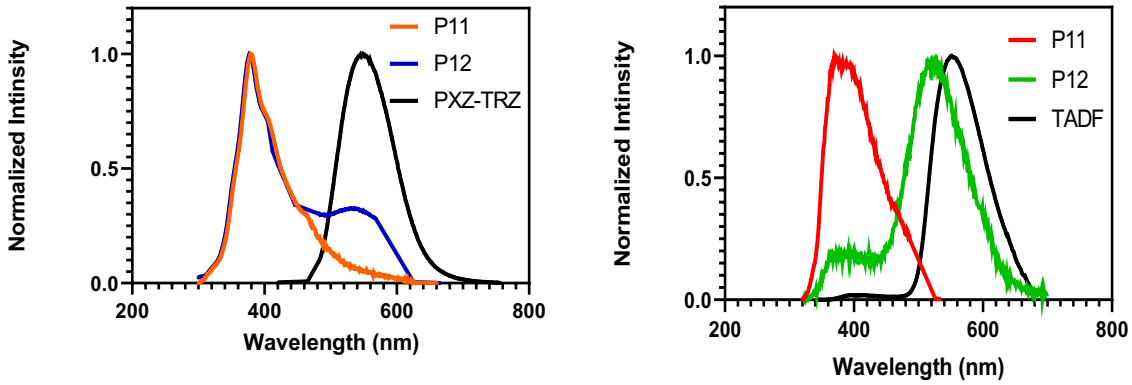

Figure 3. 5 Normalized intensity of P11, P12 and TADF unit in a) toluene solution and in b) thin film

3.2.4 Elechtrochemical Analysis

Cyclic voltammetry (CV) experiments were performed on a Princeton Potentiostat / Galvanostat 263A electrochemical workstation. The experiment used a three-electrode setup, with Ag/Ag^{+} as the reference electrode, a platinum disc as the working electrode, and a platinum wire as the auxiliary electrode. The electrochemical characteristics of the polymers were assessed using thin films cast in anhydrous acetonitrile and tetrabutylammonium perchlorate as an electrolyte. In the application of organic light-emitting diodes, determining the positions of the HOMO and the LUMO energy levels of semiconducting materials is

important. The value of the onset oxidation potential is therefore used to calculate the HOMO level, whilst the value of the onset reduction potential is used to calculate the LUMO level. As a result, the electrochemical band gap (Eg(elec)) is defined as the difference between them. The electrochemical band gaps of this chapter's polymers (P9-P12) are summarised in Table 3.4. Figure 3.6 displays the reduction and oxidation of each polymer.

Table 3. 4 CV analysis data for P9-P12

Polymers	HOMO (eV)[a.]	LUMO (eV)[b.]	Eg (elec) (eV)[c]
P9	-5.28	-3.43	1.85 ± 0.0022
P10	-5.04	-3.46	1.58 ± 0.0036
P11	-5.33	-3.36	1.97 ± 0.0018
P12	-5.09	-3.39	1.70 ± 0.0025

a. HOMO energy levels estimated from the onset of the oxidation peak. b. LUMO energy levels calculated from the onset of the reduction peak. c. Electrochemical band gap.

The study of the LUMO and HOMO levels for the prepared Suzuki polymers, P9 and P10, and for the Sonogashira polymers, P11 and P12, showed that P10 and P12 demonstrate shallower HOMO levels of -5.04 and -5.09 eV, respectively. P9 and P11 exhibited HOMO levels of -5.28 and -5.33, respectively. Shallower HOMO levels for P10 and P12 are due to the presence of the TADF unit. The deeper HOMO energy level of P11 resulted from the lower conjugation system. Figure 3.6 and 3.7 below shows the reduction and oxidation of the synthesised polymers, P9-P12.

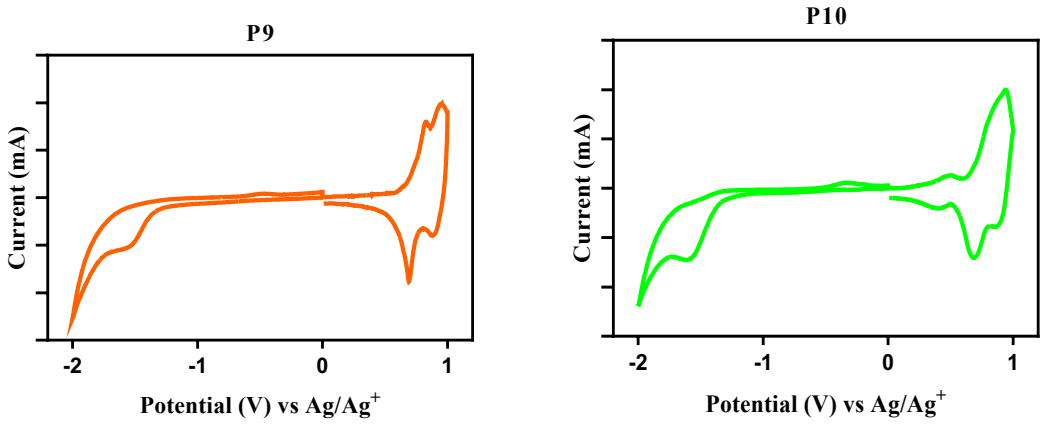

Figure 3. 6 Cyclic voltammograms for P9 and P10.

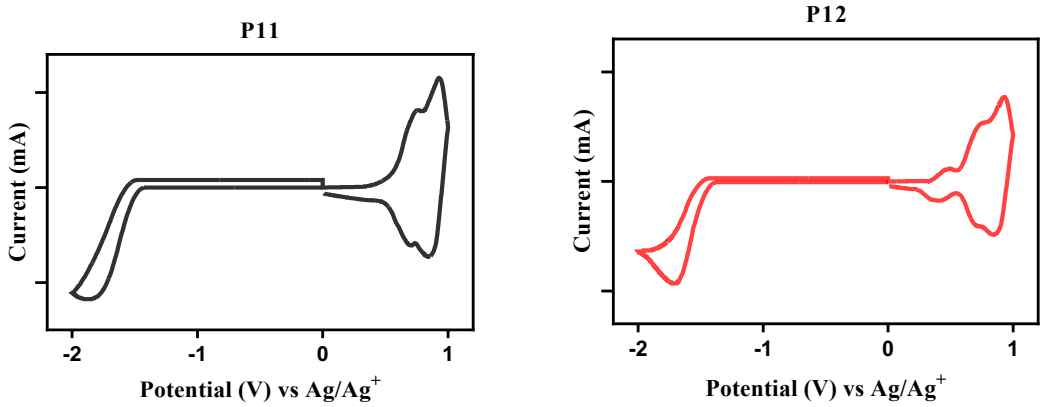

Figure 3. 7 Cyclic voltammograms for P11 and P12.

All polymers showed multiple reversible oxidation peaks. The first oxidation peaks in P10 and P12 could be ascribed to the electron donor, phenoxazine, of the TADF unit, whereas the other oxidation peaks are due to the polymers' backbone and carbazole-based host moiety. Moreover, the HOMO energy levels of these polymers are comparable to those previously prepared in Chapter 2, particularly those for P1-P2 and P5-P6. The HOMO level values for these polymers range from -5.4 to -5.43. The HOMO levels of all polymers are very close when the TADF unit is incorporated into the polymer backbone (P2, P5, P10 and P12) whereas the HOMO values for P9 and P11 are shallower than the values for P1 and P5 owing to their increased conjugation. This indicates that replacing the backbone with a fluorene or acetylene unit will only affect the HOMO level values in the absence of the TADF unit.

3.2.5 Thermal Analysis

All polymers were tested for thermal stability using thermogravimetric analysis (TGA). A plot of the thermal degradation curves for each polymer is shown in Figure 3.8. Table 3.5 shows the temperature at which each polymer started to decompose. Heating was carried out at a speed of 10 °C min^{-1} in an inert nitrogen atmosphere.

Table 3. 5 Thermal properties of P9-P12

Polymers	Td (℃)[a]
P9	360
P10	362
P11	288
P12	291

[a] Degradation onset of polymers determined by thermogravimetric analysis with a heating rate of 10℃ min^{-1} under an inert nitrogen atmosphere.

All polymers in this chapter displayed good thermal stability with a decomposition onset temperature in excess of 355 °C for the Suzuki copolymers, P9 and P10, and in excess of 285 °C for the Sonogashira polymers, P11 and P12. P9 and P10 showed similar onset degradation temperatures of approximately 361 °C, whereas P11 and P12 exhibited almost the same but lower onset decomposition temperatures of ~290 °C. This can be attributed to the cleavage of the alkyl side chain of the TADF polymers; these degradations showed weight losses comparable with the side chains in the polymers. Amongst all the polymers that have been prepared in this report (Chapters 2 and 3), P10, followed by P9, displays the greatest thermal stability compared with those prepared in Chapter 2 (P1-P8) and in this chapter (P11 and P12). It is hypothesised that P9 and P10 possess larger conjugation backbones than the other polymers in this study which result in an increase in degradation temperature.

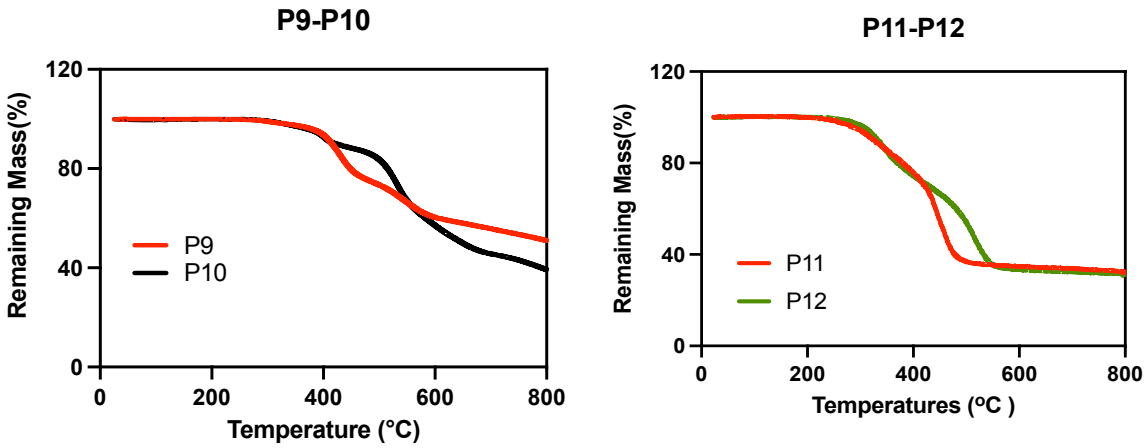

Figure 3. 8 Thermogravimetric analysis of polymers, P9-P10, carried out at a heating rate of 10 °C min^{-1} in an inert nitrogen atmosphere.

3.3 Conclusion

OLED host molecules must possess significant high triplet energy to enable an efficient energy transfer to the incorporated emitter. Introducing a high triplet host material such as SiCz into TADF polymers can enhance the quantum efficiency as well as overcome the quenching of triplet excitons of high triplet emitters. Therefore, designing successful host materials is extremely important for optimising the performance of OLED devices. This chapter describes a series of fluorene-based polymers (P9, P10) and 1,7-octadiyne-based polymers (P11, P12) that were successfully made using palladium-catalysed Suzuki coupling and Songashira cross-coupling reactions. Different spectroscopic analyses were used to study the properties of these copolymers. In addition to the advantages of the Suzuki polycondensation, which was discussed in Chapter 1, P11 and P12 were designed from aryl bromides and 1,7-octadiyne followed the Sonogashira procedure, which was carried out under mild conditions. The successful incorporation of the TADF unit in the copolymers (P10 and P12) was verified by ^{1}H NMR and ^{13}C NMR, and the TADF character of these polymers was confirmed by photoluminescence spectroscopy. Gel permeation chromatography was used to estimate the Mn and Mw of the resulting polymers. Thermogravimetric analysis was also performed to test thermal stability, while ultraviolet-visible spectroscopy confirmed the optical properties. Finally, cyclic voltammetry was used to understand the electrochemical properties of these polymers.

The Mw and Mn were both estimated by GPC, which gave larger values for P9 and P10. The polymers continuing fluorene displayed a higher Mn and Mw due to the presence of 2,7-linked fluorene, which enhanced the conjugation length in these non-conjugation polymers. In addition, the large molecular weight of these two polymers is due to soluble alkyl chins, which promotes further polymerization.

The optical properties of polymers P9-P12 were tested in solutions and solid states using UV-Vis spectroscopy. All of these polymers exhibited red-shifted behaviour when applied to thin films. This is attributed to the planar conformation of the polymers' backbones in a solid state. Cyclic voltammetry analysis showed different band gaps for these polymers with lower values for P9 and P10. In addition, P9 and P10 exhibited a lower band gap compared to other polymers described in this chapter, which could be explained by the use of 2,7-linked fluorene in P9 and P10. This boosts the conjugation length to adopt a more coplanar structure.

3.4 References

(1) Wang, Q.; Tian, Q.-S.; Zhang, Y.-L.; Tang, X.; Liao, L.-S. High-Efficiency Organic Light-Emitting Diodes with Exciplex Hosts. *Journal of Materials Chemistry C* **2019**, *7* (37), 11329–11360.

(2) Segal, M.; Baldo, M. A.; Holmes, R. J.; Forrest, S. R.; Soos, Z. G. Excitonic Singlet-Triplet Ratios in Molecular and Polymeric Organic Materials. *Physical Review B* **2003**, *68* (7), 075211.

(3) Gray, V.; Dreos, A.; Erhart, P.; Albinsson, B.; Moth-Poulsen, K.; Abrahamsson, M. Loss Channels in Triplet–Triplet Annihilation Photon Upconversion: Importance of Annihilator Singlet and Triplet Surface Shapes. *Physical Chemistry Chemical Physics* **2017**, *19* (17), 10931–10939.

(4) Thompson, M. The Evolution of Organometallic Complexes in Organic Light-Emitting Devices. *Mrs Bulletin* **2007**, *32* (9), 694–701.

(5) Reineke, S.; Thomschke, M.; Lüssem, B.; Leo, K. White Organic Light-Emitting Diodes: Status and Perspective. *Reviews of Modern Physics* **2013**, *85* (3), 1245.

(6) Li, Y.; Gao, X.; Wang, L.; Tu, G. Deep-Red Organic Light-Emitting Diodes with Stable Electroluminescent Spectra Based on Zinc Complex Host Material. *RSC Advances* **2017**, *7* (64), 40533–40538.

(7) Tung, Y.; Lee, S.; Chi, Y.; Chen, L.; Shu, C.; Wu, F.; Carty, A. J.; Chou, P.; Peng, S.; Lee, G. Organic Light-Emitting Diodes Based on Charge-Neutral RuII Phosphorescent Emitters. *Advanced Materials* **2005**, *17* (8), 1059–1064.

(8) Cocchi, M.; Virgili, D.; Fattori, V.; Rochester, D. L.; Williams, J. A. G. N∧ C∧ N-Coordinated Platinum (II) Complexes as Phosphorescent Emitters in High-Performance Organic Light-Emitting Devices. *Advanced Functional Materials* **2007**, *17* (2), 285–289.

(9) Wei, Q.; Fei, N.; Islam, A.; Lei, T.; Hong, L.; Peng, R.; Fan, X.; Chen, L.; Gao, P.; Ge, Z. Small-Molecule Emitters with High Quantum Efficiency: Mechanisms, Structures, and Applications in OLED Devices. *Advanced Optical Materials* **2018**, *6* (20), 1800512.

(10) Zheng, H.; Zheng, Y.; Liu, N.; Ai, N.; Wang, Q.; Wu, S.; Zhou, J.; Hu, D.; Yu, S.; Han, S. All-Solution Processed Polymer Light-Emitting Diode Displays. *Nature Communications* **2013**, *4* (1), 1–7.

(11) Joo, C. W.; Huseynova, G.; Yifei, J.; Yoo, J.-M.; Kim, Y. H.; Cho, N. S.; Lee, J.-H.; Kim, Y.-H.; Lee, J. Highly Efficient Solution-Processed Blue Organic Light-Emitting Diodes Based on Thermally Activated Delayed Fluorescence Emitters with Spiroacridine Donor. *Journal of Industrial and Engineering Chemistry* **2019**, *78*, 265–270.

(12) Uoyama, H.; Goushi, K.; Shizu, K.; Nomura, H.; Adachi, C. Highly Efficient Organic Light-Emitting Diodes from Delayed Fluorescence. *Nature* **2012**, *492* (7428), 234–238.

(13) Nakagawa, T.; Ku, S.-Y.; Wong, K.-T.; Adachi, C. Electroluminescence Based on Thermally Activated Delayed Fluorescence Generated by a Spirobifluorene Donor–Acceptor Structure. *Chemical Communications* **2012**, *48* (77), 9580–9582.

(14) Zhang, D.; Cai, M.; Zhang, Y.; Zhang, D.; Duan, L. Sterically Shielded Blue Thermally Activated Delayed Fluorescence Emitters with Improved Efficiency and Stability. *Materials Horizons* **2016**, *3* (2), 145–151.

(15) Dias, F. B.; Bourdakos, K. N.; Jankus, V.; Moss, K. C.; Kamtekar, K. T.; Bhalla, V.; Santos, J.; Bryce, M. R.; Monkman, A. P. Triplet Harvesting with 100% Efficiency by Way of Thermally Activated Delayed Fluorescence in Charge Transfer OLED Emitters. *Advanced Materials* **2013**, *25* (27), 3707–3714.

(16) Jankus, V.; Data, P.; Graves, D.; McGuinness, C.; Santos, J.; Bryce, M. R.; Dias, F. B.; Monkman, A. P. Highly Efficient TADF OLEDs: How the Emitter–Host Interaction Controls Both the Excited State Species and Electrical Properties of the Devices to Achieve near 100% Triplet Harvesting and High Efficiency. *Advanced Functional Materials* **2014**, *24* (39), 6178–6186.

(17) Gazvoda, M.; Virant, M.; Pinter, B.; Košmrlj, J. Mechanism of Copper-Free Sonogashira Reaction Operates through Palladium-Palladium Transmetallation. *Nature Communications* **2018**, *9* (1), 1–9.

(18) Sonogashira, K.; Tohda, Y.; Hagihara, N. A Convenient Synthesis of Acetylenes: Catalytic Substitutions of Acetylenic Hydrogen with Bromoalkenes, Iodoarenes and Bromopyridines. *Tetrahedron Letters* **1975**, *16* (50), 4467–4470.

(19) Dieck, a H. A.; Heck, F. R. Palladium Catalyzed Synthesis of Aryl, Heterocyclic and Vinylic Acetylene Derivatives. *Journal of Organometallic Chemistry* **1975**, *93* (2), 259–263.

(20) Cassar, L. Synthesis of Aryl-and Vinyl-Substituted Acetylene Derivatives by the Use of Nickel and Palladium Complexes. *Journal of Organometallic Chemistry* **1975**, *93* (2), 253–257.

(21) Ye, S.; Liu, Y.; Di, C.; Xi, H.; Wu, W.; Wen, Y.; Lu, K.; Du, C.; Liu, Y.; Yu, G. Wide-Energy-Gap Host Materials for Blue Phosphorescent Organic Light-Emitting Diodes. *Chemistry of Materials* **2009**, *21* (7), 1333–1342.

(22) Brunner, K.; van Dijken, A.; Börner, H.; Bastiaansen, J. J. A. M.; Kiggen, N. M. M.; Langeveld, B. M. W. Carbazole Compounds as Host Materials for Triplet Emitters in Organic Light-Emitting Diodes: Tuning the HOMO Level without Influencing the Triplet Energy in Small Molecules. *Journal of the American Chemical Society* **2004**, *126* (19), 6035–6042.

(23) Suzuki, A. Organoboron Compounds in New Synthetic Reactions. *Pure and Applied Chemistry* **1985**, *57* (12), 1749–1758.

(24) Grätz, S.; Wolfrum, B.; Borchardt, L. Mechanochemical Suzuki Polycondensation–from Linear to Hyperbranched Polyphenylenes. *Green Chemistry* **2017**, *19* (13), 2973–2979.

(25) Terao, J.; Wadahama, A.; Matono, A.; Tada, T.; Watanabe, S.; Seki, S.; Fujihara, T.; Tsuji, Y. Design Principle for Increasing Charge Mobility of π-Conjugated Polymers Using Regularly Localized Molecular Orbitals. *Nature Communications* **2013**, *4* (1), 1–9.

Chapter 4: Developing a New Series of TADF Copolymers Based on a Fluorene Derivative for OLED Applications

Abstract

In this chapter, a series of TADF copolymers were synthesised and characterised based on a mixture of conjugated polyfluorene derivatives and a non-conjugated chain as the backbone. P13-P16 were designed following a side-chain engineering strategy in which the Suzuki polycondensation coupling method was used to make them. Different molar ratios of PXZ-TRZ were incorporated into the side chain of P14, P15 and P16, while P13 was made without a TADF unit for analysis comparison purposes. The successful polymerisations were verified by NMR, and the LUMO and HOMO energy levels were measured using cyclic voltammetry. The (Mw) was calculated using GPC and was in the range of 15300 g/mol and 27000 g/mol. The polymer free of the TADF unit (P13) produces only one peak in its photoluminescence spectrum, while P14-P16 show dual emission peaks. In addition, the optical band gap of all polymers was measured; they show comparable values based on their absorption onset in the UV-Vis solid state. All polymers exhibit good thermal stability with large decomposition temperatures. Furthermore, the designed polymers show high solubility in most common organic solvents, which make them a good candidate as an emitting layer for solution-processed polymer light-emitting diodes (PLEDs).

4.1. Introduction

Considerable efforts have been made to design and develop organic electroluminescent molecules for application in OLEDs. When comparing OLEDs with liquid crystal displays, OLEDs offer better colour contrast and a wider viewing angle; they also demand less input energy and can be designed thinner.[1] Bernanose[2] was the first to report the organic electroluminescence compound in the fifties, the noticeable development in this field started in 1987 when Tang and Van Slyke made a new luminescent device containing tris(8-hydroxyquinoline) aluminum.[3] The first OLED polymer, in which the emissive layer was made from the poly(p-phenylenevinylene)(PPV), was reported in the early nineteen-nineties by Friend et al.[4] Since then, a variety of non-conjugated and conjugated polymers based on phosphorescence, TADF and fluorescence have been studied for high-performance PLEDs such as, poly(thiophene), poly(1,4-phenylene) and polyfluorene. TADF polymers were introduced to enhance the IQE without using rare, heavy metals. That can be possible by using materials that have a small (ΔE_{ST}).[5,6] However, small TADF molecules described in the literature are inappropriate for vapor evaporatin proccesing.[7] Polymeric TADF materials are different from small molecules, as they can be applied into the high quality solid-state *via* solution processing techniques, such as roll printing and coating, which is easy to operate and results in reduced commercial costs. However, numerous types of solution-processable TADF polymers have been innovated and made using various strategies. These include dendrimers[8], conjugated and non-conjugated side chain polymers[9,10] and through-space charge transfer polymers.[11]

Poly(fluorene)s[12] have been shown to have high quantum yield and have been used in electroluminescent devices because the fluorene derivative materials possess many features, such as their emissions can cover all the visible range[13]. Also, their emissive properties can be easily managed by manipulating the functionalisation of the methylene bridge and they have good thermal stability. All these advantages together with other unique features make copolymers of polyfluorene excellent components for luminescent layers in TADF devices. Thus, colour tuning is possible by copolymerising fluorene monomer derivatives with different aromatic groups and adjusting the band gap. Many attempts have been made to examine the spectroscopic and electrochemical properties of fluorene and its derivatives. Fluorene derivatives have chemical, electrical and optical characteristics that make them ideal for use as functional units in organic compounds. They emit light and support both hole and electron transport in OLEDs. They have also been designed to work as host materials in phosphorescent

organic light-emitting diode applications.[14,15] Incorporating a fluorene moiety into the molecular structure enhances the thermal stability as well as the durability of organic molecules.

As discussed here, various homopolymers and copolymers were developed using fluorene and its derivatives. Fluorene-based polymers have been applied and utilised either as the active emissive layer in PLEDs or as the host molecule to make another colour by taking the energy into the lower energy of fluorophores.[16,17] The good solubility nature, elevated thermal stability and high fluorescence quantum yields of solid-state polyfluorenes make them particularly appropriate for blue light-emitting diode devices (LEDs).[17–19] Poly(9,9-di-n-octylfluorene)[20] is an example of a homopolymer of fluorene, which is used as an efficient blue emitter. However, polyfluorenes might form excimers or become aggregated during the operation of electroluminescent devices, which leads to a redshift and limit the efficiency as a result.[21] Thus, the position of carbon nine (C9) in fluorene is filled with large substituents to overcome the efficiency limitation. In addition, the pure blue emission of the polyfluorene main chain can be sustained by inserting a saturated sp^3 in the C9 position of the fluorene ring, which results in the inhibition of the conjugated system between the polymer's backbone and side chain.

The polymeric materials that make the emissive layers of solution-processed devices can negatively impact the efficiency and output performance of TADF devices, as external quantum efficiency can be restricted by the polymers that are used. As shown in the first chapter, the singlet to triplet ratio is in a range of 1:1 to 1:3 for polymer-based OLEDs; over 50% of triplet excitons are nullified by the process of non-radiative decay of excited excitons. The mechanisms of TADF from organic emissive molecules provide a good method of improving the external quantum efficiency of polymeric devices. In this chapter, PXZ-TRZ is used as the TADF pendant unit and is attached to the side chain of the polymers to generate a channel of TADF in a single polymer system. According to the side chain engineering strategy, incorporating TADF units into polymers' side chains together with the polymer's backbone provides a single polymer system with two unique advantages. The electrical properties of the backbone, which serves as the host and charge-transporting channel, are unaffected by the side chain.[22,23] Therefore, polymers described in this chapter (P13-P16) were designed following this technique, whereby the TADF unit is attached to M3.

4.2. Results and Discussions

4.2.1. Monomer Preparation for the Fluorene-based Copolymers (P13-P16)

The targeted polymers of this chapter were made from 1,6-bis(4-[4,4,5,5-tetramethyl-1,3,2-dioxaborolan]phenoxy)hexane, 2,7-di(bromo)-9,9-di-n-octylfluorene (M7) and M3, which contains a TADF unit. M2 was successfully prepared with a high yield in two steps as shown in Chapter 2. The mechanism of the involved steps is discussed and explained in Schemes 2.10 and 2.11 (Chapter 2). Regarding fluorene-based monomer (M7), it was made via the bromination of fluorene in the first step, followed by the alkylation of C9 in 2,7-dibromofluorene. The preparation of M7 is illustrated in Scheme 4.1. The appearance of this monomer was a light yellowish crystalline solid, which was obtained after recrystallising the crude product with methyl alcohol. The purity of this structure was confirmed, first by TLC, and then by mass spectrometry, which displayed the required peaks. In addition, the chemical structure of this monomer was identified via ^{1}HNMR, which showed that the singlet peak of the 9-position proton disappeared at 3.90 ppm. Furthermore, the aliphatic region in the ^{1}HNMR spectrum displayed the expected numbers of protons as shown in Figure 4.1. The ^{13}C NMR spectrum of this monomer shows nine peaks for nine different carbons in the aliphatic region and six peaks for six different carbons in the aromatic region. Also, elemental analysis of M7 gave a result as follows: C,63.12: H, 7.31: Br, 30.63 which was in agreement with its proposed formula.

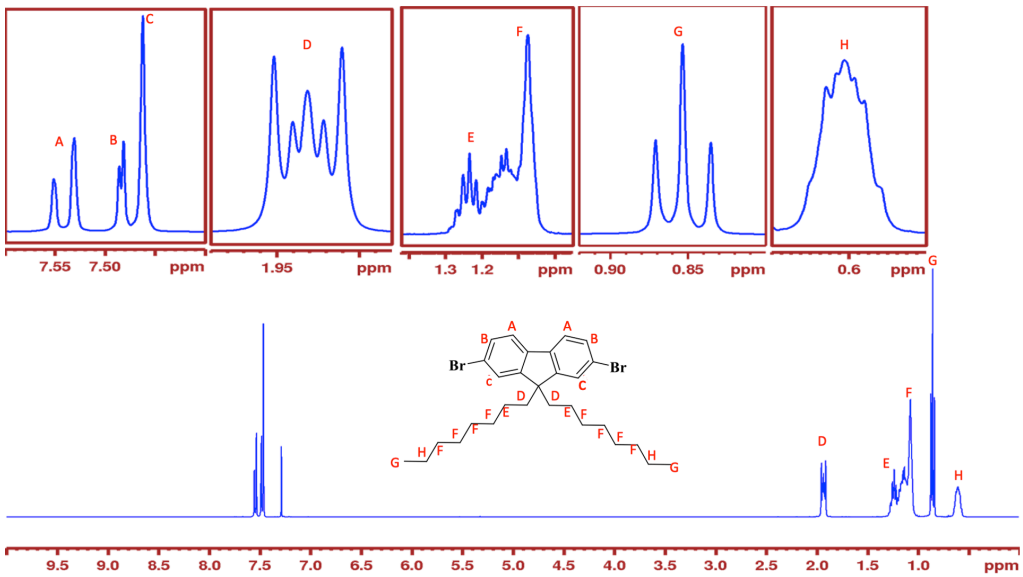

Figure 4. 1 ^{1}H-NMR spectrum of M7 in $CDCl_3$.

The mechanism of this reaction involves two steps, bromination and alkylation; these were described in-depth in Chapter 3. Furthermore, M3 was also included in the structure of P14, P15 and P16. This monomer was prepared via many steps, as shown in Chapter 2. TADF dye was prepared and introduced into this monomer as described in the second chapter.

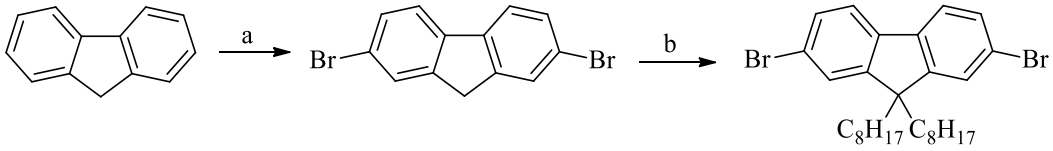

Scheme 4. 1 Preparation route to M7.

Reagents & conditions; a) Br_2, dry chloroform, H_2SO_4, RT, 30h; b) KOH, KI, 1-bromooctane, DMSO RT, 22h,

4.2.2. Preparing Alternating Fluorene-based Copolymers (P13-P16)

In order to minimise the conjugation system of fluorene-based polymers, an alkyl chain was introduced into a series of alternating copolymers that were created in this chapter (P13-P16). The backbone of these polymers involves the fluorene unit, which is presented as a repeating unit in all of the designed polymers. The fluorene moiety was selected to provide these polymers with a strong fluorescence property. The ordered chemical structure and high thermal stability of fluorene-based polymers are fundamental to promote electrons and holes mobility. It is also important to disconnect the conjugation to optimise the high triplet energy, thus, preventing the reverse transfer of energy from the TADF guest to the host in TADF polymers. In addition, the concept of bearing alkyl chains on fluorene units is extremely beneficial to increase the solubility of the resulting polymers. Therefore, the fluorene-based monomer described in this chapter contained chains.10-(4-(5-Phenyl-1,3,4-oxadiazol-2-yl)phenyl)-10H-phenoxazine (PXZ-TRZ) was used for TADF attachment, due to its high and well-known quality as a green TADF emitter. PXZ-TRZ was synthesised and attached to M3, as described in Chapter 2. The TADF unit was grafted onto the side chain of P14, P15 and P16, while P13 was prepared without M3 to compare their properties. It is worth mentioning that the TADF dye unit was incorporated into these polymers with different percentages P16>P15>P14. All of this chapter's polymers were synthesised following a Suzuki palladium catalytic coupling mechanism. Scheme 4.2 shows the synthetic path for monomers polycondensation.

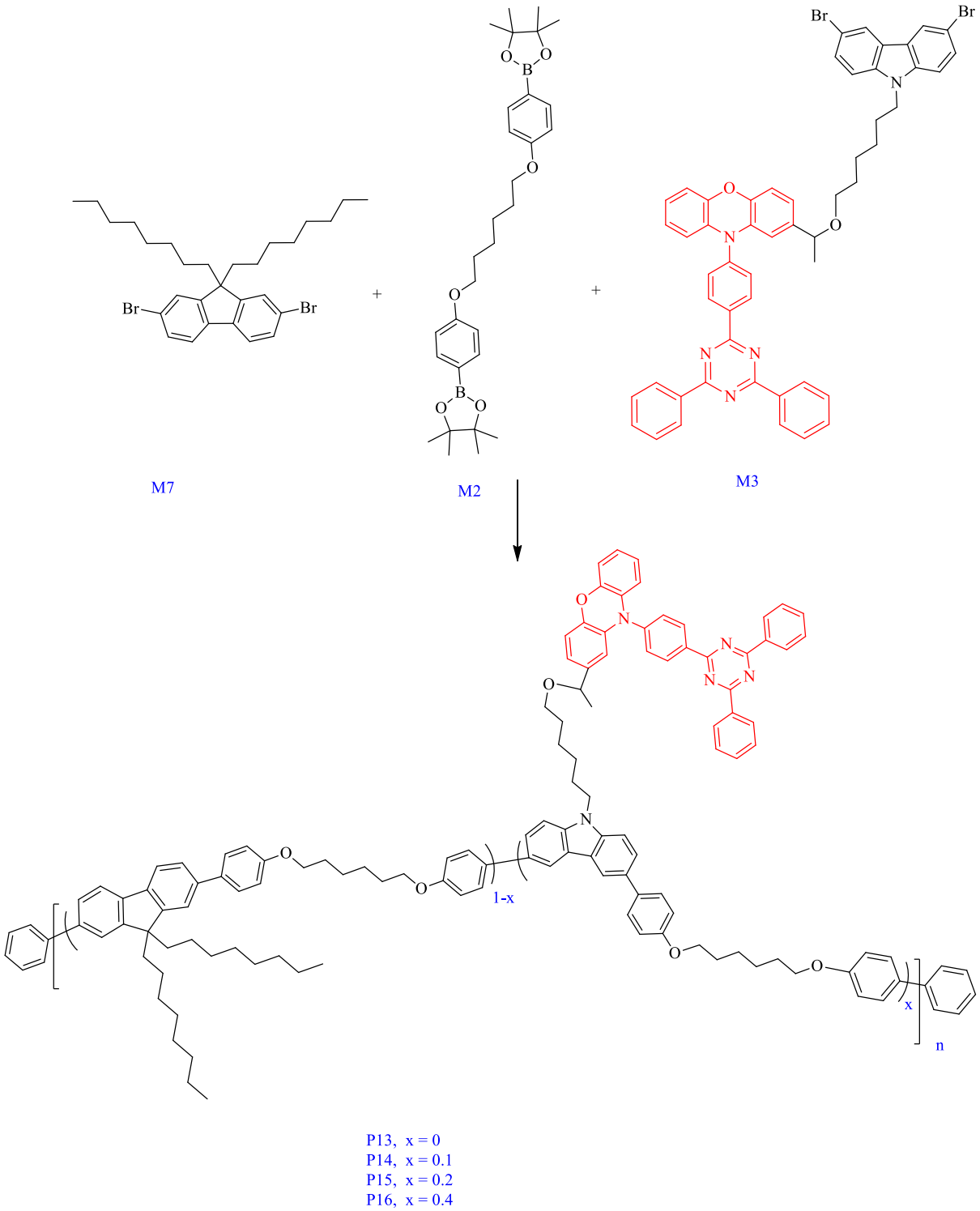

Scheme 4.2 Synthetic route to polymers (P13-P16).

Reagents & conditions; $NaHCO_3.H_2O$, dry THF, $P(o\text{-}tol)_3$, $Pd(OAC)_2$, Ar, 80°C-90°C.

All the monomers' polymerisations were carried out under argon atmosphere conditions. The reaction duration varied from polymer to polymer, based on the amount of precipitate that

formed at the bottom of the reaction flask. These polymers were obtained with very reasonable yields; they also displayed high solubility in most organic solvents, such as THF, $CHCl_2$, $CHCl_3$ and acetone, which makes them viable candidates for solution-processed devices. ^{1}HNMR confirmed the chemical structure of all the designed polymers. The spectral results exhibited good accordance with the proposed structures. The actual percentage of TADF unit in these copolymers can be seen and calculated from the NMR spectra (table 4.1). It is clear that the intensity of PXZ-TRZ peaks in the spectrum increased from P14 to P16 as the molar feed ratio increased. In P14, P15 and P16, the peaks at 9.02, 8.80, 6.57 and 6.02 ppm are assigned to hydrogen atoms in PXZ-TRZ. While fluorene characteristic peaks appeared at 7.53 and 7.46 ppm, the protons of alkyl chains are shown between 1.10 and 1.95 ppm.

Table 4. 1 ^{1}H NMR results of TADF percentage ratio in P13,P14, P15 and P16

Polymers	feed ratio	actual ratio
P13	0%	0%
P14	5%	4.4%
P15	10%	10.8%
P16	20%	20.2%

The polymers' weight average molecular weight (Mw) and the number average molecular weight (Mn) were estimated by gel permeation chromatography (GPC) using tetrahydrofuran (THF) as the eluent and calibration of polystyrene as a standard. The weight average molecular weight of the synthesised polymers in this chapter was in the range of 16000 and 29000. P13, which does not contain M3 in its chemical structure, displayed the highest molecular weight (29000 g/mol). This might be due to the absence of M3, as the steric hindrance of this monomer may lead to chain twists resulting in a vigorous repulsion between the chains. This interaction between the polymer chain prevents high molecular weight copolymers from forming during

polymerisation.[24,25] P16 appeared to have the lowest molecular weight (16000) due to π–π stacking. It is understood that larger steric hindrance of M3 increases π–π stacking of the P16 backbone, and as a result bigger aggregation of polymers' backbone. Therefore, the polymer (P16) precipitates faster during polymerization, hence, lower Mw.

However, all designed polymers in this section displayed larger molecular weights than those described in Chapters 2 and 3. It is frequently prescribed for the planer structure of fluorene unit (M7), which boost reducing steric repulsion between polymers' chains during the polymerisation process. Therefore, extending the polymers' chains results in polymers with a large molecular weight. The data of GPC analysis, including the Mw, Mn and polydispersity index (PDI) is presented in Table 4.2.

Table 4. 2 GPC analysis date for P13, P14, P15 and P16.

Polymer	M_n (Da)	M_w (Da)	PDI	Yield	Fraction
P13	26500	29000	1.09	65%	Chloroform
P14	22300	26800	1.20	59%	Chloroform
P15	19600	22900	1.17	60%	Chloroform
P16	13500	16000	1.19	60%	Chloroform

4.2.3. UV-Vis and Photoluminescence Analysis of the Polymers

UV-Vis was used to evaluate the optical characteristics of the normalised UV-visible absorption spectra of the polymers P13, P14, P15 and P16. The polymers' energy optical band gaps were determined according to the absorption onset of the polymers in the thin film. Table

4.3 below summarises the optical behaviours of all polymers. The UV-Vis spectra were firstly taken in a dilute solution of chloroform (Figure 4.2(a)), then as drop cast thin film in the solid state (Figure 4.2(b)).

Table 4. 3 The optical data for P13, P14, P15 and P16.

Polymer	λ_{max} in Solution (nm)	λ_{max} in Film (nm)	λ_{max} Onset of thin film (nm)	$E_{g\ opt}$ (eV)
P13	349	353	408	3.04 ± 0.0024
P14	346.5	350	406.5	3.05 ± 0.0018
P15	345	349	407	3.05 ± 0.0038
P16	341	345	402	3.08± 0.0022

P13, P14, P15 and P16 in chloroform solution demonstrate maxima absorption at 349, 346.5, 345 and 341 nm respectively. As shown in the data, all polymers display an intense peak in the ultraviolet region as result of the polymeric backbone absorption. The 2,7-functionalised fluorene repeat units increase the electronic delocalisation across the polymer's backbone by optimising the conjugation system, which results in a greater red-shifted absorption for the fluorene-based polymers in this chapter compared with those described in Chapter 2 and Chapter 3. In addition, the normalised UV-Vis absorption of the PXZ-TRZ unit was calculated in order to be compared with the optical data of P14, P15 and P16. However, the absorption of the TADF units did not appear in P14 and P15, while a very weak peak showed in the P16 spectra, which was attributed to the low molar ratio loading of TADF unit into these polymers. Furthermore, these polymers showed no obvious differences between them in neat films. When these polymers are applied to thin film, the UV-Vis absorption peak displayed a red shifted behaviour compared to the dilute solution. It is ascribed to a stronger planarity of the polymers in film, which leads to π-π interchain stacking, resulting in a red shifted absorption. P13-P16 optical band gaps demonstrated comparable values, ranging from 3.04 to 3.08 eV. However, these values are lower than those reported in previous chapters due to the high delocalisation

of electrons along the backbone of conjugated fluorene-based polymers, which result in lower band gaps.

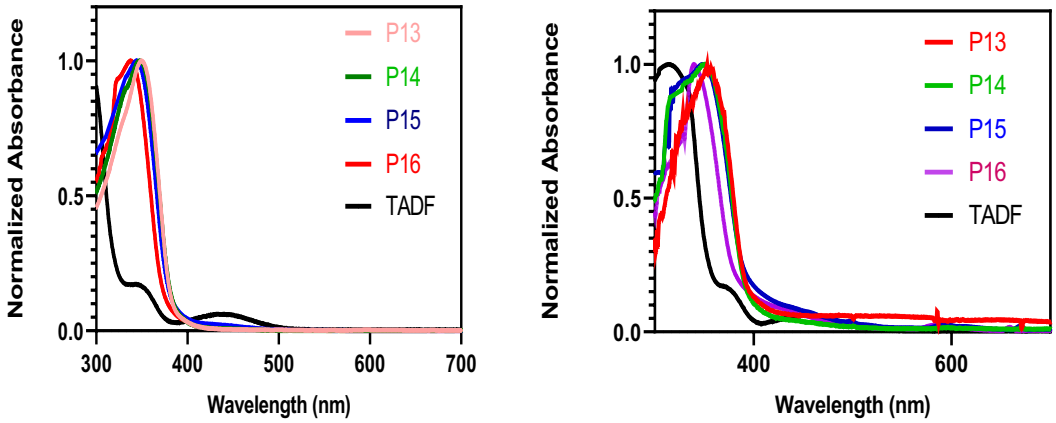

Figure 4. 2 UV-Vis absorption of P13-P16 in (a) a dilute chloroform solution and (b) solid thin film.

The spectra of photoluminescence spectroscopy analysis in toluene solution (a) and neat film (b) are depicted in Figure 4.3. In the solution of toluene, polyfluorene-based P14 and P15 emit distinct dual emission peaks at 400 and 550 nm respectively. The former is assigned to the polymer backbone while the latter is attached to the green TADF emitter. Increasing the molar feed of M3 from 0.1 in P14 to 0.4 in P16 led to a gradual increase in the peak intensity at 550 nm, which indicates a higher energy transfer from the polymer's backbone to the attached TADF unit. Interestingly, the photoluminescence spectra of these polymers in the solid state exhibited extremely different behaviours; there was almost no emission originating from the polymer's backbone. All of them showed the main emission at ~554 nm, which denotes a total energy transfer from the polymers' backbone to the TADF unit. When photoluminescence runs at higher concentrations, it is obvious that the TADF emission peak gradually controls the spectra while the emission from the backbone of the polymers is minimised. This is attributed to the aggregation effect; that is, when the neighbouring chains stay a short distance from each other, more energy is transferred from the backbone of the polymers to the side chain. Thus, the TADF emissions dominate the photoluminescence spectra. Moreover, the enhancement of the TADF aggregation effect from P14 to P16 as the loading of M3 increased, a progressively red shift from 540 nm for P14 to 550 nm for P16 occurred.

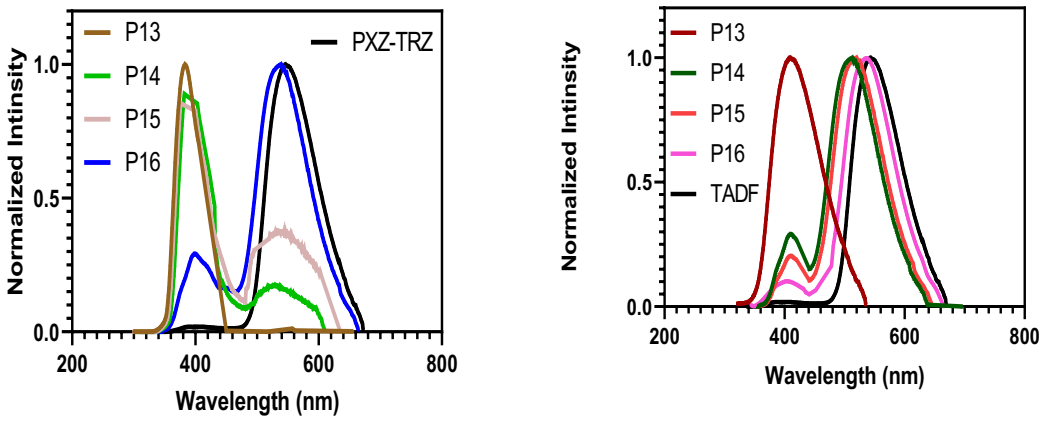

Figure 4. 3 Photoluminescence (PL) spectra of P13-P16 in (a) toluene solution and (b) in neat film

4.2.4 Electrochemical Analysis

The electrochemical properties of the polymers, P13, P14, P15 and P16, have also been investigated. Figure 4.4 shows the results of a CV analysis of the electrochemical characteristics of the polymers. In comparison to the *vacuum* level, the onsets of oxidation and reduction were used to calculate the HOMO and LUMO energy levels for each polymer. The experiments were carried out on drop-cast polymer films utilising a platinum-disc electrode as the working electrode in dry acetonitrile with 0.1M tetrabutylammonium perchlorate as the electrolyte and silver nitrate (Ag/Ag^{+}) as the reference electrode at a scan rate of 100 mV s^{-1}. As shown in Table 4.3, the electrochemical band gaps were calculated using the difference between HOMO and LUMO levels. The HOMO and LUMO levels were determined from the onset of the oxidation (Eox) and reduction (Ered) potentials, respectively, based on the following equations:

$$\text{HOMO} = -\left[(E_{onset\,(ox)} - E_{foc}) + E_{ref}\right] (\text{eV})$$

$$\text{LUMO} = -\left[(E_{onset\,(red)} - E_{foc}) + E_{ref}\right] (\text{eV})$$

where E_{foc} is the potential of the ferrocene/ferrocenium ion, and E_{ref} is the reference energy level for ferrocene (4.8 eV below the *vacuum* level; the *vacuum* level is defined as zero).

The polymer's band gap was calculated by subtracting the LUMO level from the HOMO level using the following equation:

$$Eg_{elec} = - (HOMO - LUMO)\ eV$$

Table 4. 4 CV analysis data for P13-P16

Polymers	HOMO (eV)[a]	LUMO. (eV)[b]	Eg (elec) (eV)[c]
P13	-5.35	-3.38	1.97 ± 0.0011
P14	-5.04	-3.44	1.60 ± 0.0025
P15	-4.98	-3.45	1.53 ± 0.0016
P16	-4.90	-3.46	1.44 ± 0.0037

a. HOMO energy levels estimated from the onset of the oxidation peak. b. LUMO energy levels calculated from the onset of the reduction peak. c. Electrochemical band gap.

Table 4.4 and Figure 4.4 show how the HOMO and LUMO levels for these TADF polymers are determined by their chemical structures. The HOMO levels for the fluorene-based polymers, P13, P14, P15 and P16, were -5.35, -5.04, -4.98 and -4.90 eV, and the LUMO levels, -3.38, -3.44, -3.45 and -3.46, respectively. Cyclic voltammograms for these polymers displayed similar behaviours to those for polyfluorene products, exhibiting a semi-reversible wave. The results indicate that polymers with PXZ-TRZ units (P14, P15 and P16) showed a gradual increase in HOMO levels and a small decrease in LUMO levels. This observation can be attributed to the phenoxazine donor moiety and triazine acceptor unit, respectively. Figure 4.4 shows the reduction and oxidation onsets for the copolymers.

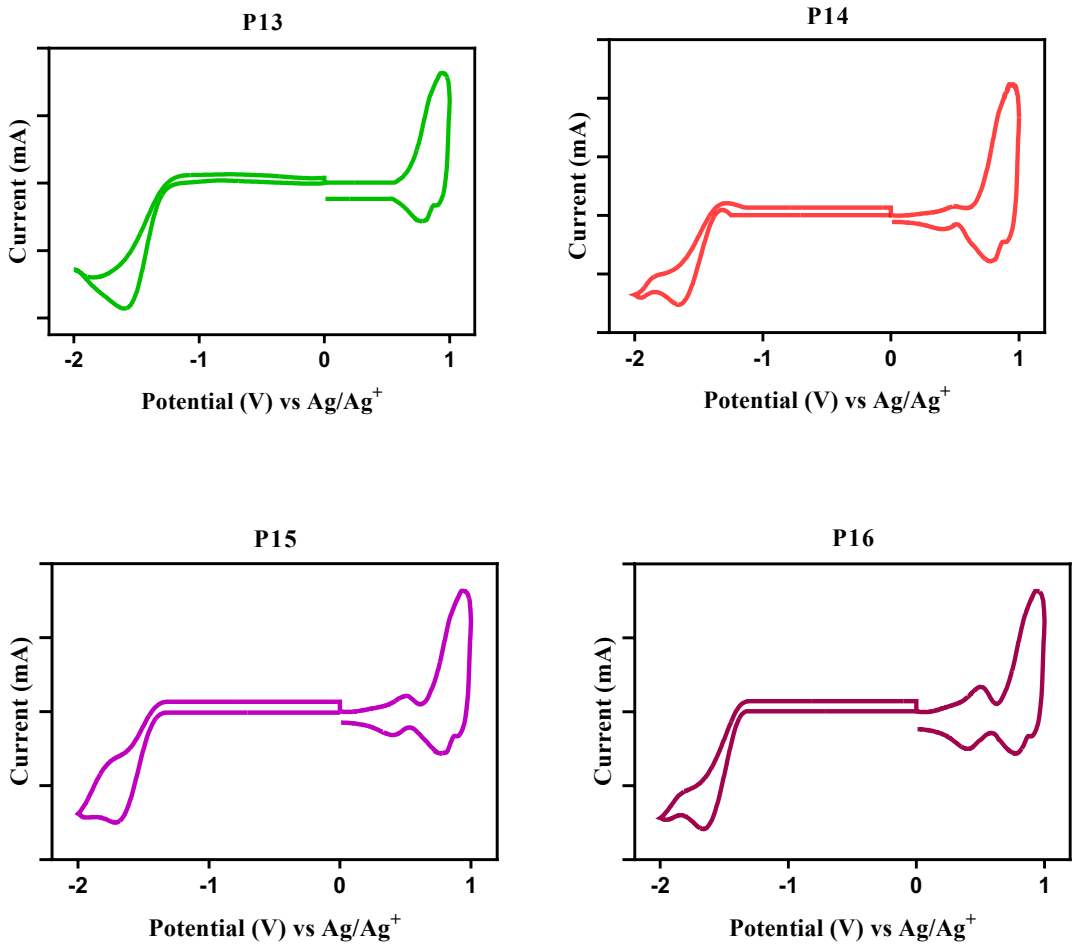

Figure 4. 4 Cyclic voltammograms for P13, P14, P15 and P16.

The electrochemical behaviours of these copolymers show different oxidation peaks as illustrated in Figure 4.4. P13 displayed one oxidation peak located at 0.63 V, which was assigned to the polymer backbone. P14, P15 and P16 exhibited extra oxidation peaks located at 0.32 V, 0.26 V and 0.18 V, respectively, which related to the phenoxazine unit in the TADF polymers; little difference was seen in the reduction peaks for all the polymers. The LUMO levels of these polymers are in the range of -3.38 to -3.46, which implies a good electron-transporting ability for organic light-emitting diodes.[26] The CV results indicated that the synthesised polymers could be promising candidates as electron-transporting materials in OLEDs. It is obvious in this report that there are two main trends with increasing PXZ-TRZ content within the polymer structure: i) the lower potential oxidation wave intensity was gradually increased (larger HOMO level); ii) the electron bandgap was decreased from 1.60

eV in P14 to 1.44 eV in P16. These results show total agreement with those published by Zhao et al..[26]

A comparison of the electrochemical behaviours of this chapter's polymers (P13-P16) with those of Chapter 1 (P1-P4), which were based on carbazole, shows that the HOMO levels for P13, P14, P15 and P16 were shallower than those for P1, P2, P3 and P4, respectively. Additionally, the fluorene-based polymers displayed a slightly lower band gap than those polymers based on carbazole. The electrochemical band gaps for P1, P2, P3 and P4 were 2.06 eV, 1.66 eV, 1.61 eV and 1.54 eV, respectively, and for P13, P14, P15 and P16, 1.97 eV, 1.60 eV, 1.53 eV and 1.44 eV, respectively. This could be explained by the different conjugation systems of the fluorene-based and carbazole-based polymers.

4.2.5 Thermal Analysis

Thermal gravimetric analysis (TGA) was used to examine the thermogravimetric properties of the synthesised polymers in an inert nitrogen atmosphere at a heating rate of 10 °C min^{-1}. Figure 4.5 depicts the degradation curve for each polymer; Table 4.5shows the temperatures at which decomposition began (Td).

Table 4. 5 Thermal properties for P13- P16.

Polymers	Td (℃)[a]
P13	328
P14	330
P15	332
P16	340

[a] Degradation onset of polymers determined by using thermogravimetric analysis with a heating rate of 10℃ min^{-1} in an inert nitrogen atmosphere

All the polymers have decomposition temperatures of above 300 °C at 5% weight loss (Td), which is due to the presence of the conjugated fluorene structure in the polymer backbone. This high thermal stability makes these compounds good candidates for OLED devices. P13 has the

lowest Td value (328 °C) followed by P14 (330 °C), P15 (332 °C) and P16 (340 °C). The onset degradation temperature is slightly reduced as the TADF content diminishes. This can be attributed to the decrease in hindrance structure from P16 to P13. The degradation curve is a result of the alkyl chain cleavage in the polymer backbone and side chain. As the decomposition plot shows, all these polymers degrade until 25% of the weight remains, and then the curves stabilise until the end of measurement at 800 °C. Polymers with large alkyl chains are hypothesised to become less volatile during combustion. As a result, during the decomposition of P13, P14, P15 and P16, thick charred layers were generated on the virgin polymer, which isolated the virgin polymers from heat flux due to their low thermal conductivity. Polymer thermal decomposition would be retarded by this mechanism.[27]

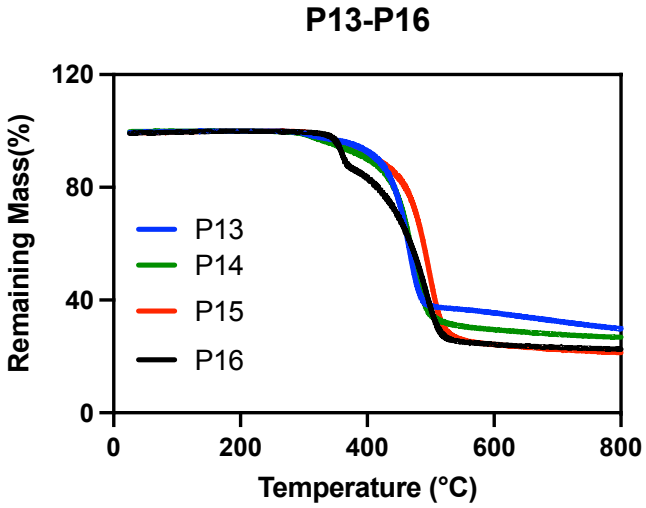

Figure 4. 5 Thermogravimetric analysis of polymers, P13, P14, P15 and P16.

4.3. Conclusion

A series of PF derivatives were synthesised based on Suzuki polycondensation. The polymers' backbones consisted of both conjugated 2,7-linked fluorene and non-conjugated alkyl chains. PXZ-TRZ moiety was incorporated with different feed molar ratios into P14, P15 and P16. Polymer P13 was purposely made without the TADF moiety for comparison. All these polymers were synthesised with a good yield and a reasonable molecular weight. They all exhibited good solubility in many organic solvents, such as DCM, THF and chloroform. Fluorene has been used in this section due to its good electron/hole-transporting properties, high stability and good linking abilities.

Thermogravimetric analysis was used to investigate the thermal stability of these polymers, in which all of them displayed good stability against the increased temperature. Furthermore, due to the conjugation system of fluorene, all of the designed TADF polymers in this chapter exhibited relatively shallow HOMO levels when their electrochemical properties were tested using cyclic by voltammetry. The UV-Vis absorption of P13, P14, P15 and P16 was investigated in a dilute solution as well as in a solid state. The maximum peak absorption of all polymers was observed in the ultraviolet region (~340 nm) in both solution and solid states. Finally, the resultant polymers (P14-P16) offered an effective energy transfer in solid states, which enabled them to maintain the property of TADF from the attached guest, giving an intense peak at ~550 nm.

4.4. References

(1) Mitschke, U.; Bäuerle, P. The Electroluminescence of Organic Materials. *Journal of Materials Chemistry* **2000**, *10* (7), 1471–1507.

(2) Bernanose, A. The Mechanism of Organic Electroluminescence. *Journal of Chemical Physics* **1955**, *52*, 396–400.

(3) Tang, C. W.; VanSlyke, S. A. Organic Electroluminescent Diodes. *Applied Physics Letters* **1987**, *51* (12), 913–915.

(4) Burroughes, J. H.; Bradley, D. D. C.; Brown, A. R.; Marks, R. N.; Mackay, K.; Friend, R. H.; Burns, P. L.; Holmes, A. B. Light-Emitting Diodes Based on Conjugated Polymers. *Nature* **1990**, *347* (6293), 539–541.

(5) Zhou, X.; Huang, M.; Zeng, X.; Zhong, C.; Xie, G.; Gong, S.; Cao, X.; Yang, C. Sky-Blue Thermally Activated Delayed Fluorescence Polymers with π-Interrupted Polymer Mainchain via Friedel-Crafts Polycondensation. *Polymer* **2020**, *204*, 122722.

(6) Khammultri, P.; Chasing, P.; Chitpakdee, C.; Namuangruk, S.; Sudyoadsuk, T.; Promarak, V. Red to Orange Thermally Activated Delayed Fluorescence Polymers Based on 2-(4-(Diphenylamino)-Phenyl)-9 H-Thioxanthen-9-One-10, 10-Dioxide for Efficient Solution-Processed OLEDs. *RSC Advances* **2021**, *11* (40), 24794–24806.

(7) Albrecht, K.; Matsuoka, K.; Fujita, K.; Yamamoto, K. Carbazole Dendrimers as Solution-Processable Thermally Activated Delayed-Fluorescence Materials. *Angewandte Chemie International Edition* **2015**, *54* (19), 5677–5682.

(8) Li, Y.; Chen, T.; Huang, M.; Gu, Y.; Gong, S.; Xie, G.; Yang, C. Tuning the Twist Angle of Thermally Activated Delayed Fluorescence Molecules via a Dendronization Strategy: High-Efficiency Solution-Processed Non-Doped OLEDs. *Journal of Materials Chemistry C* **2017**, *5* (14), 3480–3487.

(9) Luo, J.; Xie, G.; Gong, S.; Chen, T.; Yang, C. Creating a Thermally Activated Delayed Fluorescence Channel in a Single Polymer System to Enhance Exciton Utilization Efficiency for Bluish-Green Electroluminescence. *Chemical Communications* **2016**, *52* (11), 2292–2295.

(10) Ren, Z.; Nobuyasu, R. S.; Dias, F. B.; Monkman, A. P.; Yan, S.; Bryce, M. R. Pendant Homopolymer and Copolymers as Solution-Processable Thermally Activated Delayed

Fluorescence Materials for Organic Light-Emitting Diodes. *Macromolecules* **2016**, *49* (15), 5452–5460.

(11) Shao, S.; Hu, J.; Wang, X.; Wang, L.; Jing, X.; Wang, F. Blue Thermally Activated Delayed Fluorescence Polymers with Nonconjugated Backbone and Through-Space Charge Transfer Effect. *Journal of the American Chemical Society* **2017**, *139* (49), 17739–17742.

(12) Inagi, S.; Hayashi, S.; Fuchigami, T. Electrochemical Polymer Reaction: Selective Fluorination of a Poly (Fluorene) Derivative. *Chemical Communications* **2009**, No. 13, 1718–1720.

(13) Bernius, M. T.; Inbasekaran, M.; O'Brien, J.; Wu, W. Progress with Light-emitting Polymers. *Advanced Materials* **2000**, *12* (23), 1737–1750.

(14) Zhao, X.-H.; Zhang, Z.-S.; Qian, Y.; Yi, M.-D.; Xie, L.-H.; Hu, C.-P.; Xie, G.-H.; Xu, H.; Han, C.-M.; Zhao, Y. A Bulky Pyridinylfluorene-Fuctionalizing Approach to Synthesize Diarylfluorene-Based Bipolar Host Materials for Efficient Red, Green, Blue and White Electrophosphorescent Devices. *Journal of Materials Chemistry C* **2013**, *1* (21), 3482–3490.

(15) Ye, S.; Liu, Y.; Di, C.; Xi, H.; Wu, W.; Wen, Y.; Lu, K.; Du, C.; Liu, Y.; Yu, G. Wide-Energy-Gap Host Materials for Blue Phosphorescent Organic Light-Emitting Diodes. *Chemistry of Materials* **2009**, *21* (7), 1333–1342.

(16) Chen, F.-C.; Yang, Y.; Thompson, M. E.; Kido, J. High-Performance Polymer Light-Emitting Diodes Doped with a Red Phosphorescent Iridium Complex. *Applied Physics Letters* **2002**, *80* (13), 2308–2310.

(17) McGehee, M. D.; Bergstedt, T.; Zhang, C.; Saab, A. P.; O'Regan, M. B.; Bazan, G. C.; Srdanov, V. I.; Heeger, A. J. Narrow Bandwidth Luminescence from Blends with Energy Transfer from Semiconducting Conjugated Polymers to Europium Complexes. *Advanced Materials* **1999**, *11* (16), 1349–1354.

(18) Leclerc, M. Polyfluorenes: Twenty Years of Progress. *Journal of Polymer Science Part A: Polymer Chemistry* **2001**, *39* (17), 2867–2873.

(19) Neher, D. Polyfluorene Homopolymers: Conjugated Liquid-crystalline Polymers for Bright Blue Emission and Polarized Electroluminescence. *Macromolecular Rapid Communications* **2001**, *22* (17), 1365–1385.

(20) Grice, A. W.; Bradley, D. D. C.; Bernius, M. T.; Inbasekaran, M.; Wu, W. W.; Woo, E. P. High Brightness and Efficiency Blue Light-Emitting Polymer Diodes. *Applied Physics Letters* **1998**, *73* (5), 629–631.

(21) Klärner, G.; Davey, M. H.; Chen, W.; Scott, J. C.; Miller, R. D. Colorfast Blue-light-emitting Random Copolymers Derived from Di-n-hexylfluorene and Anthracene. *Advanced Materials* **1998**, *10* (13), 993–997.

(22) Luo, J.; Xie, G.; Gong, S.; Chen, T.; Yang, C. Creating a Thermally Activated Delayed Fluorescence Channel in a Single Polymer System to Enhance Exciton Utilization Efficiency for Bluish-Green Electroluminescence. *Chemical Communications* **2016**, *52* (11), 2292–2295.

(23) Xie, G.; Luo, J.; Huang, M.; Chen, T.; Wu, K.; Gong, S.; Yang, C. Inheriting the Characteristics of TADF Small Molecule by Side-Chain Engineering Strategy to Enable Bluish-Green Polymers with High PLQYs up to 74% and External Quantum Efficiency over 16% in Light-Emitting Diodes. *Advanced Materials* **2017**, *29* (11), 1604223.

(24) Fu, Y.; Kim, J.; Siva, A.; Shin, W. S.; Moon, S.; Park, T. Parameters Influencing the Molecular Weight of 3, 6-carbazole-based D-π-A-type Copolymers. *Journal of Polymer Science Part A: Polymer Chemistry* **2011**, *49* (20), 4368–4378.

(25) Nayana, V.; Kandasubramanian, B. Polycarbazole and Its Derivatives: Progress, Synthesis, and Applications. *Journal of Polymer Research* **2020**, *27* (9), 1–24.

(26) Zong, W.; Qiu, W.; Yuan, P.; Wang, F.; Liu, Y.; Xu, S.; Su, S.-J.; Cao, S. Thermally Activated Delayed Fluorescence Polymers for High-Efficiency Solution-Processed Non-Doped OLEDs: Convenient Synthesis by Binding TADF Units and Host Units to the Pre-Synthesized Polycarbazole-Based Backbone via Click Reaction. *Polymer* **2022**, *240*, 124468.

(27) Patel, P.; Hull, T. R.; Lyon, R. E.; Stoliarov, S. I.; Walters, R. N.; Crowley, S.; Safronava, N. Investigation of the thermal decomposition and flammability of PEEK and its carbon and glass-fibre composites. *Polymer Degradation and Stability* **2011**, 96 (1).

Chapter 5: Conclusions and Future Work

5.1. Conclusions

Polymer light-emitting devices are one of the most researched topics in flexible electronics due to their cost-effective wet production process, which gives the produced devices a pricing advantage. The key organic emissive materials used in OLEDs have rapidly evolved. The new generation of materials with TADF features can up-convert all formed triplet excitons into singlet excitons, resulting in an exciton utilisation efficiency of about 100% without the use of heavy metals. Many TVs and mobile devices are already made from thin layers of OLED. Unlike small molecule-OLEDs (SM-OLEDs), materials based on polymeric molecules are mostly suffering from low efficiency and short lifetimes, but they are readily soluble; therefore, they are used in solution processing. Moreover, only a few efficient TADF polymers have been reported so far, because it is challenging to produce an effective separation between the LUMO and HOMO levels while generating a minimised energy gap between the singlet and triplet states in conjugated polymers. Thus, many non-conjugated hosts have been introduced to enhance the triplet energy and to be incorporated into TADF polymers by a host-guest interaction system.

The main aim of this study was to create an efficient host (Br-SiCz-Br) and then design a different series of TADF-OLED polymers using the Suzuki polycondensation and Sonogashira polymerisation procedures. This thesis describes the use of a side-chain engineering strategy that inserts the TADF unit onto the polymer side chain to create a single polymer system with a TADF channel. In addition, the backbone of these polymers purposely included alkyl chains to increase the solubility and the molecular weight of the resultant polymers. The purity and chemical structure of all of the involved materials were identified and then confirmed using a variety of analytical techniques, such as elemental analysis, mass spectrometry, ^{1}HNMR and ^{13}CNMR. In each chapter, the project's principal findings were studied and discussed; the findings were summarised, and polymers were compared where relevant.

The second chapter followed a side-chain engineering technique to generate TADF polymers. A well-known TADF unit (PXZ-TRZ) was made and different molar ratios were incorporated into the side chain of the polymer's backbone. As a consequence, a range of non-conjugated polymers (P1-P8), containing SiCz, as a host was successfully prepared with a variation in the PXZ-TRZ content following the Suzuki polycondensation reaction. The optical properties of the resultant polymers, together with thermal and electrochemical characteristics, were studied and tested. Introducing the alkyl chain in these polymers resulted in their enhanced solubility

in most organic solvents, such as THF, DCM and toluene, which make them good candidates for solution processing techniques. The polymers' chemical structure and the actual percentage of TADF unit were confirmed by ^{1}HNMR, and GPC was performed to determine their molecular weight. That showed that the second series of polymers (P5-P8) have lower molecular weights than (P1-P4) due to the steric hindrance of involving monomers that limits the polymerisation chain. In addition, the polymers' optical properties in dilute solution and solid-state were investigated using UV-Vis and photoluminescence. The former displayed a red shift for all of the polymers when applied to a thin film, which is ascribed to the higher planarity of the polymers' backbone in a solid state. The photoluminescence also confirmed the successful incorporation of the TADF unit, by displaying the complete energy transfer from the polymer backbone to the TADF unit in a solid state. Finally, cyclic voltammetry and thermogravimetric analysis were both used to explore the polymers' bandgap and thermal stability respectively; in which they all showed expected bandgaps and high thermal stability.

Chapter 3 proposed a new series of non-conjugated polymers (P9, P10, P11 and P12), which have been designed using the Suzuki polycondensation reaction for P9 and P10 and based on the palladium Sonogashira reaction for P11 and P12. Furthermore, a TADF moiety was introduced into the polymers' structure (P10 and P12) with only 10% molar ratio. The chemical structure of the first two polymers of this chapter (P9 and P10) included fluorene and carbazole tetraphenyl silane, while the other two polymers (P11 and P12) incorporated 1,7-octane. Different spectroscopic analyses were used to characterise the resultant TADF polymers. The advantage of using Sonogashira cross-coupling was that the coupling reaction between aryl acetylenes and aryl bromides was carried out under mild reaction conditions. ^{1}HNMR and photoluminescence were applied to verify the structure of these TADF polymers. Other analyses, such as TGA, GPC, UV and CV were used to study the properties of the resultant polymers. The fluorene-based polymers (P9 and P10) displayed a higher molecular weight than Sonogashira-based polymers (P11 and P12), which is attributed to the 2.7-linked fluorene, which improves the planarity of these polymers. In addition, all designed polymers exhibited a red shift when applied to a solid-state film due to the high planarity of the polymers' backbone in the film state. Cyclic voltammetry also provides a reasonable band gap with small values of HOMO level.

Finally, a range of polyfluorene derivatives P13, P14, P15 and P16 were synthesised, as described in Chapter 4. All polymers were made according to side-chain engineering techniques, in which a PXZ-TRZ unit was inserted into the side chain of the polymer's

backbone using the Suzuki cross-coupling reaction. The polymer's backbone was made from conjugated fluorene and a non-conjugated chain to increase the triplet energy. While TADF was introduced into polymers P14, P15 and P16 with different molar ratios, P13 was made free of the TADF moiety for comparison. All polymers described in this chapter were made with a good yield, showing a high solubility in many organic solvents, such as THF, toluene and $CHCl_3$. The final polymer structure, together with the percentage of TADF units, was identified via ^{1}HNMR. In addition, TGA was performed to study their thermal stability and all of the polymers exhibited good stability against the high temperature. The Cyclic voltammetry estimated the HOMO level of all these polymers, as well as the energy bandgap. The maximum peak of these polymers was close in both dilute solution and thin film. The resultant polymers (P14-P16) offered an effective energy transfer in solid states, which enabled them to maintain the property of TADF from the attached guest, giving an intense peak at ~550 nm.

To conclude, all polymers (P1-P16) exhibited good solubility in most organic solvents, and they showed high thermal stability with decomposition temperatures of above 320 °C at 5% weight loss (Td) except Sonogashira polymers (P11-P12), which they have lower Td (288 °C) for P11 and (291°C) for P12. Unlike fluorene-based polymers in this study (P9, P10) and (P13-P16), carbazole-based polymers showed more blue-shifted absorption in UV-Vis spectra. This can be understood as the nonconjugated system increase in the polymers backbone of carbazole-based polymers due to the presence of silicon and alkyl chains in these polymers' structures (P1-P8) and (P11 and P12).

These findings highlight the difference in the electronic properties of these materials as a direct result of the linkage positions in the polymer's backbone and as a result of the structure of the monomers involved in polymerization. Therefore, (P1-P4) seem to be the best material among all designed polymers in this study in terms of high triplet energy due to the (Sicz) (M1) and alkyl chin (M2), which formed these polymers (P1-P4). It is hypothesized that polymers with a high triplet energy host in their backbone have a small Δ_{EST} and high k_{RISC}. Thus, these polymers (P1-P4) may have better EQE compared with other polymers in this study. On the other hand, fluorene-based polymers (P9, P10, P13, P14, P15 and P16) might display better charge transporting properties due to the 2,7 linkages of fluorene which increase the planarity. Among all polymers in this research, (P11 and P12) are believed to be less efficient materials as TADF emissive layers, this is because these polymers have very low Mw, lower thermal stability, and poorer solubility compared to other polymers in this study.

5.2 Future Work

In this study, carbazole-based polymers, as well as fluorene-based polymers, have been discussed as successful organic materials for OLED applications. In addition, we showed the importance of using host materials such as SiCz in TADF. Therefore, it is hoped that incorporating a high triplet energy host into the polymer's backbone will enhance the efficiency of electroluminescent devices. Moreover, the optical and electrical properties of certain polymers synthesized and discussed in this thesis inspire further research into their use as active layers with various ratios of TADF unit for applications in OLED.

In this project, an efficient TADF-small unit (PXZ-TRZ) was made and then incorporated as a copolymerisation moiety into a side chain of the host polymers' backbone, giving a series of non-conjugated polymers with different molar ratios of TADF units. The resultant polymers successfully derived the TADF properties from the small-attached molecule (PXZ-TRZ). It would be motivated to investigate the polymers' charge mobility as well as thin-film properties. As a result, the electroluminescence characteristics of those polymers should be additionally tested in cooperation with the physics department. All of the polymers in this thesis (P1-P16) exhibited good solubility in most organic solvents indicating that they will be easily deposited via the solution processing technique.

The sets of polymers in this research are developed for use in OLED devices, therefore, the future study requires further investigation into their potential use in practical devices. Measurement of the triplet energy of designed polymers is significant in order to find out whether Sicz-based polymers possess the same triplet energy as Sicz molecule. This measurement could be undertaken upon running time-resolved photoluminescence experiments at low temperatures on P1, P5, P9 and P11. Calculating the emission lifetime of the designed polymers is also significant to demonstrate the properties of TADF. Therefore, future work should involve these measurements to test the TADF properties of this study's polymers and compare their characteristic to counterparts in the literature. In addition, The future study will also include EL devices investigated on all these polymers. Polymers with promising EL properties could be further analysed for their properties on a variation of their molecular weights. Future work may involve studies on using polymers with no TADF dyes as hosts in blends with TADF dyes and comparing their properties to those where the TADF dyes are covalently attached to these polymers.

Chapter 6: Experimental Part

6.1. Materials

All involved materials including starting substances and other needed chemicals were bought and obtained from available commercial suppliers and were directly used without any further modification or purifications. Grubbs solvent purification system was the main source of the anhydrous solvents. Other reagents, drying agents and needed solvents such as the deuterated chloroform were purchased from the internal department store. All polymerization and most other synthesis were carried out in absence of oxygen atmosphere using an Argon gas, well-dried glassware and Schlenk line.

6.2. Measurement Techniques and Analytical Approaches

6.2.1. Nuclear magnetic resonance spectra (NMR)

All ^{1}H and ^{13}C NMR spectra for the monomers and polymers were recorded on Bruker Avance AV 3HD 400 (400 MHz) and Bruker Avance 100 (100 MHz) spectrometer using deuterated solutions such as deuterium oxide D_2O, chloroform-d_1, acetone-d_6 and DMSO-d_6 at room temperature. All deuterated were ordered from a commercial supplier (Merk) and utilised as received. Chemical shift calibrations (δ) were set according to internal standard tetramethylsilane (TMS). The coupling constant (J) of NMR spectra was recorded using Hertz (Hz) unit, and the measurement of the spectra was in part per million (ppm). Typical NMR splitting patterns are abbreviated as follows: s (singlet), d (doublet), dd (doublet of doublet), t (triplet), qt (quartet), m (multiplet), bs (broad singlet), bd (broad doublet), bm (broad multiplet). Bruker TopSpin 3.2 software was used to analyse NMRs' spectra.

6.2.2 Elemental analysis (EA)

The elemental analysis and the percentage of nitrogen (N), hydrogen (H), and sulphur was calculated via a Perkin Elmer 2400 series II while the Schoniger oxygen-flask combustion method was applied to obtain the elemental analysis of halide anions. The required amount for the analysis was about 6 mg for the halide anions and 5mg for other mentioned elements.

6.2.3. Thin layer chromatography (TLC)

Thin layer chromatography was applied on plates of silica silica-coated aluminium. The ultraviolet (Uv) light was needed to trace the chromophores. The plate of TLC was rarely heated by heat gun after applying a spray of *p*-anisaldehyde solution to activate non-UV's compounds. TLC was mainly used to confirm the purity of the compound in which a drop of

product solution was applied on a TLC plate and then ran on selective eluents. The purity was decided by the presented spots as displaying one spot in different eluent confirmed the product purity.

6.2.4. Gel permeation chromatography analysis (GPC)

The molecular weight average and the number of designed polymers were both calculated using The GPCmax VE2001 GPC solvent/sample module along with the Waters 410 Differential Refractometer using a method of RI-detection. The curve of the GPC was calibrated based on a series of polystyrene. Tetrahydrofuran (THF) was used as an eluent as well as a solvent in which all polymers dissolved in drops of toluene, which was used as a reference, were added to the prepared sample. The index of polydispersity (PDI) was calculated according to the equation shown below.

$$PDI = Mw/Mn$$

Where:

Mw stands for (the polymer weight average molecular weight); and

Mn stands for (the polymer number-average molecular weight).

6.2.5. Ultraviolet-Visible absorption spectroscopy analysis (UV-Vis)

The Uv-vis optical properties of all prepared polymers were studied via A Hitachi U-2010 Double Beam UV/Visible Spectrophotometer. The prepared polymer samples were firstly applied into quartz cuvettes with minimized length (~1cm) using diluted chloroform ($CHCl_3$), and then in solid state as manageable drop-cast thin films on quartz substrates with about 1.2 mg of the sample dissolved in $CHCl_3$.

6.2.6. Thermogravimetric analysis (TGA)

The curves of TGA were collected through the Perkin Elmer TGA-1 Thermogravimetric Analyser device. 2.5 mg of each polymer sample was analysed in an inert nitrogen atmosphere at a 10˚C min^{-1} scan rate.

6.2.7. Cyclic voltammetry (CV)

The Voltammograms of CV were recorded on Princeton Applied Research Model 263A Potentiostat/Galvanostat. CV measurements of all samples were carried out in 0.1 M solutions

of tetrabutylammonium perchlorate electrolyte in acetonitrile (CH_3CN). The system consists of three different electrodes; (i) a referencing electrode prepared from Ag/Ag+, (ii) a working electrode made from a platinum disc, (iii) a counter electrode derived from a platinum wire. During the measurements, the prepared electrolyte covered all the electrode cells. Ferrocene was utilized as the redox system reference based on recommendations from the IUPAC.

6.2.8. Melting Point (M.P.)

The melting point of all designed polymers was tested via Gallenkamp Melting Point Apparatus. The prepared sample is located in the detected area on the apparatus after being installed in tubes of the open-ended capillary.

6.3. Synthesis of monomers.

6.3.1 Tetrakis (4-bromophenyl) silane)[1,2]

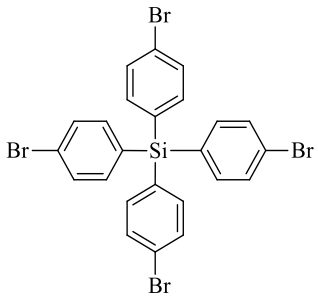

In 250 ML 2-necked flask, 50 ml of freshly anhydrous tetrahydrofuran (THF) was added to 1,4- dibromobenzene (5g, 21.5 mmol). The solution was then cooled to -78 ^{0}C using a bath of dry ice and acetone. 2.5 M of n-Buli in hexane (6.3 g, 21.5 mmol) was drop-wisely injected into the solution and stirred for 3 h at -78 ^{0}C. A solution of Silicon trichloride ($SiCl_4$) (0.62 g, 3.5 mmol) in THF was slowly added to the reaction mixture at that low temperature. The reaction mixture was kept at low temperature for 20 mins then the temperature was gradually increased to the room temperature allowing the reaction to stir for 20 h. The mixture was extracted using diethyl ether after washing with deionized water, dried over magnesium sulphate. The final pure product was received, as white powder (68% yield), from column-chromatography using petroleum ether as the eluent.

^{1}H NMR (400 MHz; $CDCl_3$, (δ) ppm): 7.55 (d, *J*= 8.2 Hz 8H); 7.38 (d, *J*=8.2 Hz 8H).

^{13}C NMR (100 MHz; $CDCl_3$, (δ) ppm): 135.6, 131.5, 130.4, 124.2.

MS (EI) *m*/*z*:(M^+); theoretically calculated for $C_{24}H_{16}Br_4Si$; 651,7, found: 649, 651, 653.

Elemental analysis for $C_{24}H_{16}Br_4Si$: calc. C, 44.21; H, 2.47; Br, 49.01, found: 44.14; H, 2.33; Br, 48.88.

Melting point; 240-243 ^{0}C.

6.3.2. Bis(4-(9*H*-carbazol-9-yl)phenyl)bis(4-bromophenyl)silane (M1)[3]

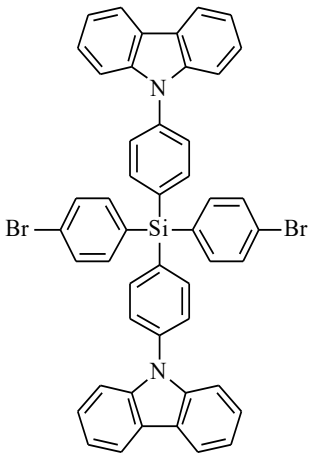

M1

A mixture of tetrakis(4-bromophenyl) silane (5.0 g, 7.5 mmol), carbazole (2.51 g, 15 mmol), Potassium tetraoxidophosphate (1.64 g, 22.5 mmol), trans-1,2 diamino cyclohexane (43 mg, 0.38 mmol), and copper (I) iodide (28 mg, 0.16 mmol) was dissolved in a freshly dried toluene (80 ml) in a 250 ml dried clean 2 necked flask. The reaction mixture was left stirring under argon atmosphere at Rt for 20 min, the reaction then was heated to reflux for one day. The reaction mixture was allowed to cool down to RT, then washed with water followed by extraction by DCM, and dried over sodium sulphate. The crude product was purified through column-chromatography using silica gel and a mixture of DCM/PE (2:5) the methanol was then used to recrystallize the final product giving 1.44 g of the product (23%).

^{1}H NMR (400 MHz; $CDCl_3$, (δ) ppm): 8.17 (d, *J* = 7.6 Hz, 4H), 7.84 (d, *J* = 8 Hz, 4H), 7.71 (d, *J* = 8 Hz, 4H), 7.66 (d, *J* = 7.8 Hz, 4H), 7.56 (m, 8H), 7.44 (td, *J* = 7.8 Hz, *J* = 2Hz, 4H), 7.37 (td, *J* = 7.8 Hz, *J* = 2Hz, 4H).

^{13}C NMR (100 MHz; $CDCl_3$, (δ) ppm): 140.2, 139.4, 137.8, 137.6, 137.5, 131.9, 131.4, 126.3, 126.0, 125.3, 123.6, 120.3, 120.2, 109.8

MS (EI) *m*/*z*:(M^+); theoretically calculated for $C_{48}H_{32}Br_2N_2Si$: 824.07; found: 8.22, 824, 826.

Elemental analysis for $C_{48}H_{32}Br_2N_2Si$: Calc. C, 69.91; H, 3.91; Br, 19.38; N, 3.40; found: C, 69.93; H, 3.90; Br, 19.40; N, 3.38.

6.3.3. 1,6-Bis(4-bromophenoxy) hexane [4]

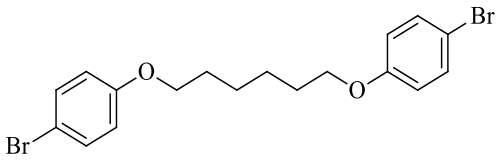

1,6-dibromohexane (3.45 mL, 22.5 mmol), 4-bromophenol (8.55 g, 33 mmol) and anhydrous potassium carbonate (12.40 g, 90 mmol) were added in dry clean 500 ml, two-necked, (round-bottomed flask) and then dissolved in 170 mL DMF. After that, the mixture was maintained and stirred under an argon atmosphere and the temperature was increased gradually to 70^0C. The reaction mixture was stirred at that temperature for three days. Upon completion, ethyl acetate and deionized water were added after cooling the mixture down. The aqueous layer was extracted four times with Et_2O. The organic layer was washed with deionized water multi times and the saturated aqueous solution of Na_2HCO_3, dried by Na_2SO_4. Reduced pressure was used to remove all remaining volatiles. The crude product was recrystallization from methyl alcohol to yield 73% (7g colourless solid).

^{1}H NMR (400 MHz; $CDCl_3$, (δ) ppm): 7.37 (d, J = 9.0 Hz, 4H), 6.77 (d, J = 9.0 Hz, 4H), 3.94 (t, J = 7.0 Hz, 4H), 1.85-1.78 (m, 4H), 1.57-1.46 (m, 4H).

^{13}C NMR (100 MHz; $CDCl_3$, (δ) ppm): 158.5, 132.5, 116.5, 112.9, 68.4, 29.3, 25.9.

MS (EI) *m/z*:(M^+); theoretically calculated for $C_{18}H_{24}O_2N_{79}Br_2$: 427.98; found: 425, 427, 429.

Elemental analysis for $C_{18}H_{24}O_2N_{79}Br_2$: Calc. C, 50.49; H, 4.71; Br, 37.32; found: C,50.62; H, 4.79; Br 37.38.

Melting point; 98 – 102.

6.3.4. 1,6-bis(4-[4,4,5,5-tetramethyl-1,3,2-dioxaborolan]phenoxy)hexane (M2)[5]

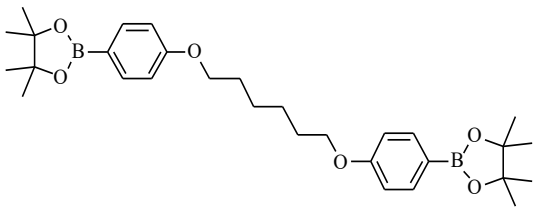

M2

In an oven-dried two necks round bottomed flask, 1,6-Bis(4-bromophenoxy)hexane (3.18g, 7.49 mmol) was dissolved in anhydrous tetrahydrofuran (40 ml), and cooled in dry ice to 195.1K. After that, A solution of *n*-BuLi (2.5 M in hexane, 6.28 mL, 15.7 mmol) was added slowly over 10 mins, the mixture was then kept stirring at low temperature for 3h before a solution of isopropoxy-4,4,5,5-tetramethyl-1,3,2-dioxaborolan (3.38 mL,16.6 mmol) in THF was added. The reaction mixture was left at that low temperature for further hour. Finally, the temperature was raised to room temperature and the mixture was stayed under stirring for 18 h. Upon completion, the reaction was quenched with a saturated solution of (NH_4Cl) and extracted three times with ethyl acetate. The collected organic layer was dried from the water using magnesium sulphate. The reduced pressure was applied to remove all volatiles. The crude product was purified using flash column chromatography using SiO_2 and a mixture of hexane, Et_2O and MeOH (20:2:0.5) to yield 90% of the final product as a glass solid (3.51g).

^{1}H NMR (400 MHz; $CDCl_3$, (δ) ppm): 7.75 (d, J = 9.0 Hz, 4H), 6.90 (d, J = 9.0 Hz, 4H), 4.01 (t, J = 7.0 Hz, 4H), 1.88-1.79 (m, 4H), 1.61-1.51 (m, 4H), 1.34 (s, 24H).

^{13}C NMR (100 MHz; $CDCl_3$, (δ) ppm): 161.9, 136.7, 114.1, 83.7, 67.8, 29.4, 26.02, 24.10.

MS (EI) *m*/*z*:(M^+); theoretically calculated for $C_{30}H_{44}B_2O_6$; 523.33, found 522, 523, 524.

Elemental analysis for $C_{30}H_{44}B_2O_6$; Calc. C, 68.99; H, 8.49; B, 4.14; O, 18.38, found: C, 69.03, H, 8.55.

Melting point; 122-125 ^{0}C.

6.3.5. 10- acetylphenoxazine [6]

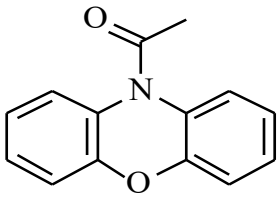

Two different two necked round bottom flask were used in this this reaction, where a solution of acetyl chloride (2.88 g, 2.61 ml, 36.8 mmol) in dry methylene chloride (18 ml) from first flask was slowly transferred to a solution of phenoxazine (4.8 g, 26.2 mmol) and triethylamine (4 g, 5.55 ml, 39.5 mmol) in dry methylene chloride (45 mL) at 0 °C. The reaction left stirring at low temperature for 1 h, then at room temperature for further 5 hours. The reaction was quenched in a solution of hydrochloride acid (300 mL, 0.5 M). The aq. portion was separated by extraction in methylene chloride (DCM). The collected layers were dried over $MgSO_4$, and the solvent was evaporated. The final pure product was obtained in 75% yield after using the silica gel column chromatography for purification (2 ethyl acetate/n-hexane 6.5).

^{1}H NMR (400 MHz; $CDCl_3$, (δ) ppm): 7.53 (dd, J = 8.0 Hz, J = 2.0 Hz, 2H), 7.24 (td, J = 8.0 Hz, J = 2.0 Hz, 2H), 7.20-7.14 (m, 6H), 2.37 (s, 3H).

^{13}C NMR (100 MHz; $CDCl_3$, (δ) ppm): 169.5, 151.3, 129.7, 126., 125.4, 123.6, 116., 23.3.

MS (EI) *m/z*:(M^+); theoretically calculated for $C_{14}H_{11}NO_2$; 225.25, found: 225.

Elemental analysis for $C_{14}H_{11}NO_2$; Calc. C, 74.66; H, 4.91; N, 6.23: found: C, 74.83; H, 4.95; N 6.09.

Melting point: 140-142 ^{0}C.

6.3.6. 2-actetylphenoxazine [7]

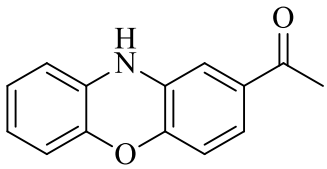

The synthesis of this product was carried out in two steps: first, a partially dissolved of 10-acetylphenoxazine (11.3 g, 50 mmol) in 150 mL carbon di-sulphide was added in a potion while stirring to anhydrous aluminium chloride (20 g, 15 mmol), the mixture was stirring under

reflux for 60 min. After that, acetyl chloride (6 g, 8 mmol) was added via syringe at moderate temperature to keep boiling. The stirred reaction mixture was left refluxing and monitored by TLC. After 120 min, the mixture was cooled. Concentrated hydrochloric acid together with Crushed ice was then utilized to decompose the resulting gummy residue. The formed precipitation was washed after being collected and finally suspended through glacial acid (100 mL) and 20% HCl (25 mL) and refluxed for an extra 20 min. The final precipitate was filtered using continuous toluene extraction. The final product was obtained as a crystal with a greenish-yellow colour with a yield of 55%.

^{1}H NMR (400 MHz; DMSO, (δ) ppm): 8.44 (bs, 1H), 7.27 (dd, *J* = 8.0 Hz, *J* = 2.0 Hz, 1H), 6.98 (d, *J* = 2.0 Hz, 1H), 6.78 (td, *J* = 8.0 Hz, *J* = 2.0 Hz, 1H), 6.71 (d, *J* = 8.0 Hz, 1H), 6.66 (dd, *J* = 8.0 Hz, *J* = 2.0 Hz, 1H), 6.61 (td, *J* = 8.0 Hz, *J* = 2.0 Hz, 1H), 6.47 (dd, *J* = 8.0 Hz, *J* = 2.0 Hz, 1H), 2.46 (s, 3H).

^{13}C NMR (100 MHz; DMSO, (δ) ppm): 196.7. 147.7, 142.8, 133.7, 133.2, 132.3, 125.0, 122.1, 121. 3, 116.0, 115.5, 114.2, 112.6, 26.9.

MS (EI) *m*/*z*:(M^+); theoretically calculated for $C_{14}H_{11}NO_2$; 225.25: found: 225.

Elemental analysis for $C_{14}H_{11}NO_2$: Calc. C, 74.66; H, 4.91; N, 6.23; found: C, 74.83; H, 4.95; N,6.09.

Melting Point: 203-208 ^{0}C.

6.3.7. 1-(2-phenzazinyl) ethanol [7]

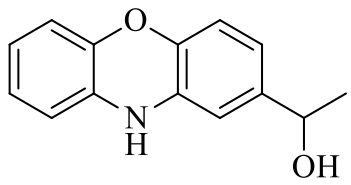

A sample of 0.75 g of sodium borohydride was added to a dried 50 ml two necks round-bottomed flask and then isopropanol (22 mL) was poured in to dissolve the sample. The dissolved sample was added to in another flask where 2.77 g of 2-acetyl phenoxizine was dissolved in dioxane. The resulting mixture was stirred at room T for 3 h and then heated to 60 ^{0}C for one more hour. The mixture was allowed to cool down before the decomposition of any excess hydride take place by acid. The mixture was extracted using ethyl acetate (3 times) and

washed with water. The solvent was removed in vacuo and the final product was formed as a white crystal giving a 72% yield (2.20 g) after recrystallization from a mixture of petroleum ether and toluene then a mixture of toluene and cyclohexane.

^{1}H NMR (400 MHz; DMSO, (δ) ppm): 8.15 (bs,1H), 6.66 (td, *J*= 7Hz, *J*= 1.5 Hz 1H), 6.22 (m,5H), 6.09 (d, *J*= 1.5Hz, 1H), 4.51 (q, *J* = 6.5 Hz 1H), 4.18 (bs, 1H), 1.27(d, *J* = 6.5 Hz, 3H).

^{13}C NMR (100 MHz; DMSO, (δ) ppm): 143.7 ,143.3 ,141,8 ,132.9 ,132.4 ,124.3 ,120.7 ,117.6 ,115.5,114.9 ,113.8 ,110.9, 67.9, 26.4.

MS (EI) *m/z*:(M^+); theoretically calculated for $C_{14}H_{13}NO_2$: 227.09; found, 227.

Elemental analysis for $C_{14}H_{13}NO_2$: estimated: C, 73.97; H, 5.75; N, 6.14: found; C, 74.63; H, 5.08; N, 6.21.

Melting Point: 92-98 ^{0}C.

6.3.8 Synthesis of 2-Chloro-4,6-diphenyl-1,3,5-triazine (6)[8]

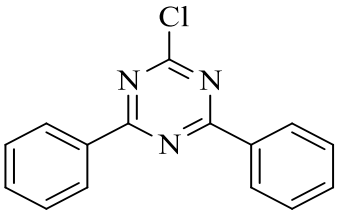

Under dry conditions using argon gas, to a solution of iodine activated Mg (0.33 g 12.5 mmol) in freshly anhydrous THF (12 mL), was dissolved bromobenzene (1.62 g, 10.5 mmol) in 12 mL THF was added slowly over 10 min to generate a Grignard reagent. That then was transferred at 0^{0}C drop wisely to a mixture of cyanuric chloride (0.63 g, 3.5 mmol) in 25 mL dry tetrahydrofuran. The reaction solution was stirred and heated to 55 ^{0}C for 12 hours. After it was cooled to room temperature, 14% aq. solution of hydrochloric acid (45 mL) was poured slowly and mixed. The resultant crude product was extracted with dichloromethane and dried over sodium sulphate, the solvents were evaporated under reduced pressure to receive a solid form of crude product which was purified through silica gel chromatography in which petroleum ether and DCM (3:1) were used as an eluent. The final 2-Chloro-4,6-diphenyl-1,3,5-triazine was obtained as a white solid with a yield of 70%.

^{1}H NMR (400 MHz; $CDCl_3$, (δ) ppm): 8.67 (dd, *J* = 7.5 Hz, *J* = 1.5 Hz, 4H), 7.67 (t, *J* = 7.5 Hz, 2H), 7.59 (t, J = 7.5 Hz, 4H).

^{13}C NMR (100 MHz; $CDCl_3$, (δ) ppm): 173.6, 172.4, 134.6, 133.8, 129.6, 128.9.

MS (EI) *m/z*:(M^+); theoretically calculated for $C_{15}H_{10}ClN_3$: 267.0, found: 266.

Elemental analysis for $C_{15}H_{10}N_3Cl$: calculated: C, 67.33; H, 3.80; N, 15.67, found: C, 67.51; H, 3.98; N, 15.73.

Melting Point: 133-136 ^{0}C.

6.3.9. 2-Amino-4,6-diphenyl-1,3,5-triazine [8]

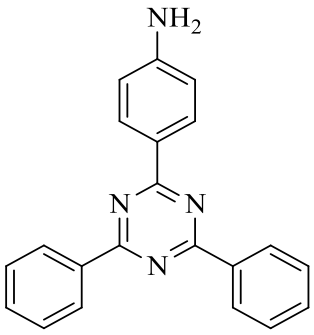

An aqueous solution of K_2CO_3 (4.16 g, 30 mmol) was slowly added to two necked round bottom flask which include a mixture of 4-(4,4,5,5 tetrame-thyl1,3,2-dioxaborolan-2-yl) aniline (3.62 g, 16.54 mmol), 2-chloro-4,6-diphenyl-1,3,5-triazine (4.02 g, 15 mmol) and tetrakis(triphenylphosphine)palladium (0.872g, 0.752mmol) in THF (85 ml). The reaction mixture was stirred at reflux for 55 h. After was cooled, the mixture of deionized water and ethyl acetate was used to quench and extract the reaction. After extraction, the organic part was collected and washed with brine followed by drying over magnesium sulphate, which was then filtrated and the solvent was evaporated under reduced pressure. The resultant crude was precipitated in 70 mL $CHCl_3$ to form a brown product which was dried through a vacuum. The brown precipitate was washed twice by chloroform and finally collected by filtration to give the final desired product with a yield of 70% (4.57 g).

^{1}H NMR (400 MHz; DMSO, (δ) ppm): 8.71 (dd, J =7.5 Hz, J =1.5 Hz, 4H), 8.48 (d, J =8.5 Hz, 2H), 7.72-7.62 (m, 6H), 6.76 (d, J = 8.5 Hz, 2H), 4.16 (bs, 2H).

^{13}C NMR (100 MHz; DMSO, (δ) ppm): 171.3, 170.6, 154.4, 136.3, 133.2, 131.3, 129.4, 128.9, 122.1, 113.8.

MS (EI *m/z*:(M^+); theoretically calculated for $C_{21}H_{16}N_4$: 324.1, found:324.

Elemental analysis for $C_{21}H_{16}N_4$: Calc. C, 77.80; H, 4.94; N, 17.26 Found C, 74.42; H, 4.93; N, 15.71.

Melting Point: 270-273 ^{0}C.

6.3.10. 2-Bromo-4,6-diphenyl-1,3,5-triazine [8]

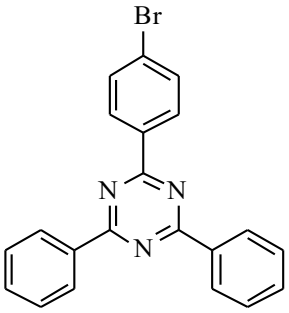

Under argon atmosphere and schlenk line system technique, a solution of 2-amino-4,6-diphenyl-1,3,5-triazine (3.34 g, 10.3 mmol) in 15 ml of HBr (48%) was stirred under an ice bath for 30 min before a cooled mixture of 15 mL water and sodium nitrate (900 mg) was added over 10 min time. The mixture was stirred at 0 ^{0}C for 45 min. After that, 0.89 g of Cu(I)Br (6.19 mmol) in 6 ml HBr was slowly transferred to the above mixture and the solution was kept stirring for 15 min at RT before raising the reaction temperature to the reflux for one day. The reaction mixture was maintained stirring while gradually reducing the temperature to 0 ^{0}C and neutralized the resulting residue using $NaHCO_3$. $CHCl_3$ was then added, the organic phase was separated and the aqueous one was further extracted by $CHCl_3$. The collected organic phases were washed using brine, dried over a magnesium sulphate and the solvent was evaporated in vacuo. The final pure product was afforded (3.20 g) (60% yield) after chromatography using an eluent of hexane and chloroform (4/1).

^{1}H NMR (400 MHz; $CDCl_3$, (δ) ppm): 8.76 (dd, J =7.5 Hz, J =1.5 Hz, 4H), 8.63 (d, J = 8.5 Hz, 2H), 7.70 (d, J = 8.5 Hz, 2H), 7.66-7.54 (m, 6H).

^{13}C NMR (100 MHz; $CDCl_3$, (δ) ppm): 171.9, 170.8, 135.8, 135.2, 132,7, 131.9, 130.5, 128.9, 128.7, 127.5.

MS (EI *m/z*:(M^+); theoretically calculated for $C_{21}H_{14}BrN_3$: 388.2, found: 388, 389.

Elemental analysis for $C_{21}H_{14}BrN_3$: Calc. C, 64.97; H, 3.64; Br, 20.57, Found C, 64.66; H, 3.95; Br, 22.65.

Melting Point: 385-388 ^{0}C.

6.3.11. 1-(10-(4-(4,6-diphenyl-1,3,5-triazin-2-yl)phenyl)-10*H*-phenoxazin-2-yl)ethanol [8,9]

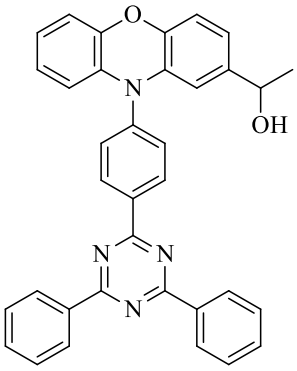

A dried magnetic bar was placed inside a two neck round bottomed flask where a solution of pallidum (II) acetate (40 mg, 0.18 mmol), tri-tertbutyl phosphine (133 mg, 0.66 mmol) in 60 mL toluene was added to a solution of 1-(2-phenzazinyl) ethanol (1.4 g, 6.6 mmol), 2-bromo-4,6-diphenyl-1,3,5-triazine (2.33 g, 6mmol) in 60 mL toluene. The mixture was stirred at room temperature for 30 min then heated to reflux for 18 h. Upon completion, the mixture was cooled to 0 ^{0}C and partitioned between deionized water and chloroform. The aqueous part was extracted with $CHCl_3$ after separating the organic phase. The brine was used to wash as well. The collected organic phase was dried over magnesium sulphate and the remaining solvents were evaporated in a vacuum to concentrate the crude product. The resulting residue was purified using silica gel chromatography (eluent; $CHCl_3$: n-hexane= 1/3) to finally receive the pure product as a light yellowish-white solid (65%).

^{1}H NMR (400 MHz; $CDCl_3$, (δ) ppm): 9.01 (d, *J* = 8.50 Hz, 2H), 8.81 (dd, *J* =7.5 Hz, 1.5 Hz, 4H), 8.70-8.59 (m, 8H). 6.75-6.62 (m, 4H), 6.04 (td, *J* =8.0 Hz, *J* =2.0 Hz, 1H), 6.10-6.02 (m, 2H), 4.55 (q, *J*= 6 Hz 1H), 4.22 (bs, 1H).1.31(d, *J*= 6 Hz, 3H).

^{13}C NMR (100 MHz; $CDCl_3$, (δ) ppm):171.9, 170.8, 143.9, 143.3, 142.8, 141.1, 136.5, 136.1,133.9, 132.8, 131.8, 131.1, 129.1, 128.6, 123.3, 121.7, 118.3, 115.6, 115.5, 113.4, 110.6, 69.9, 24.9.

MS (EI) *m*/*z*:(M^+); theoretically calculated for $C_{35}H_{26}N_4O_2$: 534.21, found; 533.

Elemental analysis for $C_{35}H_{26}N_4O$: C,78.64; H, 4.91; N,10.46, Found C,78.66; H,5.05; N, 9.85.

Melting Point: 114 ^{0}C.

6.3.12. 3,6-Dibromo-9H-carbazole [10]

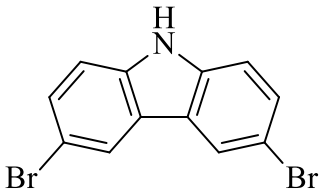

In a 250 mL two-neck round-bottomed flask fitted with a magnetic stirrer bar, an additional funnel and argon gas was also connected to the reaction system. 6.5 g of 9-H carbazole (38.9 mmol) was dissolved in 40 mL dried toluene was placed in the flask that was left stirring on ice path. Using the additional funnel, a solution of 15 g NBS (48.18 mmol) in 100 mL DMF was transferred to the previous flask. The reaction then was stirred for 45 min. After that, the reaction mixture was poured into cooled water to form the precipitate, which was then filtered, washed twice with very cold methyl alcohol, and finally recrystallized through a mixture of hexane and methanol (1:5) to yield 91% of the titled product (11.5 g).

^{1}H NMR (400 MHz; DMSO, (δ) ppm): 11.57 (bs, 1H), 8.42. (s, 2H), 7.46(m, 4H).

^{13}C NMR (100 MHz; DMSO, (δ) ppm): 139.2. 129,2, 123.8, 123.8, 113.7, 111.4.

MS (EI) *m/z*:(M^+); theoretically calculated for $C_{12}H_7\ Br_2\ N$; 324.89, found: 322, 324, 326

Elemental analysis for $C_{12}H_7Br_2\ N$: C,44.34; H 2.15; Br, 49.119; N,4.32, Found C,44.38; H 2.30; Br, 49.05; N,4.35.

Melting Point: 211 ^{0}C.

6.3.13. 3,6-Dibromo-9(6-bromohexane) –carbazole [11]

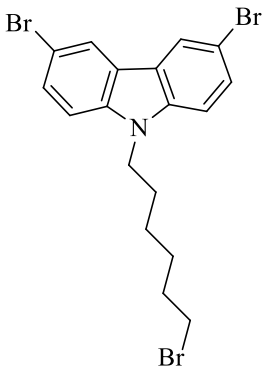

To a stirring solution of 3,6- dibromo-9H- carbazole (3.6 g, 10.75 mmol) in 15 mL dry DMF, anhydrous powder of potassium hydroxide (1.8 g, 32 mmol) was added. The mixture was stirred at 25 ^{0}C for 2.5 h. After that, the mixture was transferred slowly via a dropping funnel to 21.42 g of 1,6-dibromohexane (87.1 mmol) while stirring. The reaction mixture was left stirring for 2 days. Upon completion, the reaction mixture was poured into H_2O and extracted using $CHCl_3$ (3 times). The combined organic phase was dried over anhydrous $MgSO_4$ and the remaining solvents and unreacted substance were removed in vacuo. The crude product was purified by recrystallization in methyl alcohol to finally yield 73%.

^{1}H NMR (400 MHz; $CDCl_3$, (δ) ppm): 8.13(s, 2H), 7.55(dd, *J*=8.5Hz, *J*=2Hz 2H) 7.23(d, *J*= 8.5Hz, 2H), 4.23(t, J=7.5 Hz, 2H), 3.37(t, *J*=7.5 Hz, 2H), 1.80-1.66 (m, 4H), 1.43-137(m, 2H) 1.31-1.22(m, 2H).

^{13}C NMR (100 MHz; $CDCl_3$, (δ) ppm): 139.3, 129.1, 123.5, 123.3, 111.9, 110.2, 43.1, 33.6, 32.4, 28.7, 27.8, 26.3.

MS (EI) *m/z*:(M^+); theoretically calculated for $C_{18}H_{18}Br_3N$: 486.8, found: 487.

Elemental analysis for $C_{18}H_{18}Br_3N$: C,44.32; H 3.72; Br, 49.11; N,2.85, Found C,44.39; H 3.68; Br, 48.45; N,2.72.

Melting point: 278-281 ^{0}C.

6.3.14. 2-(1-((6-(3,6-dibromo-9H-carbazol-9-yl)hexyl)oxy)ethyl)-10-(4-(4,6-diphenyl-1,3,5-triazin-2-yl)phenyl)-10H-phenoxazine (M3) [10]

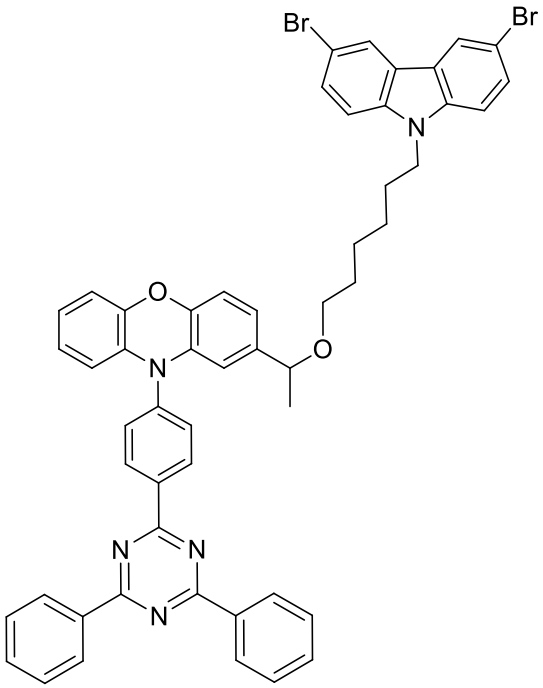

In a 100 ml round-bottomed flask, a mixture of a functionalized PXZ-TRZ (0.64g, 1.18 mmol) and anhydrous powder of potassium hydroxide was dissolved in freshly dried DMF (5 mL). The solution mixture was kept stirring for 2.5 h before the slow addition of 3,6- dibromo-9-(6-bromohexyl)-9-carbazole (4.66g, 9.64 mmol) in 30 mL DMF. The reaction mixture was stirred at 60 ^{0}C for 20 h. The deionized water was used to quench the reaction and chloroform to extract the crude product. The organic layers were separated, and the aqueous phase was further extracted by chloroform three times followed by brine wash. The combined organic parts were dried using sodium sulphate and the solvents were removed by reduced pressure. The final pure product was obtained as a light yellowish solid after separating the crude product in column chromatography (eluent; petroleum ether/ ethyl acetate, 10:2) yielding over 60% of the M3.

^{1}H NMR (400 MHz; $CDCl_3$, (δ) ppm): 9.02 (d, *J* = 8.5 Hz, 2H), 8.80 (dd, *J* =7.5 Hz, *J* =1.5 Hz, 4H), 8.02 (d, *J*=1.5 Hz, 2H), 7.65-7.53 (m, 8H), 7.40 (dd, *J*=7.5 Hz, *J*=1.5Hz, 2H), 7.12 (d *J*=7.5, 2H), 6.76-6-57 (m, 5H), 6.07-6.02 (d, *J*=6.5 2H), 4.04 (q, J = 6.5 Hz, 1H), 3.87 (t, J = 6.5 Hz, 2H), 3.19 (t, J = 6.5 Hz, 2H), 1.77-1.66 (m, 4H), 1.48-1.22 (m, 4H), 1.21(t, *J*=2.5Hz, 3H).

^{13}C NMR (100 MHz; $CDCl_3$, (δ) ppm): 171.7, 170.7, 143.8, 143.2, 142.9, 141.4, 139.3, 136.4, 136.1, 133.9, 133.8, 132.6, 131.6, 131.2, 129.1, 129.0, 128.6, 123.5, 123.2, 121.6, 118.4, 115.6, 115.5, 113.3, 112.1, 110.7, 110.3. 69.6, 43.1, 40.2, 29.7, 28.7, 26.8, 24.8.

MS (EI) *m*/*z*:(M^+); theoretically calculated for $C_{53}H_{43}Br_2N_5O_2$: 941.18, Found: 941, 943, 945.

Elemental analysis for $C_{53}H_{43}Br_2N_5O_2$: C,67.60; H, 4.61; N,7.42; Found C,66.90; H,4.41; N, 7.40.

Melting point: 268 ^{0}C.

6.3.15. Bis(4-(9H-carbazol-9-yl)phenyl)bis(4-(4,4,5,5-tetramethyl-1,3,2-dioxaborolan-2-yl)phenyl)silane (M4)[12]

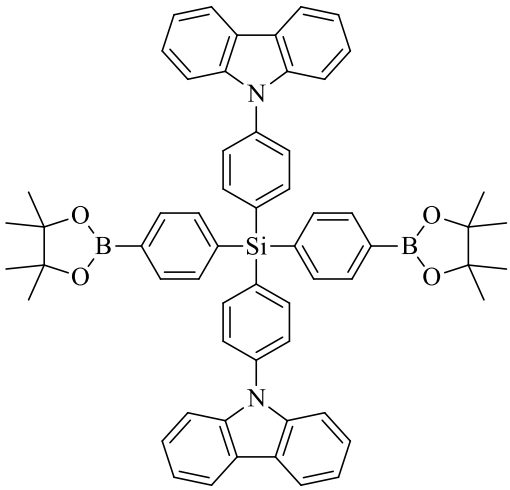

M4

In dried 100 ml two necked round flask, a mixture of bis(4-(9H-carbazol-9-yl) phenyl) bis(4-bromophenyl) silane (**M1**) (2.1 g, 2.6 mmol), octamethyl-2,2′-bi-1,3,2-dioxaborolane(1.94 g, 7.8 mmol), CH_3COOK (1.14 g, 11.8 mmol), and Pd $(PPh_3)_4$ (60 mg, 0.052 mmol) were all mixed in anhydrous 40 ml DMF and purged with argon gas for 30 min. The reaction solution was stirred at a high temperature (95 ^{0}C) for 20 hours. Celite powder was used to filter the mixture after it was cooled to Rt. The obtained crude product was extracted by ethyl acetate (4 times) and dried over sodium sulphate. The solvent was removed by reduced pressure and the pure product was received from the SiO_2 column chromatography with hexane and ethyl acetate (10:1, 10:4) as the eluent. The resultant oily product was turned to a white solid by recrystallization twice from methyl alcohol to give 1.07 g (45%).

^{1}H NMR (400 MHz; CDCl3, (δ) ppm): 8.19 (d, *J* = 7.8 Hz, 4H), 7.93 (d, *J* = 7.5 Hz, 4H), 7.88 (d, *J* = 8.0Hz, 4H), 7.76 (d, *J* = 7.5 Hz, 4H), 7.68 (d, *J* = 8.0 Hz, 4H), 7.54 (d, *J* = 8.1 Hz, 4H), 7.44 (t, *J* = 7.8 Hz, 4H), 7.36 (t, *J* = 7.8, Hz, 4H), 1.34 (s, 24H).

^{13}C NMR (100 MHz; $CDCl_3$, (δ) ppm):140.8, 138.7, 137.2, 135.4, 135.1, 134.8, 132.3, 132.1, 128.4, 128.2, 123.2, 120.9, 112.0, 109.8, 83.8, 24.9.

Elemental analysis for ($C_{60}H_{56}B_2N_2O_4Si$): C, 78.43; H, 6.14; N, 3.05; found: C, 78.57; H, 6.23; N, 2.98.

MS (EI) *m*/*z*:(M^+); theoretically calculated for ($C_{60}H_{56}B_2N_2O_4Si$): calc. 919.62, found: 919, 920, 921.

6.3.16. 2,6-Dibromo-9H-Fluorene [13]

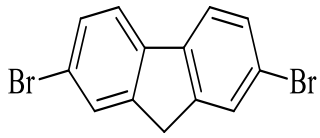

A solution of 11.2 g bromine (69.7 mmol) in 5 ml chloroform was added drop-wisely into a solution of 5 g 9-H-fluorene (30 mmol) in 20 mL anhydrous chloroform, then the reaction mixture was folded by the foil of aluminium and kept stirring in a dark environment at room temperature for 30 hours. After that, a light brown precipitate was produced that was ffilterated, washed by chloroform and finally collected to be crystallized from ethyl alcohol. The resulting product was formed as light white crystals. (8 g, 80% yield).

^{1}H NMR (400 MHz; $CDCl_3$, (δ) ppm): 7.70 (s, 2H), 7.63 (d, *J* = 8.02 Hz, 2H), 7.53 (d, *J* = 8.02 Hz, 2H), 3.90 (s, 2H).

^{13}C NMR (100 MHz; $CDCl_3$, (δ) ppm): 144.7, 139.6, 130.1, 128.2, 121.1, 120.9, 36.5.

MS (EI) *m*/*z*:(M^+); theoretically calculated for ($C_{13}H_8Br_2$): 323.9. Found: 324, 326, 328.

Elemental analysis for ($C_{13}H_8Br_2$): C,48.20; H 2.51; Br,49.30, Found: C,48.62; H 2.69; Br,49.02.

Melting Point: 139 ^{0}C.

6.3.17. 9,9-Dioctyl-2,7-dibromofluorene (M7)[14]

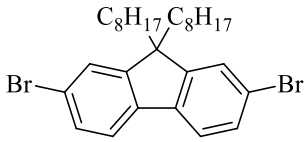

In dried cleaned 250 mL two-necked flask, and under an argon gas atmosphere 12 mL of DMSO was added to dissolve a mixture of 4 g 2,7 dibromofluorene, 0.29 g KI (1.77 mmol) and 2.75 g of KOH (48.95 mmol) were placed with a dried magnetic bar. A dropwise of 1-bromooctane (5.90 g, 30.8 mmol) was added to the mixture and left stirring overnight at 25 ^{0}C. A deionized H_2O was added and immediately extracted with dichloromethane. The organic layer was taken and dried using anhydrous sodium sulphate, filtrate and the crude was concentrated in vacuo. The concentrated crude product was purified through SiO_2 chromatography using a mixture of petroleum-ether and DCM as an eluent to yield the final product as a light yellow solid. (5.72 g, 85%).

^{1}H NMR (400 MHz; $CDCl_3$, (δ) ppm): δ (ppm) 7.55 (d, J = 2.0 Hz, 2H), 7.48 (d, J = 2.0 Hz, 2H), 7.46 (s, 2H) 1.95-1.98(m, 2H), 1.26-1.03 (m, 20H), 0.86 (t, J = 7.0 Hz, 6H), 0.62-0.57 (m, 4H).

^{13}C NMR (100 MHz; $CDCl_3$, (δ) ppm): 152.4, 138.7, 130.1, 125.0, 121.3, 121.5, 55.4, 40.1, 31.6, 29.7, 29.0, 26.3, 23.5, 22.5, 13.9.

MS (EI) *m/z*:(M^+); theoretically calculated for ($C_{29}H_{40}Br_2$): 548.4, found: 548, 550, 552.

Elemental analysis for ($C_{29}H_{40}Br_2$): C, 63.53; H 7.37; Br, 29.10, Found: C,63.12; H 7.31; Br,30.63.

Melting point: 56-60 ^{0}C.

6.3.18. 9,9-Dioctyl-9-fluorene-2,7-diboronic acid bis(pinacol) ester (M5)[15]

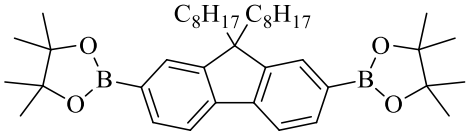

In dried one hundred mL two necked round bottom flask, a freshly dried 25 mL DMF was added to dissolve a combine mixture of 2,7 dibromo-9,9-dibutyl-9H-fluorene (1.1g, 2 mmol), bis(pinacolato)diboron (1.76 g, 7 mmol), potassium acetate (1.13g, 12 mmol) and $PdCl_2$

(dppf)Cl_2 (66 mg, 0.088mmol). After purging the system with argon gas, the reaction mixture was stirred at room temperature for 30 min before the temperature was gradually increased to 95 ^{0}C for 48 h. Upon completion of the reaction, the round bottom flask was allowed to cool down to RT before the reaction was quenched with 100 mL water followed by extraction with diethyl ether (3 times. 200ml), the separated organic layer was collected, washed with deionized water, and dried over anhydrous $MgSO_4$. The diethyl ether and other organic solvents were removed via reduced pressure under a high vacuum. The final pure product was accomplished by recrystallization from methyl alcohol, which was then passed through the basic alumina to get rid of any acidic protons to receive 5.70 g of the product (84 % yield).

^{1}H NMR (400 MHz; $CDCl_3$, (δ) ppm): 7.79 (dd, *J*= 7.5Hz, *J*=1.3Hz, 2H), 7.43 (m, 4H), 1.97 (m, 4H),1.38(s, 24H) 1.26-0.92 (m, 20H), 0.79 (t, J= 7.04Hz, 6H), 0.51 (m, 4H).

^{13}C NMR (100 MHz; $CDCl_3$, (δ) ppm): 150.4, 143.7, 133.1, 128.8, 119.2, 83.6, 55.0, 39.9, 31.6, 29.8, 29.1, 29.1, 23.5, 22.4, 14.0.

MS (EI) *m/z*:(M^+); theoretically calculated for ($C_{41}H_{64}B_2O_4$): 642.5, found: 642, 643, 644.

Elemental analysis for ($C_{41}H_{64}B_2O_4$): C, 76.65; H 10.05; Found C,76.50; H 9.70.

Melting point: 129-131 ^{0}C.

6.4. General Procedure to Prepare Suzuki Polymers (1-10) (13-16)[16,17]

The general polymerization procedure was carried out according to Suzuki polycondensation of palladium-based catalyst. Different ratios of previously prepared monomers (M1, M2, M3, M4 and M7) were reacted under argon gas. The required polymers was designed from related monomers, $Pd(AcO)_2$ (0.1 eq.) and tri*(*o-tolyl*)*-phosphine (0.2 eq.). A saturated aqueous solution of $NaHCO_3$ (2- 4 mL), which had been left bubbling and degassing under argon gas for 180 min was added to the mixture. Under inert condition, a freshly anhydrous THF (3-6 mL) was after that added to the reaction mixture. The rection mixture was heated under argon atmosphere to 85-90 ^{0}C after left stirred at Rt for 15 min. It was stirred at that temperature for 24-72 h based on formed precipitants. The reaction was allowed to cool down to 25 ^{0}C then bromobenzene (~0.2 mL) was added, degassed, and heated again while stirring to reflux (~ 90 ^{0}C) for 1.5 hours. After the solution was cooled to room temperature, phenylboronic acid (~100mg) was transferred to the solution, which was then degassed and heated to reflux for further 3.5 hours. Trichloromethane (250 mL) was used upon completion to dissolve the resulted mixture. An aqueous solution of ammonium hydroxide (60 mL) was carefully poured

into that mixture and kept stirring overnight. The organic layer was collected and washed with water; the aqueous phase was extracted with trichloromethane (4 times). The remaining solvents were evaporated and concentrated to about 30 mL after being dried over magnesium sulphate. The 30 mL of polymer crude was poured slowly into 250 mL methanol, followed by stirring for 18 h at rt. The solid was at the end collected from a membrane filter. The Soxhlet was then performed to purify the collected solid.

6.4.1 Preparation of Polymers (P1-P4)

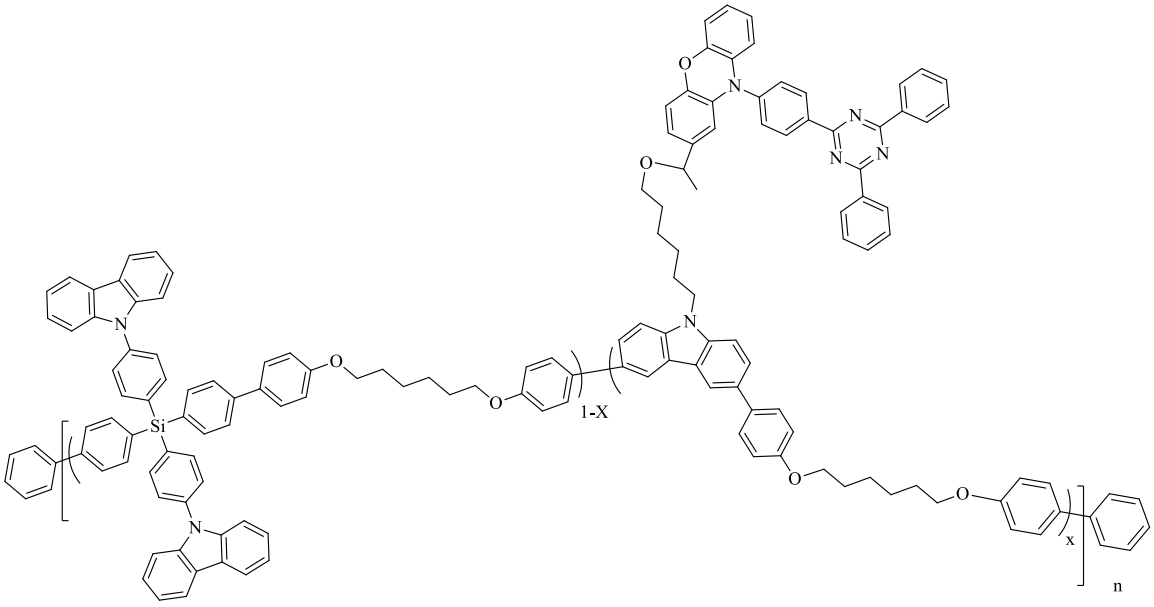

P1 - P4

P1: According to the general procedure: M1(0.165 g, 0.2 mmol), M2 (0.105 g, 0.2 mmol), $Pd(OAc)_2$ (0.0045 g, 0.02 mmol), tri(otolyl)phosphine (0.012 g, 0.04 mmol), 1 mL of saturated aqueous solution of $NaHCO_3$, and 3 mL THF. The reaction mixture was stirred at 85 ^{0}C for 50 h to give polymer (1) as a white solid.

^{1}H NMR (400 MHz; $CDCl_3$, (δ) ppm): 8.18 (bs, 4H), 7.90 (bs, 4H), 7.88 (bs, 4H), 7.76 (bs, 4H), 7.66-7.54 (bm, 12H), 7.44(bs, 4H), 7.40- 7.35 (m, 4H), 7.05-6.96 (bm, 4H), 4.05 (bs, 4H), 1.92 (bs, 4H), 1.55 (bs, 4H).

GPC: Toluene fraction, Mn = 17100 g mol^{-1} , Mw = 22100 g mol^{-1}, PDI = 1.292.

P2: **M1** (0.22 g, 0.27 mmol), **M2** (0.16 g, 0.3 mmol), **M3** (0.028 g, 0.03), $Pd(OAc)_2$ (0.0067 g, 0.03 mmol), tri(otolyl)phosphine (0.018 g, 0.06 mmol), 1.5 mL saturated aqueous solution of

$NaHCO_3$, and 4 mL THF. The reaction mixture was stirred at 90 ^{0}C for 72 h to give polymer 3 as a light yellowish solid.

^{1}H NMR (400 MHz; $CDCl_3$, (δ) ppm): 9.01 (bs, 0.11H), 8.83 (bs,0.22H), 8.20 (bs, 3.78H), 7.94 (bs, 3.89H), 7.88 (bs, 4H), 7.76-7.30 (bm, 23.18H), 7.10-6.93 (bm, 4.11H), 6.78-6.62 (m, 0.23H), 6.10 (bs, 0.1H) 4.05 (bs, 4.05H), 3.20 (bs, 0.1H), 1.90 (bs, 4H), 1.76-1.22 (m, 4.55H).

GPC: Toluene fraction, Mn = 20000 g mol^{-1} , Mw = 24900 g mol^{-1}, PDI = 1.245.

P3: **M1** (0.197 g, 0.24 mmol), **M2** (0.16 g, 0.3 mmol), **M3** (0.056 g, 0.06), $Pd(OAc)_2$ (0.0067 g, 0.03 mmol), tri(otolyl)phosphine (0.018 g, 0.06 mmol), 1.5 mL of saturated aqueous solution of $NaHCO_3$, and 4 mL THF. The reaction mixture was stirred at 90 ^{0}C for 72 h to give polymer 2 as a yellow solid.

^{1}H NMR (400 MHz; $CDCl_3$, (δ) ppm): 9.01 (bs, 0.21H), 8.83 (bs,0.43H), 8.20 (bs, 3.57H), 7.96 (bs, 3.78H), 7.88 (bs, 4H), 7.72 (bs, 3.78H), 7.69-7.60 (bm, 11.5H), 7.48 (bs, 3.79H), 7.33 (bs, 3.57H), 7.10-6.93 (bm, 4.2H), 6.78-6.62 (m, 0.54H), 6.10 (bs, 0.22H), 4.10 (bs, 0.1H), 4.05 (bs, 4H), 3.20 (bs, 0.22H), 1.90 (bs, 4H), 1.76- 1.51 (bm, 4.4H), 1.47-1.20 (bm, 0.76H).

GPC: Chloroform fraction, Mn = 19000 g mol^{-1}, Mw = 22100 g mol^{-1}, PDI = 1.163.

P4: **M1** (0.148 g, 0.18 mmol), **M2** (0.16 g, 0.3 mmol), **M3** (0.100 g, 0.12 mmol), $Pd(OAc)_2$ (0.0067 g, 0.03 mmol), tri(otolyl)phosphine (0.018 g, 0.06 mmol), 1.5 mL of saturated aqueous solution of $NaHCO_3$, and 4 mL THF. The reaction mixture was stirred at 90 ^{0}C for 72 h to give polymer 4 as a yellow solid.

^{1}H NMR (400 MHz; $CDCl_3$, (δ) ppm): 9.01 (bs, 0.45H), 8.83 (bs,0.88H), 8.20 (bs, 3.11H), 7.97 (bs, 4.2H), 7.88 (bs, 4H), 7.72 (bs, 3.56H), 7.69-7.60 (bm, 11.5H), 7.48 (bs, 3.6H), 7.33 (bs, 3.11H), 7.10-6.93 (bm, 4.9H), 6.78-6.62 (m, 1.1H), 6.10 (bs, 0.45H), 4.10 (bs, 0.22H), 4.05 (bs, 4H), 3.20 (bs, 0.4H), 1.90 (bs, 4H), 1.76- 1.51 (bm, 4.9H), 1.47-1.20 (bm, 1.5H).

GPC: Chloroform fraction, Mn = 18000 g mol^{-1}, Mw = 21500 g mol^{-1}, PDI = 1.194.

6.4.2. Preparation of Polymers (P5- P8)

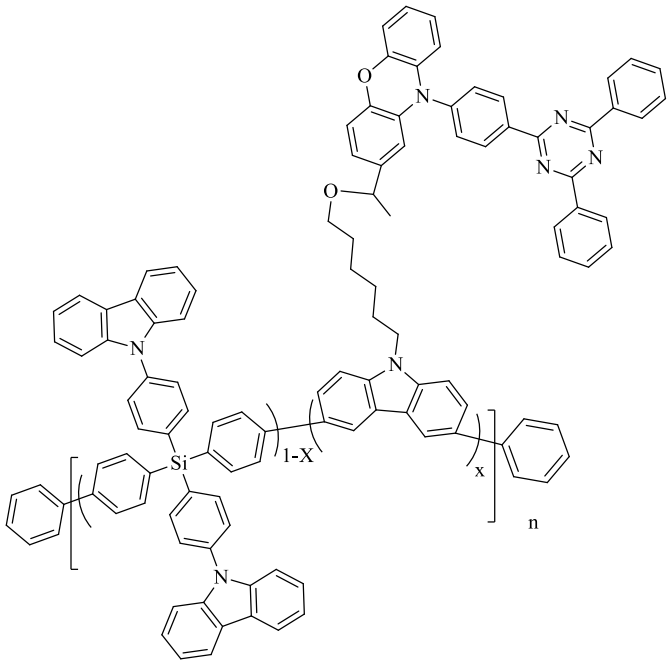

P5 - P8

P5: Followed the same general procedure that used for previous polymers, **M1** (0.124 g, 0.15 mmol), **M4** (0.14 g, 0.15 mmol), $Pd(OAc)_2$ (0.0034 g, 0.015mmol), tri(otolyl)phosphine (0.009 g, 0.03 mmol), 1mL of saturated aqueous solution of $NaHCO_3$, and 2.5 mL THF. The reaction mixture was stirred at 80^0C for 24 h to give polymer 5 as a white solid.

^{1}H NMR (400 MHz; $CDCl_3$, (δ) ppm): 8.22 (bs, 8H), 8.00-7.80 (bm, 24H), 7.72-7.62 (bm, (bm, 8H), 7.57 (bs, 8H), 7.48 (bs, 8H), 7.34 (bs, 8H).

GPC: Toluene fraction, Mn = 5400 g mol^{-1}, Mw = 15600 g mol^{-1}, PDI = 2.888.

P6: M1 (0.185 g, 0.225 mmol), **M4** (0.23 g, 0.25 mmol), **M3** (0.024 g, 0.025 mmol), $Pd(OAc)_2$ (0.006 g, 0.025 mmol), tri(otolyl)phosphine (0.015 g, 0.05 mmol), 2 mL of saturated aqueous solution of $NaHCO_3$, and 3.5 mL THF. The reaction mixture was stirred at 85 ^{0}C for 72 h to give polymer 6 as a light yellowish solid.

^{1}H NMR (400 MHz; $CDCl_3$, (δ) ppm): 8.99 (bs, 0.08H), 8.78 (bs, 0.17H), 8.22 (s, 7.8H), 8.00-7.75 (bm, 23.7H), 7.57 (bs, 7.9H), 7.48 (bs, 8.1H), 7.37-7.13 (bm, 7.8H), 7.12 (bs, 0.08H), 6.72-6.63 (bm, 0.21H), 6.10 (bs, 0.08H).

GPC: Chloroform fraction, Mn = 6800 g mol^{-1}, Mw = 14800 g mol^{-1}, PDI = 2.176.

P7: M1 (0.165 g, 0.20 mmol), **M4** (0.23 g, 0.25 mmol), **M3** (0.047 g, 0.05 mmol), $Pd(OAc)_2$ (0.006 g, 0.025 mmol), tri(otolyl)phosphine (0.015 g, 0.05 mmol), 2 mL of saturated aqueous solution of $NaHCO_3$, and 3.5 mL THF. The reaction mixture was stirred at 85 ^{0}C for 72 h to give polymer 7 as a yellow solid.

^{1}H NMR (400 MHz; $CDCl_3$, (δ) ppm): 9.01 (bs, 0.18H), 8.82 (bs, 0.36H), 8.20 (s, 7.64H), 8.00-7.72 (bm, 23.02H), 7.57 (bs, 7.9H), 7.48 (bs, 8.16H), 7.37-7.13 (bm, 7.6H), 7.13 (bs, 0.18H), 6.72-6.63 (bm, 0.4H), 6.10 (bs, 0.18H).

GPC: Chloroform fraction, Mn = 6300 g mol^{-1}, Mw = 13400 g mol^{-1}, PDI = 2.127.

P8: M1 (0.124 g, 0.15 mmol), **M4** (0.23 g, 0.25 mmol), **M3** (0.094 g, 0.1 mmol), $Pd(OAc)_2$ (0.006 g, 0.025 mmol), tri(otolyl)phosphine (0.015 g, 0.05 mmol), 2 mL of saturated aqueous solution of $NaHCO_3$, and 3.5 mL THF. The reaction mixture was stirred at 85 ^{0}C for 48 h to give polymer 6 as a yellow solid.

^{1}H NMR (400 MHz; $CDCl_3$, (δ) ppm): 9.01 (bs, 0.37H), 8.82 (bs, 0.74H), 8.20 (bs, 7.25H), 8.00-7.72 (bm, 22.14H), 7.57 (bs, 8.7H), 7.48 (bs, 7.6H), 7.37-7.13 (bm, 7.3H), 7.13 (bs, 0.3H), 6.72-6.63 (bm, 0.9H), 6.10 (bs, 0.37H).

GPC: Chloroform fraction, Mn = 4200 g mol^{-1}, Mw = 8600 g mol^{-1}, PDI = 2.04.

6.4.3. Preparation of Polymers (P9 and P10)

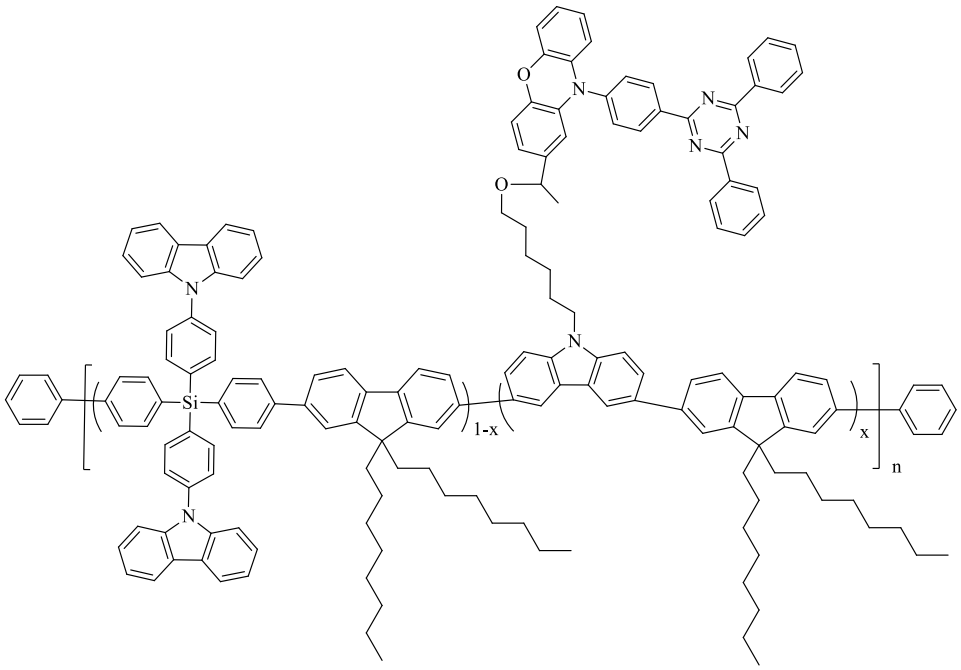

P9 - P10

P9: According to the general procedure that was described and used previously in this section, **M1** (0.247 g, 0.3 mmol), **M7** (0.19 g, 0.3 mmol), (0.0067 g, 0.03 mmol), tri(otolyl)phosphine (0.018 g, 0.06 mmol), 1.5 mL saturated aqueous solution of $NaHCO_3$, and 3.5 mL THF. The reaction mixture was stirred at 85 ^{0}C for 30 h to give polymer 9 as a white plastic solid.

^{1}H NMR (400 MHz; $CDCl_3$, (δ) ppm): 8.20 (bs, 4H), 8.10-7.80 (m, 10H), 7.72 (bs, 8H), 7.60 (bs, 4H), 7.48 (bs, 8H), 7.38-7.33 (bm, 4H), 2.10 (bs, 4H), 1.17 (bs, 20H), 0.88 (bs, 0.10H).

GPC: Chloroform fraction, Mn = 23600 g mol^{-1}, Mw = 38100 g mol^{-1}, PDI = 1.61.

P10: **M1** (0.22 g, 0.27 mmol), **M7** (0.19 g, 0.3 mmol), **M3** (0.028 g, 0.03), $Pd(OAc)_2$ (0.0067 g, 0.03 mmol), tri(otolyl)phosphine (0.018 g, 0.06 mmol), 1.5 mL saturated aqueous solution of $NaHCO_3$, and 4 mL THF. The reaction mixture was stirred at 90 ^{0}C for 3 days to give polymer 10 as a light yellowish solid.

^{1}H NMR (400 MHz; $CDCl_3$, (δ) ppm): 9.00 (bs, 0.08H), 8.80(bs, 0.16H), 8.20 (bs, 3.48H), 8.10-7.80 (m, 9.7H), 7.72 (bs, 7.7H), 7.60 (bs, 3.8H), 7.48 (bs, 7.8H), 7.38-7.33 (bm, 3.8H),

7.15-7.10 (bm, 0.08), 7.72-6.65 (bm, 0.20H), 6.10 (bs, 0.08H), 2.10 (bs, 4H), 1.65-1.44 (bm, 0.33H), 1.17 (bs, 20H), 0.88 (bs, 0.10H).

GPC: Chloroform fraction, Mn = 14200 g mol^{-1}, Mw = 18200 g mol^{-1}, PDI = 1.277.

6.4.4. Preparation of Polymers (P13-P16)

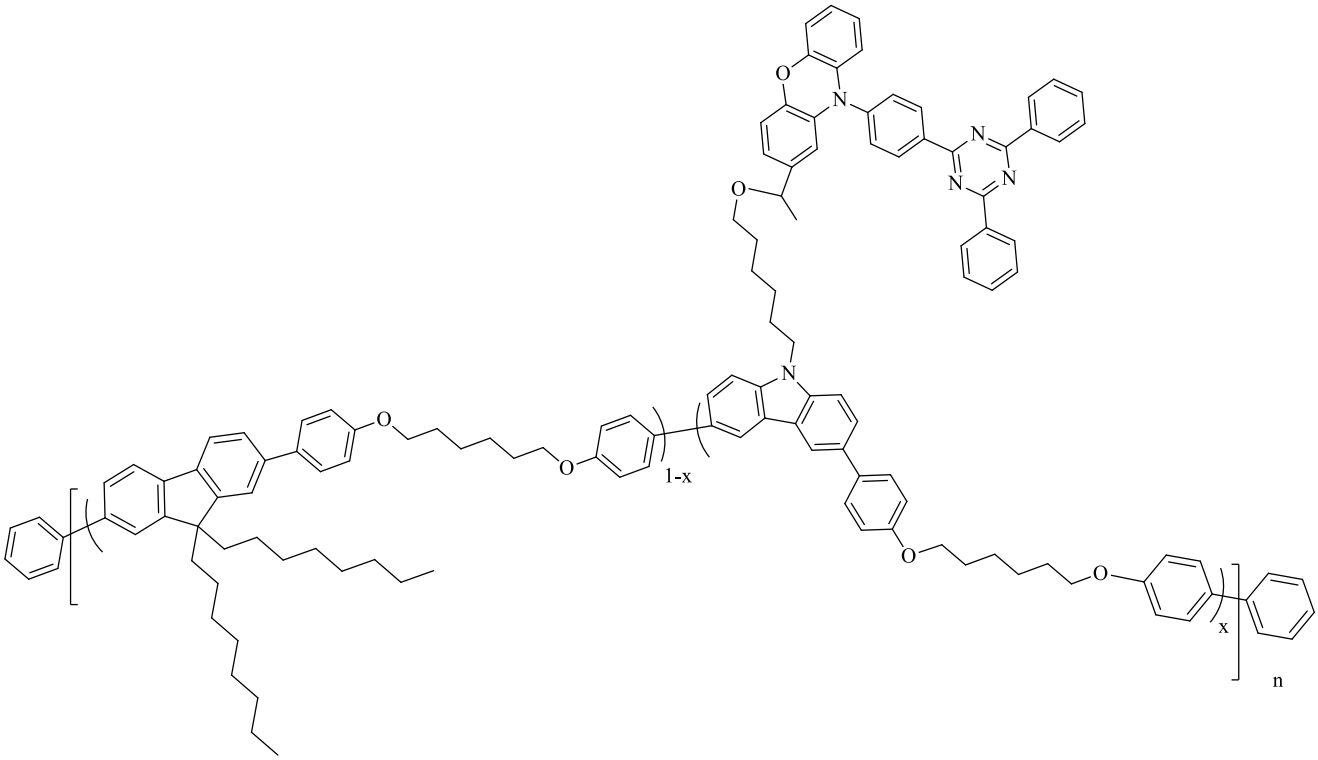

P13 - P16

P13: According to general procedure that was describe earlier in this part, **M5** (0.22 g, 0.40 mmol), **M2** (0.21 g, 0.40 mmol), palladium acetate (0.009 g, 0.04 mmol), tri(otolyl)phosphine (0.024 g, 0.08 mmol), 2.5 mL of saturated aqueous solution of $NaHCO_3$, and 6 mL THF. The reaction mixture was stirred at 90 ^{0}C for 65 h to give polymer 2 as a white solid.

^{1}H NMR (400 MHz; $CDCl_3$, (δ) ppm): 7.76 (d, *J* = 6.5 Hz, 4H), 7.64-7.60 (m, 2H), 7.57-7.52(m,2H), 7.50-7.45 (m, 2H), 7.10-6.92 (bm, 4H), 4.10 (bs, 4H), 2.02 (bs, 2H), 1.90 (bs, 4H), 1.60 (bs, 4H), 1.30-1.10 (m, 20H), 0.90-0.79 (m, 10H).

GPC: Chloroform fraction, Mn = 26500 g mol^{-1}, Mw = 29000 g mol^{-1}, PDI = 1.09.

P14: M5 (0.197 g, 0.36 mmol), **M2** (0.21 g, 0.4 mmol), **M3** (0.038 g, 0.04), palladium acetate (0.0067 g, 0.03 mmol), tri(otolyl)phosphine (0.018 g, 0.06 mmol), 2.5 mL of saturated aqueous solution of $NaHCO_3$, and 6 mL THF. The reaction mixture was stirred at 90 ^{0}C for 3 days to yield polymer 14 as a light yellowish solid.

^{1}H NMR (400 MHz; $CDCl_3$, (δ) ppm): 9.02 (bs, 0.08H), 8.82 (bs, 0.176H), 7.76 (bs, 4H), 7.62-7.59 (m, 2.3H), 7.57-7.52 (m,1.9H), 7.50-7.45 (m, 1.98H), 7.10-6.92 (bm, 4.1H), 6.71-6.62 (bm, 0.2H), 6.01 (bs, 0.08H), 4.10 (bs, 4H), 2.07 (bs, 1.9H), 1.92 (bs, 4.2H), 1.60-1.53 (bm, 4.0H), 1.30-1.10 (m, 19.3H), 0.90-0.79 (m, 9.6H).

GPC: Chloroform fraction, Mn = 22300 g mol^{-1}, Mw = 26800 g mol^{-1}, PDI = 1.20.

P15: M5 (0.175 g, 0.32 mmol), M2 (0.21 g, 0.4 mmol), **M3** (0.075 g, 0.08), palladium acetate (0.0067 g, 0.03 mmol), tri(otolyl)phosphine (0.018 g, 0.06 mmol), 2.5 mL of saturated aqueous solution of $NaHCO_3$, and 6 mL THF. The reaction mixture was stirred at 90 ^{0}C for 72 h to give polymer 15 as a yellow solid.

^{1}H NMR (400 MHz; $CDCl_3$, (δ) ppm): 9.02 (bs, 0.21H), 8.82 (bs, 0.43H), 7.80-7.55 (bm, 10.7H), 7.10-6.92 (bm, 4.2H), 6.71-6.62 (bm, 0.5H), 6.01 (bs, 0.21H), 4.10 (bs, 4.1H), 3.20 (bs,0.21H), 2.07 (bs, 1.8H), 1.92 (bs, 4.4H), 1.40 (bs, 22.3H), 0.80 (bs, 8.9H).

GPC: Chloroform fraction, Mn = 19600 g mol^{-1}, Mw = 22900 g mol^{-1}, PDI = 1.17.

P16: M5 (0.131 g, 0.24 mmol), **M2** (0.21 g, 0.4 mmol), **M3** (0.151 g, 0.16), palladium acetate (0.0067 g, 0.03 mmol), tri(otolyl)phosphine (0.018 g, 0.06 mmol), 2.5 mL of saturated aqueous solution of $NaHCO_3$, and 6 mL THF. The reaction mixture was stirred at 90 ^{0}C for 78 h to produce polymer 16 as a yellow solid.

^{1}H NMR (400 MHz; $CDCl_3$, (δ) ppm): 9.02 (bs, 0.4H), 8.82 (bs, 0.81H), 7.80-7.55 (bm, 11.2H), 7.05 (bs, 4.4H), 6.71-6.62 (bm, 0.98H), 6.01 (bs, 0.39H), 4.10 (bs, 4.2H), 3.20 (bs, 0.4H), 2.07 (bs, 1.6H), 1.92 (bs, 4.8H), 1.40 (bs, 20.7H), 0.80 (bs, 7.9H).

GPC: Chloroform fraction, Mn = 13500 g mol^{-1}, Mw = 16000 g mol^{-1}, PDI = 1.19.

6.5 General procedure for the synthesis of Sonogashira Polymers (P11 and P12)[18]

To a solution of various ratios of M1, M3 and M6 in anhydrous tetrahydrofuran, the terminal acetylene was added together with copper (I) iodide, $Pd(PPh_3)_2Cl_2$ and PPh_3. The solution mixture was degassed three times and purged with argon gas before was left stirring at 75 ^{0}C for three days. Drops of an aqueous solution of HCl (37%) (0.5M) was added to the reaction mixture after was cooled to room temperature. The resulting solution was stirred at RT for 60 min, followed by extraction with DCM. The organic phases were washed with distilled H_2O and dried over anhydrous magnesium sulphate. The solvents were evaporated, and the crude was concentrated via reduced pressure. The 20 mL crude product was precipitated in methanol twice and finally filtered to obtain pure polymers.

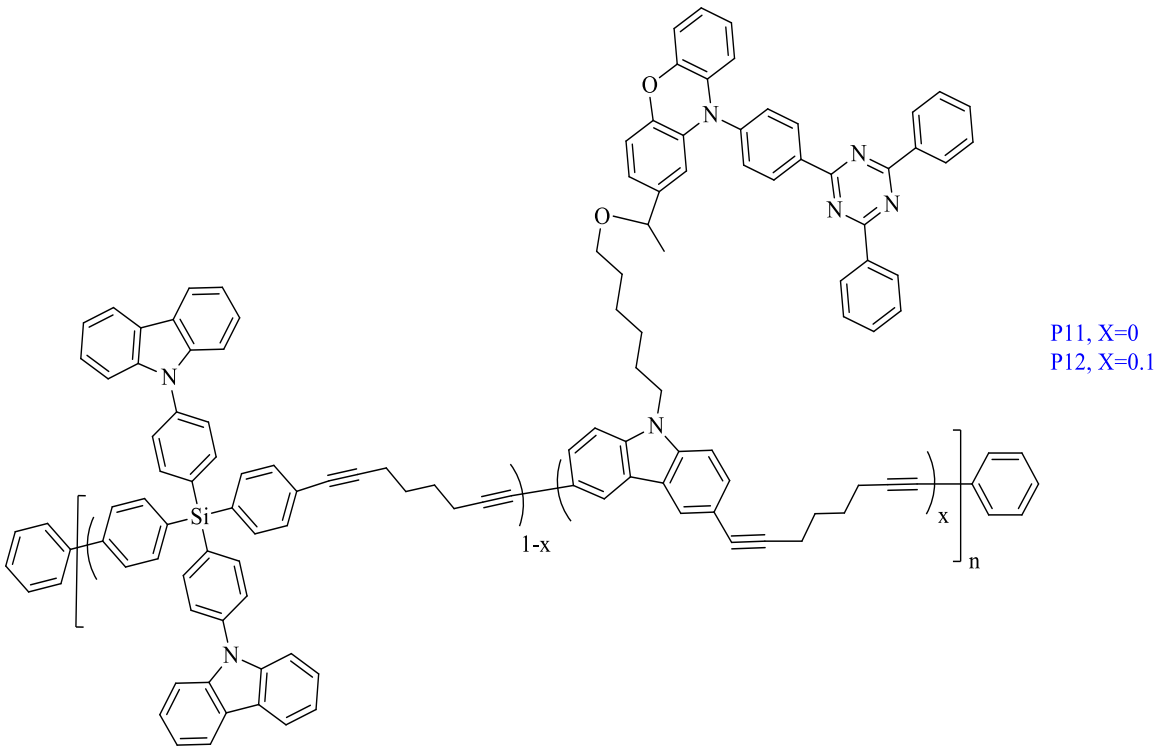

P11, X=0
P12, X=0.1

P11-P12

P11: **M1** (0.29 g, 0.35 mmol), **M6** (0.04 g, 0.35 mmol) CuI (0.14 g, 0.08 mmol), $Pd(PPh_3)_2Cl_2$ (0.005 g, 0.085mmol), PPh_3 (0.0035 g , 0.15mmol, 0.04g), were dissolved in 4 mL THF. The reaction was stirred at 75 ^{0}C for 3 days to yield P11 as a white solid.

^{1}H NMR (400 MHz; $CDCl_3$, (δ) ppm): 8.18 (bs, 4H), 7.83 (bs, 4H), 7.68 (bs, 8H), 7.60 (bs, 8H), 7.46-7.33 (bm, 8H), 2.55-2.49 (bm, 4H), 1.90-1.75 (m, 4H).

GPC: Toluene fraction, Mn = 5700 g mol^{-1}, Mw = 7500 g mol^{-1}, PDI = 1.30.

P12: **M1** (0.26 g, 0.315 mmol), **M6** (0.04 g, 0.35 mmol), **M3** (0.034 g, 0.035 mmol), CuI (0.14 g, 0.08 mmol), $Pd(PPh_3)_2Cl_2$ (0.005 g, 0.085mmol), PPh_3 (0.0035 g , 0.15mmol, 0.04g), were dissolved in 5 mL THF. The reaction was stirred at 75 ^{0}C for 3 days to yield P12 as a light yellowish solid.

^{1}H NMR (400 MHz; $CDCl_3$, (δ) ppm): 9.00 (bs, 0.07H), 8.81 (bs, 0.13H), 8.20 (bs, 3.9H), 7.88 (bs, 3.93H), 7.71-7.63 (bm, 8.1H), 7.59 (bs, 7.7H), 7.48-7.33 (bm, 7.8H), 7.12 (bs, 0.07H), 7.69-6.53 (m, 0.17H), 6.02 (bs, 0.07H), 2.51-2.47 (bm, 4H), 1.90-1.75 (m, 4H).

GPC: Toluene fraction, Mn = 3000 g mol^{-1}, Mw = 3400 g mol^{-1}, PDI = 1.12.

6.5 References

(1) Xue, R.; Zhang, M.; Xu, G.; Zhang, J.; Chen, W.; Chen, H.; Yang, M.; Cui, C.; Li, Y.; Li, Y. Molecular Design with Silicon Core: Toward Commercially Available Hole Transport Materials for High-Performance Planar p–i–n Perovskite Solar Cells. *Journal of Materials Chemistry A* **2018**, *6* (2), 404–413.

(2) Kim, S.-O.; Zhao, Q.; Thangaraju, K.; Kim, J. J.; Kim, Y.-H.; Kwon, S.-K. Synthesis and Characterization of Solution-Processable Highly Branched Iridium (III) Complex Cored Dendrimer Based on Tetraphenylsilane Dendron for Host-Free Green Phosphorescent Organic Light Emitting Diodes. *Dyes and Pigments* **2011**, *90* (2), 139–145.

(3) Choi, S.; Godumala, M.; Lee, J. H.; Kim, G. H.; Moon, J. S.; Kim, J. Y.; Yoon, D.-W.; Yang, J. H.; Kim, J.; Cho, M. J. Optimized Structure of Silane-Core Containing Host Materials for Highly Efficient Blue TADF OLEDs. *Journal of Materials Chemistry C* **2017**, *5* (26), 6570–6577.

(4) Zhang, R.; Peterson, J. P.; Fischer, L. J.; Ellern, A.; Winter, A. H. Effect of Structure on the Spin–Spin Interactions of Tethered Dicyanomethyl Diradicals. *Journal of the American Chemical Society* **2018**, *140* (43), 14308–14313.

(5) Komber, H.; Müllers, S.; Lombeck, F.; Held, A.; Walter, M.; Sommer, M. Soluble and Stable Alternating Main-Chain Merocyanine Copolymers through Quantitative Spiropyran–Merocyanine Conversion. *Polymer Chemistry* **2014**, *5* (2), 443–453.

(6) Hernandez-Olmos, V.; Abdelrahman, A.; El-Tayeb, A.; Freudendahl, D.; Weinhausen, S.; Müller, C. E. N-Substituted Phenoxazine and Acridone Derivatives: Structure–Activity Relationships of Potent P2X4 Receptor Antagonists. *Journal of Medicinal chemistry* **2012**, *55* (22), 9576–9588.

(7) Vanderhaeghe, H. Phenoxazines. I. Ring-Substituted Derivatives. *The Journal of Organic Chemistry* **1960**, *25* (5), 747–753.

(8) Liu, X.-K.; Zheng, C.-J.; Xiao, J.; Ye, J.; Liu, C.-L.; Wang, S.-D.; Zhao, W.-M.; Zhang, X.-H. Novel Bipolar Host Materials Based on 1, 3, 5-Triazine Derivatives for Highly Efficient Phosphorescent OLEDs with Extremely Low Efficiency Roll-Off. *Physical Chemistry Chemical Physics* **2012**, *14* (41), 14255–14261.

(9) Hwang, S.; Moon, Y. K.; Jang, H. J.; Kim, S.; Jeong, H.; Lee, J. Y.; You, Y. Conformation-Dependent Degradation of Thermally Activated Delayed Fluorescence Materials Bearing Cycloamino Donors. *Communications Chemistry* **2020**, *3* (1), 1–11.

(10) Ku, C.-H.; Kuo, C.-H.; Chen, C.-Y.; Leung, M.-K.; Hsieh, K.-H. PLED devises Containing Triphenylamine-Derived Polyurethanes as Hole-Transporting Layers Exhibit High Current Efficiencies. *Journal of Materials Chemistry* **2008**, *18* (12), 1296–1301.

(11) Liu, Y.; Wang, C.; Li, M.; Lai, G.; Shen, Y. Synthesis and Spectroscopic and Electrochemical Properties of TTF-Derivatized Polycarbazole. *Macromolecules* **2008**, *41* (6), 2045–2048.

(12) Choi, S.; Yoon, J. W.; Godumala, M.; Kim, H. J.; Park, S. H.; Kim, S. K.; Lee, H.; Kwon, J. H.; Cho, M. J.; Choi, D. H. 2D-σ-2A Type Cruciform Host Material with Silane Core for Highly Efficient Solution-Processable Green Thermally Activated Delayed Fluorescence Organic Light Emitting Diodes. *Dyes and Pigments* **2019**, *167*, 120–126.

(13) Li, Q.; Guo, H.; Ma, L.; Wu, W.; Liu, Y.; Zhao, J. Tuning the Photophysical Properties of N^ N Pt (II) Bisacetylide Complexes with Fluorene Moiety and Its Applications for Triplet–Triplet-Annihilation Based Upconversion. *Journal of Materials Chemistry* **2012**, *22* (12), 5319–5329.

(14) Singh, V.; Wang, S.; Kool, E. T. Genetically Encoded Multispectral Labeling of Proteins with Polyfluorophores on a DNA Backbone. *Journal of the American Chemical Society* **2013**, *135* (16), 6184–6191.

(15) Miyaura, N.; Suzuki, A. Palladium-Catalyzed Cross-Coupling Reactions of Organoboron Compounds. *Chemical Reviews* **1995**, *95* (7), 2457–2483.

(16) Yi, H.; Al-Faifi, S.; Iraqi, A.; Watters, D. C.; Kingsley, J.; Lidzey, D. G. Carbazole and Thienyl Benzo [1, 2, 5] Thiadiazole Based Polymers with Improved Open Circuit Voltages and Processability for Application in Solar Cells. *Journal of Materials Chemistry* **2011**, *21* (35), 13649–13656.

(17) Bautista, M. v; Varni, A. J.; Ayuso-Carrillo, J.; Tsai, C.-H.; Noonan, K. J. T. Chain-Growth Polymerization of Benzotriazole Using Suzuki–Miyaura Cross-Coupling and

Dialkylbiarylphosphine Palladium Catalysts. *ACS Macro Letters* **2020**, *9* (9), 1357–1362.

(18) Gazvoda, M.; Virant, M.; Pinter, B.; Košmrlj, J. Mechanism of Copper-Free Sonogashira Reaction Operates through Palladium-Palladium Transmetallation. *Nature Communications* **2018**, *9* (1), 1–9.

Chapter 7 Supplementary Information

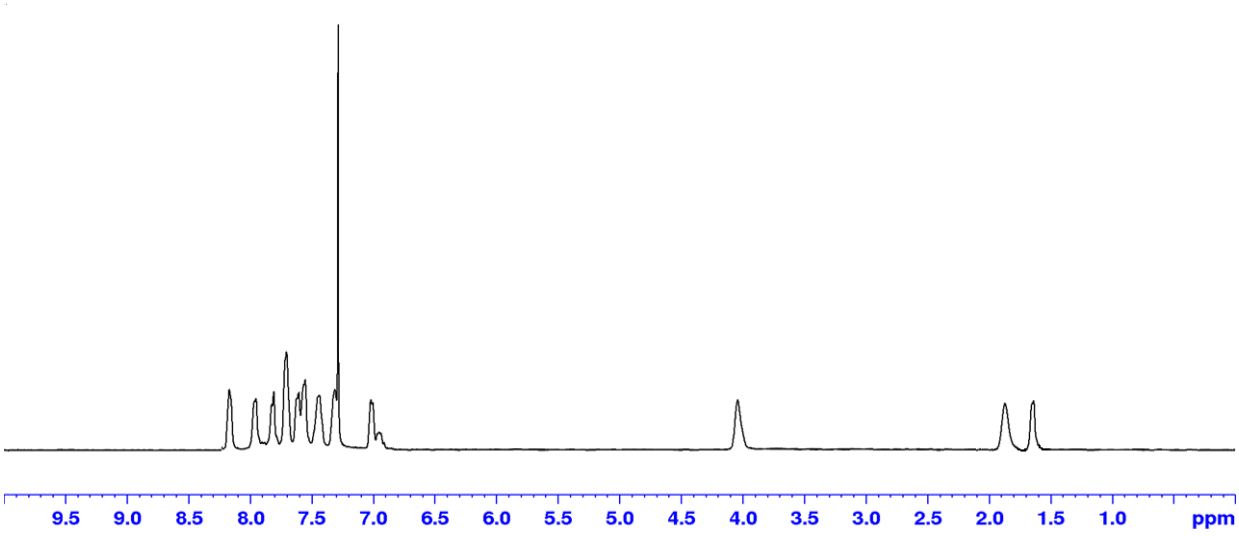

Figure 0. 1 ^{1}HNMR Spectrum of P1 in $CDCl_3$

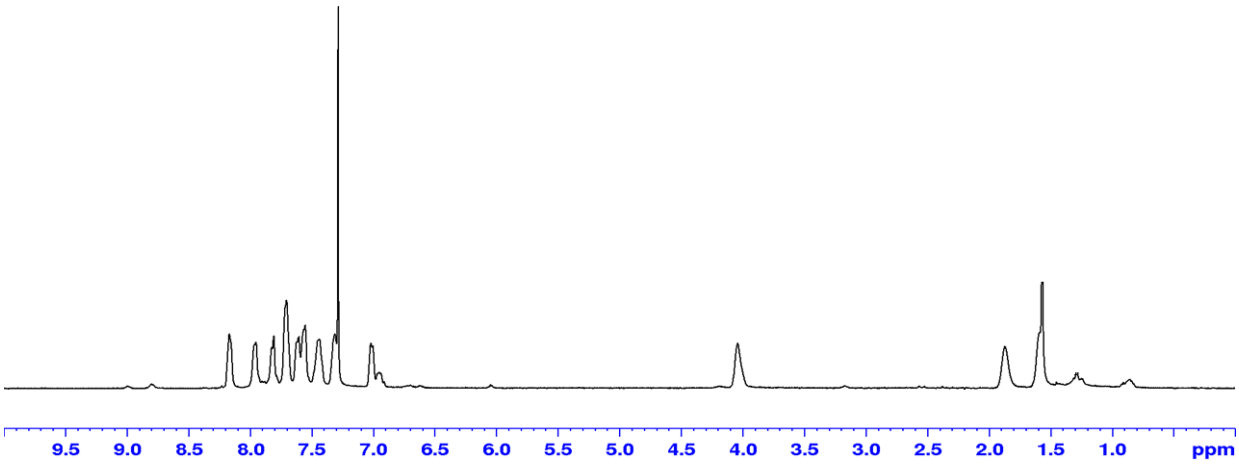

Figure 0. 2 ^{1}HNMR Spectrum of P2 in $CDCl_3$.

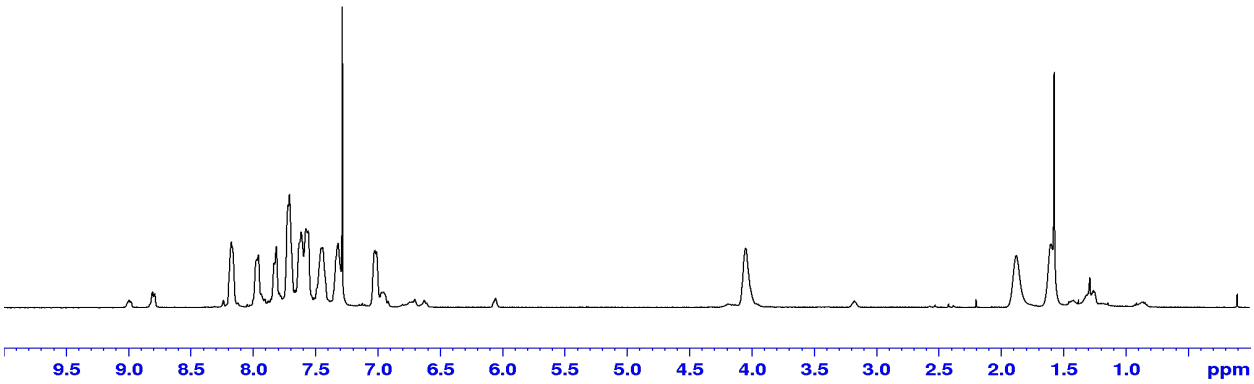

Figure 0. 3 ^{1}HNMR Spectrum of P3 in $CDCl_3$.

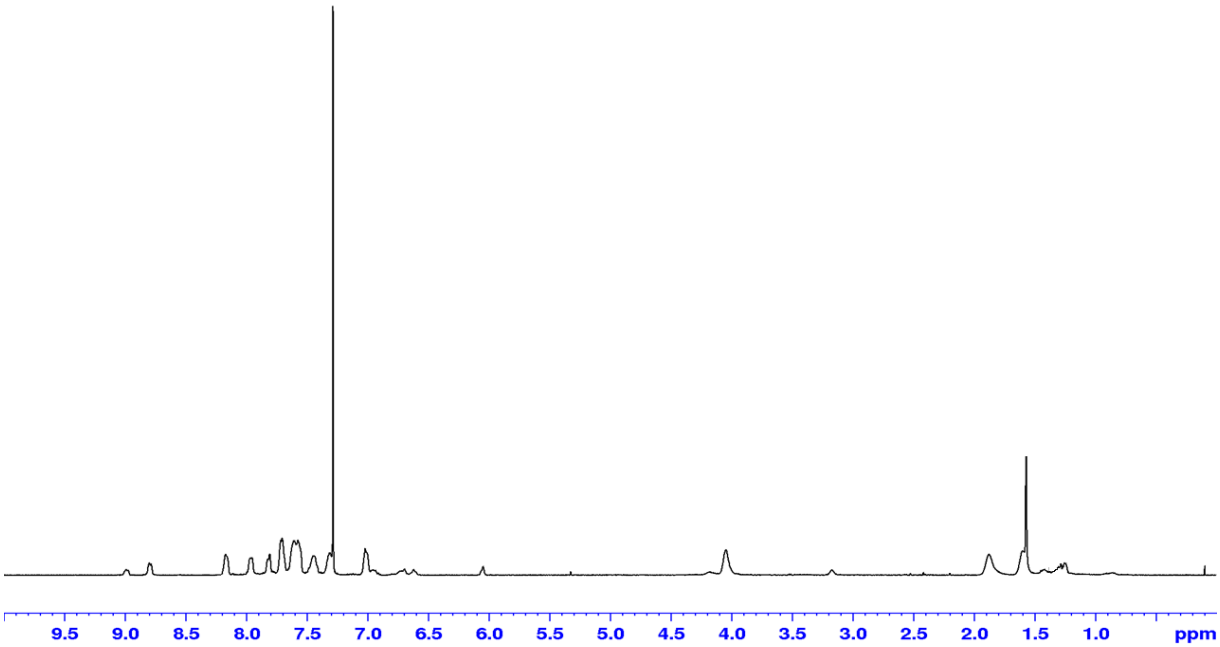

Figure 0. 4 ^{1}HNMR Spectrum of P4 in $CDCl_3$.

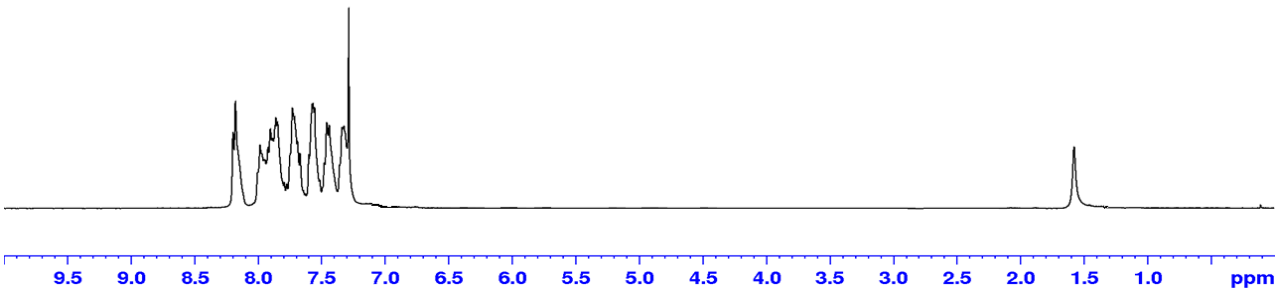

Figure 0. 5 ^{1}HNMR Spectrum of P5 in $CDCl_3$

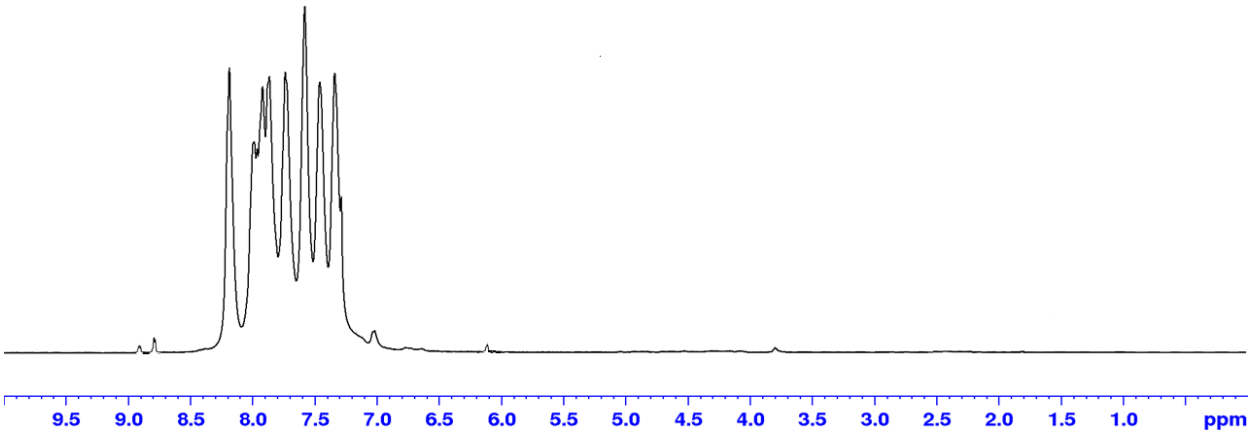

Figure 0. 6 ^{1}HNMR Spectrum of P6 in $CDCl_3$.

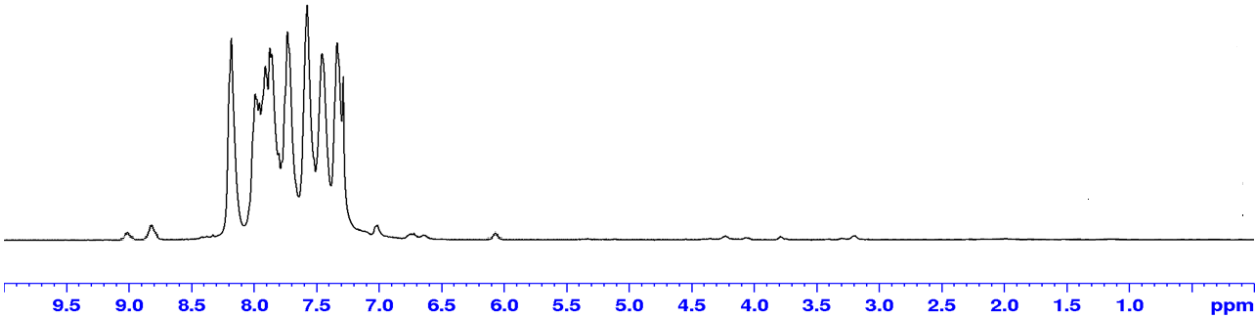

Figure 0. 7 ^{1}HNMR Spectrum of P7 in $CDCl_3$

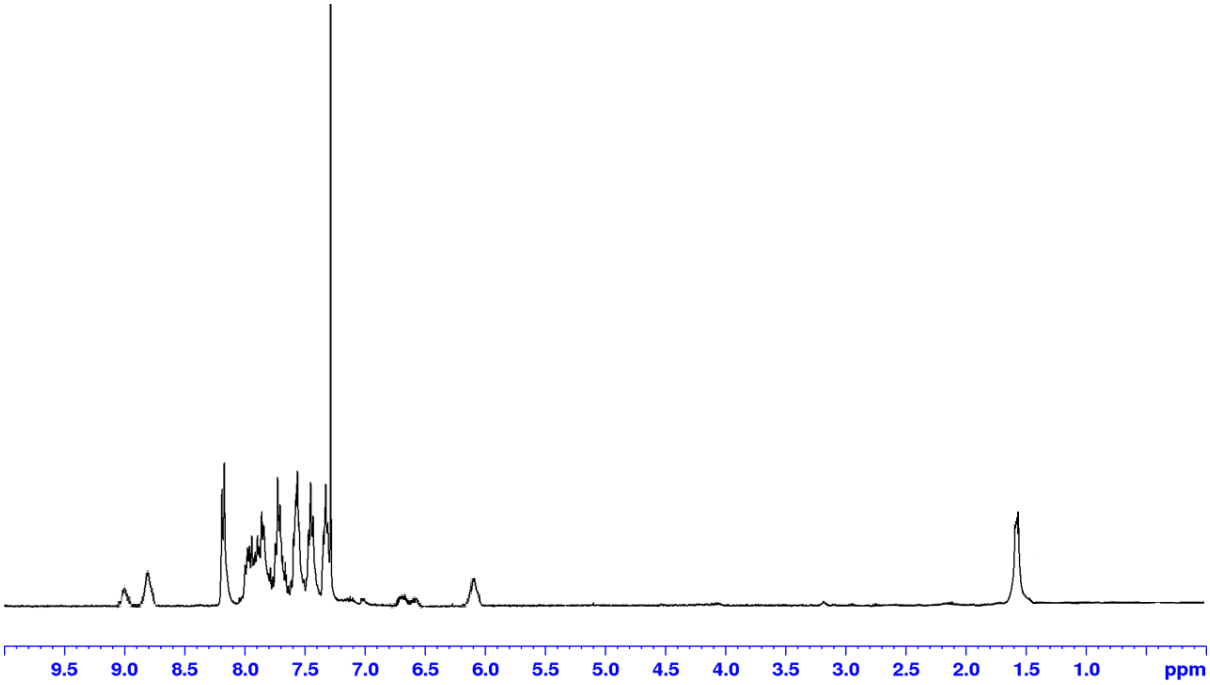

Figure 0. 8 ^{1}HNMR Spectrum of P8 in $CDCl_3$.

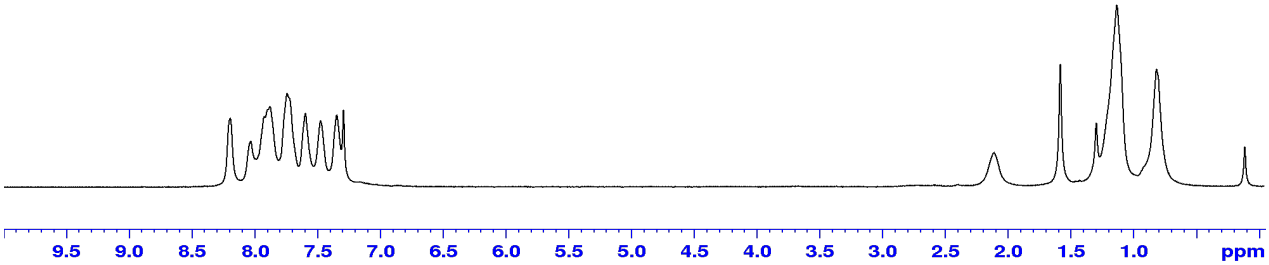

Figure 0. 9 ^{1}HNMR Spectrum of P9 in $CDCl_3$.

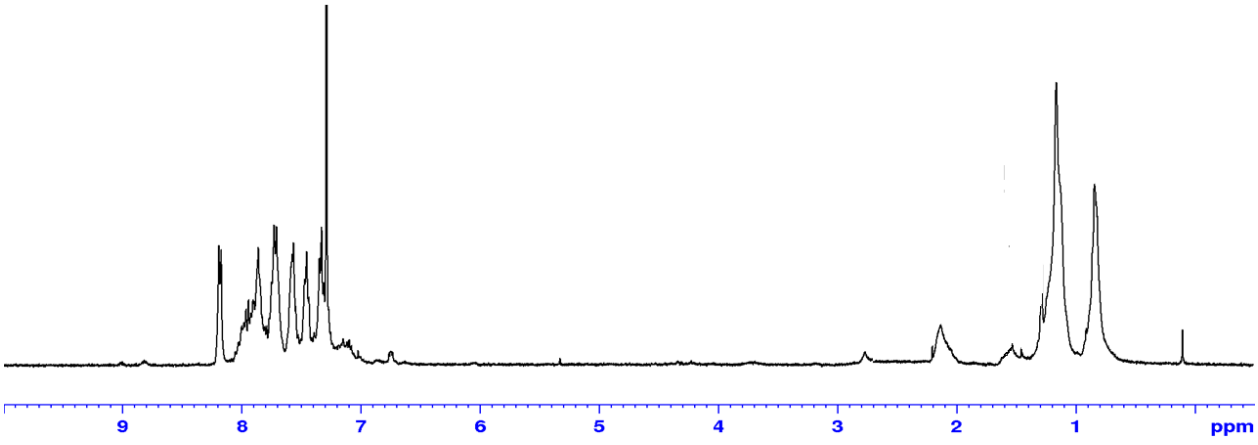

Figure 0. 10 ^{1}HNMR Spectrum of P10 in $CDCl_3$

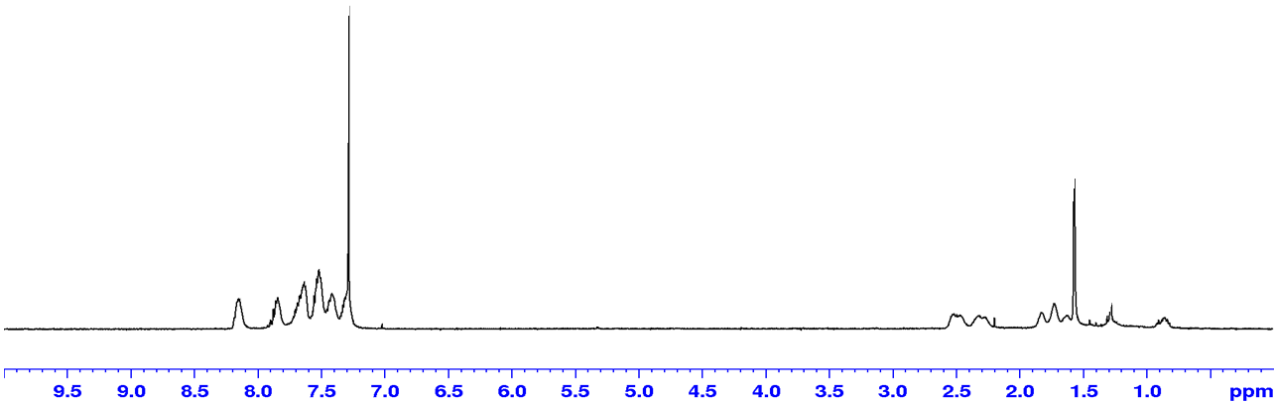

Figure 0. 11 ^{1}HNMR Spectrum of P11 in $CDCl_3$.

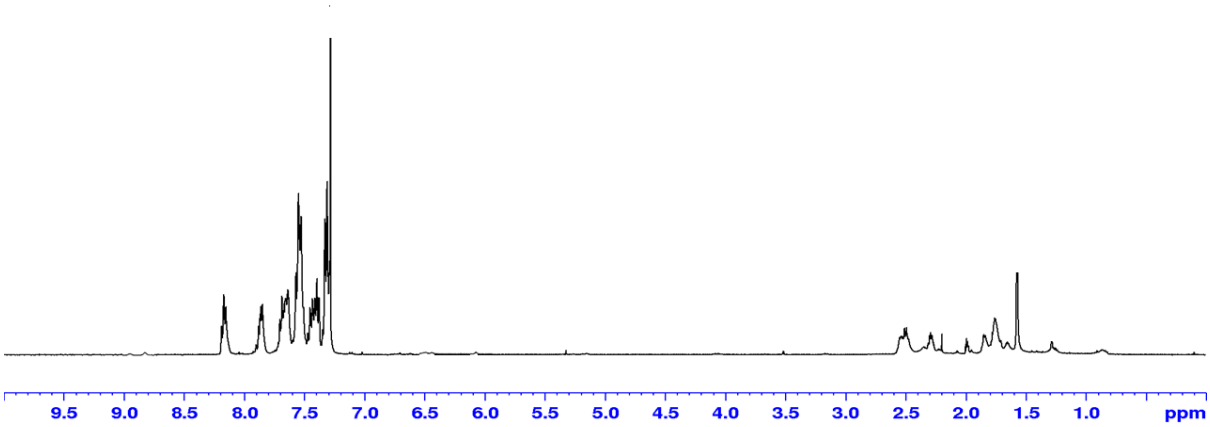

Figure 0. 12 ^{1}HNMR Spectrum of P12 in $CDCl_3$.

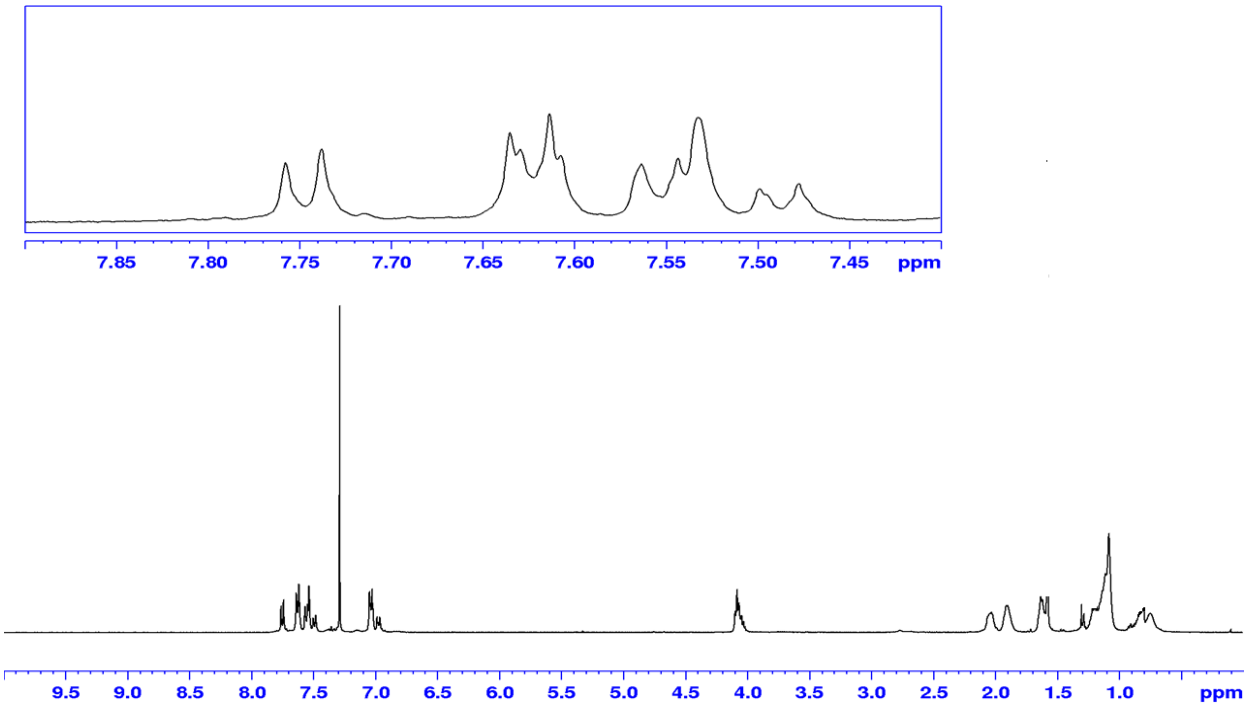

Figure 0. 13 ^{1}HNMR Spectrum of P13 in $CDCl_3$.

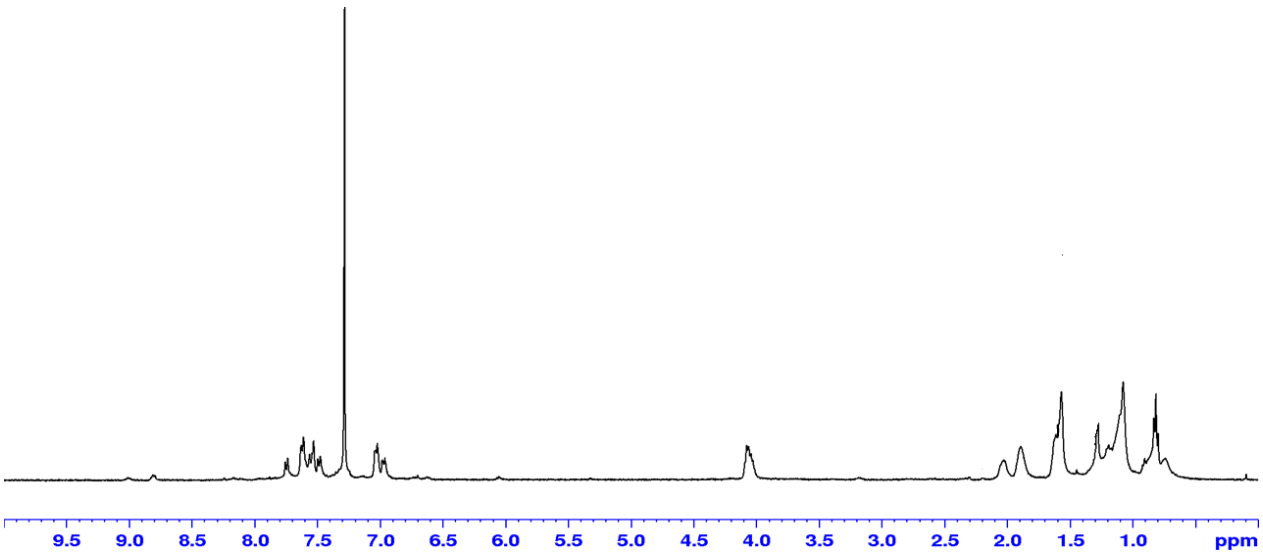

Figure 0. 14 ^{1}HNMR Spectrum of P14 in $CDCl_3$.

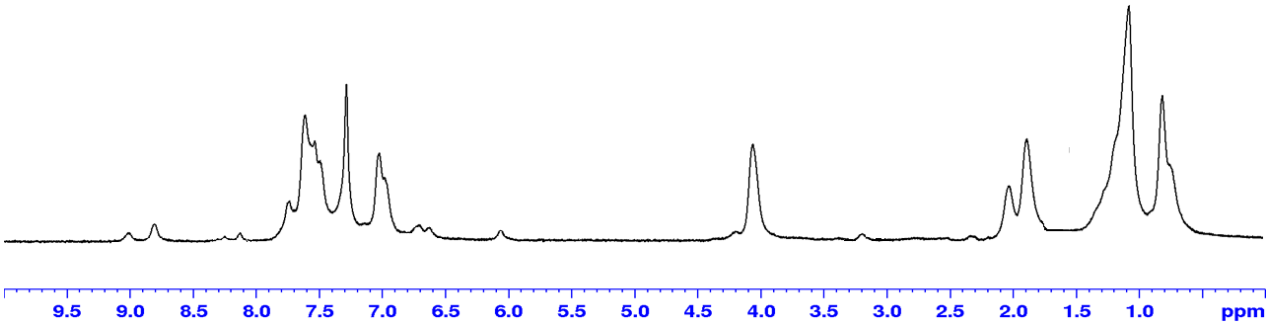

Figure 0. 15 ^{1}HNMR Spectrum of P15 in $CDCl_3$.

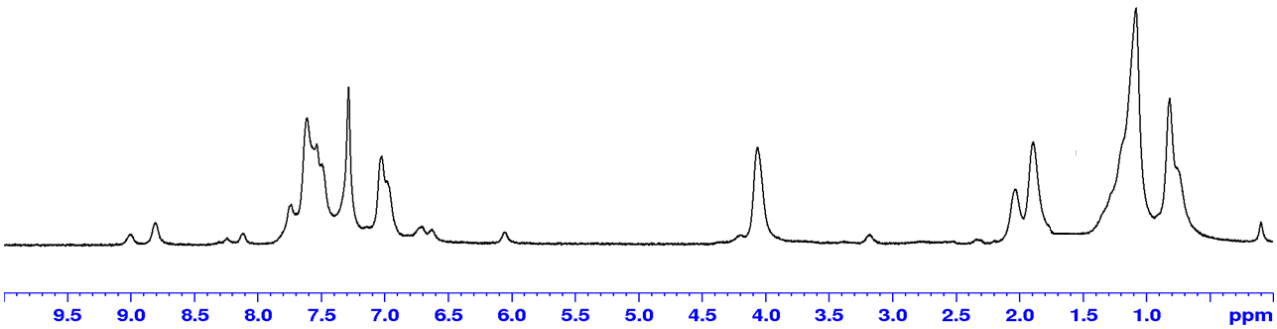

Figure 0. 16 ^{1}HNMR Spectrum of P16 in $CDCl_3$.